THE
PHYSICAL REVIEW
A Journal of Experimental and Theoretical Physics Established by E. L. Nichols in 1893
VOL. 54, NO. 9 NOVEMBER 1, 1938 SECOND SERIES

Nuclear Transformations Produced in Zinc by Alpha-Particle Bombardment

WILFRID B. MANN
Radiation Laboratory, Physics Department, University of California, Berkeley, California
(Received August 23, 1938)

Zinc has been bombarded with 17 Mev alpha-particles and the consequent radioactivity observed. The disintegration products are mainly positrons; the half-lives of the observed activities are 19.8∓0.4 minutes, 37∓1.5 hours, 79∓2 hours and about 195 days. A chemical separation indicates that the first and third of these activities are due to gallium and the remaining two to germanium. The two gallium activities may be respectively assigned to Ga^{70} and Ga^{67}. No very definite assignment has been possible, however, with respect to the activities associated with germanium.

WITH the 17 Mev alpha-particles from the cyclotron at Berkeley the transmutations produced in the bombardment of zinc with alpha-particles have been further studied. A preliminary report of the results obtained was given at the Stanford meeting of the American Physical Society in December, 1937. The results given at that meeting, however, require modification on account of the reported long-lived activity having been found to have a much longer half-life than was estimated. As a result, the half-life of 32 hours assigned to germanium has been found to be 37 hours while that of 55 hours ascribed to Ga^{67} has been increased to 79 hours.

RADIOACTIVE PRODUCTS

The activity obtained when a piece of chemically pure zinc was bombarded for about 4 microampere hours with alpha-particles was followed by means of a Lauritsen-type quartz fiber electroscope. It was found that the resulting decay curve could be resolved into four components, representing activities having half-lives of about 20 minutes, 37 hours, 79 hours, and one of about 195 days. The last part of the decay curve, together with the corrected 79-hour activity, is shown in Fig. 1. At first it was suspected that the long 195-day activity might be due to deuteron contamination and was in fact the seven-month activity found by Livingood and Seaborg[1] on bombarding zinc with deuterons. No trace, however, of the accompanying one-hour gallium activity could be detected, so that this explanation was therefore ruled out. Extrapolated to zero time after bombardment the 20-minute, 37-hour, 79-hour and 195-day activities had intensities corresponding respectively to 0.002, 0.4, 3.0 and 40 microcuries, giving yields of 4×10^{-7}, 5×10^{-7}, 1×10^{-7} and 4×10^{-8}. The electroscope was calibrated with a uranium standard.

In order to identify the various radioactive products, a target was prepared for bombardment with a view to effecting a chemical separation. By using a chemically pure zinc sulphate bath and following the procedure given by Bar-

[1] J. J. Livingood and G. T. Seaborg, San Diego Meeting, June 1938.

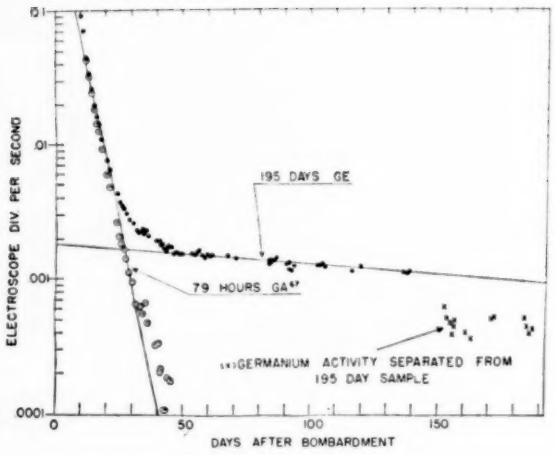

FIG. 1. Activity of zinc after bombardment by alpha-particles.

clay and Hainsworth,[2] a layer of zinc was electrolytically deposited onto a sheet of carbon to a thickness of about one-fiftieth of an inch. This target was bombarded with alpha-particles for 5.7 microampere hours; great care was taken to avoid deuteron contamination. Such contamination was not difficult to avoid since the deuteron and alpha-particle peaks were quite adequately resolved in the cyclotron.

After bombardment, the zinc target was dissolved off the carbon by boiling in a mixture of concentrated hydrochloric and nitric acids contained in a flask provided with a reflux condenser to prevent volatilization of the germanium chloride which might be present. Carriers of germanium and gallium were added and a separation for zinc, germanium and gallium carried out, according to the procedure recommended by Noyes and Bray.[3]

The solution obtained from dissolving the target to which the appropriate carriers had been added was diluted to about 6*N* and treated with hydrogen sulphide. Under this condition of acidity only germanium can be precipitated, while gallium and zinc remain in solution. The germanium precipitate was washed several times with 6*N* sulphuric acid saturated with hydrogen sulphide. The gallium and zinc filtrate was now evaporated to dryness and the residue redissolved in 6*N* hydrochloric acid. From this solution the gallium was extracted by the ether method of extraction; the ether was washed several times with acid before it was finally evaporated. The zinc in hydrochloric acid, after washing with ether, was then evaporated to dryness and the residue dissolved in water. The zinc was then precipitated by treatment with hydrogen sulphide. The results are shown plotted in Figs. 2 and 3. In Fig. 2 are shown the decay curves of the

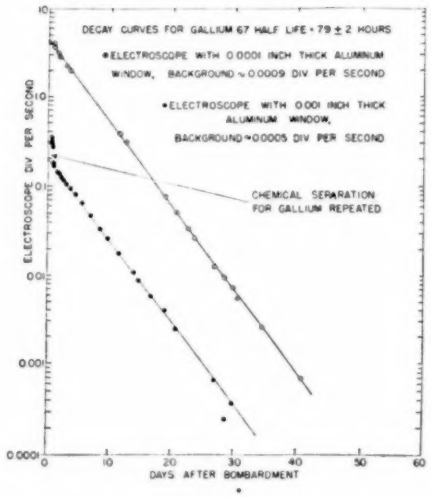

FIG. 2. Decay curves for gallium.

gallium activity observed on two electroscopes, one having an aluminum window 0.0001 inch thick and the second having an aluminum window 0.001 inch thick. In Fig. 3 is shown the decay curve of the germanium activity. The zinc showed a weak activity, having a half-life of about 38 hours, but this is probably due to a trace of germanium.

The gallium activity after a short time of rapid decay, presumably due to the 20-minute activity of Ga^{70}, settled down to a rate of decay corresponding to 79 hours, which was followed well into the background of the electroscope. The germanium activity decayed with a half-life of about 39 hours but started lengthening out just above background. By making a correction for the presence of this longer period the half-life of main activity was reduced to one of 37 hours, in agreement with that obtained without chemical analysis.

The 195-day activity is still, however, not

[2] W. R. Barclay and C. H. Hainsworth. *Electroplating* (Edward Arnold, London).
[3] A. A. Noyes and W. C. Bray. *Qualitative Analysis For the Rare Elements* (Macmillan, New York).

chemically identified. The 20-minute and 79-hour activities may be attributed to Ga^{70} and Ga^{67}, respectively. The 37-hour germanium activity is probably to be identified with that of 26 hours reported by Sagane for Ge^{69}. While the possibility of isomerism cannot be overlooked, the identification with Ge^{69} seems reasonable. The lengthening out observed in Fig. 3 leads one to suspect that the 195-day activity is due to germanium and might possibly be due to the radioactive isotope Ge^{67}. There is no sign at all that there is any long period activity due to gallium. The ratio of the 79-hour and 195-day activities in Fig. 1 extrapolated to zero time after bombardment is such that if this activity were due to gallium, then it should most certainly be observed in the data given in Fig. 2, which were obtained after a bombardment of about the same duration. If, however, the activity be due to Ge^{67}, then there should also be present activity due to Ga^{67} which would be formed by the disintegration of a Ge^{67} nucleus. Accordingly the sample from which the readings in Fig. 1 were obtained was added to another which had aged until only the 195-day period was present and a chemical separation was made for zinc, gallium and germanium. The activities obtained in the various fractions were weak. The germanium showed an activity about equal to background, the gallium about a third background, and the zinc about one-eighth background. The activity separating

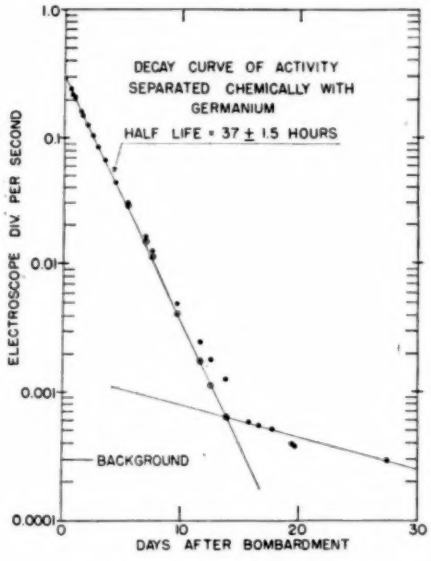

FIG. 3. Decay curves for germanium.

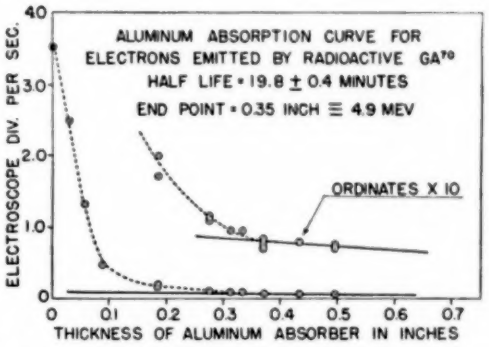

FIG. 4. Aluminum absorption curve for electrons emitted by radioactive Ga^{70}.

out with the gallium was, however, long-lived, nor did it show the characteristic absorption of Ga^{67}. Thus, as will be discussed in the next section, the soft beta-particles should have been practically completely absorbed by 0.001 inch of aluminum. This was not the case. However, since it is extremely improbable that any zinc or gallium will be precipitated in acid solution by hydrogen sulphide while any germanium left in solution would separate out with both these elements, it seems fairly reasonable to conclude that the 195-day activity should be ascribed to germanium.

With the identification of the 20-minute and 79-hour activities with Ga^{70} and Ga^{67}, correction for the isotopic abundance of Zn^{67} and Zn^{64} from which the radioactive isotopes of gallium would be formed by alpha-particle capture and emission of a proton, gives respective absolute yields of 9×10^{-6} and 3×10^{-7}.

Disintegration Products

By examination in a magnetic field, the emitted electrons were found to be predominantly positive. It is known, however, that the two gallium isotopes, Ga^{67} and Ga^{70}, give rise to negative electrons, the former by conversion of a gamma-ray and the latter by emission in the process of transforming to stable Zn^{70}. The chemically separated germanium was found to be positron active, corresponding, if the identification be correct, to a transformation from Ge^{69} to Ga^{69}. The germanium activity was investigated for soft x-rays but none was found. Absorption measurements were made using aluminum absorbers and the results are shown in Figs. 4, 5 and 6. From Feather's empirical formula, values of 5.0

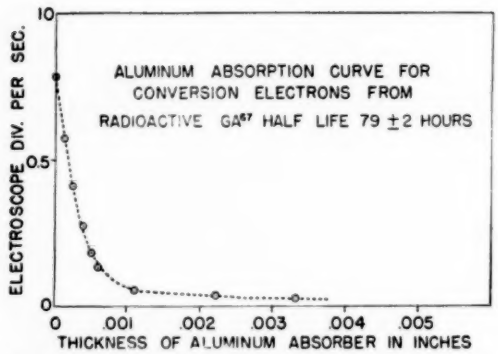

FIG. 5. Aluminum absorption curve for conversion electrons from radioactive Ga^{67}.

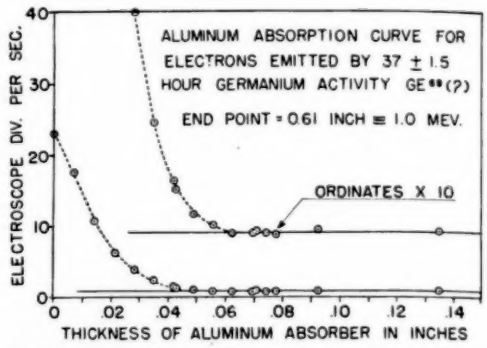

FIG. 6. Aluminum absorption curve for electrons emitted by 37 ±1.5 hour germanium activity Ge^{69}(?).

Mev and 1.0 Mev were obtained, respectively, for the maximum energies of the electrons emitted by Ga^{70} (19.8 minutes) and Ge^{69} (37 hours). The disintegration products of Ga^{67} (79 hours) have been exhaustively investigated by Alvarez[4] who found that Ga^{67} transformed to Zn^{67} by capture of a K shell electron followed by emission of an x-ray characteristic of zinc. The soft electrons which are emitted, the absorption curve for which is shown in Fig. 5, have been found by Alvarez to be due to conversion of a 100 kev gamma-ray in the K and L shells. In the present instance, the absorption coefficients of the x-rays have also been measured and a complete identification of the results with those obtained by Alvarez has been established.

It is again a pleasure to be able to express my thanks to Professor E. O. Lawrence and to the staff of the Radiation Laboratory for all their help and cooperation. My thanks are also due to the Commonwealth Fund for the award of a fellowship which has made my stay here possible. The research has also been aided by grants to the laboratory from the Research Corporation, the Chemical Foundation and the Josiah Macy, Jr., Foundation. The experiments have been facilitated by assistance from the W.P.A.

[4] L. W. Alvarez, Phys. Rev. **53**, 606 (1938).

NOVEMBER 1, 1938 PHYSICAL REVIEW VOLUME 54

Note on K-Electron Capture in Be^7

G. BREIT AND J. K. KNIPP
University of Wisconsin, Madison, Wisconsin

(Received August 5, 1938)

There is no observed positron emission in Be^7. This sets an upper limit of 2.09 mc^2 for the mass difference Be^7–Li^7 from Fermi's theory and 2.3 mc^2 from the Konopinski-Uhlenbeck theory. This upper limit is compared with other estimates of the same mass difference. The gamma-ray emission accompanying the disintegration probably takes place after the K capture from an excited state of Li^7 having a spin $\frac{1}{2}$. The K-capture transition to $i=\frac{1}{2}$ from $i=\frac{3}{2}$ is according to experiment only $\frac{1}{10}$ as weak as that to $i=\frac{3}{2}$. This speaks for the Gamow-Teller type of selection rules. The mean lives of He^6, Be^7, C^{11} are compared. It is found that the observed mean lives are relatively shorter for the lighter nuclei than Fermi's theory predicts. This is in apparent contradiction with the preference shown for the Fermi theory by the alpha-particle distribution from Li^8. From a theory without derivatives, the facts seem to point either to an appreciable increase in the many-body aspect of nuclei from He^6 to C^{11} or else to a decrease in the intrinsic β-emitting powers of nuclear particles in heavier nuclei. On the Konopinski-Uhlenbeck theory some of the disagreement can be removed but the β-particle distribution from Li^8 (Gamow and Teller) speaks strongly against using this theory for mean lives.

THE experiments of Roberts, Heydenburg and Locher[1] show that Be^7 captures its K electron to form Li^7. They observe roughly one gamma-ray quantum per every ten Be^7 atoms produced. The gamma-radiation is explained by them as being due to capture of a K electron into an excited state. Their measurements give

[1] R. B. Roberts, N. P. Heydenburg, G. L. Locher, Phys. Rev. **53**, 1016 (1938); R. B. Roberts and N. P. Heydenburg, Abstract No. 78, 1938, Washington Meeting American Physical Society.

425 ± 25 kev for the energy of the gamma-ray. This agrees within experimental error with the position of the level of Li^7 (450 kev) determined by the reaction[2] $Li^6+H^2=Li^7+H^1$. Richardson[3] finds that N^{13} emits in addition to the annihilation radiation also another somewhat softer γ-ray. The gamma-radiation of N^{13} was used as a comparison standard in the determination of the radiation from Li^7. The energy $(Li^7)^*-Li^7$ is, therefore, possibly lower than stated and the level responsible for gamma-radiation may be different from that observed in $Li^6+H^2=Li^7+H^1$. The exact identity of the level makes little difference for the discussion below as long as its spin is $\frac{1}{2}$. It is likely and it will be assumed below that the level in question is identical with that observed in proton emission and that its spin is $\frac{1}{2}$ because the energy measurements of gamma-rays are difficult and because it is difficult theoretically to explain the presence of two levels within 450 kev of the ground state.

TABLE I. *Approximate values of* $lg_{10}(P_+/P_K)$.

$511(\Delta w-1)$kev	10.2	41	101	172	278	511	590 kev
$[lg_{10}(P_+/P_K)]_F$	4.4	2.6	0.0	0.7	1.4	2.3	2.5
$[lg_{10}(P_+/P_K)]_{K\text{-}U}$				2.7	1.7		1.2

The mass difference Be^7-Li^7 is not known directly with great certainty. The neutron distribution from Li^6+H^2 obtained by Rumbaugh, Roberts and Hafstad[4] indicates that their maximum energy is at least 3.3 Mev for 800 kev incident neutrons. This gives $Li^6+H^2\geqq Be^7+n$ +3.2 Mev. From the measurements of Cockcroft and Walton, Bethe and Livingston obtain $Li^6+H^2=Li^7+H^1+5.02\pm0.12$ Mev and Rumbaugh, Roberts and Hafstad[4] obtain 5.0(3) Mev. This gives $Be^7<Li^7+1.8$ Mev $-0.00080=0.00091$ $=1.6(7)$ $mc^2=0.91$ mmu. Using the mass of Li^6 as given by Livingston and Bethe[5] and Bethe's revised neutron mass[6] one obtains from the Be^7+n process; $Be^7=Li^7+1.9(0)$ $mc^2=Li^7+1.04$ mmu. The disagreement between these estimates makes it desirable to estimate the upper limit of the energy by making use of the apparent improbability of the positron emission from Be^7.

This was done by using the formulas of Yukawa and Sakata[7] for the ratio of the positron probability P_+ to K-capture probability P_K. It was supposed that the neutrino mass is zero. One has then in a sufficiently good approximation

$$\frac{P_+}{P_K}=\frac{\int_1^{\Delta w}F(\epsilon,0)d\epsilon}{2\pi(\alpha Z)^3(1+\Delta w)^2}. \qquad \text{(Fermi)} \quad (1)$$

$$\frac{P_+}{P_K}=\frac{\int_1^{\Delta w}F(\epsilon,0)(\Delta w-\epsilon)^2d\epsilon}{2\pi(\alpha Z)^3(1+\Delta w)^4}. \qquad \text{(Konopinski-Uhlenbeck)} \quad (2)$$

Here $\Delta w-1$ is the energy available for positron emission in mc^2 units, $\alpha=1/137$ and $Z(=4)$ is the atomic number of the unstable nucleus.

$$F(\epsilon,0)=\epsilon(\epsilon^2-1)^{\frac{1}{2}}(\Delta w-\epsilon)^2\frac{x}{e^x-1};$$

$$x=2\pi\alpha Z\epsilon(\epsilon^2-1)^{-\frac{1}{2}}.$$

The α-particle distribution from Li^8 indicates, according to Gamow and Teller,[8] that the Fermi theory accounts for mean lives as a function of available energy in β-decay better than the Konopinski-Uhlenbeck theory for the disintegrations of light nuclei. It appears safest, therefore, to use the formulas of the Fermi theory in this case also. One obtains the approximate values given in Table I of $lg_{10}(P_+/P_K)$ on the Fermi (F) and the Konopinski-Uhlenbeck theories.

Experiment shows that the number of γ-rays is about 1/10 of the number of neutrons. An emitted positron should give two γ-rays. The number of emitted positrons is, therefore, less than 1/20 of the number of Be^7 atoms which is practically the same as $P_+/P_K<1/20$. According to Table I this corresponds to $Be^7-Li^7<45$ kev $+2$ $mc^2=2.08(8)$ mc^2 on the Fermi theory and $Be^7-Li^7<172$ kev $+2$ $mc^2=2.34$ mc^2 on the K-U theory. Since the K-U theory underestimates the emission at the end of the range the K-U calculation should give too low values of

[2] L. H. Rumbaugh and L. R. Hafstad, Phys. Rev. **50**, 681 (1936).
[3] J. R. Richardson, Phys. Rev. **53**, 610 (1938).
[4] L. H. Rumbaugh, R. B. Roberts and L. R. Hafstad, Phys. Rev. **54**, 657 (1938); the writers are indebted to Messrs. Rumbaugh, Roberts and Hafstad for communicating to them their results before publication.
[5] M. S. Livingston and H. A. Bethe, Rev. Mod. Phys. **9**, 245 (1937).
[6] H. A. Bethe, Phys. Rev. **53**, 313 (1938).
[7] H. Yukawa and S. Sakata, Proc. Phys. Math. Soc. of Japan **17**, 467 (1935); **18**, 128 (1936); C. Moller, Phys. Rev. **51**, 84 (1937).
[8] Considerations of Gamow and Teller quoted by L. H. Rumbaugh, R. B. Roberts and L. R. Hafstad, Phys. Rev. **51**, 1106 (1937).

P_+/P_K for the correct energy and too high values of Be^7-Li^7 for a given P_+/P_K. The estimate from Fermi's theory is preferable. Positrons with 45 kev maximum energy would easily escape detection and the only direct contradiction to assuming the mass difference to be $2.09\ mc^2=1.14$ mmu lies in the neutron energy. Plotting the mass differences He^3-H^3, $C^{11}-B^{11}$, $N^{13}-C^{13}$, $O^{15}-N^{15}$, $F^{17}-O^{17}$ against Z one estimates that 0.9 mmu $<Be^7-Li^7<1.2$ mmu. These estimates are seen to agree with each other. From the fact that $C^{11}-B^{11}$, $O^{15}-N^{15}$ have relatively larger values than $N^{13}-C^{13}$, $F^{17}-O^{17}$ values below 1.0 mmu appear unlikely so that the range between 1.0 mmu $=1.8\ mc^2$ and 1.14 mmu $=2.09\ mc^2$ appears to be available for Be^7-Li^7.

Since the normal state of Li^7 has a spin $\frac{3}{2}$, it is natural to suppose that the same is true for the normal state of Be^7. There is some probability that the level of Li^7 at 450 kev has a spin $\frac{1}{2}$ and that it is the $^2P_{1/2}$ partner of the $^2P_{3/2}$ normal level. If so, the K capture occurs here into two nuclear states differing from each other mainly through the relative orientation of total particle spin with respect to total orbital angular momentum. On the Fermi theory one would expect the transition to $^2P_{1/2}$ to have negligible intensity in comparison with that to $^2P_{3/2}$. Experiment indicates the opposite and speaks in favor of the Gamow-Teller type of selection rules.[9] With the interaction energy given by their Eq. (2) the transition probabilities are proportional to 5 and 4 for $^2P_{3/2}$ and $^2P_{1/2}$ respectively (for $l=1$, the ratio is $2l+3:4l$ on a single particle model with $l=$orbital angular momentum) and besides to $(1+\Delta w)^2$. Using the ratio 10 : 1 for the transition probabilities and $0.88\ mc^2$ for $(Li^7)^*-Li^7$ one obtains Δw by solving

$$\frac{(1+\Delta w)^2}{(0.12+\Delta w)^2}=\frac{4}{5}\frac{9}{1}.$$

This gives $\Delta w=0.40$ which makes $Be^7-Li^7=1.4\ mc^2=0.8$ mmu. This value is too low. For a mass difference of $2.09\ mc^2$ the expected ratio of the transition probabilities for $^2P_{3/2}$ and $^2P_{1/2}$ is 3.7 which corresponds to 1/4.7 as many γ-rays as neutrons. The difference between 1/4.7 and 1/10 may not be significant in view of the difficulty of γ-ray intensity measurements and the uncertain nature of the theory. On the K-U theory modified with spin terms for heavy particles the ratio 10 : 1 gives in the same way $\Delta w=1.3$ which corresponds to $Be^7-Li^7=2.3\ mc^2$ and is only slightly too high. For $2.09\ mc^2$ the expected ratio of the transition probabilities is 12 which agrees better with experiment than the Fermi-like theory. This comparison is, however, only apparently favorable to the K-U form because Gamow and Teller's[9] matrix element M_2 cannot be used by itself. Their matrix element M_1 will increase the ratio considerably making the Fermi-like result approach the experimental value and the K-U value recede from it.

An appreciable intrinsic preference for a transition to $^2P_{3/2}$ in comparison to $^2P_{1/2}$ is apparently ruled out by the approximate value 10 : 1 of $Be^7:\gamma$. Thus even if there were only a factor 10 favoring $^2P_{3/2}$ the ratio of transitions to $i=\frac{3}{2}$ and $i=\frac{1}{2}$ would be on the Fermi theory $10(1+\Delta w)^2/(0.12+\Delta w)^2$. The smallest possible value of Δw is 0.7 which gives 40 for this ratio and the largest Δw is 1.1 which gives 30. On a K-U theory with an intrinsic preference 10 : 1 for $\frac{3}{2}$ one has a ratio of 180 for $\Delta w=0.7$ and 90 for $\Delta w=1.1$. All of these values are appreciably greater than 10.

The Be^7 nucleus differs from Li^7 presumably only through the conversion of a proton into a neutron. The matrix element M of the β-ray theory should be, therefore, of the order of magnitude 1 for the transition $\frac{3}{2}\rightarrow\frac{3}{2}$. It is thus natural to expect that the mean life of Be^7 should correspond to an anomalously high $|M|^2$ with Fermi's g which was obtained from more complicated and, therefore, less probable transitions. The increase of $|M|^2$ with decreasing atomic number has been pointed out by Nordheim and Yost[10] and has been attributed by them to the increasing importance of the many-body aspect for heavier nuclei. A comparison will be made here with the period $C^{11}\rightarrow B^{11}$ which gives about the same value of $|M|^2$ as $N^{13}\rightarrow C^{13}$. Before discussing the numerical relations it is necessary to consider the dependence of $|M|^2$ on other nuclear properties. The isotopic spin notation is the most

[9] G. Gamow and E. Teller, Phys. Rev. **49**, 895 (1936).

[10] L. W. Nordheim and F. L. Yost, Phys. Rev. **51**, 943 (1937).

convenient.[11] The wave function is then antisymmetric for simultaneous interchanges of space coordinates x, spins σ and isotopic spins τ.

The matrix element for positron emission is on Fermi's theory

$$M=(\varphi, \sum_k \tfrac{1}{2}(\tau_k^\xi + i\tau_k^\eta)\psi). \tag{3}$$

Here ψ, φ are the wave functions of initial and final nuclei. The operators τ^ξ, τ^η, τ^ζ are Pauli's matrices for isotopic spin so that $(\tau^\xi)^2=1$ etc. $\cdots$. The wave-lengths of the light particles are supposed to be long compared with the nuclear radius, so that there is no difference in the values of the light particle wave functions at the different heavy particles within the nucleus. The above formula takes into account the interference of the light particle field due to emissions from different heavy particles. For a symmetric Hamiltonian the normal state of the final nucleus has

$$\varphi=\sum \tfrac{1}{2}(\tau_k^\xi + i\tau_k^\eta)\psi, \qquad \text{so that} \quad M=(\psi, (T_\xi - iT_\eta)(T_\xi + iT_\eta)\psi). \tag{3'}$$

Evaluating the operator in the scalar product one finds

$$M=T(T+1)-T_\zeta(T_\zeta+1) = (T-T_\zeta)(T+T_\zeta+1), \tag{4}$$

where one has set $(\psi, \psi)=1$ since the wave function must be normalized. Here T_ζ is $\frac{1}{2}(N-Z) = \frac{1}{2}\Sigma\tau_k^\zeta$ and $T(T+1)$ is the characteristic value of $T_\xi^2+T_\eta^2+T_\zeta^2$ where T_ξ, T_η are defined similarly to T_ζ. If the number of protons is the minimum possible with a given T then $T_\zeta=T$ and $M=0$. This should be the case because there can be no final nucleus with the same T with a smaller number of protons. The values T_ζ, $T_\zeta+1$ are seen to be the values of T_ζ in the initial and final nucleus. For the disintegrations $Be^7\rightarrow Li^7$, $C^{11}\rightarrow B^{11}$, $N^{13}\rightarrow C^{13}$, $T_\zeta=-\frac{1}{2}$ so that

$$M=(T+\tfrac{1}{2})^2.$$

There is considerable probability[11] that $T=\frac{1}{2}$ for the ground states. This gives $M=1$ for the three cases.

The validity of Eq. (3′) was essential for Eq. (4). If the Hamiltonian is symmetric the φ of Eq. (3′) will be a solution of the wave equation and will correspond to a possible final nucleus. For a Hamiltonian that is not symmetric this is not the case. Even the inequality between unlike particle and like particle forces matters. For example, the Heisenberg interaction between unlike particles can be expressed as

$$\tfrac{1}{2}\sum_{k>j}(\tau_k^\xi\tau_j^\xi+\tau_k^\eta\tau_j^\eta)J(r_{ij}).$$

For long range forces this becomes

$$[(T_\xi^2+T_\eta^2+T_\zeta^2)-T_\zeta^2-(n/2)]J(0).$$

The term T_ζ^2 does not commute with $T_\xi+iT_\eta$ and Eq. (3′) does not hold in general. This is due to the fact that an "unsymmetric Hamiltonian" is not invariant to rotations of the isotopic spin and does not commute with $T_\xi+iT_\eta$. The equation $H(T_\xi+iT_\eta)\psi=0$ then does not follow from $H\psi=0$. If, on account of a difference between like and unlike particle forces, the four neutrons of Li^7 should be somewhat farther out than the three protons, then similarly in Be^7 the four protons will be somewhat farther out than the three neutrons. When a K capture occurs the neutralized proton finds itself in the right position to be a neutron of Li^7 but the three remaining protons are too far out. Such a condition would be expected to decrease the transition probability. The model just mentioned is meant only as an illustration of principle and not in a literal way. Similarly an inequality between proton-proton and proton-neutron interactions introduces terms in T_ζ and T_ζ^2. A surplus repulsion between protons will make Be^7 slightly larger than Li^7 and C^{11} slightly larger than B^{11}. Due to this cause, however, one will expect only very small effects because the Coulomb barrier in carbon is at the most 6 mc^2 and changes at the most by 1 mc^2 in the positron emission. The mass differences $Be^8+H^3-B^{11}=0.012$ and $Be^8+He^3-C^{11}=0.0097$ show that H^3 and He^3 must be quite thoroughly distorted in B^{11} and C^{11}. It is probable that these nuclei do not have any loosely attached particles for which the Coulomb effect is especially important. In Li^7 the H^3

[11] The most complete account of this is given by E. Wigner, Phys. Rev. **52**, 106 (1937); first introduced by W. Heisenberg, Zeits. f. Physik **77**, 1 (1932); cf. also B. Cassen and E. U. Condon, Phys. Rev. **50**, 846 (1936). Wigner's notation is used here.

combination is bound only by 0.0028 mass units and here the H^3 combination may be behaving somewhat as a unit. The Coulomb field in H^3 is too weak, however, to cause much distortion in H^3. It is difficult to see, from such average field effects, a reason for a smaller $|M|^2$ in $C^{11} \rightarrow B^{11}$ than in $Be^7 \rightarrow Li^7$.

Using the Fermi theory and disregarding the presence of transitions that violate the selection rules, one obtains, with $g = 4.0 \times 10^{-50}$, $C^{11} - B^{11} - 2\ mc^2 = 2.26\ mc^2$, $|M|^2 = 1$ an expected mean life of 270 minutes. The observed mean life is 20.5 min./0.694 = 29.6 min. This requires $|M|_C^2 = 9.(0)$. In Be^7 with the same g and $|M|^2$ and with $Be^7 - Li^7 = 2\ mc^2$, the expected mean life is 5.3 years. The observed mean life is 43 days/0.694 = 62 days. This requires $|M|_{Be}^2 = 30$. The ratio of the two $|M|^2$ is 3.3. One can try to lower the ratio by increasing the value of $Be^7 - Li^7$ used in the calculation of the expected mean life. The small number of emitted positrons makes it impossible to assume more than 2.1 mc^2 for $Be^7 - Li^7$. The transition probability due to K capture is then increased by 10 percent in the total transition probability due to positron emission. The discrepancy is then still represented by a factor ~ 2.6.

According to Bjerge and Bjerge and Brostrum[12] the half life of He^6 is ~ 1 sec. and the available energy ~ 3.7 Mev corresponding to $|M|^2 \sim 120$. This $|M|^2$ is even larger than that in Be^7 and is more surprising because He^6 and Li^6 are not homologous. The β-disintegrations of the light elements show in this way an interesting contradiction in pointing for Li^8 to the dependence of probability on energy predicted by Fermi's theory, as has been noticed by Gamow and Teller, and in showing besides a systematic increase in the probability with decreasing Z.

The K-U theory when applied to C^{11} and Be^7 gives approximate agreement of $|M|_C^2$ and $|M|_{Be}^2$ with the use of the inspection limit for C^{11} and $\Delta w = 1$ for Be^7. It is difficult to believe that this agreement means much because the K-U theory does not account for the α-particle distribution of Li^8 but it should be noted that the extreme shortness of the life of He^6 in comparison with that of C^{11} is accounted for more easily on the K-U than on the Fermi theory. According to Gamow and Teller, however, the alpha-particle distribution from Li^8 speaks strongly against the K-U theory.

The approximate regularity of mass differences in $He^3 - H^3$, $C^{11} - B^{11}$ and their partial agreement with expected Coulomb energies indicates the partial validity of Eqs. (3′) and (4). To be sure, Eq. (4) holds only for the Fermi interaction and not for the generalization of Gamow and Teller. Nevertheless the increase in the probability with decreasing Z appears to be too strong to be explicable by the geometrical factors that may be expected to appear in Gamow and Teller's theory. It is, perhaps, worth while to consider the possibility of a decrease in the intrinsic β-emitting powers of nuclear particles with increase in atomic weight. This would amount to a change of g in the calculations. Such an effect is conceivable if the interactions between nuclear particles are intimately connected with the β-ray field.

It should also be remembered that the equality of unlike and like particle interactions which is essential for (3′) has so far its experimental support only for particles with zero relative angular momentum.

The authors would like to thank the Wisconsin Alumni Research Foundation for its support and the University of Michigan Physics Symposium for its hospitality.

[12] The anomalous behavior of He^6 was noticed independently by H. A. Bethe. For measurements on He^6 see Bjerge, Nature **138**, 400 (1936); Bjerge and Brostrum, Nature **138**, 400 (1936).

Nuclear Transmutations of the Lithium Isotopes

L. H. RUMBAUGH,*
Bartol Research Foundation of the Franklin Institute, Swarthmore, Pennsylvania

R. B. ROBERTS† AND L. R. HAFSTAD,
Department of Terrestrial Magnetism, Carnegie Institution of Washington, Washington, D. C.

(Received September 13, 1938)

Yield curves have been obtained for eight of the more important reactions of Li^6 and Li^7 produced by proton and deuteron bombardment in the energy range from 200 to 1000 kev. Each curve was obtained with an accuracy of about five percent, and a set of intercomparisons served to determine the relative yields between the different reactions within 20 percent. A special set of observations on a single reaction then gave the absolute yield for all the reactions within a factor of about three. An investigation was made of the reactions involved in the formation and decay of Li^8, the mass of which was found to be 8.02499 ±0.00020. The range-distribution of the delayed alpha-particles from Li^8 was measured and the interpretation of this distribution is discussed. Observations on the reaction $Li^6+n\rightarrow He^4+H^3$ gave a value of 4.97 Mev for the reaction energy as compared to a value of 4.56 Mev derived from the masses involved. No evidence could be obtained for the production of Li^8 by the process $Li^7+n\rightarrow Li^8$. Measurements of the energies of the neutrons produced by deuteron bombardment of Li^6 indicated that Be^7 is formed by the reaction $Li^6+D^2\rightarrow Be^7+n$. Further experiments showed that Be^7 is radioactive and is converted to Li^7 by K-electron capture. It was found that this process is followed by gamma-ray emission in roughly ten percent of the transitions.

A. INTRODUCTION

LITHIUM was the first element to be disintegrated by artificially accelerated ions and its transmutation processes have been studied by many investigators, but at the time this work was undertaken there still remained much valuable information to be obtained from a more comprehensive investigation and correlation of the various processes involved in its transmutations. The products of disintegration have long been known and the energy balances have been measured for most of the possible modes of disintegration, but very little information was available concerning the yields of the various reactions and the variations of the yields with the energy of the bombarding particles. For a more complete understanding of the nucleus, measurements of the relative yields of different particles from the same compound nucleus are highly important. While the types of reactions which will occur and their energy balances can be predicted from a knowledge of the masses involved, and the general shape of most of the yield curves can be calculated by consideration of the penetration probabilities, the differences between yield curves for different isotopes or different projectiles probably depend on the arrangement of the nuclear constituents themselves, and thereby furnish definite criteria for testing the success of any theory of the structure of the nucleus.

It was the object of the present work to supplement the investigation of the transmutation processes of lithium previously reported[1] by obtaining accurate data on the yields of the various processes and by measuring quantitatively several other features of the reactions which had been studied only in a qualitative fashion. Some of the material covered by this paper has been reported briefly in the *Physical Review*.[2]

Because of the large number of possible reactions involved, they are collected in Table I for the convenience of the reader.

B. EXPERIMENTAL PROCEDURE

In general, the experimental procedure was similar to that of the previous work. The particles used in bombardment were accelerated by the two-meter electrostatic generator of the Department of Terrestrial Magnetism. Voltages were measured by the high resistance voltmeter,

* Now at the University of Minnesota.
† Carnegie Institution Fellow.

[1] L. H. Rumbaugh and L. R. Hafstad, Phys. Rev. **50**, 681–689 (1936).

[2] L. H. Rumbaugh, R. B. Roberts, and L. R. Hafstad, Phys. Rev. **51**, 1013 (1937); **51**, 1106–1107 (1937); R. B. Roberts, L. R. Hafstad, and L. H. Rumbaugh, Phys. Rev. **52**, 247 (1937); R. B. Roberts and N. P. Heydenburg, Phys. Rev. **53**, 929 (1938); R. B. Roberts, N. P. Heydenburg, and G. L. Locher, Phys. Rev. **53**, 1016 (1938).

previously described,[3] the absolute calibration of which has since been checked independently by observations of the scattering of protons in nitrogen and argon. The ion current could be varied at will from 0.2 to 5.0 microamperes, which was a great convenience in maintaining suitable counting rates. Molecular ions were employed for very low voltage work on deuteron produced reactions. The ion current was measured by a current integrator.

Targets

As in the previous work, a set of 18 isotopic targets which ranged from 10 micrograms to 4 milligrams in mass was available for use in any case where the disintegration products of the two isotopes might be confused. All yield curves were taken with thin targets.

Detecting apparatus

The apparatus used in detecting the various products of disintegration included several ionization chambers and Geiger-Müller counters with their associated amplifiers and counting circuits, a shielded Lauritsen electroscope, and a Wilson cloud chamber. Special features of the equipment will be described in conjunction with the experiment in which the apparatus was used.

TABLE I. *Nuclear reactions of lithium.**

$Li^6+H^1\rightarrow \mathbf{He^3}_{1.2\text{ cm}}+\mathbf{He^4}_{8\text{ cm}}+3.72$ Mev
$Li^7+H^1\rightarrow \mathbf{He^4}_{8\text{ cm}}+\mathbf{He^4}_{8\text{ cm}}+17.13$ Mev
$Li^7+H^1\rightarrow (Be^8)^*\rightarrow Be^8+h\nu+(17$ Mev$)$
$Li^6+D^2\rightarrow \mathbf{He^4}_{13\text{ cm}}+\mathbf{He^4}_{13\text{ cm}}+22.07$ Mev
$Li^6+D^2\rightarrow Li^7+\mathbf{H^1}_{30\text{ cm}}+5.03$ Mev
$Li^6+D^2\rightarrow (Li^7)^*+\mathbf{H^1}_{25\text{ cm}}+4.58$ Mev
$(Li^7)^*\rightarrow Li^7+h\nu+0.455$ Mev
$Li^6+D^2\rightarrow He^3+He^4+n+(1.56$ Mev$)$
$Li^6+D^2\rightarrow Be^7+n+(3.1$ Mev$)$
$Be^7+e_K\rightarrow Li^7+\eta+(1$ Mev$)$
$Be^7+e_K\rightarrow (Li^7)^*+\eta+(0.55$ Mev$)$ (half-life 43 days)
$(Li^7)^*\rightarrow Li^7+h\nu+0.45$ Mev
$Li^7+D^2\rightarrow Be^8+n+(14.5$ Mev$)$
$Li^7+D^2\rightarrow He^5+\mathbf{He^4}_{7\text{ cm}}+(14.3$ Mev$)$
$(He^5)\rightarrow \mathbf{He^4}_{2-6\text{ cm}}+n+(0.8$ Mev$)$
$Li^7+D^2\rightarrow \mathbf{He^4}_{0-8\text{ cm}}+\mathbf{He^4}_{0-8\text{ cm}}+n+(14.9$ Mev$)$
$Li^7+D^2\rightarrow Li^8+H^1-0.2$ Mev
$Li^8\rightarrow \mathbf{He^4}_{0-6\text{ cm}}+\mathbf{He^4}_{0-6\text{ cm}}+\beta^-+\eta+15.9$ Mev (half-life 0.85 sec.)
$Li^6+n\rightarrow \mathbf{He^4}_{1\text{ cm}}+\mathbf{H^3}_{6\text{ cm}}+4.9$ Mev
$Li^6+n\rightarrow He^6+H^1-2.8$ Mev (probable)
$Li^7+n\rightarrow Li^8+h\nu$ (not observed)
$Li^7+n\rightarrow He^6+H^2-2.7$ Mev (probable)

* The ranges given are for identification only, and are taken from the well-known original work in which the existence of such groups were established, no adjustment being made for differences in bombarding energies in different experiments. The disintegration products which have been observed are shown by boldface type. Those reaction energies included in parentheses are approximate.

[3] L. R. Hafstad, N. P. Heydenburg, and M. A. Tuve, Phys. Rev. **50**, 504–514 (1936).

Range measurements

In all measurements of the ranges of the immediate products of disintegrations, the observations were made at 90° to the incident beam. The smallest aperture which would give adequate counting rates was used. Two sets of calibrated mica windows mounted on wheels provided a means of rapidly varying the stopping power in 5-mm steps. A screw on the ionization chamber furnished a fine adjustment. In all cases where accurate range measurements were desired the stopping power of the window of the target chamber and of the effective air path to the ionization chamber was calibrated by placing a clean polonium source at the target position and measuring the range of the emitted alpha-particles. In converting to energy, the revised Cornell range-energy curves of 1937 were used for protons and those of 1938 for alpha-particles.

Elimination of spurious effects

In the first attempt to obtain accurate yield curves, some difficulty was encountered in getting reproducible results. The source of the difficulty was soon traced to the current measurements which recorded as effective current some ions which entered the target chamber but were not effective in producing observable disintegrations; that is, ions missing the target area or striking parts of the target shielded from the detector. To correct this condition the target chamber was placed at the end of a 60-cm collimating tube. At each end of this tube was a diaphragm with a $\frac{3}{16}$-inch hole, which insured a well-defined beam at the target which was located approximately ten cm below the last diaphragm. The collimating tube was built in insulated sections so that it also served as a trap for the electrons liberated from the diaphragms. Very little ion current was sacrificed by this arrangement due to the sharp focus of the accelerating tube. Fluctuations of the current caused no errors since the current was measured by an integrator. Voltage fluctuations

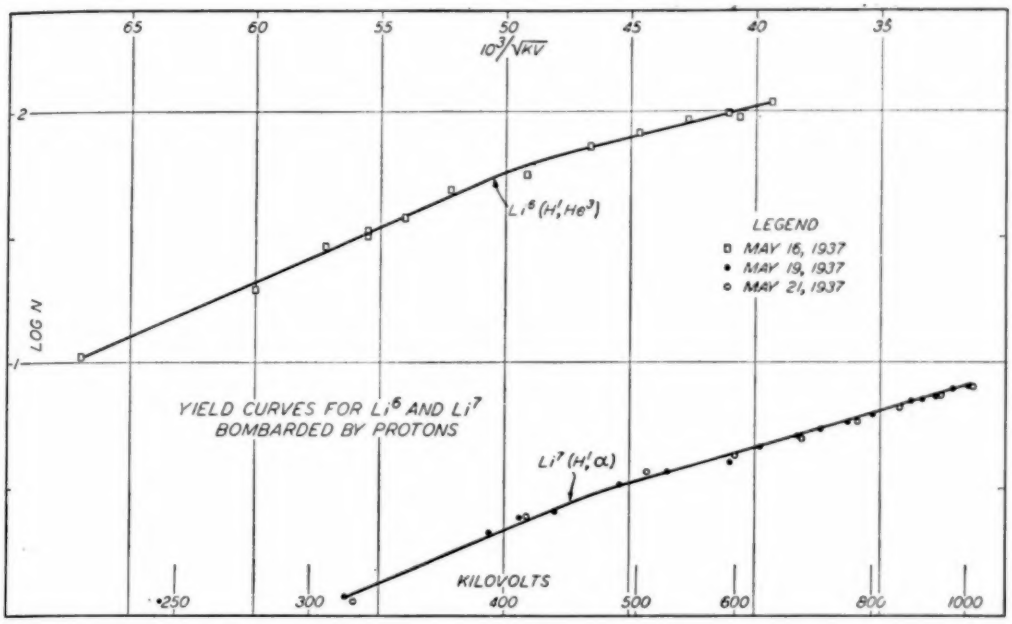

FIG. 1. Yield curves for Li^6 and Li^7 bombarded by protons.

were also eliminated because of the high resolution given by the magnetic field in combination with the slit system. As soon as this arrangement was installed, there was no further difficulty in repeating any observation with agreement better than five percent.

The possibility of changes in the calibration of the voltmeter was eliminated by checking the voltmeter occasionally with a measurement of the lithium gamma-ray resonance at 440 kev. The same measurement applied to the thin targets of Li^7 used for the yield curves showed the thicknesses of the targets and the amount of carbon (contamination) which had accumulated on them.

Despite the magnetic analysis of the ion beam it was possible, of course, to have molecular hydrogen present in the mass 2 spot. Its presence readily could be detected and its percentage estimated by observing the current carried by the mass 1, 3, and 4 spots. This error was never serious as the mass 2 spot was almost invariably better than 95 percent deuterons.

Confusion due to contamination by carbon or oxygen on the target was easily avoided in most cases since the characteristic groups of charged particles arising from these elements are well known. In counting the beta-rays from lithium, however, it was necessary to use a coincidence pair of Geiger-Müller counters shielded by lead to avoid spurious effects from x-rays produced in the tube and from beta- and gamma-rays from carbon. Carbon neutrons also had an appreciable effect when counting neutrons at the higher voltages.

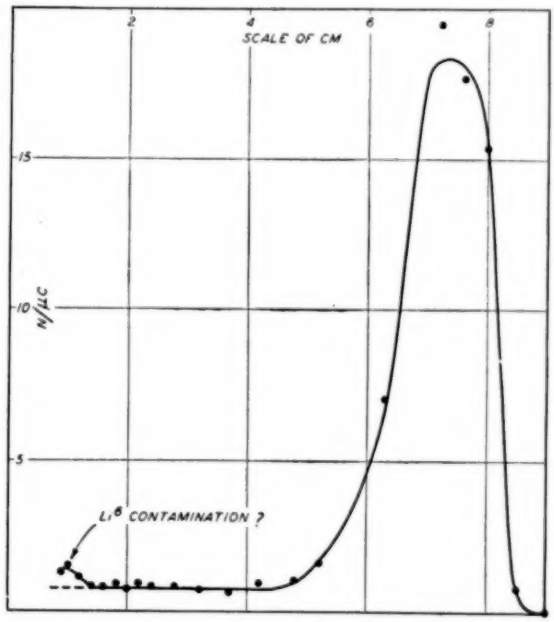

FIG. 2. Alpha-particles from Li^7+H^1.

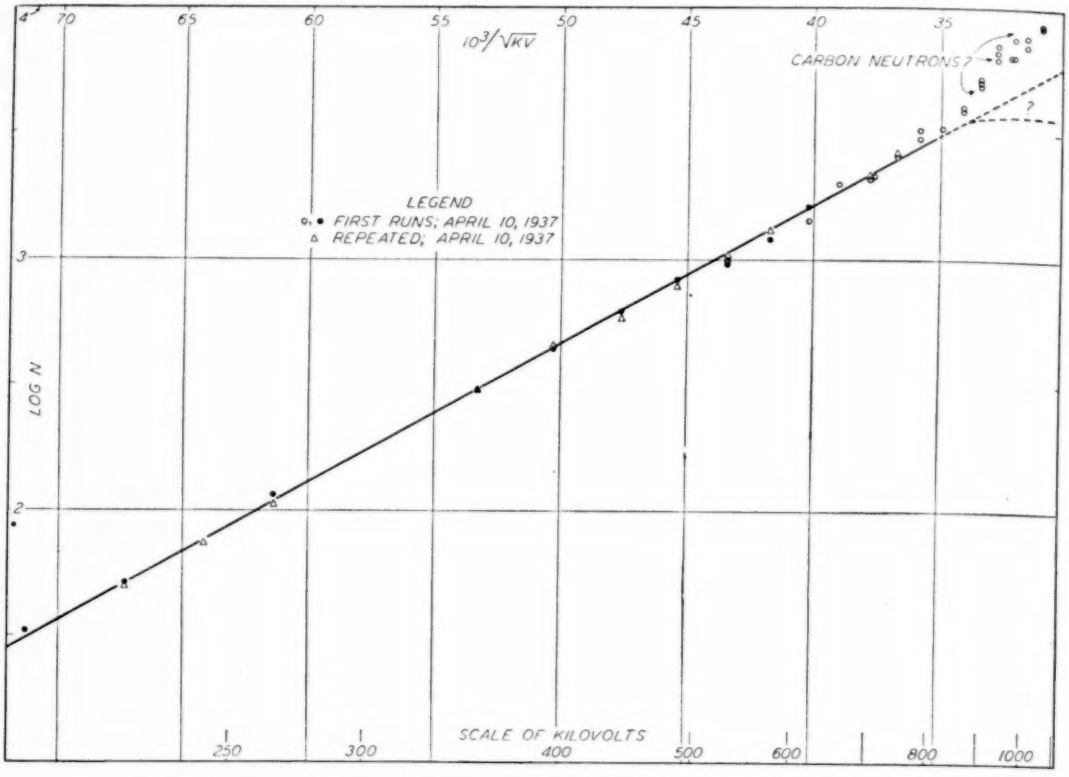

FIG. 3. Neutrons from Li^6+D^2.

C. YIELD CURVES

(1) Li^6+H^1

Figure 1 shows the yield curves for the proton produced reactions in lithium. The yield of the reaction $Li^6+H^1 \rightarrow He^3+He^4$ was measured with an ionization chamber by counting He^3 particles emitted from a thin isotopic target. It was impossible to carry the investigation to voltages higher than 600 kv because the range of the scattered protons there became sufficient to interfere with the counting of the He^3 particles. A thin isotopic target was used.

(2) Li^7+H^1

Thin targets of ordinary lithium, as well as thin Li^7 targets, were used in investigating the yield curve for the reaction $Li^7+H^1 \rightarrow He^4+He^4$. The alpha-particles from this reaction have a range of about eight cm, so all alpha-particles of ranges greater than six cm were counted with an ion chamber connected to a counting system set at medium bias.

The resulting yield curve, shown in Fig. 1, is in satisfactory agreement with the yield functions which have been published previously.[3, 4] The possibility that short-range alpha-particles are emitted in the reaction $Li^7+H^1 \rightarrow He^4+He^4+h\nu$ was investigated by the use of a Li^7 target to eliminate the short-range particles from Li^6+H^1. The range-number curve (Fig. 2) was taken at 475 kv, and the Li^7 target was sufficiently thick to insure the observation of any contribution from the 440 kev resonance. No evidence for a reaction emitting short-range alpha-particles was found.

The weak peak at 1.2 cm was ascribed to a Li^6 contamination of roughly one part in 500, since the cross section for the Li^6+H^1 reaction is approximately 30 times greater than for Li^7+H^1. While the contamination assumed is about 40 times greater than that measured for the thin isotopic lithium targets, it was expected to be large in the present instance because of the very high deposition current (0.6 milliampere) used in

[4] R. G. Herb, D. B. Parkinson, and D. W. Kerst, Phys. Rev. **48**, 118–124 (1935).

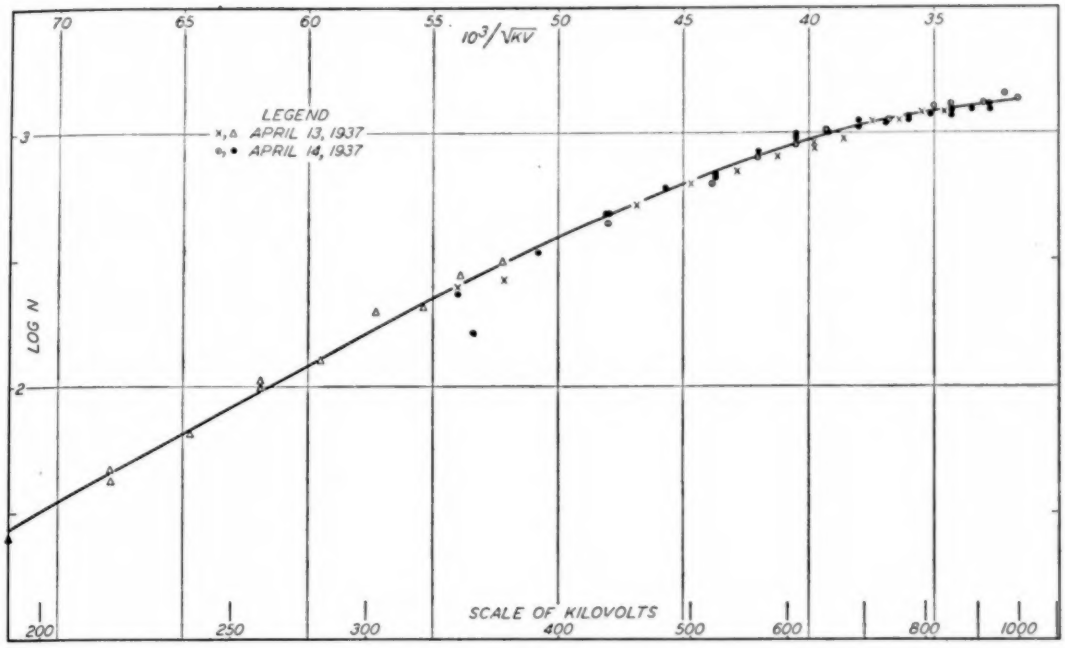

FIG. 4. Alpha-particles from Li^6+D^2.

collecting the thick Li^7 target in the mass spectrometer.

(3) Li^6+D^2

The yield of neutrons from a thin Li^6 target is shown in Fig. 3. The target was placed at the center of a large block of paraffin and the neutrons were counted in a boron lined ionization chamber. It was believed that neutrons from carbon deposited on the target made an appreciable contribution to the number of neutrons observed at the higher voltages (over 800 kv). The effect of the carbon contamination was negligible below 800 kv because of the very steep excitation curve for the production of carbon neutrons. A qualitative method of correcting for the carbon effect above 800 kv is indicated below, in the discussion of the neutrons from Li^7, where a similar carbon effect is estimated by recourse to the alpha-particles which are emitted in the same reaction as the Li^7 neutrons.

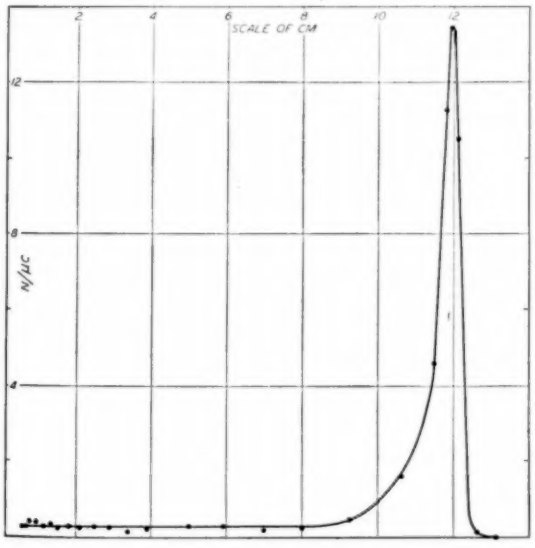

FIG. 5. Alpha-particles from Li^6+D^2, high counter bias.

Figure 4 shows the voltage-yield curve measured for the reaction $Li^6+D^2 \rightarrow He^4+He^4$. A thin isotopic target was used in order to minimize any contaminations, which otherwise would be more abundant by amounts corresponding to the proportional increase in useless Li^7. The alpha-particles were counted in an ionization chamber and the thyratron counter was biased to discriminate against protons. The same isotopic target was used in extending the number-range curve for Li^6+D^2 through the region ordinarily obscured by alpha-particles from Li^7+D^2. Fig. 5 indicates that reactions of the type $Li^6+D^2 \rightarrow He^4+He^4+h\nu$ are highly improbable.

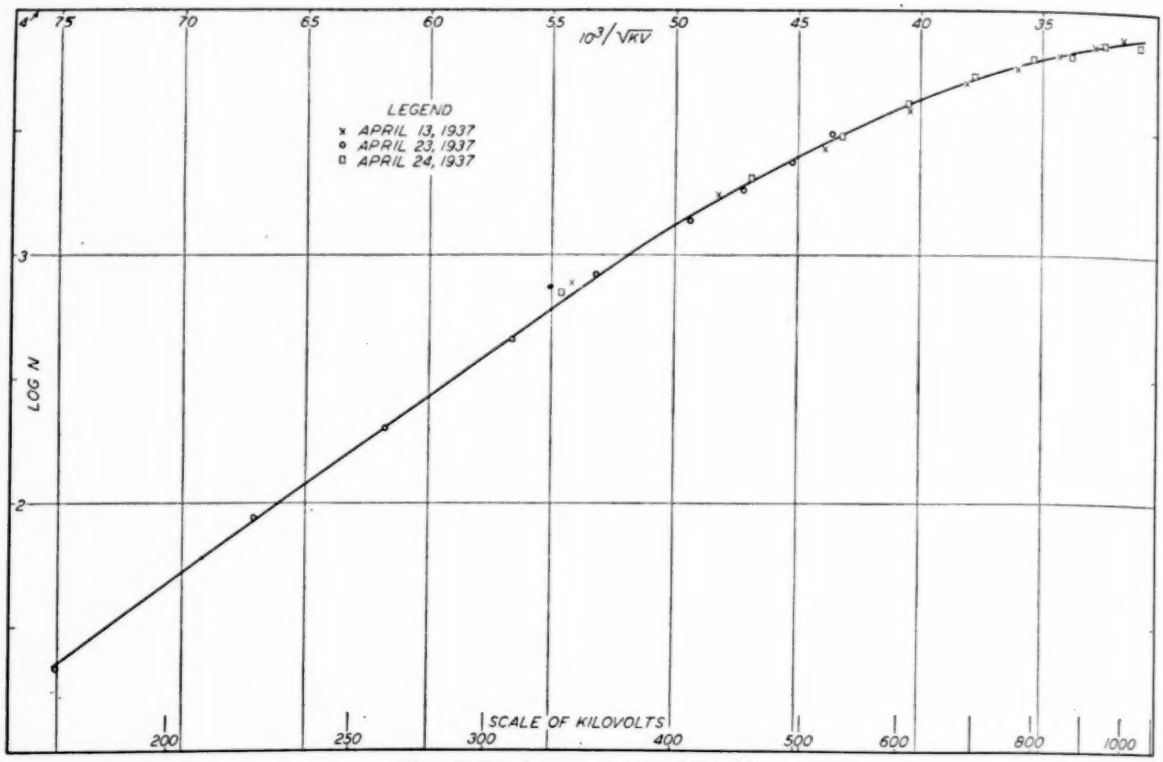

FIG. 6. Total protons from Li^6+D^2.

The total yield of protons from the two processes $Li^6+D^2\rightarrow Li^7+H^1$ and $Li^6+D^2\rightarrow Li^{7*}+H^1$ is shown in Fig. 6 as a function of the deuteron energy. The thyratron counter was biased to count both fast and slow protons, and the ionization chamber was adjusted for ranges sufficiently short to include both Li^6 proton groups but sufficiently long to stop the alpha-particles from Li^6 and the proton groups from carbon and oxygen which comprised the only appreciable charged particle groups to be avoided.

The relative yields of the two Li^6 proton groups at various deuteron bombarding energies, as given in Fig. 7, indicate clearly that the relative probability of forming Li^7 in an excited state increases at higher bombarding voltages. The gradual increase in this probability observed by Williams, Shepherd, and Haxby[5] from 100 to 225 kv continues through the interval from 200 to 500 kv but becomes more rapid for deuteron energies above 500 kev. The mean energy separation of the two states of Li^7, as measured from the proton groups of Fig. 7, is 455 ± 15 kev.

[5] J. H. Williams, W. G. Shepherd, and R. O. Haxby, Phys. Rev. **52**, 390–396 (1937).

(4) Li^7+D^2

The yield of neutrons from deuteron bombardment of Li^7, shown in Fig. 8, was measured by counting neutrons and by counting alpha-particles produced in the same reaction, $Li^7+D^2\rightarrow He^4+He^4+n$. The alpha-particles were counted in the usual ionization chamber with the thyratron counter lightly biased to record all alpha-particles, both fast and slow. The alpha-particles produced in the radioactive disintegration of Li^8 were avoided by placing the ionization chamber at a range of four cm where the relative numbers of these alpha-particles become negligible. A thin Li^7 target was used in order to escape the uncertainty of corrections for the 13-cm group of alpha-particles emitted from Li^6. In counting the neutrons the target was surrounded with paraffin and the neutrons were detected in a boron lined ionization chamber.

These two independent methods of measurement gave identical results for bombarding energies between 200 and 770 kev, but at bombarding energies above 770 kev the alpha-particle yield ceased increasing and no longer corresponded to

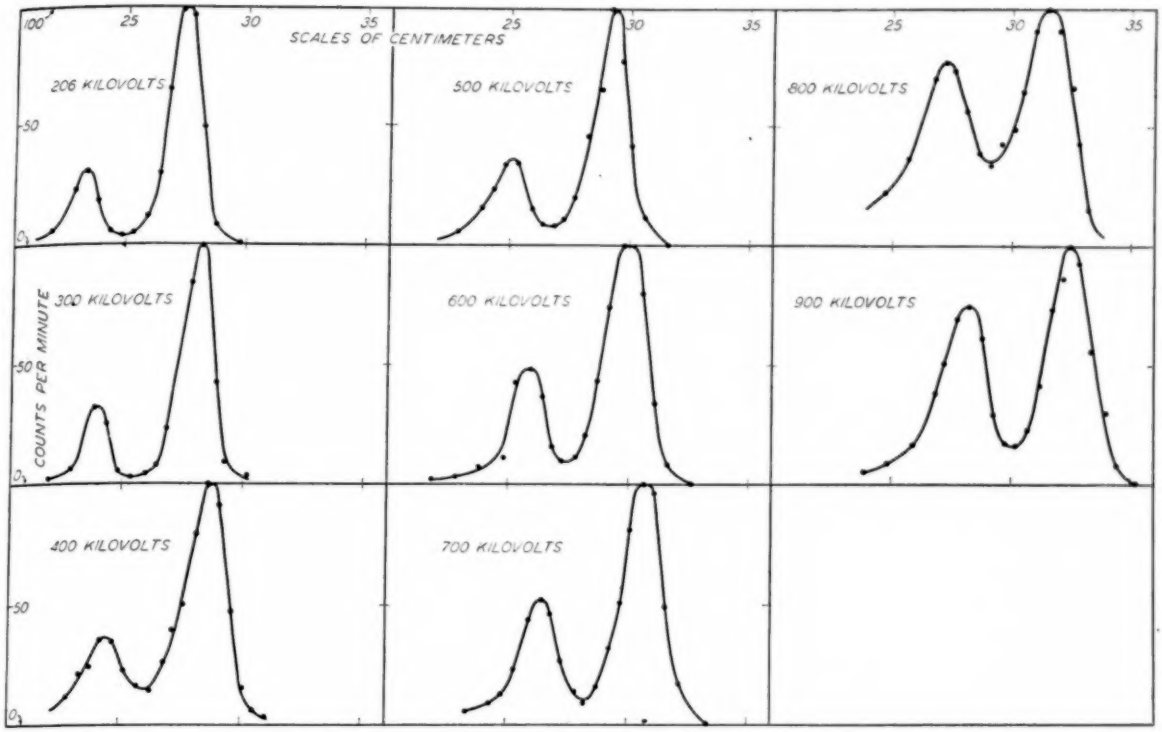

FIG. 7. Proton doublet from Li^6+D^2.

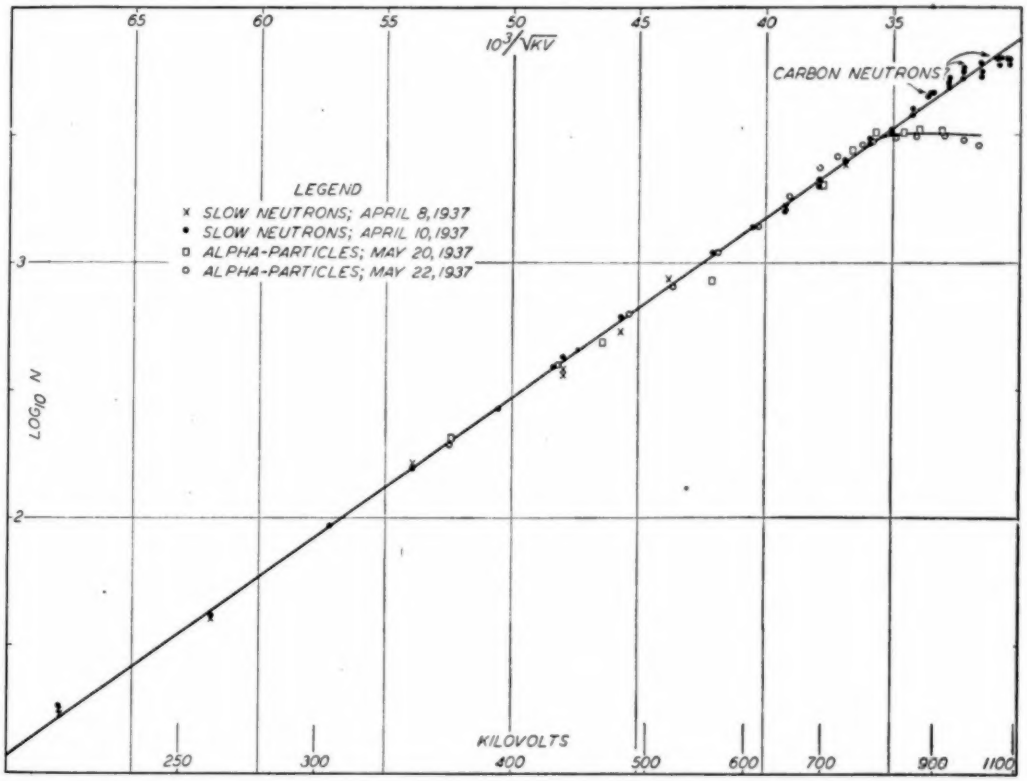

FIG. 8. Neutrons from $Li^7+D^2=He^4+He^4+n$.

the neutron yield. This discrepancy must be ascribed to the production of neutrons in some other process than the one mentioned above. One possible explanation is that the reaction $Li^7+D^2 \rightarrow Be^8+n$ only becomes relatively probable at deuteron energies above 770 kev since, according to Bonner and Brubaker,[6] this reaction contributes only a small fraction of the total lithium neutrons at voltages below 800 kv. A much more plausible explanation is that the excess observed above 800 kv was due to neutrons produced in carbon contamination on the target. The similar effect observed above 800 kv in the yield curve for neutrons from Li^6 indicates that the latter explanation is the correct one.

Figure 9 shows the yield curve for the production of radioactive Li^8 which was measured by counting the alpha-particles as well as the beta-particles released in the decay of Li^8. A double coincidence pair of Geiger-Müller counters was employed in counting the beta-particles. The counters were shielded with lead so that the background count remained very low even when the high voltage was applied to the tube. The counters viewed the lithium target through a small window in the lead covered with Dow metal to screen out the less energetic beta-particles from the carbon contamination on the target. The solid angle subtended by the counters was adjusted to give counting rates such that the correction for the recovery time of the counters (about 10^{-5} sec.) was negligible. The resolving time for coincident discharges was about 5×10^{-6} second. The effect of the carbon contamination was shown to be negligible by the fact that no increase in the background counting rate was observed after the target had been bombarded for some time. The effect of gamma-rays from carbon also was proved negligible by comparing continuous counting rates (that is, rates during bombardment) with the numbers of counts observed in five-second intervals after bombardment.

The alpha-particles emitted by Li^8 can be observed effectively only if some arrangement is made to separate them from the instantaneously emitted alpha-particles from the reaction $Li^7+D^2 \rightarrow He^4+He^4+n$. This separation was accomplished by using a target deposited on a wheel which was rotated during the bombardment. Only those alpha-particles were observed which were emitted after the wheel had rotated 90° from its position during bombardment. A thin target of ordinary lithium was used since a separate experiment proved Li^6 did not emit any delayed alpha-particles. The particles were counted with the usual ionization chamber. Counting rates also were taken with the wheel at rest to measure the background of neutron recoils.

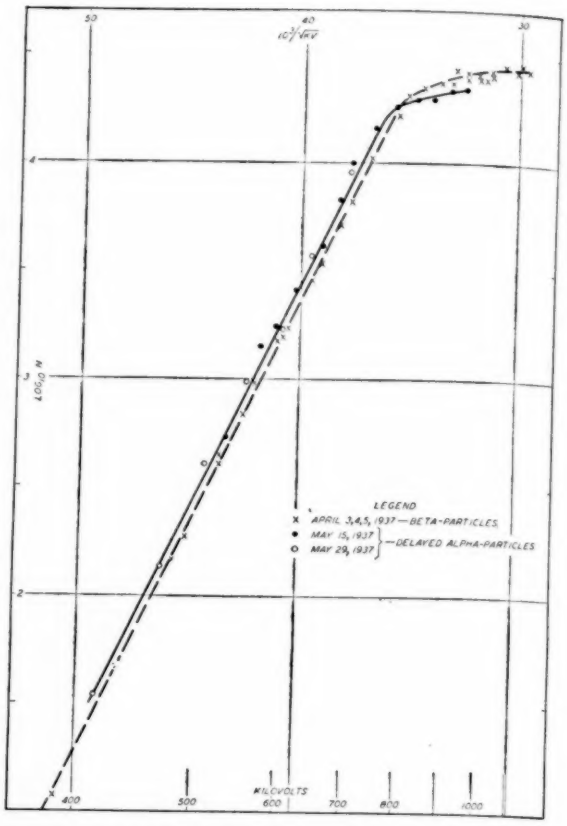

FIG. 9. Yield of delayed particles from Li^7+D^2.

All points of the yield curves represent 1000 or more counts, except for a very few at the lowest voltages. Because of the great variations in the yields with incident particle energy, it was sometimes necessary to change the solid angle of the detector as well as to vary the current to maintain usable counting rates. The curves were fitted at all points at which it was necessary to change the solid angle. In most cases the two portions of the curve have a large overlap. Different portions of the curves, taken with different apertures, are

[6] T. W. Bonner and W. M. Brubaker, Phys. Rev. **48**, 742–746 (1935).

indicated on the curves by different symbols for the points.

D. Relative Reaction Cross Sections for the Lithium Reactions

The curves shown above give only the forms of the yield curves, since the observed number of particles is plotted against energy. For many theoretical considerations a knowledge of relative reaction cross sections of different reactions, as shown in Fig. 10, is of value, so a special effort was made to obtain dependable relative yields by a system of intercomparisons carefully chosen to avoid conflicting groups. In order to obtain the ratio

$$\frac{Li^7+H^1\rightarrow He^4+He^4}{Li^7+D^2\rightarrow He^4+He^4+n}$$

for instance, it was necessary to use an isotopic Li^7 target to avoid counting the 13-cm alpha-group from Li^6 and further to make the observation at a voltage so low that the contribution due to the delayed alpha-particles from the reaction $Li^7+D^2\rightarrow Li^8+H^1$ was negligible. For this reason a bombarding voltage of 380 kv was chosen. All alpha-particles of ranges greater than eight mm in the continuous distribution were counted. The ratios

$$\frac{Li^7+H^1\rightarrow 2He^4}{Li^6+H^1\rightarrow He^4+He^3}$$

$$\frac{Li^6+D^2\rightarrow 2He^4}{Li^6+D^2\rightarrow Li^7+H^1}$$

$$\frac{Li^7+H^1\rightarrow 2He^4}{Li^6+D^2\rightarrow 2He^4}$$

also were obtained at 380 kv from an ordinary Li target for which Brewer's value of 11.6 for the Li^7/Li^6 ratio was assumed. An isotopic Li^6 target bombarded at 690 kv checked the ratio

$$\frac{Li^6+D^2\rightarrow 2He^4}{Li^6+D^2\rightarrow Li^7+H^1}.$$

This ratio was related to the others by means of the yield curve for the 13-cm alpha-particles given in Fig. 4.

The ratio of the neutron yields

$$\frac{\begin{matrix}Li^7+D\rightarrow Be^8+n\\ \qquad\rightarrow 2He^4+n\end{matrix}}{\begin{matrix}Li^6+D^2\rightarrow Be^7+n\\ \qquad\rightarrow He^3+He^4+n\end{matrix}}$$

was obtained by bombardment at 690 kv of isotopic targets of nearly equal masses under otherwise identical experimental conditions, using paraffin and a boron lined ionization chamber for the detector.

The relative masses of the isotopic targets were determined in two ways, namely, (a) from the integrated collector current in the mass spectrometer in which they were deposited and (b) by taking the alpha-particle ratio

$$\frac{Li^7+D^2\rightarrow 2He^4+n}{Li^6+D^2\rightarrow 2He^4}$$

for the two targets. Then this ratio was compared with all those discussed above.

The number of neutrons from Li^7+D^2 in terms of numbers of Li^7+D^2 continuous alpha-particles was obtained from Bonner and Brubaker's estimate[6] that only five percent of total neutrons from ordinary $Li+D^2$ come from reaction Be^8+n^1. It follows that the rest of the Li^7+D^2 neutrons come from He^4+He^4+n. Though the voltage distribution of the deuterons used by Bonner and Brubaker was unknown and the Li^6 and Li^7 neutron excitation functions are not parallel, correction of their data for Li^6+D^2 neutrons gives no serious uncertainty since $Li^7/Li^6 = 11.6$ in nature.

The internal consistency of the above measurements and cross checks indicated the relative reaction cross sections given in Fig. 10 to be accurate to ± 20 percent between 300 and 750 kv with the exception of the radio-lithium yield.

It proved impossible to isolate the reaction leading to radio-lithium for an accurate determination of the relative yield because of the short life of Li^8 and the presence of continuous alpha-particles from Li^7+D^2. The estimate of the relative yield of radio-lithium given in Fig. 10 is taken from comparisons between the numbers of delayed and total alpha-particles from Li^7+D^2 and may be in error by a factor of two.

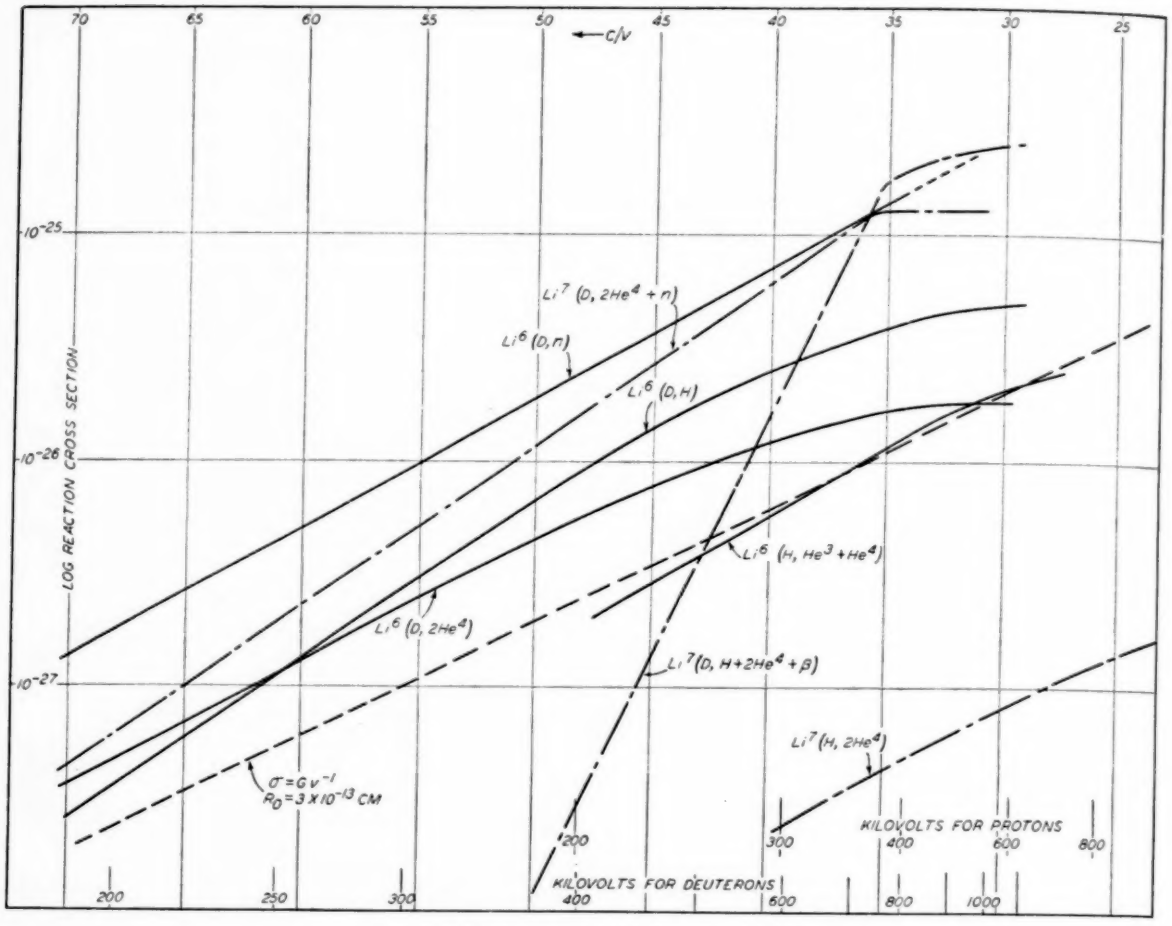

FIG. 10. Yield curves for lithium reactions.

E. ABSOLUTE CROSS SECTIONS FOR REACTIONS

The yield of He^4 from Li^6+D^2 is used to fix the scale of Fig. 8. The cross section scale adopted is the average computed from the masses of two LiOH thin targets analyzed by the National Bureau of Standards, through the kindness of Dr. C. J. Rodden, and from the mass of one Li^6 target measured in terms of collector currents during deposition in the mass spectrometer. Because of difficulty in obtaining absolutely uniform thin deposits, the various targets gave values for the absolute cross sections varying among themselves by a factor of nearly three.

It has been convenient in Fig. 10 to plot the logarithm of the reaction cross section in cm^2 against the velocity of light divided by the velocity of the bombarding particles in order to provide a common scale for the reactions resulting from both proton and deuteron bombardment. Several significant features are obvious in the collected cross section curves.

(1) The familiar exponential-like dependence of the reaction cross section upon the velocity of the incident particles appears in all the curves.

(2) The increase in the yield of Li^8 with incident deuteron velocity is exceptionally rapid. This increase will be discussed separately in connection with the radio-lithium problems of the next section.

(3) The remaining curves may be divided into two groups according to slope so that below 400 kv the rate of increase in cross section is approximately the same function of the incident particle velocity, v, for all the reactions within the same group. The rate for the first group, which consists of the two reactions $Li^6(D^2, H^1)$ and $Li^7(D^2, 2He^4+n)$, is greater than the rate for

the second group of reactions by approximately a factor $v^{\frac{1}{2}}$.

(4) The curves for the two reactions resulting from deuteron bombardment of Li^7 both break rather sharply near 770 kv and their cross sections become comparable.

(5) Deuteron bombardment of either lithium isotope leads to a high neutron yield, but the two neutron yield curves are different functions of v.

(6) The cross section for the reaction $Li^7(H^1, 2He^4)$ is much smaller than for any other reaction considered.

The exponential form of the yield functions may be explained in the usual way by assuming that the governing term resembles the Gamow factor for penetration through the potential barrier, $G \sim \exp(-2\pi\alpha Zzcv^{-1})$, where α is the fine structure constant, Z and z are the atomic numbers of the reacting particles, v is their relative velocity, and c is the velocity of light. The various reactions, excepting the case of radio-lithium, involve penetration of the potential barrier by the incident particle only, since the emitted particles receive energies considerably greater than the barrier heights. Theoretical discussions of reaction cross sections have been given by Gamow,[7] Breit and his colleagues,[8, 9] Bethe,[10, 11] and others. At bombarding energies that are small compared to the barrier heights, the various derived expressions generally are asymptotic to the simplified formula for the cross section, $\sigma \sim Gv^{-2}$, where v^{-2} has the significance of an absolute cross section proportional to the square of the wave-lengths of the incident particles. The simplified formula gives relative cross sections which increase too slowly by, roughly, a factor of v through the intermediate range of bombarding energies (200 to 400 kev) to agree with even the least steep excitation curves of Fig. 10.

An interpretation of the yield curve for the reaction $Li^7(H, 2He^4)$, as measured by Herb, Parkinson, and Kerst,[4] and by Hafstad, Heydenburg, and Tuve,[3] at bombarding energies overlapping those of the present experiments, has been given by Ostrofsky, Breit, and Johnson.[9] They calculated the reaction cross section as proportional to the density of incident protons within a potential well of chosen breadth and depth. Both the rate of increase with incident particle energy and the form of the calculated yield function then became sensitive to the positions of the resulting resonances. However, their expression for the cross section at low bombarding energies simplified to the formula $\sigma \sim Gv^{-2}$ when the density factor was included. On the other hand, a reaction cross section proportional to the flux of incident particles through the nucleus simplified to a prior expression, also given by Breit,[8] $\sigma \sim Gv^{-1}$. This oversimplified formula for the cross section is the one plotted in Fig. 10 for purposes of comparison, since the cross sections observed in the present experiments appear to agree more nearly with this expression.

The final levels available for a given disintegration process include, of course, excited levels

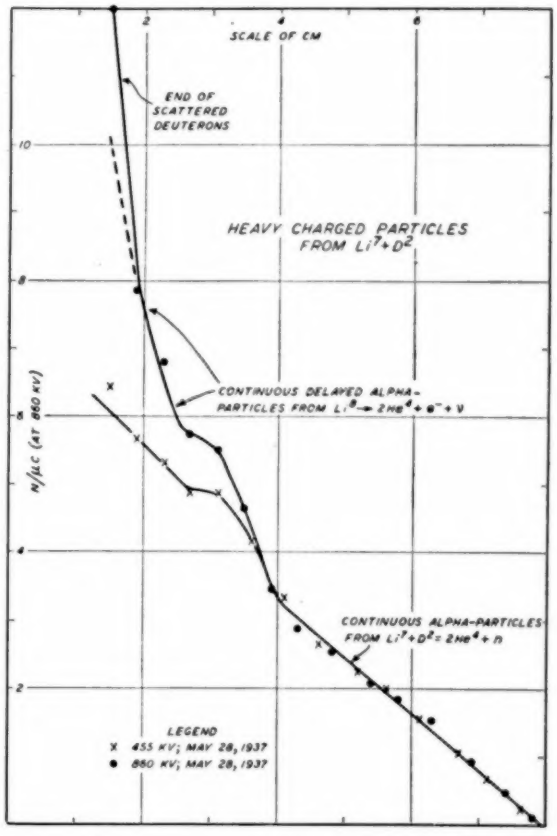
SCALE OF CM
END OF SCATTERED DEUTERONS
HEAVY CHARGED PARTICLES FROM Li^7+D^2
CONTINUOUS DELAYED ALPHA-PARTICLES FROM $Li^8 \rightarrow 2He^4 + e^- + \nu$
N/μC (AT 860 KV)
CONTINUOUS ALPHA-PARTICLES FROM $Li^7+D^2 = 2He^4 + n$
LEGEND
× 455 KV; MAY 28, 1937
• 860 KV; MAY 28, 1937

FIG. 11. Heavy charged particles from Li^7+D^2.

[7] G. Gamow, *Atomic nuclei and radioactivity* (Cambridge, 1937).
[8] G. Breit, Phys. Rev. **34**, 817 (1929).
[9] M. Ostrofsky, G. Breit, and D. P. Johnson, Phys. Rev. **49**, 22–34 (1936).
[10] H. A. Bethe, Rev. Mod. Phys. **9**, 186–219 (1937).
[11] E. J. Konopinski and H. A. Bethe, Phys. Rev. **54**, 130–138 (1938).

as well as the ground levels of the disintegration products. Consequently the cross section curves of Fig. 10 in some instances represent the measured sums of the cross sections for more than one final level, since such measurements were the experimentally practical ones. Two states of Li^7 are summed in the cross section curve for the reaction $Li^6(D^2, H^1)$, but the curve for either Li^7 state singly may be obtained by reference to Fig. 7. Only a small part of the steeper initial increase with relative velocity in the total cross section for the reaction $Li^6(D^2, H^1)$ may be attributed to the increased probability of forming Li^7 in the excited state, since the yield of this state relative to the ground state increases but slowly between 200 and 500 kv according to Fig. 7. However, at higher voltages the form of the curve is influenced considerably by the more rapid increase in the relative strength of the excited state. Likewise, in the reaction $Li^7(D^2, 2He^4+n)$ a part of the observed variation of the cross section might be related to accompanying changes in the distribution of the disintegration products among the numerous available final levels, since several known levels cover a range of about 12 Mev, and the bombarding energy was varied by nearly one Mev in obtaining the yield curve. However, there is no evidence of such changes in the distribution of available final states for this reaction since (1) the only discernible variation in the distribution of the associated alpha-particles which occurred when the bombarding energy was varied by 400 kev is actually due to the delayed alpha-particles from Li^8 (see Fig. 11), and (2) the cross-section curve from neutron measurements and that from alpha-particles of ranges greater than four cm appear identical in shape except for the effect ascribed to carbon neutrons at high bombarding voltages (Fig. 8). The final levels for the reaction $Li^6(D^2, n)$ are unknown except that they are perhaps about equally divided between $Li^6+D^2 \rightarrow He^3+He^4+n$ and $Li^6+D^2 \rightarrow Be^7+n$. The number of final levels is probably small because the energy released in the disintegrations is not large. The disintegrations $Li^7+H^1 \rightarrow 2He^4$ and $Li^6+D^2 \rightarrow 2He^4$ seem able to occur only to the ground levels according to Fig. 2 and Fig. 5. Likewise, the reaction $Li^7+D^2 \rightarrow Li^8+H^1$ seems to involve only the ground state of Li^8 since the energy release is small and no gamma-radiation has been detected (see Section F). However, the apparent absence of gamma-radiation is not very conclusive evidence by itself due to the experimental difficulties of detecting it.

The break in the cross-section curves for Li^7 under deuteron bombardment at 770 kv cannot be due solely to the effect of competing reactions in the compound nucleus since both curves break at apparently identical deuteron energies. According to the views of Breit and his colleagues,[9] a high resonance in Be^9 might account for either or both breaks. Such a resonance would need to be located in the neighborhood of $(Li^7+D^2-Be^9)+(7/9)(0.77)$ Mev ≈ 17.2 Mev above the ground state of Be^9, and at the same time would account, at least qualitatively, for the observation that the cross section for the reaction $Li^7(D^2, 2He^4+n)$ increases faster with voltage than do the cross sections for most lithium reactions.

Above 800 kv the cross section for the formation of radio-lithium appears to be somewhat larger than the cross section for neutron emission in Li^7, though this has not been established definitely due to the uncertainty in the beta-ray yield, as described in Section D. Various investigators have identified a considerable number of final levels associated with neutron emission in the reaction $Li^7(D^2, 2He^4+n)$,[6, 12] but radio-lithium appears to be formed only in the ground state (no gamma-radiation). Consequently, it may be inferred that in light nuclei other factors can be more important in determining relative yields of competing reactions than is Bethe's rule[10] that at emission energies above the potential barrier the relative yields of competing reactions are approximately proportional to the relative numbers of final levels available for the reactions. On the other hand, this rule more successfully approximates the relative yields of the competing processes in Li^6 under deuteron bombardment.

It should be noted that at the lower bombarding energies the cross section for neutron emission from Li^6 is sufficiently larger than that from Li^7 to account for an appreciable fraction of all the neutrons observed during deuteron bombardment of ordinary lithium, and such neutrons must be taken into account in studies of the distribution in energy of ordinary Li neutrons.

The comparatively low yield of the reaction

[12] W. E. Stephens, Phys. Rev. **53**, 223–226 (1938).

$Li^7(H^1, 2He^4)$ relative to other lithium reactions has been discussed by Goldhaber,[13] by Breit and his colleagues,[9] and by Konopinski and Bethe[11] in connection with the influence of the orbital momentum of the incident particle upon the probability that it will penetrate the barrier.

F. Radio-Lithium

The reaction usually assumed for the production of radio-lithium, $Li^7+D^2\rightarrow Li^8+H^1+Q_1$, seems the only possible one fitting the experimental facts, although the proton group from the reaction never has been found. During the previous work with isotopic targets, the upper limit of the range of this group had been set at eight cm.[1] Consequently, in the present investigation, a special effort was made to find the proton group superimposed upon the continuous distribution of alpha-particles ending at eight cm from the reaction $Li^7+D^2\rightarrow He^4+He^4+n$.

It is obvious, according to the reaction cross sections of Fig. 10, that such a proton group should be especially conspicuous at bombarding energies of 800 kev or more but should decrease at lower voltages much more rapidly than do the yields of other lithium reactions. Accordingly, range-number curves were obtained at 860 kv and at 455 kv, using a bias on the detector such as to count protons near the ends of their range. These curves are shown in Fig. 11 with ordinates adjusted to bring the two curves into juxtaposition for easy comparison. There is no proton group of range greater than 1.7 cm associable with Li^8, since the two curves apparently are identical except for the effect at shorter ranges on the 860-kv curve due to the delayed alpha-particles from short life radioactive disintegration of Li^8. This effect readily could be estimated, either from the results of Fig. 10 and Fig. 13, or, independently, by observing the number of delayed alpha-particles after interrupting the bombarding beam of deuterons. The proton group sought should appear in numbers large compared to the delayed alpha-particles of Fig. 11, being in equilibrium with the delayed alpha-particles of all energies after a few seconds' bombardment. The group at 3.5 cm clearly is not due to the formation of Li^8 for (1) it is far too weak, (2) it still persists at 455 kv whereas the yield of Li^8 has decreased by a factor of 100 according to Fig. 10, and (3) it appears to be a broad alpha-particle group belonging to the reaction $Li^7+D^2\rightarrow He^4+He^4+n$.

[13] M. Goldhaber, Proc. Camb. Phil. Soc. **30**, 561–566 (1934).

Mass of Li^8

The 860-kv curve of Fig. 11 can be used to fix an upper limit for the energy release, Q_1, in the formation of Li^8. Since the energy of the bombarding deuterons was 0.860 Mev and since 1.7 cm protons have an energy of 0.830 Mev, it follows that Q_1 is less than $(1+\frac{1}{8})(0.830)-(1-2/8)(0.860)=0.290$ Mev. A lower limit on Q_1 can be set by the fact that disintegrations of radio-lithium were observed for bombarding energies as low as 360 kev. The kinetic energy of the incident deuteron available to the center of mass system is, at the latter bombarding voltage, $(\frac{7}{8})(0.360)=0.280$ Mev, so Q_1 is greater than -0.280 Mev since the escaping proton must have positive kinetic energy. In fact, the exceedingly low yield of the reaction at 360 kev suggests that Q_1 is considerably nearer to -0.280 Mev than to $+0.290$ Mev.

A better value for Q_1, and consequently for the mass of Li^8, can be obtained as follows. Assuming that the proton is emitted with very low energy, it can escape the system only by penetrating out through the potential barrier. Hence, two penetration factors must be included in computing the cross section for the reaction. Using the approximate formula due to Breit[8] we have

$$\sigma \leqq K v_D^{-1} \exp(-2\pi 3\alpha c v_D^{-1}) \exp(-2\pi 3\alpha c v_p^{-1}),$$

where v_D and v_p are the relative velocities for the deuteron and for the proton, and c and α are the velocity of light and the fine structure constant, respectively. The quantity v_p is unknown but is related to v_D by the momentum and energy relations which give

$$E_p=9/8Q_1+7/8E_D,$$

where E_p and E_D are the kinetic energies of the proton and deuteron. By means of these equations, σ can be calculated as a function of E_D for various values of Q_1 and compared with the cross-section curve of Fig. 9 in the range 400 to 600 kv. In this way, the best fitting value of Q_1 was found to be -0.200 ± 0.010 Mev. It is not certain

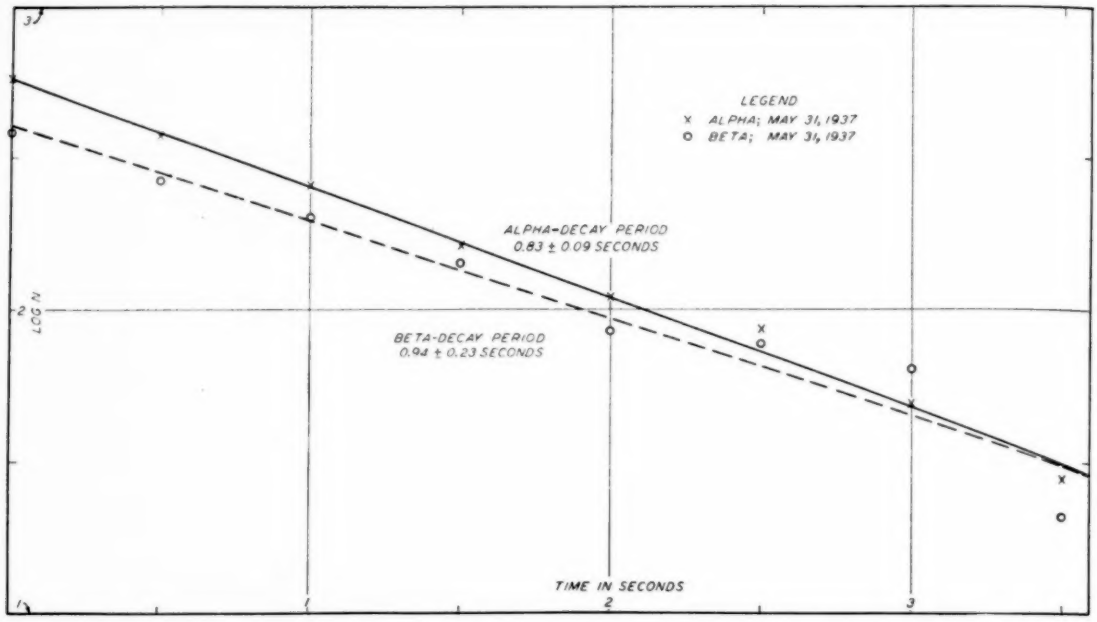

FIG. 12. Periods of alpha- and beta-particles from Li^8.

that the factor $1/v_D$ is correct in this application and the observed form of the cross-section curve probably is influenced by resonances, as discussed in the preceding section. In spite of this uncertainty, it is very probable that Q_1 is -0.200 ± 0.030 Mev, because the double penetration factor is by far the more important in the formula. When Livingston and Bethe's masses for Li^7, D, and H are used, this value of Q_1 gives a mass of 8.02499 for Li^8. The error in this mass principally depends upon the error in the mass of Li^7.

Disintegration of Li^8

An effort to detect gamma-rays from Li^7 bombarded by deuterons was unsuccessful, and a similar result has been reported by Bayley and Crane.[14] Hence it may be assumed that, of the possible reactions[1] in the radioactive decay of Li^8, only the reaction $Li^8 \rightarrow 2He^4 + e^- + Q$ is of importance. This conclusion is supported by the fact that the number of (delayed) alpha-particles of range greater than six mm is slightly greater than (1.1 times) the total number of beta-particles observed. Corrections for alpha-particles of shorter range and for the geometry of the beta-counter[15] would tend to make this ratio closer to two, which is the factor necessary if Li^8 always disintegrates with alpha-emission. Furthermore, the facts that the two yield curves taken with beta-particles and with alpha-particles are identical (Fig. 9) and that the decay periods, determined for both kinds of particles by least-square adjustment, are the same within the experimental error (Fig. 12) also suggest that the alpha-particles and the beta-particles are emitted in the same reaction. As a final check numerous cloud chamber photographs were obtained of the simultaneous emission of two charged heavy particles of equal ranges in approximately opposite directions from a very thin film of lithium previously bombarded by deuterons. Since the heavy particles therefore have equal masses and equal charges and were observed to behave like doubly

[14] D. S. Bayley and H. R. Crane, Phys. Rev. **52**, 604–609 (1937).

[15] The relative numbers of alpha- and beta-particles were obtained by counting the delayed particles of each type where they emerged through a one-mm hole in a six-mm thick lead plate at the end of a tube about eight cm distant from a thin target. Even the use of turned lead baffle plates, carefully spaced and aligned, apparently did not eliminate excessive counts due to the "piping" of beta-particles by small angle scattering. The beta-particle yields obtained in this manner did not agree with those obtained with more distant beta-counters viewing a wide-windowed target chamber through air when no alpha-particles were being counted.

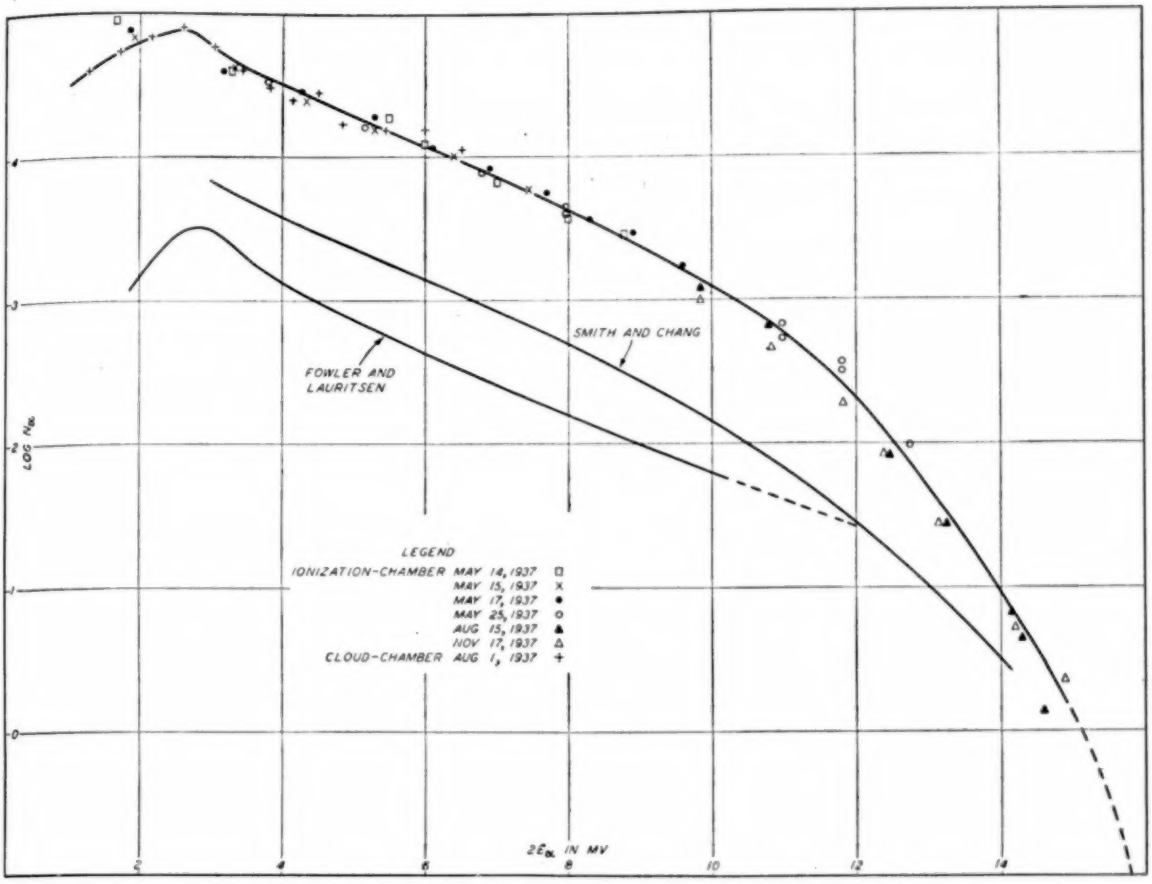

FIG. 13. Li^8 alpha-particle distribution curve.

charged particles in an ion chamber, it follows that they can be only He^4.[16]

Alpha-particles from Li^8

Breit and Wigner[17] have suggested that the radioactive disintegration of Li^8 is associated with the emission of alpha-particles from a rather broad excited state in the neighborhood of three to five Mev in Be^8, and a somewhat similar explanation has been advanced by Kronig.[18] The most crucial test of such a hypothesis should be given by the form of the energy distribution curve for the delayed alpha-particles. Three different methods were found necessary to observe these particles effectively at short, intermediate, and long ranges because of their wide variations in number and range.

An ion chamber in combination with the thin lithium target deposited on a rotating wheel (described above) was suitable for observing alpha-particles of intermediate range. The number-energy distribution at constant bombarding voltage was readily measured for ranges between one and four cm with the aid of this device and showed a decrease in intensity by a factor of over 100 as four cm was approached. At greater ranges the rotating wheel proved to be too inefficient since only a small fraction of the delayed alpha-particles was emitted in front of the detector.

At the longer ranges, an intermittent rotator, devised by our colleague R. C. Meyer, was used to measure the alpha-particles. In this apparatus two targets fixed on opposite ends of a rod about 25 cm long alternately were rotated into position in the bombarding beam and in front of the detector. The magnetic coupling to the driving motor was so arranged that the targets were in

[16] See also J. C. Bower and D. P. R. Petrie, Proc. Camb. Phil. Soc. **33**, 534–539 (1937).
[17] G. Breit and E. Wigner, Phys. Rev. **51**, 593 (1937).
[18] R. de L. Kronig, Physica **4**, 171–174 (1937).

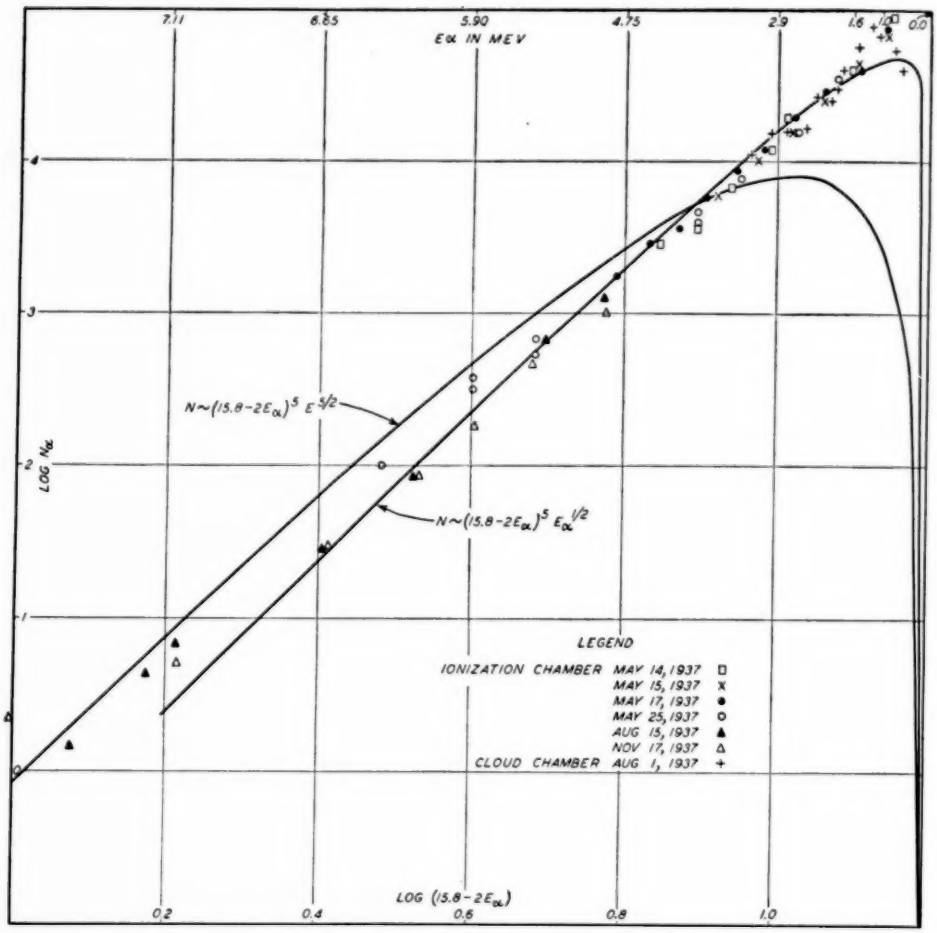

FIG. 14. Li^8 alpha-particle distribution curve, comparison with Gamow-Teller theory.

position for roughly one second and then rapidly exchanged in a fraction of a second. By means of this apparatus it was possible to fix the end point of the distribution of delayed alpha-particles at 15.8 ± 0.5 Mev, the large error mainly being due to the manner in which the alpha-particle intensity approaches zero.

In the low energy region the determination of range-number distributions by electrical counting methods is unsatisfactory because of the short ranges of the emitted particles. If the counter is set to differentiate sharply the effective range is reduced, and if differentiation is not used a maximum in a distribution appears only as an inflection. Though an inflection at short ranges was observed during the present experiments by using a counter without electrical differentiation, not enough points could be obtained on the low energy side of the inflection to establish its position with any certainty. These observations merely check qualitatively a better determination made with a cloud chamber. The use of windows in the cloud chamber was avoided by mounting a thin target on an arm which could be moved from the outside. The target proper was a lithium film deposited on a foil of one mm of air equivalent thickness. This target could be swung into a side tube of the chamber where it was bombarded by deuterons entering through a metal foil. The arm was moved to the center of the cloud chamber before expansion, thus permitting the tracks of all charged particles taking part in a disintegration to be photographed, without any intervening windows or wall effects to mar observation of the shortest tracks. The cloud chamber observations showed a definite maximum at about seven mm air equivalent in the range distribution but this maximum was less

sharp on the low energy side than that found by Fowler and Lauritsen.[19] The observations of Smith and Chang[20] do not show this maximum, but it would not be expected to appear in their experiments since they used a counter technique.

The energy distribution resulting from observations covering an intensity range of nearly 10^5 is plotted in Fig. 13 with the Pasadena and the Cavendish results shown for comparison. This distribution curve indicates that the excited level in question lies between 2.5 and 3 Mev rather than at the higher value previously reported from the Cavendish.[21] The lower value agrees well with the excited level of Be^8 found by Dee and Gilbert[22] in the disintegration of boron.

Discussion

Gamow and Teller[2] have pointed out that the main features of the distribution curve can be explained as a four-body disintegration by considerations based on the Fermi theory of beta-neutrino decay. According to this view the equation for the disintegration is

$$Li^8 \rightarrow He^4 + He^4 + e^- + v + Q_2,$$

where v signifies the neutrino. The disintegration energy, Q_2, is divided between the energy of the light particles, $E_L = E_e + E_v$, and the energy of the two alpha-particles which is $2E_\alpha$ since the two heavy particles must receive nearly equal energies if momentum is to be conserved. Then

$$Q_2 = 2E_\alpha + E_e + E_v = 2E_\alpha + E_L.$$

The probability of beta-decay, $N(E_L)$, is proportional to ${E_L}^5$ in the Fermi theory and therefore to $(Q_2 - 2E_\alpha)^5$, but in the present case there is an additional factor ${E_\alpha}^n$ describing the separation into two alpha-particles, where n is $\frac{1}{2}$ or $5/2$ corresponding to alpha-particles of angular momenta zero or 2. Consequently, on the basis of the Fermi theory, the number-energy distribution function for the alpha-particles is given by $N(E_\alpha) \sim (Q_2 - 2E_\alpha)^5 {E_\alpha}^n$, since $N(E_L)$ must be proportional to $N(E_\alpha)$ if charge is to be conserved.

The observed number-energy distribution of the delayed alpha-particles has been replotted in Fig. 14 using as abscissa the logarithm of the energy $(Q_2 - 2E_\alpha)$ available to the light particles. It is seen that the Gamow-Teller formula with $n = \frac{1}{2}$ agrees fairly well with the experimental points except in the region of low alpha-particle energies, which indicates that the effect of the potential barrier must be included before a calculation of the above type can be made exact. The Konopinski-Uhlenbeck beta-neutrino field would predict a seventh power dependence on the energies of the light particles, in marked disagreement with the observed distribution.

Consequently, it appears that the Fermi beta-theory should account satisfactorily for most features of the observed distribution of alpha-particles from the radioactive decay of Li^8. However, it is important to emphasize that in the region of the high energy alpha-particles (where the energy available to the light particles becomes small) the definiteness of agreement with the Gamow-Teller calculations becomes quite sensitive to the values of $(Q_2 - 2E_\alpha)$. $Q_2 = 15.8$ Mev, the observed end point of the distribution of delayed alpha-particles, is used in Fig. 14.

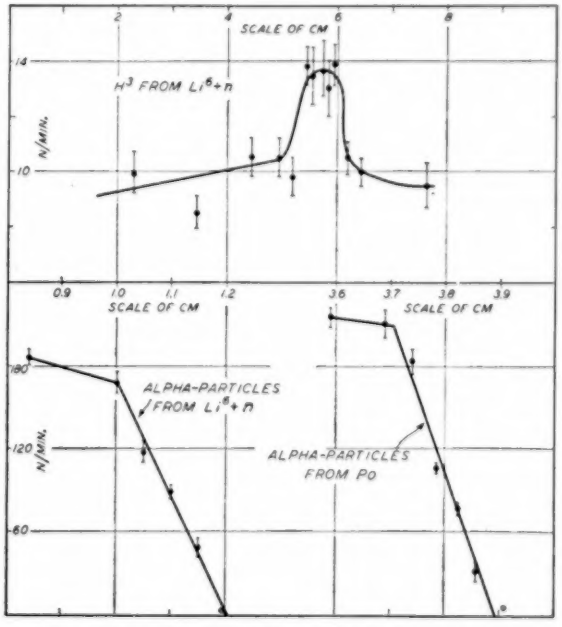

FIG. 15. Range curves for particles from $Li^6 + n$.

[19] W. A. Fowler and C. C. Lauritsen, Phys. Rev. **51**, 1103 (1937).
[20] C. L. Smith and W. Y. Chang, Proc. Roy. Soc. **166**, 415–424 (1938).
[21] W. B. Lewis, W. E. Burcham and W. Y. Chang, Nature **139**, 24 (1937).
[22] P. I. Dee and C. W. Gilbert, Proc. Roy. Soc. **154**, 279–296 (1936).

The value of Q_2 may be computed on the basis of the observation that Li^8 disintegrates into two alpha-particles without gamma-radiation, if negligible rest mass for the neutrino is assumed. Direct computation from the mass of Li^8, as determined above, and from the mass of He^4, gives $Q_2=16.03$ Mev to which the uncertainty in the mass of Li^7 alone contributes about 0.170 Mev in probable error. It seems better to compute Q_2 by taking the mass of Li^7 as equivalent to $2He^4-H^1+17.13$ Mev. Subtracting the equation $Li^7+H^1=He^4+He^4+17.13\pm0.06$ Mev from $Li^7+D^2=Li^8+H^1-0.20\pm0.03$ Mev, gives $Li^8=D^2-2H+2He^4-17.33$ Mev. Then, since $Li^8=2He^4+Q_2$, $Q_2=D^2-2H^1+17.33$ Mev $=15.90$ Mev, where Bainbridge and Jordan's[23] value for the separation of the mass-spectrographic doublet $(H_2^1-D^2)$ is used. It is, of course, pointless to attempt to use the less accurate end point of the alpha-particle distribution from Li^8 as a check on any of the above values.

G. Disintegration of Lithium by Neutrons

Two thin, square isotopic deposits, 2.5 cm on a side, were prepared upon flat silver plates especially for study of the disintegration of lithium by slow neutrons. One target contained 400 micrograms of Li^6 and the other 4600 micrograms of Li^7. These targets were interchangeable in a target holder located close to a neutron source at the center of a large block of paraffin in order to obtain a maximum flux of slow neutrons through the lithium.

The neutron produced disintegration particles from the lithium were observed by means of a linear amplifier connected to a broad but shallow ion chamber whose face was parallel to the lithium target and target holder. The face of the chamber carried a collimator made from a plate five mm thick drilled with $\frac{1}{2}$-mm diameter holes closely spaced in hexagonal pattern, so that only those disintegration particles whose paths lay within 6° of the normal to the target could enter the ion chamber. The chamber could be moved with respect to the target by means of an attached screw and each setting was read with a micrometer.

[23] K. T. Bainbridge and E. B. Jordan, Phys. Rev. **49**, 883 (1936).

Li^6+n

The alpha-particles and the H^3 particles emitted in the disintegration of Li^6 by neutrons, according to the reaction $Li^6+n\rightarrow He^4+H^3$, were observed with this apparatus. The neutron source, equivalent in strength to 7000 millicuries of (Rn − Be), was produced by bombarding a graphite plate with ten microamperes of 1-Mev deuterons.[24] Carbon neutrons produced in this manner are of relatively low energies and, through the consequent elimination of high energy recoil particles, give only a fraction of the background effects of other neutron sources. When the electrical counter was biased to count H^3 particles near the end of their range, the background was about equal to the effect produced by the H^3 particles, but the H^3 peak was still clearly defined; when the counter was biased to count only alpha-particles, the background was negligible. The range-number curves for both types of particles are plotted in Fig. 15. The alpha-particles are more suitable for an accurate determination of the energy released in the disintegration, since their energy-range relation is well established in the range interval under consideration. The less accurately measurable range and energy of H^3 are chiefly useful for determining the disintegration which occurs and for checking the experimental value of the reaction energy obtained from the alpha-particle measurements.

Immediately after the range-number curve was taken for the alpha-particles from Li^6, their range was compared directly with the range of polonium alpha-particles under identical conditions of geometry and counter bias by replacing the Li^6 target with a clean polonium source prepared on a silver square similar to that carrying the lithium. This comparison gave 2.13 Mev as the energy of the alpha-particles from Li^6 exposed to slow neutrons, when the Cornell range curves for alpha-particles (1938) were used and 3.842 cm was assumed as the mean range of the polonium alpha-particles.[25b] The corresponding reaction energy is then $(7/3)(2.13)=4.97$ Mev, in sufficient agreement with the

[24] E. Amaldi, L. R. Hafstad and M. A. Tuve, Phys. Rev. **51**, 896–912 (1937).

[25] M. G. Holloway and M. S. Livingston, Phys. Rev. **54**, 18–38 (1938).

value of 4.86 Mev observed by Livingston and Hoffman,[26] but definitely in disagreement with the energy release of 4.56 Mev calculated from commonly accepted values for the masses involved. The value for the energy release found in the present experiments requires an energy of $(4/7)(4.97)=2.84$ Mev for the H^3 particle. According to the Cornell proton range curve (1937 revised), the corresponding mean range expected for the H^3 particles is 6.15 cm, in good agreement with the value of 6.1 cm obtained from the range-number curve of Fig. 15.

Mass difference of H^3 and He^3

The direct measurement of the energy released in the disintegration of Li^6 by neutrons is of special interest in view of its application in establishing a value for the mass difference between He^3 and H^3. A value for this mass difference previously has been obtained by eliminating the mass of deuterium between the equations

$$D^2+D^2=H^1+H^3+Q_1, \quad (1)$$

$$D^2+D^2=n+He^3+Q_2, \quad (2)$$

which gives $(He^3-H^3)+(n-H^1)=Q_1-Q_2=0.69$ Mev, where Q_1 is taken as 3.98 Mev, according to Livingston and Bethe's[27] revision of data by Oliphant, Kempton, and Rutherford,[28] and Q_2 is 3.29 Mev according to Bonner.[29]

On the other hand, the masses of Li^6 and He^4 may be eliminated between the equations

$$Li^6+n=He^4+H^3+Q_3, \quad (3)$$

$$Li^6+H^1=He^4+He^3+Q_4, \quad (4)$$

giving $(He^3-H^3)+(n-H^1)=Q_3-Q_4=1.20$ Mev, if Q_3 is taken as 4.92 Mev (the average of the value determined in the present experiment and that of Livingston and Hoffman) and Q_4 is taken as 3.72 Mev.[27, 30]

Since the value of (Q_1-Q_2) fails to agree with the value of (Q_3-Q_4) by 0.5 Mev, there either must be considerable error in the determination of one or more of the four reaction energies or gamma-radiation must accompany at least one of the disintegrations. In the deuterium reactions, for example, if Q_1 were assigned too small a value or Q_2 were too large, or if gamma-radiation were emitted in reaction 1, the value for (Q_1-Q_2) given above would be too small. Likewise, the value of (Q_3-Q_4) given by the lithium reactions might be assumed to be too large. However, it appears difficult to explain an appreciable part of the 0.5-Mev discrepancy by the latter assumption. The gamma-radiation from lithium under proton bombardment has been investigated extensively in a number of laboratories but no gamma-radiation assignable to reaction 4 has been found, since the observed gamma-radiation can be produced from Li^7 but not from Li^6 targets and exhibits very strong resonance characteristics.[1, 2] A 0.5-Mev error would occur in the determination of Q_3 if the measured range of He^4 were 1.5 mm in error in the present investigation of reaction 3, while a like error in Q_4 would be introduced by an error of two mm in the range of He^3 as determined by Neuert[30] for reaction 4, assuming the Cornell range-energy relation to be correct. However, possible errors in the range-energy relation should have but small effect on the energy difference, (Q_3-Q_4), since the ranges of He^4 in the lithium-neutron reaction and He^3 in the lithium-proton reaction are very nearly equal. Furthermore, it seems unlikely that the value used for Q_3 is seriously in error in view of the manner in which it was obtained and the close agreement between the present experiment and that of Livingston and Hoffman.

Since $(n-H^1)=0.74$ Mev according to Bethe's adjusted mass values,[31] the evidence obtained from the Li^6 reactions predicts that He^3 is unstable by 0.46 Mev and may be transformed to H^3 by K-electron capture. Consequently, it seems important to look for possible gamma-radiation accompanying the (D+D) reactions and to reinvestigate the energy liberated in the disintegration of Li^6 by protons because of the relation of these reactions to the problem of proton-proton and neutron-neutron interactions.

[26] M. S. Livingston and J. G. Hoffman, Phys. Rev. **53**, 227–233 (1938).
[27] M. S. Livingston and H. A. Bethe, Rev. Mod. Phys. **9**, 371 (1937).
[28] M. L. E. Oliphant, A. R. Kempton, and Lord Rutherford, Proc. Roy. Soc. **149**, 406–416 (1935).
[29] T. W. Bonner, Phys. Rev. **53**, 711–713 (1938).
[30] H. Neuert, Physik. Zeits. **36**, 629–642 (1935).
[31] H. A. Bethe, Phys. Rev. **53**, 313–314 (1938).

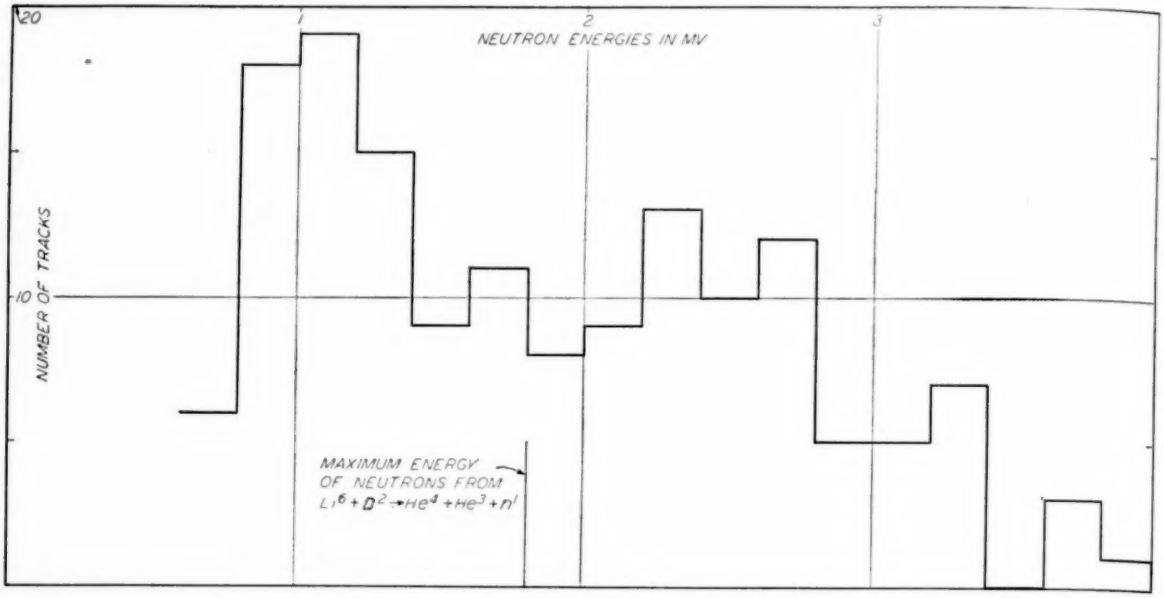

FIG. 16. Energy distribution of neutrons from Li^6+D^2.

Li^7+n

The apparatus described above also was used in a search for disintegrations produced in Li^7 by neutron bombardment. The presence of the 4600 microgram Li^7 target in front of the ion chamber under exposure to 7000 millicuries (Rn−Be) equivalent of carbon-deuteron neutrons caused no observable increase over the background counting rate at any counter bias, indicating that no appreciable number of charged heavy particles is emitted by Li^7 under these conditions. Veldkamp and Knol[32] have observed a faint beta-activity, which they attribute to Li^8, by bombarding lithium with (Rn−Be) neutrons. The observations of delayed alpha-particles from the disintegration of radio-lithium is necessary and sufficient to confirm the presence of Li^8, as discussed in Section F, but since the radioactivity observed by Veldkamp and Knol is of very low intensity, it is scarcely to be expected that such alpha-particles would be detected in the arrangement described above. Consequently, a small ionization chamber lined with ordinary lithium was placed at the center of a large block of paraffin and close to a (D−Be) neutron source equivalent to 70,000 millicuries of (Rn−Be).[24] Repeated observations failed to detect the emission of any alpha-particles after the neutron source was removed by interrupting the deuteron beam, though the ion chamber counted 4.6 Li^6 disintegrations per minute per millicurie (Rn−Be) equivalent of (D−Be) neutrons when the beam was on the target, as determined by direct count with a weak (D−Be) neutron source. With the Li^7/Li^6 ratio taken as 11.6, it was calculated that the maximum cross section for production of Li^8 from Li^7 by neutrons is less than 5×10^{-6} times the neutron disintegration cross section of Li^6.

It is difficult to compare the sensitivity of the above method with that used by Veldkamp and Knol, but it seems unlikely that their method should have been sufficiently more sensitive to compensate for the much larger number of neutrons (700 to 1) employed in the present observations. It should be pointed out that the present apparatus was sensitive only to heavy particles and therefore strictly limited to the detection of Li^8, whereas the method of Veldkamp and Knol would detect the formation of any other beta-active elements as well. Since the half-period of He^6, a beta-emitter,[33] is nearly identical with that of Li^8, it follows that they probably detected the reaction $Li^6+n\rightarrow He^6+H^1-2.8$ Mev. The endothermic nature of this

[32] J. Veldkamp and K. S. Knol, Physica **4**, 166–170 (1936).

[33] T. Bjerge, Nature **138**, 400 (1936).

reaction would account for the low intensity of the radioactivity which they observed, since only a fraction of their total (Rn−Be) neutrons would possess sufficient energy to form He^6.

H. Neutrons from Li^6

The energy distribution of the neutrons produced by deuteron bombardment of Li^6 was investigated by measuring proton recoil tracks in a cloud chamber placed to receive neutrons emitted roughly at right angles to a deuteron beam incident on a Li^6 target deposited upon silver. A bombarding energy of 800 kev was chosen in accordance with the yield curve for this process (Section C) in order to obtain the highest possible intensity of Li^6 neutrons without introducing a serious number of neutrons from carbon. Under these conditions, the maximum kinetic energy of the Li^6 neutrons was $[(\frac{7}{8})Q+\frac{5}{8}(0.8)]$ Mev, where Q is the energy released in the reaction. Only recoil proton tracks beginning and ending in the chamber and projected within 30° of the direction of the incident neutrons were measured. About 200 such recoil tracks were obtained in a preliminary survey. The distribution of the corresponding neutron energies, plotted in Fig. 16, had a range of over three Mev. Roughly one-half of the measurable tracks were produced by neutrons of more than 2.0-Mev energy, so that the corresponding values of Q were greater than 1.7 Mev, provided these neutrons originated in Li^6 reactions. A series of tests indicated that the presence of any contamination in amounts sufficient to have produced a considerable fraction of the total neutrons could have been detected easily by the accompanying characteristic groups of charged particles. Carbon on the target doubtless contributed a small part of the low energy neutrons, but the effect of deuterium upon the observed neutron distribution at higher energies apparently was inappreciable.

Deuteron bombardment of Li^6 may produce neutrons by either of two reactions

$$Li^6+D^2\rightarrow Be^7+n+Q_1, \qquad (1)$$

$$Li^6+D^2\rightarrow He^4+He^3+n+Q_2. \qquad (2)$$

Strong evidence for the occurrence of the first reaction has been obtained from the energies of recoil particles observed in an ion chamber during the previous work with lithium isotopes,[1] while the second reaction is to be expected, in analogy with the reaction $Li^7+D^2\rightarrow He^4+He^4+n$, since it is exothermic.

The energy balance, Q_1, for the first case can be predicted only in so far as the mass of Be^7 can be estimated. Since the previous observations indicated that the formation of Be^7 leads to no radioactivity of short life,[1] it may be predicted that Be^7 should be roughly one Mev heavier than Li^7, either by estimating the Coulomb energy excess of Be^7 over Li^7 or by interpolating between the relative masses of neighboring pairs of nearly stable isobars. The corresponding value of Q_1 is 3.1 Mev. In the second reaction, Q_2 can be calculated from accepted values for the masses involved and is 1.56 Mev, where the chief uncertainty is introduced by a probable error of 0.2 Mev in the mass of Li^6 according to Livingston and Bethe.[34] However, the results of experiments discussed in the preceding section indicate that the accepted mass of He^3 possibly is too small by 0.5 Mev so that Q_2 might be as low as one Mev. When the uncertainty in the mass of Li^6 is taken into account it follows that an upper limit of 1.7 Mev appears reasonable for Q_2, so neutrons of energies greater than $(\frac{7}{8})(1.7)+(\frac{5}{8})(0.8)=2.0$ Mev would not be expected to originate in reaction 2. Consequently, the neutron energy distribution of Fig. 16 constitutes strong but qualitative evidence that Be^7 is formed according to reaction 1. A greater number of recoil tracks must be measured before the mass of Be^7 can be fixed accurately or any of its energy levels determined in case Be^7 is not always left in the ground state. However, the observed distribution of neutron energies is not in disagreement with the estimate of the mass of Be^7 given above.

The relative probabilities of reactions 1 and 2 can be estimated to be very roughly equal at 800 kev if all neutrons of energies greater than 2.0 Mev are assigned to reaction 1 and all others to reaction 2. However, such an estimate is subject to considerable error, chiefly because of the uncertainty in the value of Q_2 and the large statistical variations which are probable when

[34] M. S. Livingston and H. A. Bethe, Rev. Mod. Phys. **9**, 373 (1937).

only 200 tracks are measured. In addition, the usual observational uncertainties for cloud chambers are present. The measurement of tracks tends to discriminate against very low energy neutrons because the recoil tracks are short, and against high energy neutrons because the longer recoil tracks are less apt to end within the cloud chamber. Likewise, there is the usual background from scattered neutrons and target contaminations. When all these factors are weighted the formation of Be^7 appears to be the more probable reaction, but the ratio 1 : 1 for the relative probabilities of the two reactions, as estimated by the more direct method, is believed to be within a factor of three of the true value.

I. Radioactivity of Be^7

Be^7 may be expected to be unstable since this isotope does not occur in beryllium minerals. Furthermore, the evidence outlined in the preceding section indicates that Be^7 is heavier than Li^7 and consequently should be transformed to Li^7 either through positron emission or absorption of an orbital electron by the nucleus. A previous investigation of isotopic targets bombarded by deuterons had shown that no short period activity existed which could be associated with Li^6 or the formation of Be^7.[1] Consequently, the possibility of a long half-life was investigated. Through the cooperation of Dr. G. L. Locher, a target of ordinary LiF which had been bombarded a month earlier with 35 microampere hours of 1000-kev deuterons was examined and found to exhibit radioactivity with a half-value period of 43 ± 6 days. Likewise, a thick target of lithium metal bombarded with 20 microampere hours of 1000-kev deuterons showed an activity corresponding to the increased proportion of lithium in the target. The surface of the latter target was scraped off and was found to carry the activity, which demonstrated that deuterons and not neutrons had produced the activation.

A chemical separation, carried out by Dr. M. H. Van Horn of George Washington University, concentrated the active element in a final precipitation of beryllium from 100 micrograms of beryllium carbonate added as a carrier. However, the chemical separation would not remove iron, which is a common impurity in metallic lithium. Consequently, an iron target was bombarded with 1000-kev deuterons and tested for radioactivity, but it was found that an iron impurity of more than 100 percent would have been required to account for an activity equivalent in intensity to that observed in the lithium target. It was apparent, therefore, that the radioactive element produced was a beryllium isotope and almost certainly Be^7, in view of the evidence from the Li^6 neutrons and the fact that the known isotopes Be^8, Be^9, and Be^{10} do not possess a 43-day half-period.

Proton bombardment of boron

A second reaction which should lead to the production of Be^7 is $B^{10}+H^1\rightarrow Be^7+He^4+Q$. A boron carbide target which had been bombarded with 11 microampere hours of 950-kev protons exhibited radioactive properties equivalent to those observed in the lithium targets. The intensity of this radioactivity was 75 percent as great as that produced in the lithium metal target, which indicates that transmutations producing Be^7 constitute an appreciable fraction of the disintegration processes for B^{10} under proton bombardment.

The range of the alpha-particle group from the reaction $B^{10}+H^1\rightarrow Be^7+He^4+Q$ could be used to determine the mass of Be^7. An attempt was made to observe this group superimposed upon the intense continuous distribution of alpha-particles from the four times more abundant isotope B^{11} but the experimental difficulties proved to be too great. If Be^7 is assumed to be one Mev heavier than Li^7, the expected range of the alpha-particle group from B^{10} is only about five mm for the negligible bombarding energies which are required in order to avoid protons scattered from the target. A reasonably intense superimposed group usually can be resolved by using counters with strong electrical differentiation, but differential counters cannot be used for very short range particles. Consequently, in the present experiments it was necessary to use a shallow ion chamber connected to an amplifier and counter without differentiation, but this arrangement did not reveal any significant departure from the expected continuous distribution of alpha-particles from B^{11} down to ranges as short as three mm, where scattered 200-kev protons from the target began to enter the ion chamber.

Nature of radiation

The 43-day half-life radioactivity observed in the lithium and boron targets was shown to be due to gamma-ray emission. When covered targets were alternated with uncovered targets within the chamber of a Lauritsen electroscope, the comparative discharge rates were those to be expected from gamma-ray ionization only. Likewise, no charged particles could be detected with Geiger-Müller counters having wall thicknesses equivalent to only a few centimeters of air, although the counting rates obtained with shielded counters indicated the emission of more than 100 gamma-ray quanta per second.

This unusual type of radioactivity might originate in the decay of Be^7 to form Li^7 by either of two reactions

$$\left.\begin{aligned} &Be^7 \rightarrow Li^7 + e^+ + \nu, \\ &e^+ + e^- \rightarrow 2h\nu_1, \end{aligned}\right\} \quad (1)$$

$$\left.\begin{aligned} &Be^7 + e^- \rightarrow Li^7 + \nu, \\ &Be^7 + e^- \rightarrow Li^{7*} + \nu, \\ &Li^{7*} \rightarrow Li^7 + h\nu_2, \end{aligned}\right\} \quad (2)$$

where ν signifies a neutrino. In the first case, Be^7 may emit a positron with so little energy that it does not ionize appreciably but can be detected by the resulting radiation of two simultaneous 0.5-Mev annihilation quanta. In the second case, an orbital electron may be absorbed by Be^7 so that the resulting Li^7 nucleus is formed, at least part of the time, in an excited state from which it then passes to the ground level with gamma-ray emission. In the second reaction, the expected number of gamma-ray quanta per transmutation is less than unity because part of the Li^7 nuclei may be formed in the ground state and emit no gamma-radiation.

It is evident from the above discussion that several experimental tests (involving energy, simultaneity, and number of gamma-ray quanta emitted by Be^7) may be used to discriminate between transmutations of Be^7 by positron emission and by K-electron capture. Geiger-Müller counters were used in making three such tests and it was found efficacious to compare the Be^7 radiation directly with the 0.5-Mev annihilation radiation from the positron emitter N^{13}, produced in ample quantities according to the reaction $C^{12} + D^2 \rightarrow N^{13} + n$ by bombarding a graphite target with 1000-kev deuterons. N^{13} probably decays entirely by the transmutation $N^{13} \rightarrow C^{13} + e^+ + \nu$ so that two 0.5-Mev annihilation quanta per N^{13} atom result. In addition, comparatively faint 0.2-Mev gamma-radiation (presumably corresponding to occasional formation of C^{13} in an excited state) has been reported.[35] In the present experiments, monochromatic 0.5-Mev radiation in equilibrium with its secondaries was assured after the rays had passed through $\frac{1}{8}$ inch of lead, since the absorption curve observed with greater thicknesses of lead was a simple exponential.

Absorption coefficient

The comparative absorption coefficients for the gamma-radiation from Be^7 and for the 0.5-Mev radiation from N^{13}, measured in lead under identical conditions, were found to be 0.169 ± 0.008 and 0.130 ± 0.002 g cm^{-1}, respectively, by a least-square determination. The corresponding energy for the Be^7 gamma-radiation is 425 ± 25 kev, in reasonable agreement with the energy to be expected if a K electron were absorbed by Be^7 to form Li^7 in its known excited state at 450 kev (Section C).

Simultaneity

Another test to determine the decay process was made by placing Be^7 between two Geiger-Müller counters arranged to count double coincidence discharges. No statistically significant departure from the cosmic-ray background rate of 0.6 counts per minute was observed with the Be^7 in position. If Be^7 decayed only by positron emission, the resultant simultaneous emission of two annihilation quanta in opposite directions should have increased the counting rate by a factor of three over the background rate.

Number of quanta

A third experimental test, indicative of the process by which Be^7 decays, was made by determining approximately the average number of quanta emitted per Be^7 atom. The gamma-ray counting rates from lithium targets containing Be^7 and from graphite targets containing N^{13} were measured under identical conditions with a Geiger-Müller counter shielded with $\frac{1}{8}$ inch of lead. If μ radioactive atoms having a decay constant λ sec.$^{-1}$ and emitting n gamma-rays per disintegration are presented to a counter shielded to insure equilibrium between gamma-rays and

[35] J. R. Richardson, Phys. Rev. **53**, 610 (1938).

their secondaries, the observed counting rate, C, is given by

$$C=\lambda\mu n\epsilon \text{ sec.}^{-1},$$

where ϵ is the over-all efficiency of the detecting apparatus. In the present experiment, ϵ was considered to be the same for both Be^7 and N^{13} gamma-ray quanta since their energies are practically alike and all other conditions were held constant throughout the observations. Then, the ratio of the gamma-ray counting rates for Be^7 and N^{13} is given by

$$C_1/C_2=(\lambda_1\mu_1 n_1)/(\lambda_2\mu_2 n_2),$$

where the subscripts 1 and 2 refer to Be^7 and N^{13}, respectively. The decay constants, λ_1 and λ_2, were known with considerable accuracy and n_2 was assumed to be two annihilation quanta per N^{13} atom. The ratio μ_1/μ_2 was calculated, with appropriate corrections for radioactive decay, from available information on neutron yields for the reactions in which Be^7 and N^{13} were formed. The numbers of neutrons from deuteron bombardment of lithium and carbon targets had been measured by Amaldi, Hafstad, and Tuve,[24] the relative neutron yields from Li^6 and Li^7 were obtained from Fig. 10 of the present experiments and the known isotope ratio, and the approximate fraction of Li^6 neutrons corresponding to the formation of Be^7 was estimated within a factor of three from Fig. 16. Calculations based on the above data gave n_1 as 0.1 gamma-ray quantum per Be^7 atom within limits $0.03<n_1<0.3$, which is consistent with the hypothesis of K-electron capture because transitions to the ground state of Li^7, which produce no gamma-radiation, should be more probable than the less energetic transitions to excited levels.

Possibility of positron emission

The experiments enumerated above did not preclude the possibility of the emission of low energy positrons by a small fraction of the Be^7 atoms. Accordingly, a bare LiF target which had been bombarded some weeks previously was placed inside a cloud chamber. Repeated expansions failed to reveal any particle track of any length whatsoever which definitely originated in the target, nor was there any evidence of ionization in the immediate neighborhood of the target. However, the gamma-ray emission was sufficiently intense that occasional Compton electron tracks were observed in various parts of the chamber. The total number of Be^7 atoms decaying during the sensitive periods of the cloud chamber could be estimated, since the decay constant and the approximate number of Be^7 atoms present in the target were known, as outlined above. Thus, it was possible to estimate that, provided positron emission occurs at all, probably not more than one Be^7 atom per thousand decays with the emission of a positron of more than a few kilovolts' energy.

Discussion

There are four separate lines of experimental evidence in all, which strongly indicate that positron emission does not occur and that Be^7 decays only through the absorption of an orbital electron to form Li^7 sometimes in the ground state and sometimes in the 450-kev excited level. It follows that the upper and lower limits for the mass difference (Be^7-Li^7) may be set at 1.0 Mev and 0.45 Mev, respectively, since for greater differences positron emission would become probable and for lesser differences Li^7 could not be formed in the 450-kev state. Moreover, mass differences near the lower limit are not to be expected, since the transition probability for the 450-kev state should decrease more rapidly than Be^7-Li^7-450 kev, the energy available for this transition, in analogy with all other known radioactive processes. For example, if the relative transition probabilities for the two Li^7 states, as given by the number of gamma-rays observed per Be^7 atom, arbitrarily are taken to be proportional to the fourth power of the relative transition energies,[36] then the mass difference (Be^7-Li^7) is approximately one Mev for 0.1 gamma-ray quantum per Be^7 atom, and 0.8 Mev for 0.03 quantum per Be^7 atom.

J. Acknowledgment

The support and encouragement of Drs. J. A. Fleming and W. F. G. Swann, the directors of the laboratories in which this work was done, is gratefully acknowledged. We are also indebted to Drs. G. Breit, G. Gamow, N. P. Heydenburg, G. L. Locher, R. C. Meyer, C. J. Rodden, E. Teller, M. A. Tuve, M. H. Van Horn, and E. G. Zies for important contributions at various stages in this work.

[36] H. A. Bethe and R. F. Bacher, Rev. Mod. Phys. **8**, 197 (1936).

The Alpha-Particle Model of the Nucleus

L. R. HAFSTAD
Department of Terrestrial Magnetism, Carnegie Institution of Washington, Washington, D. C.

AND

E. TELLER
George Washington University, Washington, D. C.

(Received August 26, 1938)

This paper reviews the theory of nuclei composed of alpha-particles alone, and extends it to cases where in addition to the alpha-particles, a single neutron or proton is present, and also to those light nuclei in which a single neutron or proton is missing from the complete alpha-particle structure. In the latter cases the missing particle is considered as a neutron or proton "hole." In the first section of the paper, the configuration of the alpha-particles is considered together with the motion of the neutron, proton, neutron hole, or proton hole, in the field of the fixed alpha-particles for nuclei lighter than fluorine. Rough values for the binding energies are obtained and compared with the results of the Hartree model. In the second section of the paper, rotations of the same nuclei are discussed, and the symmetry properties of the fundamental states, as well as the symmetry properties and the approximate spacing of some of the excited states are obtained. The symmetry properties of the fundamental states are in agreement with those obtained from the independent-particle model. Furthermore the excited states as obtained from the two models show a marked parallelism, although a greater number of levels is predicted by the alpha-particle model than by the independent-particle model.

INTRODUCTION

THE liquid-droplet model of the nucleus which has been recently discussed by Bohr gives an adequate description of many nuclear processes, and also provides us with some very general statements about nuclear binding energies and the distributions of excited states. More detailed results, however, may be obtained only with the help of models based on more specific assumptions. Two models of this kind have been proposed, namely, the independent-particle model and the alpha-particle model. The main difference between these two models is that, while in the independent-particle model each neutron or proton is assumed to be subject, in the first approximation, to the average force obtained from all other neutrons and protons, in the alpha-particle model the interaction of two neutrons and two protons (constituting an alpha-particle) are first considered, and then the interaction of these groups with each other and with particles outside of the groups are considered later.

It is undoubtedly true that no one is more aware of the weaknesses inherent in the use of the independent-particle model of the nucleus than those theoretical workers who have been making calculations on this basis. Such calculations are based on the model in which each of the nuclear constituents moves in a field obtained by averaging over the positions of the other particles and it neglects, therefore, in the first approximation the phase relation of the nuclear constituents. The success of a similar model in explaining atomic structure is due to the fact that all electrons are subject to the nuclear attraction, which is greater than the interaction between the electrons, and that the latter interaction, too, is a Coulomb force, that is, a long range force. It has been pointed out frequently that the absence of a central body in nuclear structure and the short range interaction between the constituents tend to make the Hartree or independent-particle approximation a very poor one. If the interaction is assumed to be of an exchange type, the independent-particle picture becomes even less justified. The impression that a considerable degree of success has been attained by this model, created perhaps especially among experimentalists, may be due to the fact that it is mainly the successes of the theory, and not its shortcomings, which are published, or at least which are emphasized in publication. It is well to remember in this connection that Breit and Rabi[1] stated at a

[1] G. Breit and I. Rabi, Phys. Rev. **46**, 230–231 (1934).

very early date in the development of nuclear theory that: "According to the usual ideas of nuclear structure the constitution of a nucleus resembles that of a polyatomic molecule or else a liquid. It is questionable whether there is much meaning to a central field which one must necessarily assume in order to assign an orbital quantum number to a particle under these conditions."

An older picture of the nucleus,[2] to which the above quotation implicitly refers, assumes that alpha-particles are present in the nuclei as comparatively stable sub-units. It has been emphasized that the alpha-activity and, to some extent, also the greater stability of nuclei of the $4n$-type may be explained by the independent-particle picture as well,[3] but still it seems impossible to obtain as good absolute values for the binding energy with the help of the Hartree model as is obtained in the zero*th* approximation from the alpha-particle picture. Again, it has been shown in some cases, and will be shown for others in this paper, that the behavior of the nuclei in the vicinity of O^{16}, which seemed to be in particularly good agreement with the closing of the "*P*-shell" in the Hartree model, can be also accounted for by the alpha-particle model.

Our purpose in this paper is to discuss the alpha-particle model for light nuclei. Such discussions have been given previously[3, 4] for nuclei composed of alpha-particles alone. We shall review the theory of these nuclei and extend it to cases where, in addition to the alpha-particles, a neutron or proton is present, and also to those light nuclei where a single neutron or proton is missing from a complete alpha-particle structure. In the latter cases we may speak of a neutron or proton "hole." Our treatment will be based on the analogy with molecular structure, just as the conventional application of the independent-particle picture is based on an analogy with atomic structure. The alpha-particles will correspond to the nuclei of the molecule, the neutron hole or proton hole to the electron moving in the field of the heavier constituents.

Obviously this picture too is inherently weak. Thus it has been pointed out that, particularly in heavy nuclei, considerations of energy and space-occupation[5] make the stability of alpha-particles as sub-units somewhat doubtful. Furthermore, our calculations, for those nuclei which are not composed of alpha-particles alone, contain the assumption that the mass of the neutron or proton is negligible as compared to that of the alpha-particle.

However, the essential reason that the independent-particle picture has been used so largely in recent theoretical investigations has been the belief that the alpha-particle picture would be more complicated for actual numerical calculations. As will be shown below, many important results can be obtained from the alpha-particle picture in a simple way.

It is a significant fact that, while the Hartree and alpha-particle approximations start from widely different assumptions, the results obtained agree in many of the main features as well as in some of the details. For example, the second approximation of the independent-particle picture, as applied to heavy nuclei,[6] brings about a distribution of neutrons and protons resembling more closely that obtained from the alpha-particle picture. A parallelism has also been found[7] with regard to the properties of the first excited states of heavy nuclei as obtained from the two points of view.

Our treatment consists of two main sections. In the first, the configuration of the alpha-particles is considered together with the motion of the neutron, proton, neutron hole, or proton hole, in the field of the fixed alpha-particles for nuclei lighter than fluorine. Rough values for binding energies are obtained and compared with results of the Hartree model.

In the second section, rotation of the same nuclei is discussed. In this section we obtain the symmetry properties of the fundamental states as well as the symmetry and approximate spacing of some of the excited states. The symmetry properties of the fundamental states are in agreement with those obtained from the

[2] G. Gamow, Proc. Roy. Soc. **A126**, 632–644 (1930).
[3] H. Bethe and R. F. Bacher, Rev. Mod. Phys. **8**, 168–171 (1936).
[4] W. Wefelmeier, Zeits. f. Physik **107**, 332–346 (1937); J. A. Wheeler, Phys. Rev. **52**, 1083–1106 (1937); C. F. von Weizsäcker, Naturwiss. **26**, 209–217, 225–230 (1938).
[5] W. Elsasser, J. de phys. et le rad. **5**, 389–397, 635–639 (1934).
[6] H. Euler, Zeits. f. Physik **105**, 553–575 (1937).
[7] E. Teller and J. A. Wheeler, Phys. Rev. **53**, 778–789 (1938).

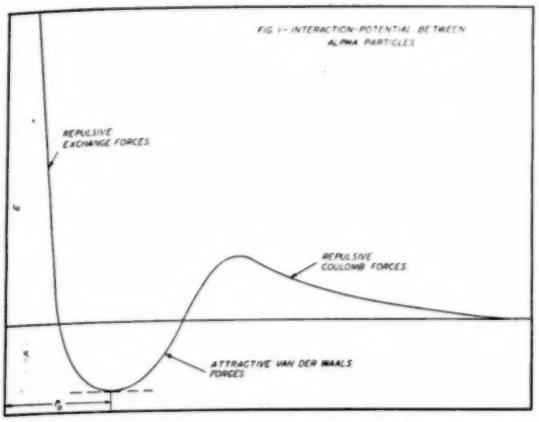
FIG. 1 - INTERACTION-POTENTIAL BETWEEN ALPHA PARTICLES
REPULSIVE EXCHANGE FORCES
REPULSIVE COULOMB FORCES
ATTRACTIVE VAN DER WAALS FORCES

FIG. 1. Interaction potential between alpha-particles.

independent-particle model. Furthermore, the excited states as obtained from the two models show a marked parallelism although a greater number of levels is predicted in the alpha-particle picture than in the independent-particle picture

The agreement of the symmetry properties in the two models seems to us to be the main result of the present paper.

Though we do not think that the model here presented is good enough to give a detailed account of experimental facts, we believe that it is not worse than the Hartree model. Explicitly, we believe that neither of these pictures can give an adequate explanation of the details of nuclear structure. However, it is of some interest to present calculations based on the alpha-particle model which give the same results as the Hartree model. Such results seem to be relatively less sensitive to the approximations which have been made and therefore might be expected with somewhat greater confidence to agree with experimental observations. Such agreement, however, seems to imply only the validity of those considerations which are fundamental to both points of view, and must not be interpreted as supporting the detailed assumptions of either model.

SECTION I

Fundamental states, proper functions, binding energies

Saturated nuclei of 4n-type.—We shall call those nuclei which contain $2n$ neutrons and $2n$ protons, and can therefore be considered as consisting of n alpha-particles, saturated nuclei. The name saturated nucleus refers to the fact that the alpha-particles are the saturated sub-units in nuclear structure. In fact, these nuclei are analogous to the rare gases and other saturated shells in molecular physics. They have, at least for light nuclei, a comparatively high binding energy, a high frequency of occurrence in nature, and no angular or magnetic momentum. These nuclei have been described in accordance with the "saturation character" of nuclear forces.[8] By "saturation character" is meant that the binding energy (and also the volume) of a nucleus is roughly proportional to the number of particles contained in it, and not to the square of the number of particles as might be expected if each particle interacted with all other particles. To obtain this condition, it can be assumed that the alpha-particles repel each other at small distances. In order to build up saturated nuclei containing more than one alpha-particle, an attraction must be introduced at larger distances. Thus an interaction potential between two alpha-particles is obtained of the form shown in Fig. 1.[9] This interaction may be compared to that between two saturated shells in atomic physics. The repulsion at small distances corresponds to the exchange interaction, the attraction at greater distances to the van der Waals, or polarization, forces.[8] The analogy with the closed atomic shells makes it plausible that the interaction forces are of an additive nature, that is, the interaction of two particles is not changed by the presence of a third alpha-particle.

According to these assumptions, alpha-particles will be held in equilibrium-positions within the nucleus, Be^{8} corresponding to a dumb-bell model, C^{12} to an equilateral triangle, O^{16} to a tetrahedron, and further saturated nuclei to more complicated structures. If, in analogy to atomic physics, a short range interaction is assumed between the closed shells, the binding energy will be proportional to the number of "bonds" between adjacent particles, that is, to the number of pairs of alpha-particles which for

[8] W. Heisenberg, Zeits. f. Physik **96**, 473–484 (1935).

[9] The effect of the Coulomb interaction at great distances will not be considered in what follows, since it is of relatively small importance for light nuclei.

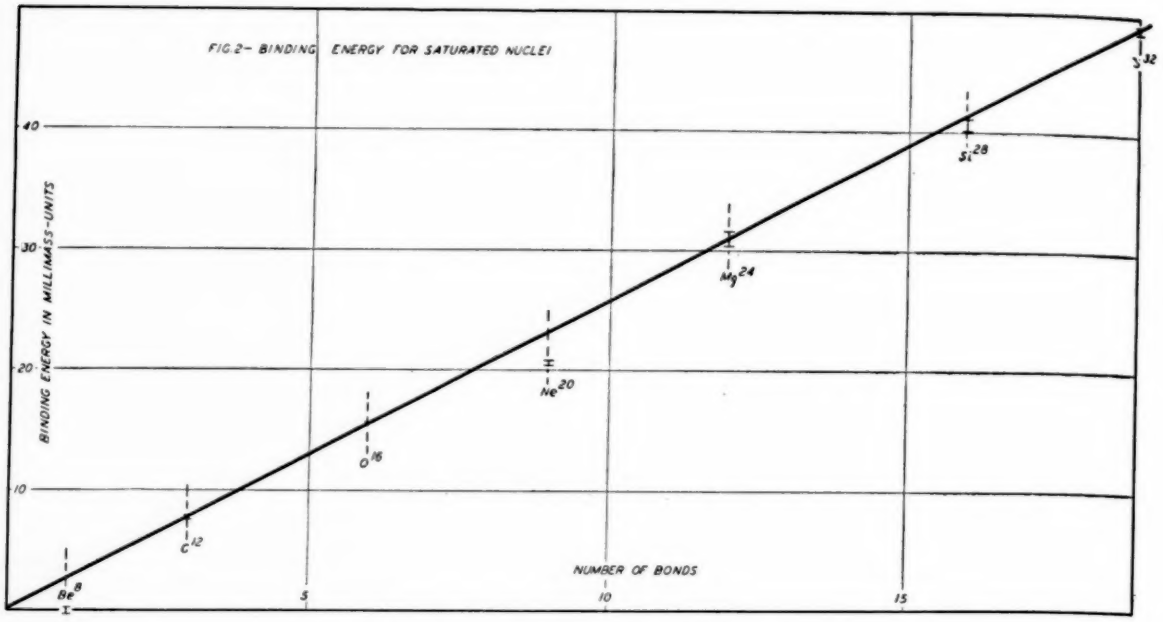

FIG. 2. Binding energy for saturated nuclei.

geometrical reasons can approach to the distance of maximum interaction r_0.

In Fig. 2 the binding energies of saturated nuclei, that is, the masses of the constituent alpha-particles minus the nuclear mass, are plotted against the number of "bonds." The experimental values are plotted with vertical lines to show their limits of error. The same procedure will be followed in Figs. 5 and 6. In agreement with the model, a very good linear relation is obtained with the exception of Be^8 and Ne^{20}, which both fall below the curve.

According to the model, Be^8 should have a binding energy corresponding to one bond, that is, 2.58 in Mev. Its actual binding energy, however, is close to zero. It has been suggested by Wefelmeier[4] that this discrepancy may be due to the effect of the zero-point energy in analogy to Wigner's explanation[10] of the surprisingly great ratio of the binding energies of the alpha-particle and the deuteron.

In order to check this explanation, we have calculated the zero-point energies for Be^8, C^{12}, and O^{16} for a simplified model, assuming that the zero-point amplitudes are small as compared to the distances between the alpha-particles and that the effects of the anharmonicity of the forces, and the interaction with rotation, may be neglected. If, furthermore, the additivity of the forces is remembered, the ratio of the zero-point energies[11] for the sequence $Be^8 : C^{12} : O^{16}$ is as $1 : [(3/2)^{\frac{1}{2}}+2(3/4)^{\frac{1}{2}}] : (\sqrt{2}+2/\sqrt{2}+3.1)$, or $1 : 2.9 : 5.8$. This ratio is very nearly equal to the ratio $1 : 3 : 6$ of the number of bonds in these nuclei so that the ratios of the total binding energy should remain $1 : 3 : 6$. Thus for the model proposed the zero-point energy does not explain the anomaly for the Be^8-nucleus.

The reason that, in comparing H^2 and H^3, the zero-point energy is of great importance while for Be^8 and C^{12} it is not, seems to us to be as follows. In H^2 and H^3 the equilibrium positions of the neutrons and protons coincide. Therefore, H^2 possesses three "vibrational" degrees of freedom and H^3 six "vibrational" degrees of freedom. Very roughly one may therefore expect the zero-point energy to increase by a factor of two. At the same time the pairs of interacting particles and therefore the number of terms in the potential energy change from one to three, that is, the potential energy increases more rapidly than the zero-point energy. On the other hand, in the models for Be^8 and C^{12} the

[10] E. Wigner, Phys. Rev. **43**, 252–257 (1933).

[11] The normal vibrations may be obtained from Table IV in the paper by Wheeler, reference 4.

number of vibrational degrees of freedom is equal to the number of bonds and it may therefore be expected that the zero-point energy and potential energy will be proportional. This qualitative consideration suggests that a rather great change of the model of saturated nuclei may be necessary to explain the low binding energy of Be^8.

In Fig. 2 it will be noticed that the number of additional bonds per particle increases markedly up to O^{16} but remains constant for the following two saturated nuclei. This corresponds to the relatively smaller binding energy for the nuclei heavier than O^{16} predicted by the "shell structure" in the independent-particle model. The fact that Ne^{20} lies below the curve shows that the break in binding energy after O^{16} is even more marked than would be expected from the alpha-particle model. It should be remembered, however, that the disagreement for Be^8 and Ne^{20} is small as compared to the disagreement as obtained in any of the direct calculations based on the independent-particle model.

The degree to which alpha-particles may retain their individuality in nuclei will decrease as the total interaction between an alpha-particle and the other constituents of the nucleus increases. It is therefore not improbable that in heavy nuclei where an alpha-particle is completely surrounded by other alpha-particles (and possibly neutrons) the alpha-particle picture is less valid than for light nuclei. This may help to explain the fact that for all heavy nuclei the binding energy of an added neutron or proton is approximately constant, whereas for light nuclei a particularly great binding energy is obtained whenever a new alpha-particle is completed.[12]

One of our reasons for restricting this discussion to light nuclei is that for these the alpha-particle model may be a reasonable approximation even though it may break down for heavy nuclei.

Nuclei of $(4n+1)$ *type.*—For nuclei containing a single neutron or proton in addition to the alpha-particles, the total binding energy will be given by the binding energy of the group of alpha-particles plus an additional energy due to the binding of the single particle to the alpha-particle group.

In the simple case of He^5 the additional energy, which we will call B, will be given directly by the difference between the masses of He^5 and (He^4+n). Thus $He^5-(He^4+n)=B$.

The independent-particle picture predicts that the fundamental state of He^5 should be a P state, consisting of four s particles and one p particle. We take this result over into the alpha-particle picture by assuming that the four s particles correspond to the alpha-particle and that the added neutron in He^5 is in a p state with a node through the center of the alpha-particle. Such a model will satisfy the exclusion principle, and make it possible in the simplest way that the ψ-function of the added neutron should be orthogonal to the ψ-function of the neutrons within the alpha-particle. One consequence of the presence of this node through the alpha-particle is that the added particle will be found with a small probability within the alpha-particle, corresponding to the notion that the density of matter within the alpha-particle closely approaches the maximum density which can be reached within a nucleus.

The case of Li^5 in which a proton is added to the alpha-particle will differ only slightly from that of He^5 due to the effect of the Coulomb forces. This difference, and those for other nuclei in which a proton is added instead of a neutron, can be calculated quite as readily for our present model as for the independent-particle picture. However, since the results are practically identical for the two models (as might be expected, since the effect of the long range Coulomb forces will not depend very greatly on the details of the configuration of nuclear constituents) and, further, since the experimental uncertainties in the available data are too great for definite conclusions to be drawn, the effects of Coulomb interactions will not be considered in this paper.

In cases of more than one alpha-particle, we may reason as follows. The force between the neutron and any one alpha-particle has a short range. This force will therefore contribute to the binding energy only when the neutron is close to some one of the alpha-particles. This fact makes it plausible that the neutron does not

[12] It should be remembered, however, that mass defects for heavy nuclei are relatively less accurately known.

simultaneously interact to a great extent with other alpha-particles which are at the average distance r_0. Thus the neutron will interact with each alpha-particle only part of the time.

For Be^9 we have two alpha-particles each with an associated ψ-function for the neutron which we will designate as ψ_1 and ψ_2, respectively. As in the case of He^5, each neutron ψ-function must have a node through the respective alpha-particle. The total wave function may be any linear combination of ψ_1 and ψ_2, but, since we are seeking the lowest energy state and since long wave-lengths correspond to smallest energies of the particle, we choose a combination $(\psi_1+\psi_2)$ with a single plane node extending through both alpha-particles. The average energy of the neutron will be given by

$$\bar{E}(\psi_1+\psi_2)=\frac{\int(\psi_1+\psi_2)H(\psi_1+\psi_2)}{\int(\psi_1+\psi_2)^2},$$

where $H=(V_1+V_2+T)$ and V_1 refers to the potential energy of the neutron due to alpha-particle number one, V_2 refers to the potential energy of the neutron due to alpha-particle number two, and T is the kinetic energy of the neutron. On expansion we find that the terms can be grouped as binding, interaction, and exchange, terms which we will designate as B, R, and Q, respectively. The B terms will have the form $\int\psi_1(V_1+T)\psi_1$ and refer to the potential and kinetic energy of the neutron due to α_1 (that is, the first alpha-particle) when the neutron is near α_1, with corresponding terms for α_2. The R terms will have the form $\int\psi_1 V_2\psi_1$ and refer to the additional potential energy of the neutron when near α_1 due to the presence of α_2, and conversely. The exchange terms are those having form $\int\psi_1 H\psi_2$ and have the usual meaning. Letting $S=\int\psi_1\psi_2$ we find

$$\bar{E}(\psi_1+\psi_2)=\frac{2(B+R+Q)}{\int\psi_1^2+\int\psi_2^2+2\int\psi_1\psi_2}=\frac{B+R+Q}{1+S}.$$

In keeping with the idea that the added neutron interacts mainly with one alpha-particle at a time and that therefore ψ_1 and ψ_2 do not overlap strongly, we assume that the overlapping of the ψ-function is small and therefore $S\ll 1$,[13] so that

$$E(\psi_1+\psi_2)\leqq[B+R+Q].$$

Applying the same type of arguments to C^{13} we will expect that the added neutron proper functions will have a plane node through all three alphas, satisfying the Pauli principle with the smallest amount of added kinetic energy. A similar argument as has been given for Be^8 leads to the energy of the neutron of $[B+2R+2Q]$. The interpretation of this formula is as follows: Since as far as the term B is concerned the neutron will interact with one alpha-particle at a time, this term will be the same as in He^5 and Be^9. On the other hand, in the interaction R, and for the proper functions which we are using also for the exchange term Q, the neutron at one alpha can interact simultaneously with the two neighboring alpha-particles. Therefore, these terms are multiplied by two for C^{13}.

We now wish to build O^{17} by adding a neutron to the tetrahedron constituting O^{16}. The wave function of the added neutron should have a node through each of the alpha-particles. This can no longer be done with one plane node. The added neutron will probably have least kinetic energy while satisfying the Pauli principle if a spherical node passes through the four alpha-particles.

It is not possible to calculate from our picture the energy of the neutron in O^{17} without introducing new constants. It follows, however, that the energy will be greater than $[B+3R+3Q]$, the value which would be obtained by extrapolating the energies of He^5, Be^9, and C^{13}. The different orientation of the nodes on different alpha-particles in O^{16} will make the wave-lengths of the neutron effectively shorter, and therefore the kinetic energy of the added neutron larger and its binding energy smaller.

Summarizing our results for nuclei of the $(4n+1)$ type, we have

$$\begin{aligned}
He^5-(He^4+n)&=B,\\
Be^9-(Be^8+n)&=B+(R+Q),\\
C^{13}-(C^{12}+n)&=B+2(R+Q),\\
O^{17}-(O^{16}+n)&>B+3(R+Q).
\end{aligned}$$

A comparison with experimental observations is given in Fig. 3; the mass-values used are those

[13] One might expect that for similar reasons $Q\ll B$ and also $R\ll B$. This however need not be true since the two terms $\int\psi_1 V_1\psi_1$ and $\int\psi_1 T\psi_1$ in B tend to cancel each other.

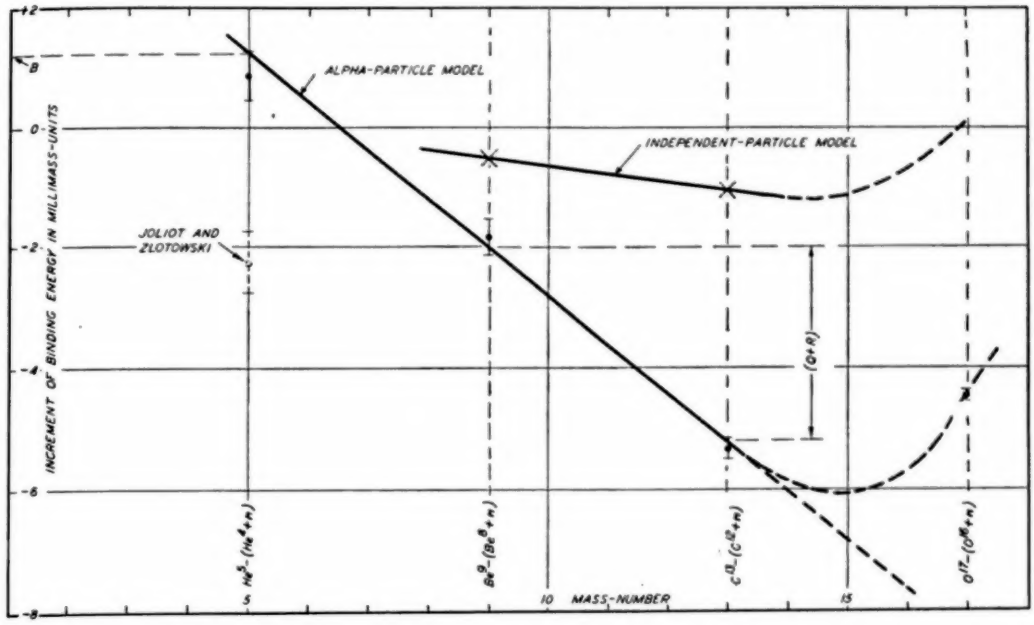

FIG. 3. Increments of binding energy for nuclei of $(4n+1)$ type.

of Livingston and Bethe.[14] This figure shows clearly the "break" in the curve at O^{17} which has been interpreted[4] as strong evidence for the independent-particle picture but which as we have seen is to be expected on the basis of the alpha-particle picture as well.

The experimental binding energies for He^5, Be^9, and C^{13} can be represented by the theory if we set $B=1.2$ Mev and $(R+Q)=-3.2$ Mev. The fact that $|R+Q|$ is actually greater than B makes our conclusions about the binding energies rather doubtful. If the presence of further alpha-particles modifies the binding of a neutron to one alpha-particle so strongly, it would seem necessary to include higher order approximations, that is, polarization terms in the calculation. However, even these extremely rough considerations account for the *trend* of the binding energies of the light nuclei as well as does the independent-particle picture. Similar statements hold for the nuclei of $(4n-1)$ type which we now proceed to discuss.

Nuclei of $(4n-1)$ type.—With our model we can treat nuclei of the $(4n-1)$ type by considering the missing particle as a "hole" and then proceeding just as in the case of the added particle. However, whereas the added particle was in a p state, with a node through the alpha-particle corresponding to the small probability of the neutron's being within the alpha-particle, the "hole" will be in an s state since it may be expected to be within the alpha-particle. Furthermore, whereas in the previous case we obtained a minimum energy for our model by arranging the wave functions of the added particle so as to have as few nodes as possible, in the present case we will get the lowest energy state for the entire nucleus by giving the "missing particle" as large an energy as possible.

For He^3 we have simply the energy $B=He^3-(He^4-n)$.

For Be^7 we have a case analogous to that of ionized molecular helium; the alpha-particles correspond to the closed shells of the two He atoms and the missing neutron correspond to the missing electron.[15] Guided by the requirement suggested above that the "missing particle" should have high energy, we proceed as in the case of Be^9 but choose $(\psi_1-\psi_2)$ as our wave function, in order to obtain the maximum

[14] M. S. Livingston and H. A. Bethe, Rev. Mod. Phys. **9**, 373 (1937); see however F. Joliot and I. Zlotowski, C. R. Acad. sci. **206**, 1256–1259 (1938) in regard to the mass of He^5.

[15] W. Weitzel and E. Pestel, Zeits. f. Physik **56**, 197–214 (1929).

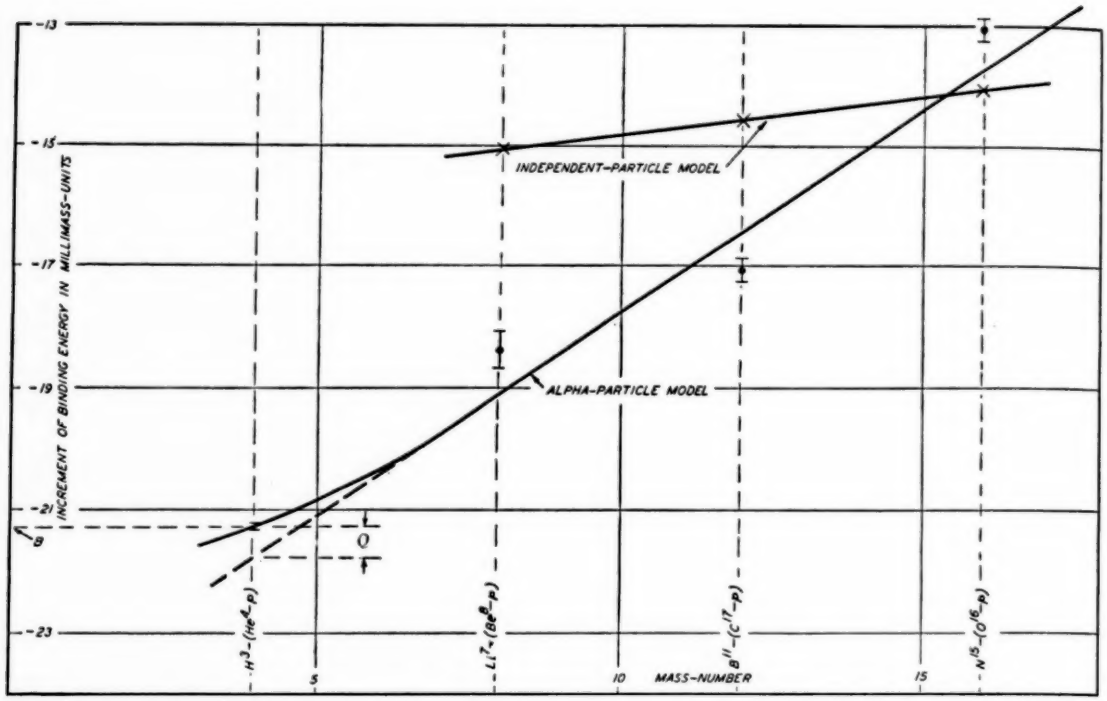

FIG. 4. Increments of binding energies for nuclei of $(4n-1)$ type. (The superscript to the carbon symbol should be 12.)

number of nodes. We evaluate

$$\bar{E}(\psi_1-\psi_2)=\frac{\int(\psi_1-\psi_2)H(\psi_1-\psi_2)}{\int(\psi_1-\psi_2)^2}$$

and find $(B-Q+R)$ as the binding energy for $Be^7-(Be^8-n)$; the negative sign in front of the exchange integral Q is due to the change in the sign of ψ_2. For the missing particle case, however, Q will probably be positive, so that $(B-Q+R)$ rather than $(B+Q+R)$—corresponding to $\psi_1+\psi_2$—will represent the lowest possible energy.

For the cases C^{11} and O^{15}, we assume again that Q is positive. We find then from group theory

$$\psi_1-(\psi_2+\psi_3)/2 \quad \text{and} \quad \psi_1+\psi_2-(\psi_3+\psi_4)$$

for proper functions corresponding to the lowest energies. The first of these functions, corresponding to C^{11}, is one of a twofold degenerate set and leads to the energy $(B-Q+2R)$. The second function corresponding to O^{15} is threefold degenerate and gives $(B-Q+3R)$. It will be seen that the exchange term remains constant regardless of the number of alpha-particles. This is due to the fact that by choosing, the wave function with a node between two alpha-particles, the third alpha-particle in the case of C^{11}, and the third and fourth alpha-particles in the case of O^{15}, lie on this node and therefore do not contribute to the exchange energy. It may be worth while to point out that, since for the case of O^{15} a spherical node such as was needed for O^{17} is not required, the break in the linear relation at O^{15} is not to be expected in the missing particle case.

A comparison with the experimentally observed values of the binding energies of nuclei of this type is given in Fig. 4. In view of the incompleteness of the data for "missing-neutron" elements, the equivalent "missing-proton" elements are used instead. According to theory the points for Li^7, B^{11} and N^{15} should lie on a straight line, whereas the point for H^3 not containing an exchange term should lie above the line by an amount Q. The agreement with experiment for the alpha-particle model obviously is not good but is certainly no worse than that given by the independent-particle model, for which the data were taken from Table V of Feenberg and Wigner.[16]

[16] E. Feenberg and E. Wigner, Phys. Rev. **51**, 95–106 (1937).

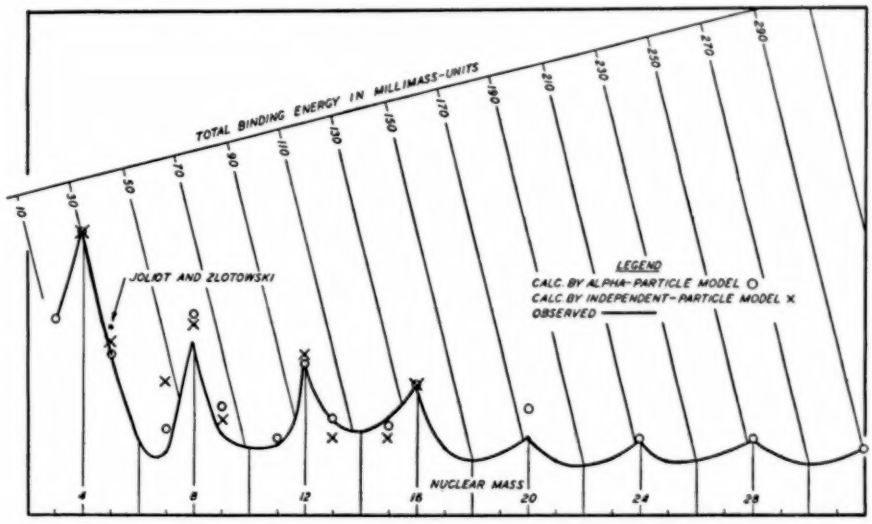

FIG. 5. Comparison of calculated and observed binding energies.

While it is not the purpose of this paper to emphasize detailed agreement with experiment, since we believe that calculations based on either model are too inaccurate to give quantitative results, we include Fig. 5 as a summary of the results so far obtained by each theory for the fundamental states. The data for the independent-particle model were obtained from Fig. 1 in the paper by Feenberg and Phillips.[17] For each model the total number of arbitrary constants used in fitting the experimental curve is large. For the alpha-particle model we determined from the experimental data constants B, R, and Q, both for the added particle and for the hole, and the mass defect of the alpha-particle, as well as the "binding energy per bond" for the saturated nuclei, making a total of eight parameters. For the independent-particle model[16] the parameters are as follows: A, α, G_1, G_3, and two from the linear correction function, making a total of six.

SECTION II

Nuclear rotation, symmetry, excited states

In the previous section nuclear proper functions have been described insofar as they bear upon the *relative* positions of alpha-particles, added neutron or proton, or missing neutron or proton. These proper functions have given us rough values of the binding energies. But if we inquire into the symmetry properties of the states in question, it will be necessary to add the description of the proper functions as depending on the orientation of the nuclear constituents in space, that is, it will be necessary to consider nuclear rotation.

This consideration will yield as a by-product some information on excited nuclear states. Further excited states would be obtained if we would include in our discussion the nuclear vibrations. However, the lowest excited levels will, as a rule, be rotational levels.

The considerable quantitative differences between theory and experiment as found in Section I indicate that no great emphasis can be laid upon the calculated spacing of excited states. Therefore the symmetry properties of both the fundamental and the excited states are of primary interest to us.

Saturated nuclei of 4n-type.—For this simple case, which we include for completeness, the results of Wheeler[4] are represented. As indicated by Wheeler, the rotational levels may be obtained very simply by comparison with the analogous molecules.

For Be^8 we have the case of a diatomic molecule, for which the energy is given by

$$E_J = (\hbar^2/2I_{Be})J(J+1).$$

However, since the alpha-particles obey Bose

[17] E. Feenberg and M. Phillips, Phys. Rev. **51**, 597–608 (1937).

statistics, and the antisymmetrical ψ-functions for $J=1, 3, 5 \cdots$ are therefore excluded, only values of $J=0, 2, 4 \cdots$ will be allowed. From the fact that reflection at the center of symmetry exchanges the two alpha-particles, we conclude that all states are even.

For C^{12} we have the case of a symmetrical top for which

$$E_{JK}=\frac{\hbar^2 J(J+1)}{2I_{\mathrm{Be}}}-\frac{\hbar^2 K^2}{4I_{\mathrm{Be}}}.$$

J is the quantum number for the total angular momentum, while K is the component of J about the figure axis, that is, about the axis perpendicular to the plane of the three alpha-particles. I_{Be} is, as above, the moment of inertia of Be. In our formula it has been implicitly assumed that the separation of the alpha-particles in Be^8 and C^{12} is the same. Since, as above, only symmetrical ψ-functions are allowed by the requirement of Bose statistics, K must be a multiple of 3. J, being the absolute value of the length of a vector, must be zero or positive. K, however, being a component of J, can be either positive or negative, but its absolute value must be smaller than or equal to J. For the case of $K=0$, that is, no rotation about the figure axis, J can have only even values just as in the case of Be^8. When $K\neq 0$, however, J may have any positive value greater than or equal to $|K|$.

The states will be odd or even according to whether K is odd or even.[18]

In the case of O^{16} we have a spherical top for which all moments of inertia are equal. Also from the tetrahedral arrangement we may conclude that $I_{\mathrm{oxygen}}=2I_{\mathrm{Be}}$ so that

$$E_J=\hbar^2 J(J+1)/4I_{\mathrm{Be}}.$$

From group theory one may find that all values of J are allowed except $J=1$, 2, and 5.

The states will be even for $J=0$, 4, and 8, and odd for $J=3$, 7, and 11. For the remaining allowed J values there will be both even and odd states with equal rotational energies.

Nuclei of $(4n+1)$ type

He^5 *or* Li^5.—From our point of view we cannot consider excited states of He^5 or Li^5 for, as in the monatomic molecule, there will be no rotational states. The fundamental state will have $J=1$ and will be odd, that is, it will have the same symmetry properties as in the independent-particle picture.

Be^9 *or* B^9.—The node of the neutron wave function through the two alpha-particles means that there is an angular momentum $\hbar$ of the neutron around the axis connecting the two alpha-particles and therefore we have the lowest state $J=1$, that is, a P state.

The excited states may be obtained by analogy with a diatomic molecule with a π_u electron, for which the nuclei obey Bose statistics. The rotational energies will be roughly given by the formula which held for Be^8. The wave function will be symmetric in the alpha-particles. Two cases arise, because the plane of the neutron wave function may be either (*a*) parallel or (*b*) perpendicular to the axis of rotation. For case (*a*) odd values of J will be permitted; the neutron function changes sign on an interchange of alpha-particles by rotation. For case (*b*) even values of J will be permitted, since now the neutron function does not change sign. All values of $J\geqq 1$ will therefore be allowed. By reflection at the center of symmetry we find no change due to the alpha-particle wave function but a change of sign due to reflection of the neutron wave function which has a node through the center. Therefore all states are odd.

O^{13} *or* N^{13}.—The rotational energies are roughly given by the formula for C^{12}. The former rule that K must be a multiple of three remains valid, because rotation about the figure axis has no effect on the neutron wave function. As in the case of C^{12}, all values of J are allowed for $K\neq 0$.

For $K=0$, the axis of rotation is perpendicular to the figure axis. As in the pure alpha-particle case, an interchange of two alpha-particles must not cause a change in sign. Such interchange of two alpha-particles can be performed by rotating through 180° around an axis passing through one of the alpha-particles and the midpoint between the other two alphas. Such a rotation, however, will also act on the neutron proper function. Since the neutron has a node in the plane of the three alphas it will change its sign. Symmetry with regard to the interchange of two alpha-particles will be obtained, therefore, whenever the rotation through 180° produces a

[18] This may be seen by rotating through π around the figure axis and reflecting in the plane of the alpha-particle.

change of sign, that is, for $K=0$ only odd values of J are allowed.

Because of the influence of the added neutron with its node, there will be even states for odd K values and odd states for even K values.

O^{17} *or* F^{17}.—The added particle will have spherical symmetry and therefore there will be no change in the conditions governing the rotations.

Since an even (spherically symmetrical) proton or neutron is added, the parity of the states will be the same as for O^{16}.

Nuclei of $(4n-1)$ type

Li^7 *or* Be^7.—As in the case of binding energies, we again may choose as our proper function either $(\psi_1+\psi_2)$ or $(\psi_1-\psi_2)$. In our consideration of the fundamental states we were guided in our choice by the fact that we wished to find the lowest possible state. This enabled us to select the $(\psi_1-\psi_2)$ for the "missing particle" case. For excited states both possibilities should be considered. Now the difference between the two cases manifests itself by a change in sign of the exchange integral Q as we have seen above, so that the separation in energy levels calculated for the two cases will be

$$[B+Q+R]-[B-Q+R]=2Q,$$

to which a contribution arising from the rotation must be added. As may be seen from the sequence for the binding energies in the missing particle case, the magnitude of the exchange term Q may be determined, in principle, from the observed binding energies, as shown in Fig. 4. (Q for the added particle case cannot be determined separately, for it appears only in the combination with R.) Actually the errors in the data are too great to permit any conclusion except within wide limits. It is possible that the Li^7 doublet[19] is due to the two states $(\psi_1+\psi_2)$ and $(\psi_1-\psi_2)$. An explanation of this doublet has been proposed by Inglis[20] but this suggestion does not seem to account for a variation in the relative intensity of the two groups with voltage which has been observed.[21] Such a variation, however, is not surprising if the explanation suggested by the alpha-particle model is accepted.

Restricting the discussion of nuclear rotation to the $(\psi_1-\psi_2)$ case, we have a proper function with a node between the two alpha-particles. Except for different values for the moments of inertia this problem is therefore the same as that for C^{13} for $K=0$ which has already been considered. The allowed states will be $J=1, 3, 5, 7 \cdots$, with the fundamental state a P state. The rotational energies are roughly given by the Be^8 formula. All states will be odd.

The analogous molecular case for He_2^+ has been investigated by Weizel and Pestel,[15] who found in this case that experimentally only states with odd values of J actually occur.

Considerations regarding the magnetic moment of the Li nucleus, as obtained with the aid of the alpha-particle model, have been given by Bethe.[22]

C^{11} *or* B^{11}.—For this case the proper function of the "hole" in the field of fixed alpha-particles must be considered more closely. The transformation properties under the effect of rotation through $2\pi/3$ and $4\pi/3$ around the figure axis are the same as those of a proper function for a particle with unit angular momentum. Thus unity must be added to, or subtracted from, the angular momentum of the alpha-particles around the figure axis. The latter will be, just as for C^{12}, a multiple of three, so that K for the missing particle case must differ from a multiple of three by ± 1. This means that K can be any integer not divisible by three.

We have seen that the proper function of the "hole" transforms as though it had unit angular momentum. Nevertheless, the actual mean value of the angular momentum of the "hole" will be smaller than $\hbar$. If we assume it to be small as compared to $\hbar$, the formula for rotational energies of C^{12} will hold roughly also for C^{11} and B^{11}. The actual values for the rotational energies, shown in Fig. 6, are obtained from that formula. If, however, the mean angular momentum of the "hole" is not small as compared to $\hbar$, interaction between the orbit of the "hole" and the rotation may influence the rotational energy considerably.

All values of $J \geqq |K|$ will be allowed with $J=1$, $K=1$ the fundamental state.

The states will be even if K is even and odd if K is odd.

[19] L. H. Rumbaugh and L. R. Hafstad, Phys. Rev. **50**, 681–689 (1936).

[20] D. R. Inglis, Phys. Rev. **50**, 783–784 (1936).

[21] L. H. Rumbaugh, R. B. Roberts, and L. R. Hafstad, Phys. Rev. **51**, 1013 (1937). J. H. Williams, W. G. Shepherd, and R. O. Haxby, Phys. Rev. **52**, 390–396 (1937). L. H. Rumbaugh, R. B. Roberts, and L. R. Hafstad, Phys. Rev. **54**, 649–672 (1938).

[22] H. Bethe, Phys. Rev. **53**, 842 (1938).

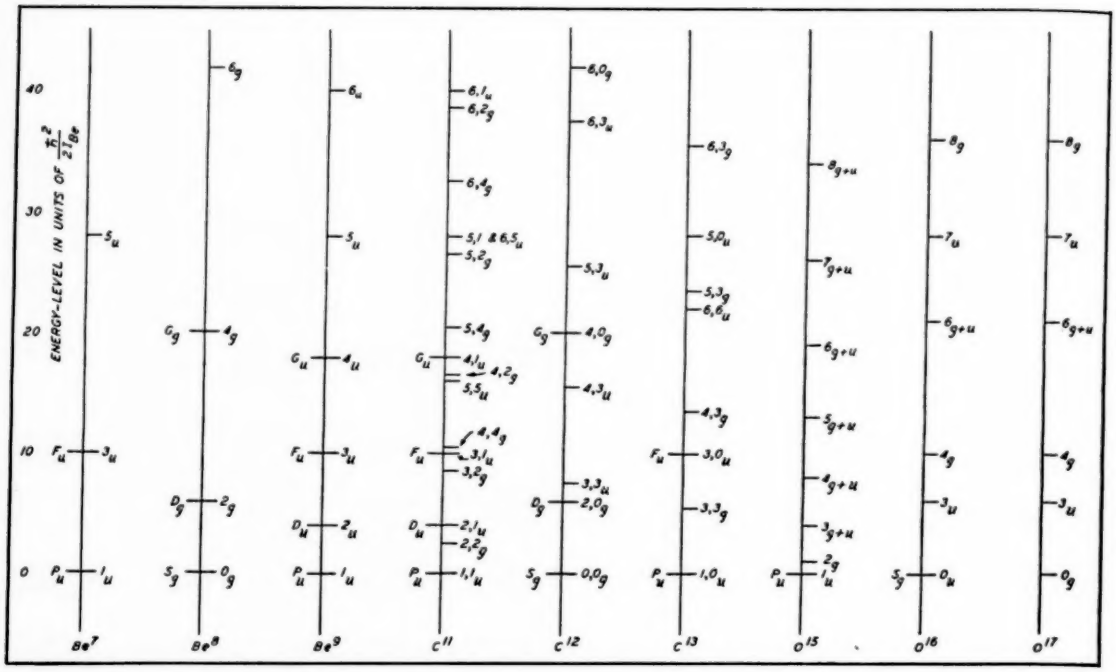

FIG. 6. Excited states of nuclei: Comparison of independent-particle model (left) to alpha-particle model (right) with energy scales adjusted to agree with D level of Be^8 ($_g$=even, $_u$=odd).

O^{15} *or* N^{15}.—Because the proper function of the "hole" transforms as that of a particle with an angular momentum unity, the state $J=0$ cannot occur. All others can.

If the mean angular momentum of the "hole" is small compared to $\hbar$, the formula for the rotation of O^{16} will roughly be applicable. Otherwise the coupling between rotation and the orbit of the "hole" must be taken into account.

The state with $J=1$ will be odd (this is the fundamental state) and that with $J=2$ will be even. States for higher J values will occur with both even and odd parity.

For convenient comparison, the permitted energy states of the various nuclei are shown in Fig. 6. The fundamental states have been assumed to have the energy zero. Actually the rotation will contribute in some cases to the energies of the fundamental states. These contributions are, however, in view of the discrepancies found in Section I, too small to be worth discussion. The excited level system predicted by the alpha-particle model (rotations only) are given to the right of the line for each element of Fig. 6, the numbers indicated referring to J when only one number is given and to the quantum numbers J and K, respectively, when two numbers appear. The levels predicted by Feenberg and Phillips,[17] taken from their Table III, are given on the left. The parity of the levels is indicated for both models.

The ordinate scale for the alpha-particle model is given in units of $\hbar^2/2I_{Be}$. This scale is fitted to that of Feenberg and Phillips by arbitrarily identifying their D level in Be^8 with our ($J=2$) level. From their Table I it may be seen that their K is exactly equal to two of our units.

It is significant that the symmetry of the fundamental states, as well as that of many of the excited states, are the same for the two models. The agreement for the nuclei Be^7, Be^8, and Be^9 is particularly good. For C^{11}, C^{12}, and C^{13} additional low excited states occur in the alpha-particle picture. They have the opposite parity as the levels obtained from the independent-particle picture. For O^{15} and O^{16} no low excited states are predicted by the independent-particle picture, whereas the alpha-particle model gives some low rotational states. These differences may tend to diminish if in the independent-particle picture excitation of neutrons or protons into higher orbits is taken into account.

An X-Ray Test of Superstructure in $FeNi_3$

F. E. HAWORTH
Bell Telephone Laboratories, New York, N. Y.

(Received September 12, 1938)

A search has been made for superstructure in permalloy of composition near $FeNi_3$. Curves of x-ray scattering power near the absorption edges of Ni and Fe show that Fe $K\beta$-radiation should give the strongest superstructure lines, and calculations indicate that reflection from (321) planes of a perfectly ordered structure should have about one-seventh the intensity of the ordinary (222) reflection. The specimen was a powdered alloy containing 70 percent nickel, annealed at 1000°C and baked at 425°C. It was placed in a focusing camera in a beam of Fe $K\beta$-rays which were selected and concentrated by a curved rocksalt crystal, and exposed for one hundred hours. No superstructure lines appeared, although superstructure in β-brass was easily detected with similar technique. This negative result, which is supported by a considerable amount of indirect evidence, indicates that no long range order exists in $FeNi_3$.

INTRODUCTION

IN the iron-nickel series of solid solutions the region from 65 to 81 percent nickel has been of outstanding interest because of the extremely high permeabilities developed by suitable heat treatments. The composition at 78.5 percent nickel has long been the standard permalloy, and the highest permeability ever reported[1] (1,330,000) was in a single crystal of permalloy of 65 percent nickel content, the same composition yielding the highest permeability for polycrystalline material.[2] Since this region includes the composition at 75 atomic percent nickel, it has been suggested for many years that the properties might be affected by the formation of a superstructure at $FeNi_3$. Such a structure is very difficult to detect by means of x-ray diffraction because iron and nickel have nearly equal scattering powers. Jette and Foote[3] looked for it in alloys of 79.4 and 66.8 percent nickel, but found no indication of superstructure lines.

However, considerable indirect evidence has appeared which strongly indicates such a superstructure. Dahl[4] has studied the effect of plastically deforming some iron-nickel alloys and found that at 35 and 100 percent nickel changes in resistivity produced by cold working an annealed specimen amounted to only one or two percent, while in the region between these compositions the effect was greater, reaching a maximum of some 34 percent at 75 atomic percent nickel. In this same region quenching also produced resistivities considerably higher than those of the annealed specimens. This is similar to the behavior of some alloys known to have superstructures, notably Cu_3Au. Two cases of large changes in resistivity with cold work where no superstructure exists are known in tungsten, with 50 percent change, and molybdenum, with 18 percent change, but as pointed out by Nix and Shockley[5] these are rather brittle substances and may not be strictly comparable with the more plastic alloys.

Another strong support for the superstructure theory occurs in the specific heat measurements of Kaya.[6] He found a sharp maximum between 500°C and 600°C in the specific heat of the aged alloy, while for the quenched alloy the maximum was much lower. Additional indications of superstructure in $FeNi_3$ are found in the measurements of the lattice spacings of the Fe–Ni series.[7] It was found that from 45 to 100 percent nickel the lattice spacing departed from the linear relation with composition, the change being a slight decrease with a maximum at about 78 percent nickel.

On the other hand, in the few cases in which magnetic measurements have been made on ordered structures exhibiting ferromagnetism, the change from order to disorder is accompanied

[1] R. M. Bozorth, J. App. Phys. **8**, 575–88 (1937).
[2] Joy F. Dillinger and Richard M. Bozorth, Physics **6**, 279–284 (1935).
[3] Eric R. Jette and Frank Foote, *Metals Technology*, Tech. Pub. No. 670 (1936).
[4] O. Dahl, Zeits. f. Metallkunde **28**, 133–138 (1936).
[5] Foster C. Nix and William Shockley, Rev. Mod. Phys. **10**, 57 (1938).
[6] Seiji Kaya, J. of the Faculty of Science, Series II, Vol. II, No. 2, Hokkaido Imperial University, Sapporo, Japan.
[7] A. J. Bradley, A. H. Jay, and A. Taylor, Phil. Mag. **23**, 545–557 (1937); E. A. Owen, E. L. Yates, and A. H. Sully, Proc. Phys. Soc. **49**, 318 (1937).

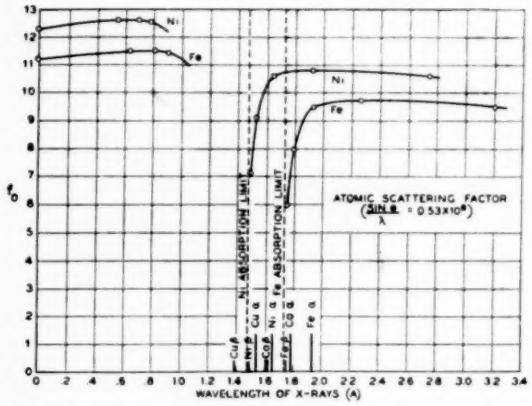

FIG. 1. Atomic scattering factors of Fe and Ni as a function of wave-length. On the wave-length scale are marked the positions of the $K\alpha$- and $K\beta$-rays from Cu, Ni, Co and Fe.

by changes in the saturation magnetization at room temperature and in the Curie point. This is especially true of those which in the disordered state have no ferromagnetism, such as Ni_3Mn and the Heusler alloy Cu_2MnAl. In the 70Ni permalloy no significant change in saturation magnetization has been found on comparing the annealed with the hard worked alloy.

All of these are indications only, not direct proof, and hence it appeared desirable that a more exhaustive test be made. Recent improvements in methods have increased the probability of obtaining x-ray diffraction lines characteristic of superstructures in cases formerly considered out of the question, and the present work was undertaken to apply these methods to $FeNi_3$. This involved choice of the x-rays of the most suitable wave-length, selecting and concentrating them into as intense a beam as possible, and using a focusing camera covering the reflection angle in which lies the strongest superstructure line.

Choice of Radiation

The difference in x-ray scattering powers of two neighboring elements may be increased if advantage is taken of the fact that near the absorption edge of an element its scattering power is greatly decreased. This was used by Mark and Szillard[8] in a study of KBr, by Bradley and Rodgers[9] in demonstrating superstructure in a Heusler alloy, and recently by Jones and Sykes[10] on β-brass. By using Zn $K\alpha$-radiation the latter were able to increase the difference between the atomic scattering powers of Cu and Zn from about 0.6 to 2.1, thus increasing the intensity of the superstructure lines by a factor of about twelve.

In Fig. 1 is shown the atomic scattering curve of Ni as determined by Jesse,[11] together with a corresponding curve for Fe, derived from it. From this it is seen that the Fe $K\beta$-radiation, which is very close to the iron absorption edge, is scattered with the greatest difference. Recently Bradley and Taylor[12] have reported that they used Co $K\alpha$-radiation in a test for superstructure of $FeNi_3$ and found no indication of any. Co $K\alpha$ gives a reflecting power for the superstructure lines somewhat less than half that for the Fe $K\beta$. Jette and Foote[3] and Kaya[6] both used Ni $K\alpha$-radiation in their studies. This wave-length lies between the absorption limits of iron and nickel and hence is strongly absorbed by iron. Very little is known of the scattering curve on the short wave-length side of the absorption limit because the reflections are weak and the background scattering high. Hence Ni $K\alpha$-radiation is very unsuitable and might even lie close to where the two curves cross, thus giving a difference in scattering power less than that for any other radiation which might be chosen.

Calculations were made of the relative intensities of all possible reflections of Fe $K\beta$-radiation from $FeNi_3$, allowing for absorption in the specimen and the effect of temperature.

TABLE I. *Calculated intensities for* $FeNi_3$.

		Intensity				Intensity	
$h\,k\,l$	θ	Ord. Line	S. S. Line	$h\,k\,l$	θ	Ord. Line	S. S. Line
100	14.3		5.4	300|221	47.7		14.3
110	20.4		8.3	310	51.3		13.3
111	25.3	703		311	54.9	1140	
200	29.6	402		222	58.7	435	
210	33.4		11.2	320	62.8		21.6
211	37.2		10.6	321	67.3		58.7
220	44.3	499		400	80.6	1350	

[8] H. Mark and L. Szillard, Zeits. f. Physik **33**, 688–691 (1925).

[9] A. J. Bradley and J. W. Rodgers, Proc. Roy. Soc. Lond. **A144**, 340 (1934).

[10] F. W. Jones and C. Sykes, Proc. Roy. Soc. Lond. **A161**, 440 (1937).

[11] Williams P. Jesse, Phys. Rev. **52**, 443–451 (1937).

[12] A. J. Bradley and A. Taylor, Proc. Roy. Soc. **166**, 353–375 (1938).

These are given in Table I, and show that the reflection from the (321) planes should be the superstructure line easiest to detect.

Experimental

The apparatus consisted of a Phillips-Metalix x-ray tube with Fe target, a bent curved crystal of rocksalt to select and concentrate the Fe $K\beta$-radiation, and a symmetrical focusing camera. These were arranged as shown in Fig. 2, a more complete description being given in an earlier paper.[13] The specimen was prepared from permalloy containing 70 percent nickel by filing powder from a quarter-inch bar. This was mixed with sufficient quartz dust to prevent sintering and annealed for 1 hour at 1000°C and then for 5 hours at 425°C. The powder was spread on a curved brass strip, and mounted on the circumference of the camera. The angular range covered by the camera was such that the (311), (222), (320), (321) and (400) reflections could be recorded. The film was exposed in this position for 100 hours and then taken out and cut in half. About an inch was cut off the end of one half and then this half was replaced in the camera with its position shifted one inch and re-exposed for about five hours. The two sections of film were then developed and fixed together. The second exposure gave reflections from the (311) and (222) planes of intensities equal to and about one-third of the expected intensity of the (321)

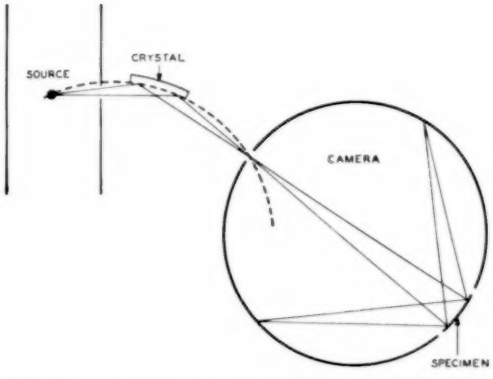

Fig. 2. Arrangement of apparatus. The Fe $K\beta$-rays from the source are brought to a focus by the bent and cut rocksalt crystal at the camera circumference. They then diverge to the specimen and after reflection are refocused at the film.

[13] R. M. Bozorth and F. E. Haworth, Phys. Rev. 53, 538–544 (1938).

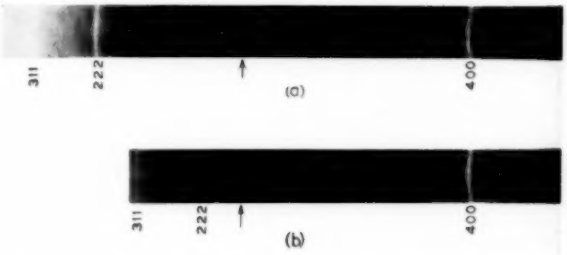

Fig. 3. X-ray diffraction pattern of $FeNi_3$ exposed to Fe $K\beta$-rays for 100 hours. Section (a) is one half as originally exposed; section (b) is the other half after cutting off the end and re-exposing for five hours in a different position, giving the fainter (311) and (222) reflections as shown. The (321) superstructure lines would be at the points indicated by the arrows and should be as intense as the (311) line on section (b) and three times as intense as the (222) line on section (b).

superstructure line, on a background of like intensity. No reflections from the (321) planes or the (320) planes could be observed although the five-hour exposure of the (222) reflection, which should have only one-third the intensity of the (321) reflection, is very plainly visible and the five-hour (311) reflection, which should be equal in intensity to the (321) reflection, has considerable intensity. The two halves of this film are reproduced unretouched in Fig. 3.

This film was the culmination of many attempts to detect superstructure lines in $FeNi_3$. In one of these the material was rolled into strips, annealed for one hour at 1000°C, and then for 100 hours at 425°C. This gives the crystallites a preferred orientation, and advantage was taken of this to set it at just the proper angle to give a maximum reflection from the (321) planes. After an exposure of 70 hours no (321) reflection appeared. As a further check of the technique some β-brass was prepared, and given sixteen hours exposure to Cu $K\beta$-radiation by the method first described. The superstructure line from the (320) planes was observed, although by calculation its intensity should be only *one twenty-eighth* that of the expected (321) reflection from the $FeNi_3$. The β-brass was given another exposure of sixty-four hours to have the reflection strong enough for reproduction and this is shown in Fig. 4.

Thus it seems reasonable to conclude from these experiments that no superstructure exists in $FeNi_3$ of sufficiently long range to form an x-ray diffraction pattern.

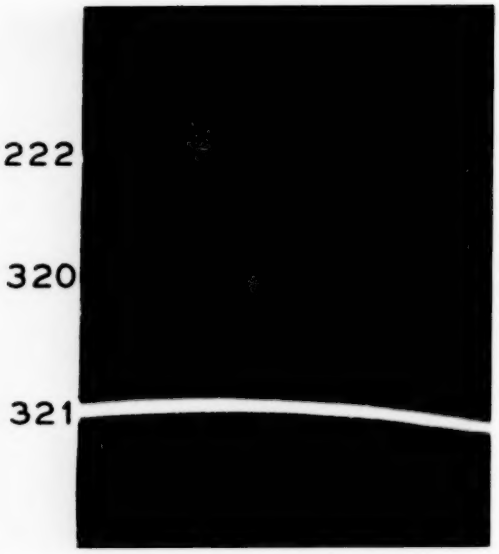

FIG. 4. X-ray diffraction pattern of Cu Zn exposed to Cu $K\beta$-rays for 64 hours. The superstructure line is the one marked (320).

DISCUSSION

There still exists the possibility that there is order in $FeNi_3$ of such a short range that no diffraction lines could be obtained, and no definite statement can be made of whether this would produce the observed change in resistivity. In the Cu_3Au alloy Sykes and Jones[14] found that for all treatments which gave it resistivities such that ordering would be expected, superstructure lines were found, and from this it seems logical that ordering sufficient to produce detectable superstructure lines and ordering sufficient to affect resistivity are concomitant, but there are not sufficient data to establish such a generalization.

Another criterion which may be useful in such problems and which I have not yet seen proposed in the literature is this: It is well known that for materials in which no superstructure exists, Matthiessen's rule is obeyed when the annealed material is cold worked, i.e., the slope of the resistivity *vs.* temperature curve does not change; this is true even for tungsten[15] which changes its resistivity by as much as 50 percent when cold worked; but for all cases of definite superstructures for which resistivity-temperature curves are reported in the literature, Matthiessen's rule is *not* obeyed in changing from the ordered to the disordered state. These data are listed in Table II.

There appear to be no data available on resistivity *vs.* temperature for cases in which superstructure is destroyed by cold work, but Dahl[4] has found that cold working the quenched Cu_3Au alloy changed its resistivity by less than

TABLE II. *Comparison of materials with and without superstructure with respect to Matthiessen's rule.*

Materials	$d\rho/dT$ (ohm cm/deg.) $\times 10^5$			Percent Change	Reference
	Quenched	Cold Worked	Annealed		
With Superstructure					
Cu_3Au	0.68		1.12	+65	16
CuAu	0.64		0.96	+50	17
Cu_3Au	0.74		1.03	+39	18
CuAu	0.90		1.28	+42	18
38% Pd, 62% Cu	0.40		0.59	+47	18
Ni_3Mn	1.2		5.8	+380	19
Without Superstructure					
W		2.60	2.64	+1.5	15
Mo		2.69	2.67	−0.7	15
Ni		5.10	4.97	−2.5	15
Pt		4.13	4.17	+1.0	15
Ni				+0.1	20

[14] C. Sykes and F. W. Jones, Proc. Roy. Soc. **A157**, 213 (1936).
[15] W. Geiss and J. A. M. v. Liempt, Zeits. f. Physik **41**, 867 (1927).
[16] C. Sykes and H. Evans, J. Inst. Metals **58**, 255 (1936).
[17] U. Dehlinger and L. Graf, Zeits. f. Physik **64**, 359 (1930).
[18] G. Borelius, C. H. Johansson and J. O. Linde, Ann. de Physik **86**, 291–318 (1928).
[19] S. Valentiner and G. Becker, Zeits. f. Physik **93**, 795–803 (1935).
[20] Heinz Bittel, Ann. de physique **31**, 219 (1938).

two percent, thus indicating that it is similar in properties to the quenched alloy.

The curves from which the values of $d\rho/dT$ for the ordered state were taken probably do not represent complete order, but for complete order the slope should be greater if any different. This may be shown by a consideration of the Cu_3Au curves, those of Sykes and Evans being reproduced in Fig. 5. On the basis of Peierls[5] application of Bethe's theory to alloys of type AB_3, the value of the critical temperature is,

$$T_c = 1.33E_0/R,$$

where E_0 is the energy of transformation from perfect order to randomness. The temperature at which the equilibrium curve departs appreciably from perfect order is $T=0.75E_0/R$. Since T_c for Cu_3Au is 654°K (381°C), T will be 368°K or 95°C. Therefore at room temperature any departure from perfect order should be due to failure to attain equilibrium rather than destruction of ordering by thermal agitation. And since we should expect the curve to be nearer equilibrium at the higher temperatures, if the experimental curve (A) of Fig. 5 is not the equilibrium curve, we should expect the latter to look more like (B), than like (C). In other words, if the material is not in equilibrium, the slope of the curve at room temperature should lie *between* that of the completely disordered state and the equilibrium curve. Hence if the changes of slope recorded in Table II are for the conditions for which equilibrium is not attained, the changes are less than the true values and Matthiessen's rule would be violated even further at equilibrium.

Resistivity data on the permalloy specimens used in the present experiments were taken by Dillinger[21] and confirmed Dahl's measurements of the change in resistivity with cold working. At the same time data were taken on $d\rho/dt$, but not published. He found that for the cold rolled specimen $d\rho/dt$ was 9.3×10^{-8} ohm cm/deg. and for the specimen annealed at 460°C it was 8.5×10^{-8}, a *decrease* of about 8.6 percent. Thus it does not obey Matthiessen's rule closely, but the fact that the change is small compared to those in the known superstructures and in the

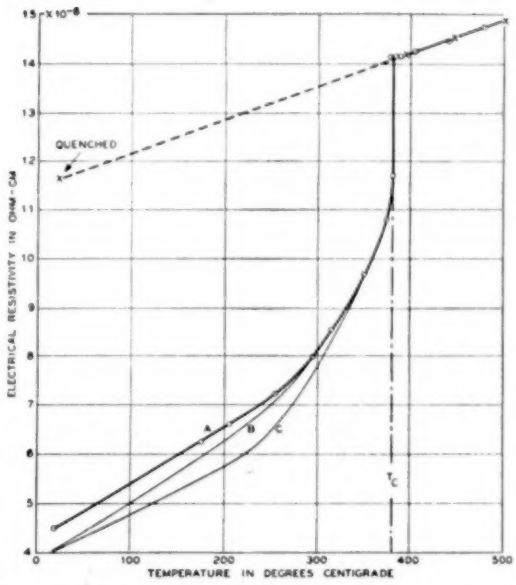

FIG. 5. Electrical resistivity-temperature curve for Cu_3Au. The experimental curve is marked A, and is in equilibrium at temperatures above 350°C.

opposite direction is indicative of the absence of superstructure.

The measurements of Kaya[6] on the specific heat of an alloy containing 24.1 percent iron provide such strong evidence of ordering that they will be considered in some detail. He found that the additional energy under the large maximum of the curve for the aged alloy was 14.57 cal./g while for the quenched alloy it was only 2.09 cal./g. His assumption was that the former represented the energy associated with the disappearance of ordering plus that of the magnetic transformation, while the latter was due to the magnetic transformation only. In accord with this idea was a calculation of the energy of ordering after the theory of Bragg and Williams, from which,

$$Q = RT_c/2.26M = 11.7 \text{ cal./g},$$

in which T_c is taken as 773° (500°C), and M is the atomic weight. But the theory as modified by Peierls for application to structures of the AB_3 type yields instead

$$Q = RT_c/1.33M = 19.0 \text{ cal./g}.$$

Stoner[22] has considered very carefully the energy change due the magnetic transformation in pure nickel as obtained from specific heat measure-

[21] J. F. Dillinger, Phys. Rev. **49**, 862 (1936).

[22] Edmund C. Stoner, Phil. Mag. **22**, 81–106 (1936).

TABLE III. *Properties of* $FeNi_3$ *for which a change by long range order would be expected and the results as known.*

PROPERTY	CHANGE	INDICATION
Resistivity, ρ	Increase on cold working or quenching	Ordering
$d\rho/dT$	−8.5% on annealing the cold worked alloy	No ordering
Magnetic saturation at room temperature	No change	No ordering
Magnetic permeability	High on quenching	None
Specific heat	15 cal./g peak	Ordering or magnetic transformation
X-ray diffraction	No superstructure lines	No long range ordering

ments, and obtains 191 cal./g-atom = 3.3 cal./g. Since from theoretical considerations one would expect the energy to vary directly with the Curie temperature and the saturation magnetization, for $FeNi_3$ the energy should be

$$Q = 3.3(870/630)(12200/6100) = 9.1 \text{ cal./g.}$$

This shows that if long range order is present we should expect the specific heat measurements to give a value of about 28 cal./g, while if it is absent a value of about 9 cal./g. Thus there is reason to expect that Kaya's value for the aged specimen, 15 cal./g, can be explained by the magnetic transformation. In this case the value for the quenched material is too small and is difficult to understand.

Kaya points out also that if there is ordering in $FeNi_3$, the high permeability is associated not with its presence but with its prevention, since the high permeability is produced by rapid cooling or quenching, and is reduced on aging. This effect would be in the direction opposite to the usual result; e.g. in Ni_3Mn the permeability at room temperature is increased by ordering.

The properties of $FeNi_3$ which one would expect to be affected by long range order and the results as known to date are summarized in Table III.

Thus the negative result of the x-ray work indicates definitely that no long range order exists in $FeNi_3$, and this nonexistence is supported by a considerable amount of less direct evidence.

The author wishes to acknowledge his indebtedness to Drs. R. M. Bozorth, F. C. Nix, and W. Shockley for many valuable discussions.

NOVEMBER 1, 1938 PHYSICAL REVIEW VOLUME 54

A Determination of e/m from the Refraction of X-Rays in a Diamond Prism

J. A. BEARDEN
Rowland Physical Laboratory, The Johns Hopkins University, Baltimore, Maryland

(Received August 29, 1938)

Measurements of the index of refraction of the copper K_β line by a diamond prism have been made with an estimated accuracy of one part in 10,000. These measurements together with the quantum theory of dispersion and the ruled grating wave-length of the copper K_β line afford a method of evaluating e/m with an accuracy comparable to that of previous determinations by other methods. The value of e/m is given by the equation

$$\frac{e}{m} = \delta\left[\frac{\lambda^2 \rho F}{2\pi W}\sum_1^s N_s\{1+A\}\right]^{-1},$$

where δ, λ, ρ, R, N_s and W have their usual meaning and A is the factor which takes into account the electronic binding. For carbon and a $\lambda^{2.75}$ law of absorption, the value of the $\sum_1^s = 6.0163 \pm 0.0006$. Using $\delta = 9224.4 \times 10^{-9}$, $W = 12.0148$, $\rho = 3.5154$, $F = 96513.1$, $\lambda = 1.39220$A, one obtains $e/m = (1.7601 \pm 0.0003) \times 10^7$ e.m.u. This bound electron value is higher than most previous spectroscopic determinations but is in excellent agreement with the free electron results of Dunnington.

IN the present unsettled state of the values of the fundamental constants it is of importance to determine the value of each constant by as many different methods as possible. In practically all of the experimental methods of evaluating constants, in reality one only measures the value of the constant of proportionality in an equation connecting a group of constants. Precise measurements of the refractive index for x-rays in material of low atomic number together with the dispersion theory afford such a method of evaluating either the wave-length of the x-rays used or the constant e/m. The other constants entering the equation are either known or can

be measured with a higher degree of precision than the value of e/m. In the present work on the dispersion of x-rays, the generally accepted ruled grating wave-length has been assumed and the value of e/m determined with a precision which appears comparable with the best previous evaluations.

The general dispersion theory equation[1] can be solved for e/m in the following convenient form:

$$\frac{e}{m}=\delta\left[\frac{\lambda^2\rho F}{2\pi w}\sum_1^s N_s\{1+A\}\right]^{-1}, \qquad (1)$$

where e/m is the ratio of the electronic charge to its mass, $\delta=1-\mu$, μ is the index of refraction, λ is the wave-length of the incident x-rays of frequency ν, ρ is the density and w the molecular weight of the refracting substance, F is the Faraday constant, N_s is the number of electrons per molecule of frequency ν_s, A is a factor which takes into account the electronic binding and the absorption of the x-rays in the refracting substance. The small corrective factor A contains the only difference between the various theories of dispersion. The value of A depends on the variation of the absorption coefficient of x-rays with wave-length. For all practical purposes a law of the form λ^n is sufficiently accurate.[2] In the present case $n=2.75$. It is very difficult to evaluate A unless n is an integer or half-integer. Therefore in the following calculations the value of e/m has been calculated on the assumptions of a λ^3 and $\lambda^{2.5}$ law and the $\lambda^{2.75}$ law value interpolated. If $X_s=\nu/\nu_s$ the formulae for A are:

$$A=(1/X_s^2)\ln(X_s^2-1) \qquad (2)$$

on the assumption of a λ^3 law and

$$A=\frac{3}{2X_s^{\frac{1}{2}}}\left(\frac{\pi}{2}-\mathrm{ctn}^{-1}X_s^{\frac{1}{2}}-\tfrac{1}{2}\ln\frac{X_s^{\frac{1}{2}}+1}{|X_s^{\frac{1}{2}}-1|}\right) \qquad (3)$$

on the assumption of a $\lambda^{2.5}$ law.

Experimental Procedure

An uncertainty in the evaluation of e/m from (1) is the factor A. This can be made small by using x-rays of short wave-length and a refracting prism of as low atomic number as possible. It is also apparent that in order for δ to be measured precisely it is necessary for the density ρ to be large and the substance homogeneous. An inspection of the available materials shows that diamond is by far the best. In a right-angle prism as used in the present work (Fig. 1) only one large optically flat surface is essential, for a negligibly small deviation is produced by the other surface. The other surface forming the prism edge should be flat but not necessarily as flat as the large surface and furthermore it need not be very large.

With the aid of a grant from the Rumford Committee of the American Academy of Arts and Sciences, the writer has been particularly fortunate in securing a perfect diamond slab 9×9×3 mm from Schenck and van Haelen of New York. Mr. van Haelen ground the large surface and one edge forming a 90 degree prism. He then attempted to polish these surfaces optically flat by the usual diamond polishing technique. This method was abandoned after repeated trials failed to give a surface flat within one wave-length of yellow light. The diamond grinding machine used for grinding ruling engine points for optical gratings in the laboratory at the Johns Hopkins University was then rebuilt. The polishing surface of the steel grinding disk was carefully finished and all bearings and the diamond holder adjusted as accurately as possible. After the necessary diamond polishing technique had been acquired, the surfaces were finally made flat within 0.1 wave-length of mercury light. The edge appeared perfectly sharp under a microscope of 300 magnification.

The methods used for determining the index of refraction are shown in Figs. 1 and 2. In Fig. 1 the x-ray beam struck the first face of the prism at a glancing angle slightly larger than the critical angle of total reflection. The continuous x-ray spectrum of longer wave-length was reflected from this face of the prism and was used to determine the angle between the direction of the incident x-ray beam and the surface of the prism. This reflected beam was recorded on the photographic plate at D, at the same time that the refracted beam was recorded at C. The prism was then moved out of the path of the x-ray beam and the direct beam recorded

[1] J. A. Wheeler and J. A. Bearden, Phys. Rev. **46**, 775 (1934).
[2] E. J. Williams, Proc. Roy. Soc. **A143**, 358 (1934).

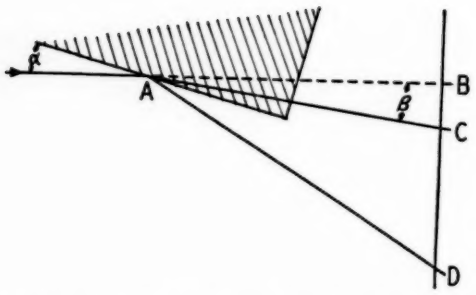

FIG. 1. The refracted x-ray line strikes the diamond prism at an angle α greater than the angle for total reflection and is refracted to C. Longer wave-lengths of the continuous spectrum are totally reflected to D. B is recorded by removing prism from path of x-ray beam.

at B. The angles α and β needed for determining μ can be obtained from the separations of the lines on the photographic plate, and the distance from the point of incidence on the prism face A to the photographic plate. The index of refraction μ may be calculated from the equation

$$\mu = 1 - \delta = \frac{\cos \alpha}{\cos (\alpha - \beta)}.$$

In Fig. 2 the direction of the x-ray beam is reversed and one needs to measure a small angular rotation of the prism in order to determine the angle α. The angle α was obtained by rotating the prism through a known angle ϕ which gave total reflection of the x-ray beam to A'. Then

$$\phi - \tan^{-1} (A'C/R) = \alpha.$$

In determining the angle β Fig. 2 the distance from the prism edge to the second plate (about 200 cm) was carefully measured and then the distance from the edge to the refracting point was subtracted from this distance. This and the distance B to C on the plate give the angle β. The advantage of this method is that, because the refracted beam is slightly convergent, very sharp lines result and all wave-lengths suffer maximum deviation simultaneously.

In previous photographic refraction measurements only the very edge of the prism could be used because of high absorption, which necessitated measurements to the edges of the photographic lines. The low absorption of the diamond made it possible to have the entire x-ray beam pass through the prism as much as 3.0 mm from the edge along the large surface. Photographs were made with the beam striking or emerging from the large surface at various positions up to the edge of the prism. The close agreement of these results indicated the perfectness of the prism.

The slits, axis of rotation of the prism, and plate holders were precisely aligned by the method used in the measurement of x-ray wave-lengths by ruled gratings.[3] The edge of the prism was placed on the axis of rotation and parallel to it with the aid of a Michelson interferometer.

The collimating gold slits were about 0.003 mm wide and 40 cm apart. The position of the prism in the x-ray beam was easily determined by the use of an ionization chamber. Normalized[3] Eastman x-ray plates were used for recording the positions of the various x-ray lines.

The average temperature of the underground room in which the experiment was performed was held within 0.05°C at all times. The variation in temperature due to the heating and cooling cycle (about 5 minutes) of the thermostat was 0.15°C. Since the massive apparatus could not follow such a rapid fluctuation in temperature, its constancy of position was affected only by the 0.05°C change, which was due to changes in heat flow through the walls and floor of the room.

In choosing an x-ray wave-length, the corrective factor A in Eq. (1) demands a short wave-length, but there is also the factor δ to be considered. From considerations of these factors and the actual measurements to be made, wave-lengths of about 1.0 to 1.5A appear best. Therefore the copper K_β line was used in the present experiments.

DENSITY OF DIAMOND

The density of the diamond was determined by measuring the density of a solution composed

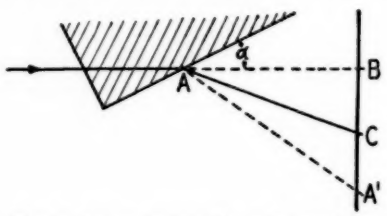

FIG. 2. X-ray beam internally refracted to C. Direct beam recorded at B by removal of prism. The angle α was measured by rotating the prism a known angle φ to give a reflected line A'.

[3] J. A. Bearden, Phys. Rev. **37**, 1210 (1931).

of thallous formate and thallous molonate in which the diamond would neither sink nor float. The density of the solution was first made less than that of the diamond and placed in a glass tube bottle 30 mm in diameter and about 100 mm long, fitted with a ground glass stopper and evacuating tube. The diamond was then placed in the solution and the space above the solution evacuated. This removed all air bubbles from the diamond and increased the density of the solution by evaporation. The evacuation was continued until the density was slightly greater than that of the diamond. Air was admitted to the bottle and the latter placed in a large clear-sided thermos bottle filled with water at 23.50°C. Water was then added and mixed thoroughly with the thallous solution until the density at 23.5°C was very close to that of the diamond.

Since the expansion coefficient of diamond is extremely small, the density of the solution can be made equal to that of the diamond by adjusting its temperature. It was found possible to make the diamond float or sink with a difference in temperature of 0.03°C, which corresponds to a difference in density of the solution of less than 2 parts in 10^5. After accurately determining the temperature of the solution that corresponded to the density of the diamond, a 10 cc pycnometer was filled with the solution. The pycnometer was placed in the thermos bottle bath and after the temperature had attained equilibrium, the excess solution was removed. The volume of the pycnometer was determined by filling it with distilled water at the same temperature. The International Critical Table value for the density of water was used. Calibrated weights were used for all weighings and buoyancy corrections applied. Four similar pycnometers were used. The average of ten entirely independent sets of measurements gave

$$\rho = 3.51536 \pm 0.00004 \text{ g/cm}^3 \text{ at } 23.5°\text{C}.$$

The probable error was calculated from the average deviation in the usual manner.

This result differs considerably from that of Tu[4] who obtained $\rho = 3.5141 \pm 0.0001$ g/cm³ and $\rho = 3.5142 \pm 0.0001$ g/cm³ on two perfect diamonds. Tu reported difficulty in making the diamonds sink or rise consistently, which indicated a non-uniformity of solution density. In the present work the thallous formate and thallous molonate solutions were carefully purified and passed repeatedly through asbestos pads held in a Gooch filtering crucible. No difficulty was experienced in making the diamond rise from the bottom to the top of the solution and back again with only a 0.03°C change in temperature.

In view of the large differences in density between the present results and those of Tu, six perfect diamonds ranging in size from one to seven carats were tested. The method used was to place the diamond used previously with one of the new ones in the thallous solution and then adjust the temperature as above until the diamonds would just rise or sink very slowly (about 2 cm/hr.). In all cases both diamonds rose and sank at the same rate. The sensitivity of the method is such that differences in density of 1 in 10^5 would have been easily detected.

While there appears to be no explanation of the discrepancy between the present densities and those of Tu, attention should be called to the fact that his density measurements on calcite crystals are also much lower than those of other experimenters. In a note to his Table XVI[4] comparing the results of different writers, he says that all values given have been reduced to 18°C, whereas only his value is given at 18°C. The others are copied from the original papers which were reduced to 20°C. This makes the difference between his results and the previous ones even greater. The Bureau of Standards has made careful determinations of the densities of the same crystals used in the previous work of the writer[5] and the average of their results is

$$\rho = 2.71029 \text{ g/cm}^3 \text{ at } 20°\text{C},$$

which is in excellent agreement with the value 2.71026 obtained by the writer. Thus it appears that Tu made some systematic error in both the diamond and calcite densities. The errors are not sufficiently large to influence his conclusion concerning the nonexistence of a mosaic effect, but are of importance in precision calculations.

[4] Y. Tu, Phys. Rev. **40**, 662 (1932).

[5] J. A. Bearden, Phys. Rev. **38**, 2089 (1931).

Results

Figure 3 shows typical contact prints from enlargements made on positive film directly from the original plates. The lines were very sharp and well defined, which made it possible to measure them with an exceedingly high degree of accuracy. The exposure times which varied from one hour to twelve hours depended upon the thickness of the prism the x-rays had to traverse.

The 15 cm range precision comparator used for measuring the separations of the lines was carefully calibrated. The periodic error was determined by using a 300 power microscope and a good quality ruled grating. The absolute length calibration was made in a similar manner, by the use of a diamond ruled glass scale which had been calibrated by the Bureau of Standards. The separation of two diamond ruled lines could be remeasured on any part of the travel used within 0.0002 mm.

The separations of the lines on the photographic plates were measured at different points along the height of the lines and all measurements were repeated with the plate reversed in position. The average of the reversed measurements agreed with the initial ones within 0.002 mm and the average of the initial and reversed measurements for the different points along the line did not exceed 0.002 mm. There was also no consistent variation in the results with position along the height of the lines.

The results for the final series of 25 plates obtained with external incidence are given in Table I. The second column gives the thickness of prism traversed by the central ray, columns three and four are the average separations of the lines of the plates, and the fifth column gives the value of δ for each plate. From the agreement of the different sets of measurements, the probable error in δ for each plate is about 2×10^{-9}. The external consistency for the 25 results is 0.375×10^{-9} and the internal consistency is 0.4×10^{-9}. The ratio of these is as near unity as can be expected, and indicates that the only errors that could have influenced the value of δ more than 0.4×10^{-9} are consistent errors that occurred throughout all the measurements.

A good series of 15 plates was taken with internal incidence, and the average of these results

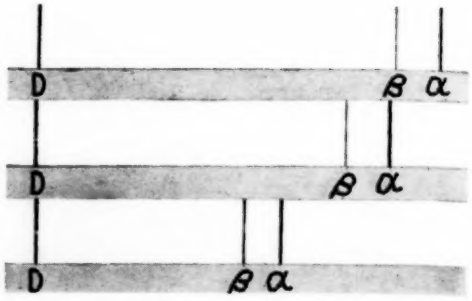

Fig. 3. Typical refraction spectra. D is the direct x-ray beam, α and β the refracted K_α and K_β lines of copper. The totally reflected line is not shown on the enlargement.

was $\delta=9223\pm3$, but because of the extra-angular measurement that has to be made when this method is used, the results are not as accurate as those obtained with external incidence. These less precise results have not been used in evaluating e/m.

The measurement of the distance from the edge of the prism to the front of the photographic plate was taken three different times during the course of the experiment and all results agreed within 0.1 mm. This distance was measured by placing a long bar[6] with parallel ends between the prism and plate and then measuring the remaining distances (about 5 cm) with inside micrometers. Any consistent error of run in the comparator was certainly negligible. Since the pencil of x-rays struck the prism face at a very small angle, the rays which passed through the most material were more highly absorbed than those nearer the edge of the prism. However, the effective shift in the position of the refracted line can be easily calculated, and such a correction was applied to all the measurements in column three of Table I. It appears safe to assume a total error in δ of about 2.5 times the internal consistency, or

$$\delta=9224.4\pm1.0\times10^{-9}.$$

In the calculation of the value of e/m by Eq. (1) one must evaluate A from Eqs. (2) and (3). X_s is the ratio of the K critical absorption wave-length of carbon to the wave-length of the copper K_β line which was used in all the measurements recorded in Table I, or

[6] The length of this bar was carefully measured by the National Bureau of Standards, Washington, D. C.

$X_s = 43.2^7/1.3922^8 = 31.03^9$; $N_s = 1.84$.[1]

These give for the $\sum_1^s$ in Eq. (1)

$\sum_1^s N_s(1+A) = 6.0194$ for a $\lambda^{2.5}$ law of absorption

and

$\sum_1^s N_s(1+A) = 6.0131$ for a λ^3 law of absorption.

From an analysis of the available x-ray absorption measurements,[10] one finds the exponent of λ to be 2.75 ± 0.05. By interpolation, the $\lambda^{2.75}$ law gives

$$\sum_1^s N_s(1+A) = 6.0163 \pm 0.0006.$$

The other constants used in evaluating e/m are:

$\delta = (9224.4 \pm 1.0)10^{-9}$; $W^{11} = 12.0148 \pm 0.0005$ g per gram mol. wt.,

$\rho = 3.5154 \pm 0.0001$ g/cm^3; $F^{11} = 96513.1 \pm 8.0$;

$\lambda = 1.39220 \pm 0.00003$.

Thus the value of e/m from the present work is

$$e/m = (1.7601 \pm 0.0003) \times 10^7 \text{ e.m.u.}$$

The two most important sources of error in this value are the exponent of the x-ray absorption law and the experimental measurement of δ. The absorption measurements of S. J. M. Allen[10] have been plotted on a large scale and the ± 0.05 variation in the exponent of λ includes every measurement from 0.88A to 2.5A. The error in δ has been discussed above and appears to be conservative. The absorption term of the complete dispersion formula has been neglected, but this introduces a negligible error in the value of e/m.

A calculation[12] was made of the value of the refractive index by using the approximate wave-mechanical theory of Hönl, in order to see how much the result would differ from that of the other laws. The result for the K shell is that $N_k(1+A) = 1.876$, and the K oscillator strength, $N_k = 1.860$. When the wave-length is far to the short wave side of an absorption edge, A becomes negligible. Since A is so small for the K edge, it will surely be safe to neglect it for the L edge. From the f sum rule, neglecting double transitions as improbable, $N = 6 - N_k = 4.140$, so that

$$\sum_1^s = 1.876 + 4.140 = 6.016,$$

which is in very good agreement with the interpolated value of the $\sum_1^s$ above.

This result is not sensitive to small changes in the wave-length or in the wave-length of the K edge. A change of 1 percent in either makes a change in the final result of about 0.004 percent. The excellent agreement between this calculation

TABLE I.

Plate	Penetration in prism mm	Distance $B-C$ in mm	Distance $B-D$ in mm	$\delta \times 10^9$
48	0.87	3.9789	20.857	9220
49	1.11	3.1815	24.298	9221
50	1.84	4.2880	19.969	9222
51	0.80	3.5358	22.538	9225
52	1.09	4.6441	19.108	9220
53	1.30	5.0470	18.362	9222
54	3.02	3.3437	23.478	9222
55	1.81	3.7486	21.682	9220
56	1.84	4.2661	20.029	9223
57	0.50	2.8210	26.627	9224
58	1.11	4.2568	20.049	9227
59	0.98	3.9862	20.846	9226
60	1.16	3.9893	20.843	9228
61	1.16	3.7382	21.726	9229
62	0.50	3.1577	24.423	9223
63	1.19	3.3261	23.539	9228
64	0.51	3.5162	22.616	9224
65	0.72	4.2599	20.029	9224
66	1.03	3.0565	25.030	9219
67	1.07	4.2671	20.022	9226
68	1.19	4.2692	20.015	9225
69	1.38	4.2692	20.018	9226
70	1.71	3.7754	21.588	9225
71	1.58	3.7734	21.597	9227
72	1.43	3.7775	21.574	9224
				Average 9224.4±.04

[7] Thibaud's value relative to Carbon K_α and the absolute scale of wave-lengths by M. Söderman, Phil. Mag. **10**, 600 (1930).

[8] J. A. Bearden, Phys. Rev. **47**, 883 (1935) for the ruled grating scale of wave-lengths, and the crystal wave-length from J. A. Bearden and C. H. Shaw, Phys. Rev. **48**, 18 (1935).

[9] X_s increases rapidly with atomic number. In the case of quartz and the copper $K_{\alpha 1}$ line, $X_s = 4$. The results obtained with the quartz prism (J. A. Bearden and C. H. Shaw, Phys. Rev. **46**, 759 (1934)) give a lower value of e/m than has been obtained with the diamond prism. The greatest uncertainty in the dispersion theory is in properly correcting for the electronic binding. In the case of quartz, where X_s is only 4, a small error in the correcting term would change the resulting value of e/m considerably more than in the case of diamond, where $X_s = 31$. This, and the uncertainty in the exponent of the x-ray absorption law for quartz, probably accounts for the difference between the diamond and quartz results.

[10] Compton and Allison, *X-Rays in Theory and Experiment*, p. 802.

[11] The writer is indebted to Professors R. T. Birge, K. T. Bainbridge, and H. C. Urey for information on the atomic weight of carbon, and to Professor Birge for the value of the Faraday.

[12] The writer is indebted to Dr. Russell Lyddane for making this calculation based on the Hönl theory.

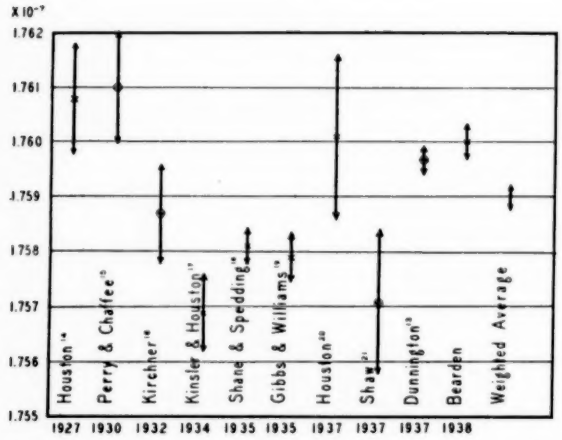

FIG. 4. A chronological plot of the best determination of e/m from 1927 to 1938. The bound electron results are indicated by $\times$, and the free electron by $\ominus$. Arrows show probable errors.

and the one above strongly supports the conclusion that adequate correction for electronic binding has been made in the present calculation of the value of e/m.

The present experiments differ markedly in one very significant way from all previous determinations, namely that in this case the electrons under observation are much more tightly bound. Here, then, is the opportunity to test whether bound and unbound electrons have different values of e/m, for the present value would be much lower than the free electron value if the binding is a significant factor. On the contrary, it is slightly higher than the excellent results of Dunnington[13] for free electrons, which seems to exclude the possibility of the value of e/m depending on the strength of electronic binding. The present status of the problem can be presented by plotting the recent values obtained by the various experimenters[13–21] together with their probable errors as in Fig. 4.

In the writer's opinion, the work of Dunnington should be given greater weight compared to other results. This has been done with the approval also of other workers in this field.

The weighted average of the bound electron results (crosses) is 1.7588×10^7 e m.u., and that of the free electron 1.7596×10^7 e.m.u. If one compares the spectroscopic values (excluding the present results) with the free electron value, then there is a marked difference which appears greater than the experimental errors. The weighted average of all the results gives

$$e/m=(1.7590\pm0.0002)\times10^8 \text{ e.m.u.}$$

A statistical analysis of the results gives for the ratio of external to internal consistency $R_e/R_i=1.64$ for the spectroscopic and 1.01 for the free electron results, and 1.63 if all results are averaged. The 1.64 and 1.63 do not prove the existence of a discrepancy in the results, but it is high enough to invoke questions as to possible consistent errors or failure of theory in some of the methods used. The free electron results as obtained by Dunnington seem to be very sound, both in the theory of the method and in the experimental procedure. Likewise in the present work the dispersion theory for x-rays in diamond is sound and the experimental procedure is the simplest of any method. In the spectroscopic method one deals with unresolved components for which ample correction is difficult. It has been shown[19, 22] that the measured fine structure separation for $D\alpha$ and the spectroscopic theory are not in satisfactory agreement. This raises some question as to the precision of e/m calculated from spectroscopic data. The need for further spectroscopic work is obvious.

Since the above was written Dr. A. E. Shaw's complete article has been published. His final result and probable error are the same as is given in Fig. 4. This value differs from the writer's by one part in 600 which is about 1.5 times the sum of the probable errors. However, the sum of the probable errors is so large that no real discrepancy is indicated by a statistical analysis of the results.

The writer is greatly indebted to the Rumford Committee of the American Academy of Science for funds with which to purchase the diamond prism. He is also grateful to Mr. C. M. Herget, who assisted in the determination of the densities of the diamonds, and to Dr. C. H. Shaw for helpful discussions and assistance.

[13] F. G. Dunnington, Phys. Rev. **52**, 475 (1937).
[14] W. V. Houston, Phys. Rev. **30**, 608 (1927).
[15] C. T. Perry and E. L. Chaffee, Phys. Rev. **36**, 904 (1930).
[16] F. Kirchner, Ann. d. Physik **8**, 975 (1931); **12**, 503 (1932).
[17] L. E. Kinsler and W. V. Houston, Phys. Rev. **45**, 104 (1934); **46**, 533 (1934).
[18] G. D. Shane and F. H. Spedding, Phys. Rev. **47**, 33 (1935).
[19] R. C. Gibbs and R. C. Williams, Phys. Rev. **48**, 971 (1935).
[20] W. V. Houston, Phys. Rev. **51**, 446 (1937).
[21] A. E. Shaw, Phys. Rev. **51**, 887 (1937).
[22] W. V. Houston, Phvs Rev. **50**, 392 (1936).

The Binding Energy of Li^6

HENRY MARGENAU AND KENNETH G. CARROLL
Yale University, New Haven, Connecticut

(Received August 8, 1938)

The mass defect of Li^6 has been calculated with the use of a symmetric Hamiltonian. Perturbation theory was employed in the main part of the work, and an upper limit for the contribution of all functions to the first and second order perturbation energies was obtained. This upper limit is 10 percent smaller than the experimental binding energy It was then shown on the basis of variational calculations that perturbation theory, carried to this stage, overshoots the mark, and the upper limit to the binding energy is reduced to 26 Mev, which is 6 Mev short of the experimental value. These figures are based on a set of nuclear constants which favor large mass defects. The perturbational effect of all doubly excited configurations upon the ^3D state of Li^6 was investigated and compared with the effect of similar functions upon the ^3S state. The result is that the first order $^3D-{}^3S$ splitting, which is about 2 Mev, is enlarged to 6 Mev, both levels being depressed.

THERE is now considerable evidence suggesting that a nuclear Hamiltonian function which is symmetrical in neutrons and protons, and in which the coordinate part of the interaction between two particles is of simple exponential type, will not be capable of correlating all experimental data. First Rarita and Present,[1] using an elaborate variational method to calculate the mass defect of H^3, showed that with the same set of constants the mass defect of He^4 comes out too great. Their most accurate variational calculation was made with potentials of the form $e^{-r/a}$, while somewhat more qualitative considerations involving the use of "equivalent two-body methods" and leading to the same results, were presented in connection with other forms of potential. Following up these interesting indications two further searching variational calculations were made[2, 3] in which potentials of the type $\exp(-r^2/a^2)$ were used and in which a single method was applied to both the H^3 and the He^4 problems, the results being further corroborated by employing two different sets of functions (functions of individual particle coordinates and of relative coordinates). While in these papers interest was concentrated chiefly on the mathematical aspects of the question of convergence, a discrepancy similar to that of Rarita and Present came to light (obscured, perhaps, in the first paper by an underestimate of the rate of convergence). The discrepancy was less strong because Margenau and Warren had chosen a smaller value of g, the ratio of Heisenberg to Majorana forces. Indeed it was shown afterward[3] that the discrepancy in the binding energies of H^3 and He^4 can be made very small by choosing $g=0.175$. This, however, leads to a bound ^1S state for the deuteron, which, at present at least, is incompatible with known facts.

Another difficulty exists in connection with the excited states of the alpha-particle which, according to the interpretation by Crane of his and his co-workers' experiments,[4] should be stable. According to theory[5] they are unstable for all acceptable values of nuclear constants. A similar situation holds with regard to the excited states of He^3: Bonner[6] finds a stable state experimentally; theory[7] denies its existence.

As soon as we depart from consideration of the lightest nuclei, definite theoretical predictions become difficult. Inglis[8] has calculated the binding energy of Li^6 and has concluded the

[1] W. Rarita and R. D. Present, Phys. Rev. **51**, 788 (1937).
[2] H. Margenau and D. T. Warren, Phys. Rev. **52**, 790 (1937); D. T. Warren and H. Margenau, Phys. Rev. **52**, 1027 (1937).
[3] H. Margenau and W. A. Tyrrell, Jr., Phys. Rev. **54**, 422 (1938).
[4] Crane, Delsasso, Fowler and Lauritsen, Phys. Rev. **48**, 125 (1935).
[5] H. Margenau, Phys. Rev. **53**, 198 (1938); S. S. Share, Phys. Rev. **53**, 875 (1938).
[6] T. W. Bonner, Phys. Rev. **53**, 711 (1938); Baldinger, Huber and Shaub, Helv. Phys. Acta **XI**, 245 (1938).
[7] L. I. Schiff, Phys. Rev. **54**, 92 (1938).
[8] D. R. Inglis, Phys. Rev. **51**, 531 (1937). To compare the results of Inglis with ours, note should be taken of errata listed by Inglis, Phys. Rev. **53**, 880 (1938). The algebraic expressions for $E_D^{(2)}$ given by Inglis are somewhat in error.

existence of another discrepancy: With a reasonable choice of the force constants, the calculated mass defect is too small. There is, however, some question as to the convergence of the contributions of the higher excited states. The interest of this example in view of the increasing doubt as to the validity of the symmetric Hamiltonian has led us to reinvestigate this problem by a different and more painstaking procedure. The present work, though its results differ in some details from those of Inglis, rather strengthens the conclusion that the theoretical mass defect is too small. It goes beyond the scope of the latter in the following respects: (1) A variational method is used in an attempt to correct the perturbational procedure; (2) An upper limit for the second order perturbational contribution to the binding energy is derived; (3) the second order effect on the ^3D state as well as the ground state is calculated. Besides, the whole calculation has been conducted with a different (but equivalent) set of functions so that an independent check on previous results is provided.

Assumptions and Method

Only the symmetric Hamiltonian is used in the present paper, the interactions being written in the following form:

$$V_{ij}=-A(w+mP_{ij}+bQ_{ij}+hP_{ij}Q_{ij}) \exp(-r_{ij}^2/a^2).$$

For A and a we use throughout the values 35.60 Mev and 2.25×10^{-13} cm, which seem in best agreement with scattering data. The other numerical parameters in (1) are varied, attention being concentrated chiefly upon the following two sets:

$$w=-2/15;\ m=14/15;\ b=7/15;\ h=-4/15 \quad (a)$$

$$=-1/12 \quad =10/12 \quad =5/12 \quad =-2/12. \quad (b)$$

They will henceforth be designated as choices (a) and (b). Both satisfy the usual requirements; the first corresponds to $g(=b+h)=0.20$, the second to $g=0.25$, two rather extreme cases. Furthermore, they are so adjusted as to give as large as possible a mass defect for Li^6 and yet satisfy the requirements.[9] The functions used are

[9] G. Breit and E. Feenberg, Phys. Rev. **50**, 850 (1936); N. Kemmer, Nature **140**, 192 (1937).

Table I. *Individual particle functions.* $\rho=(q/\pi)^{\frac{3}{4}}\exp(-qr^2/2)$.

$(1s)=\rho$
$(2s)=(\frac{2}{3})^{\frac{1}{2}}(qr^2-\frac{3}{2})\rho$
$(3s)=(\frac{2}{15})^{\frac{1}{2}}(q^2r^4-5qr^2+\frac{15}{4})\rho$
$(2p_{\pm1})=q^{\frac{1}{2}}(x\pm iy)\rho$
$(2p_0)=(2q)^{\frac{1}{2}}z\rho$
$(3p_{\pm1})=(\frac{2}{5}q)^{\frac{1}{2}}(qr^2-\frac{5}{2})(x\pm iy)\rho$
$(3p_0)=(\frac{4}{5}q)^{\frac{1}{2}}(qr^2-\frac{5}{2})z\rho$
$(4p_{\pm1})=(\frac{2}{35}q)^{\frac{1}{2}}(q^2r^4-7qr^2+\frac{35}{4})(x\pm iy)\rho$
$(4p_0)=(\frac{4}{35}q)^{\frac{1}{2}}(q^2r^4-7qr^2+\frac{35}{4})z\rho$
$(3d_{\pm2})=(\frac{1}{2})^{\frac{1}{2}}q(x\pm iy)^2\rho$
$(3d_{\pm1})=(2)^{\frac{1}{2}}q(x\pm iy)z\rho$
$(3d_0)=(\frac{1}{3})^{\frac{1}{2}}q(3z^2-r^2)\rho$
$(4d_{\pm2})=(\frac{1}{7})^{\frac{1}{2}}q(qr^2-\frac{7}{2})(x\pm iy)^2\rho$
$(4d_{\pm1})=(\frac{4}{7})^{\frac{1}{2}}q(qr^2-\frac{7}{2})(x\pm iy)z\rho$
$(4d_0)=(\frac{2}{21})^{\frac{1}{2}}q(qr^2-\frac{7}{2})(r^2-3z^2)\rho$
$(4f_{\pm3})=(\frac{1}{6})^{\frac{1}{2}}q^{\frac{1}{2}}(x\pm iy)^3\rho$
$(4f_{\pm2})=q^{\frac{1}{2}}(x\pm iy)z\rho$
$(4f_{\pm1})=(\frac{1}{10})^{\frac{1}{2}}q^{\frac{1}{2}}(5z^2-r^2)(x\pm iy)\rho$
$(4f_0)=(\frac{6}{5})^{\frac{1}{2}}q^{\frac{1}{2}}(\frac{5}{3}z^2-r^2)z\rho$

functions of individual particle coordinates; therefore the kinetic energy operator contains, besides the terms in ∇^2, terms in $\nabla_i\cdot\nabla_j$ which correct for the motion of the center of mass.[2, 8] In the greater part of the paper the Schrödinger perturbation theory up to second order terms is employed; later a variational procedure is discussed. The former involves formally the calculation of nondiagonal energy elements H_{0i}', H' being the perturbing operator, the latter involves H_{ij}. Since the unperturbed energy does not possess nondiagonal elements, H_{0i}' may be replaced by H_{0i}. This keeps the relation between the two procedures more in evidence.

Numerical calculations of the type here presented involve many details which cannot all be mentioned. Our aim is to clarify the method and to present examples of critical points in the procedure. If matters essential to an understanding of the work seem omitted, the reader will probably find them discussed in various references.[2, 3, 8] The next sections deal with an application of perturbation theory to the problem. Their aim is, after selection of a suitable set of functions for the ground state (ψ_0) and for the higher unperturbed states (ψ_i), the evaluation of

$$E=H_{00}+\sum_i{}'\frac{|H_{0i}|^2}{E_0-E_i}. \quad (2)$$

ψ_0 must be so chosen as to possess the correct symmetry of the ground state; the other ψ's need not have this property.

Functions

All unperturbed functions are linear combinations of products of six single-particle functions. We first discuss these single-particle functions. To be manageable in the integrations, they must be Gauss exponentials multiplied by polynomials. For convenience, these polynomials should make the functions orthogonal. This leads immediately to the selection of either Hermite polynomials or Legendre polynomials, as the simplest sets. Calculations including "doubly excited states" (see below) have been made with the use of both, the results being, of course, identical. This not only checked the correctness of the calculation, but also showed Legendre polynomials to be superior in practice, giving rise to fewer functions associated with a given degree of excitation. Inglis used Hermite functions throughout.

Legendre functions have the further advantage of being eigenfunctions of the angular momenta of individual particles, so that they can be designated easily in the customary spectroscopic way. The functions contain the common parameter q which will later be adjusted for minimum energy. Table I is a list of normalized functions required here.

The unperturbed energies E_i appearing in (2) are simply the sums of the six single-particle energies ϵ belonging to the functions in Table I. The ϵ's are best expressed in terms of the "oscillator quantum number" n associated with each of these functions, thus:

$$\epsilon=(n+\tfrac{3}{2})h\nu=(n+\tfrac{3}{2})(\hbar^2/M)q. \qquad (3)$$

The correspondence between the functions and n is given in Table II.

Table II. *Correspondence between the normalized functions and n.*

Function	n	Function	n	Function	n
$1s$	0	$2p$	1	$3d$	2
$2s$	2	$3p$	3	$4d$	4
$3s$	4	$4p$	5	$5d$	6 etc.

To construct the ψ_i it is most convenient to introduce the isotopic spin quantum number τ_ξ,[10] and to define four generalized spin functions:

$$\eta_1=\delta(s_z,-\tfrac{1}{2})\delta(\tau_\xi,-\tfrac{1}{2}),$$
$$\eta_2=\delta(s_z,\tfrac{1}{2})\delta(\tau_\xi,-\tfrac{1}{2}),$$
$$\eta_3=\delta(s_z,-\tfrac{1}{2})\delta(\tau_\xi,\tfrac{1}{2}),$$
$$\eta_4=\delta(s_z,\tfrac{1}{2})\delta(\tau_\xi,\tfrac{1}{2}).$$

The ground state function for the Li^6 nucleus must satisfy the following conditions:[11]

$$\left.\begin{aligned} S_z&\equiv\sum_k s_{z,k}=1,\\ T_\xi&\equiv\sum_k \tau_{\xi,k}=0,\\ Y_\xi&\equiv\sum_k s_{z,k}\tau_{\xi,k}=0,\end{aligned}\right\} \qquad (4)$$

where the summation is extended over the six particles. The last of these is not exact if the Hamiltonian contains spin dependent forces. Its imposition amounts to an omission of constituents representing spin distributions different from the normal one ($+-+$ for the neutrons, as for the protons) in the ground state function. The effect of these upon the masses of H^3 and He^4 is known to be small,[1,2] so that the approximation made here in maintaining the last condition is probably sufficient. The three conditions limit the set of η's to

$$\eta_1(1)\eta_2(2)\eta_3(3)\eta_4(4)\eta_2(5)\eta_4(6)$$

and permutations of arguments among these η's. It is here understood that 5 and 6 are the two particles which, because of the Pauli principle, are in excited states. The advantage in introducing the η-functions is that they enable us to write the complete ψ-functions as single determinants instead of a product of two determinants, one for the neutrons and one for the protons. If now the single-particle functions are designated by u with an appropriate subscript, every ψ_i has the form

[10] B. Cassen and E. U. Condon, Phys. Rev. **50**, 846 (1936).

[11] Cf. E. Wigner, Phys. Rev. **51**, 106 (1937).

$$\left(\frac{1}{n!}\right)^{\frac{1}{2}}\begin{vmatrix} u_{l1}(1)\cdot\eta_{r1}(1) & u_{l2}(1)\cdot\eta_{r2}(1) & \cdots & u_{ln}(1)\cdot\eta_{rn}(1) \\ u_{l1}(2)\cdot\eta_{r1}(2) & u_{l2}(2)\cdot\eta_{r2}(2) & \cdots & u_{ln}(2)\cdot\eta_{rn}(2) \\ \cdot\ \cdot\ \cdot\ \cdot\ \cdot\ \cdot\ \cdot\ \cdot\ \cdot\ \cdot\ \cdot & & & \\ \cdot\ \cdot\ \cdot\ \cdot\ \cdot\ \cdot\ \cdot\ \cdot\ \cdot\ \cdot\ \cdot & & & \\ u_{l1}(n)\cdot\eta_{r1}(n) & u_{l2}(n)\eta_{r2}(n)\cdot & \cdots & u_{ln}(n)\cdot\eta_{rn}(n) \end{vmatrix}, \tag{5}$$

where in our case $n=6$, and the η's are those listed above in some permutation. Henceforth this determinant will be abbreviated into $|u_{l1}\eta_{r1}\cdots u_{ln}\eta_{rn}|$.

Functions like (5), while obeying conditions (4), do not represent the correct total angular momentum, nor in general the correct total spins. The lowest state for Li^6 is presumably that for which $L=0$, $S=1$, $T=0$. In order to satisfy these conditions, linear combinations of functions like (5) must be taken. The procedure for this is well known from the theory of atomic spectra. The function which satisfies all these conditions, and which will be taken as our ψ_0, is

$$\psi_0=\left(\frac{1}{6!}\frac{1}{3}\right)^{\frac{1}{2}}\{|s\eta_1\cdot s\eta_2\cdot s\eta_3\cdot s\eta_4\cdot p_1\eta_2\cdot p_{-1}\eta_4| + |s\eta_1\cdots s\eta_4\cdot p_{-1}\eta_2\cdot p_1\eta_4| + |s\eta_1\cdots s\eta_4 p_0\eta_2 p_0\eta_4|\}. \tag{6}$$

It corresponds to the configuration $(1s)^4(2p)^2$.

Combination (6) is orthogonal to all other functions arising from this configuration. Hence there are no vanishing denominators in the summation of (2), and this relieves us of the necessity of selecting proper linear combinations for all the other ψ_i. These may then be taken in the crude form (5).

TABLE III. *List of doubly and quadruply excited configurations.*

Configurations	No. of Functions	Configurations	No. of Functions
Doubly excited		Quadruply excited	
$(1s)^4 2p3p$	6	$(1s)^4 2p4p$	6
$(1s)^4(2s)^2$	1	$(1s)^4(3p)^2$	3
$(1s)^4(3d)^2$	5	$(1s)^3 2s2p3p$	42
$(1s)^3(2p)^2 2s$	26	$(1s)^3 3d2p3p$	126
$(1s)^3(2p)^2 3d$	78	$(1s)^3 3d2p4f$	210
$(1s)^2(2p)^4$	36	$(1s)^3 3s(2p)^2$	26
		$(1s)^3 4d(2p)^2$	76
		$(1s)^2(2s)^2(2p)^2$	18
		$(1s)^2(3d)^2(2p)^2$	54
		$(1s)^2(2p)^3 3p$	96

Selection of Excited-State Functions and Determination of Their Number

Excited-state functions are best classified according to their degree of excitation, i.e., the value of $\sum n_k$ minus this sum for the ground state, the latter being obviously 2. The functions belonging to a given degree of excitation may again be subdivided into groups belonging to different configurations, and these groups can be constructed almost mechanically by writing down the permutations of a given set of symbols. This procedure will be illustrated by reference to the first of the configurations listed in Table III, which is an exhaustive tabulation of the doubly and quadruply excited configurations.[12]

Suppose we wish to construct the functions belonging to $(1s)^4(2p)3p$. We note first all combinations of orbitals which satisfy $\sum m_s=0$ (S-state). They are (omitting the four s-orbitals): $2p_{-1}3p_1$, $2p_13p_{-1}$, and $2p_03p_0$. A function is obtained by assigning six orbitals to a fixed arrangement of η's in such a way that no two equal orbitals have the same η, since otherwise the determinant (5) would vanish. Thus in our case a pair of distributions arise from each set of orbitals and we get the possible distributions listed in Table IV. Thus we have obtained six functions, the first of them being $(1/6!)^{\frac{1}{2}}|s\eta_1\cdots s\eta_4\cdot 2p_{-1}\eta_2\cdot 3p_1\eta_4|$, etc. After one has constructed all functions belonging to a given configuration, it is easy to single out by inspection

TABLE IV. *Possible distributions.*

η_1	η_2	η_3	η_4	η_5	η_6
s	s	s	s	$2p_{-1}$	$3p_1$
s	s	s	s	$3p_1$	$2p_{-1}$
s	s	s	s	$2p_1$	$3p_{-1}$
s	s	s	s	$3p_{-1}$	$2p_1$
s	s	s	s	$2p_0$	$3p_0$
s	s	s	s	$3p_0$	$2p_0$

[12] Configurations which do not combine with the ground state have been omitted.

those which will not combine with the ground state. The numbers appearing in Table III do not include these functions. It is essential in calculations of this sort to have a complete and nonredundant list of all excited functions, and the present method is one which will yield it almost automatically. Functions belonging to the same configuration do not have the same matrix elements with the ground state, but divide into a small number of groups having equal elements.

Calculation of Matrix Elements

H_{0i} consists of three parts:[13] first the terms $-(5/6)(\hbar^2/2M)\sum_k\nabla_k^2$; second the cross terms $(1/6)(\hbar^2/2M)\sum_{k>l}\nabla_k\cdot\nabla_l$; third the potential energy, a sum over (1). The first may be transformed by the relation

$$-\frac{\hbar^2}{2M}\sum_k\nabla_k^2\psi=E\psi-\frac{\hbar^2}{2M}q^2(\sum_k r_k^2)\psi. \qquad (7)$$

We introduce the abbreviations

$$T\equiv\hbar^2/Ma^2=8.10\text{ Mev};\quad \sigma\equiv qa^2. \qquad (8)$$

The nondiagonal elements of the first part of H therefore reduce, in view of (7), to the integrals

$$-\frac{5}{6}\int\psi_0^*\left(\frac{\hbar^2}{2M}\sum_k\nabla_k^2\right)\psi_i d\tau=-\frac{T\sigma}{2}\int\psi_0^*(\sum_k qr_k^2)\psi_i d\tau,$$

and these latter reduce to simple elements of the form $(u_1|qr^2|u_2)$, where the u's are single-particle functions. Of these, only the following are different from zero:

$$(1s|qr^2|2s)=(3/2)^{\frac{1}{2}},$$
$$(2p_{\pm1}|qr^2|3p_{\pm1})=(2p_0|qr^2|3p_0)=(5/2)^{\frac{1}{2}}.$$

Here again the simplicity in the use of Legendre functions is apparent.

Next we consider the second part of H. By a well-known theorem connecting momentum and coordinate matrices we have

$$\int u_\lambda^*\nabla u_\mu d\tau=\frac{M}{\hbar^2}(\epsilon_\mu-\epsilon_\lambda)\mathbf{r}_{\lambda\mu},$$

and since $\epsilon_\lambda=T\sigma(n_\lambda+3/2)$ because of (3) and (8), we find

$$\int u_\lambda^*\nabla u_\mu d\tau=q^{\frac{1}{2}}(n_\mu-n_\lambda)(q^{\frac{1}{2}}\mathbf{r})_{\lambda\mu}.$$

The expression $(1/6)(\hbar^2/2M)\sum_{k>l}\nabla_k\cdot\nabla_l$ is therefore equivalent to $(1/6)T\sigma\sum_{k>l}\Delta n_k\Delta n_l q\mathbf{r}_k\cdot\mathbf{r}_l$. Here we have written Δn for the difference of the oscillator quantum numbers of the two single-particle functions between which the matrix element is to be computed. $\Delta n=\pm1$. Thus it is seen that the second part of H_{0i} breaks down into products of two elements, each of the form $\Delta n(u_1|q^{\frac{1}{2}}\mathbf{r}|u_2)$. A list of the nonvanishing elements of this kind which are needed in the present work follows. The three values in brackets are the vector components of the elements, and r' is written for $q^{\frac{1}{2}}r$.

$$\Delta n(s|r'|2p_{\pm1})=\tfrac{1}{2}[1,\pm i,0],$$
$$\Delta n(2s|r'|2p_{\pm1})=(\tfrac{1}{6})^{\frac{1}{2}}[-1,\mp i,0],$$
$$\Delta n(s|r'|2p_0)=(\tfrac{1}{2})^{\frac{1}{2}}[0,0,1],$$
$$\Delta n(2s|r'|2p_0)=(\tfrac{1}{3})^{\frac{1}{2}}[0,0,-1],$$
$$\Delta n(2p_{\pm1}|r'|3d_0)=\tfrac{1}{2}(\tfrac{1}{3})^{\frac{1}{2}}[-1,\mp i,0],$$
$$\Delta n(2p_{-1}|r'|3d_{-2})=(\tfrac{1}{2})^{\frac{1}{2}}[1,i,0],$$
$$\Delta n(2p_1|r'|3d_2)=(\tfrac{1}{2})^{\frac{1}{2}}[1,-i,0],$$
$$\Delta n(2p_{-1}|r'|3d_{-1})=\Delta n(2p_1|r'|3d_1)=(\tfrac{1}{2})^{\frac{1}{2}}[0,0,1],$$
$$\Delta n(2p_0|r'|3d_{\mp1})=\tfrac{1}{2}[1,\pm i,0],$$
$$\Delta n(2p_0|r'|3d_0)=(\tfrac{2}{3})^{\frac{1}{2}}[0,0,1].$$

We now turn to the evaluation of the matrix elements of the potential energy, which is a little more tedious. The fundamental formulae are easily developed. Denote two general functions like (5) by ψ_A and ψ_B:

$$\psi_A=(1/n!)^{\frac{1}{2}}|u_{l1}\eta_{r1}\cdots u_{ln}\eta_{rn}|,$$
$$\psi_B=(1/n!)^{\frac{1}{2}}|u_{\lambda1}\eta_{\rho1}\cdots u_{\lambda n}\eta_{\rho n}|.$$

Then, if H is symmetrical with respect to an interchange of any two particles,

$$H_{AB}=\int(u_{l1}\eta_{r1}\cdots u_{ln}\eta_{rn})\times H|u_{\lambda1}\eta_{\rho1}\cdots u_{\lambda n}\eta_{\rho n}|d\tau. \qquad (9)$$

[13] See, for instance, reference 2, Eq. (11).

The first factor of the integrand here is no longer a determinant but a product of n single-particle functions. If H is a sum of terms each involving the coordinates of but one particle, as was the case with the ∇^2-part of the energy, (9) reduces immediately to the single integrations discussed before. If H is a sum of terms involving the coordinates of two particles, as with the $\nabla_i \cdot \nabla_j$-part and the potential energy, further reduction proceeds as follows.

Introduce the symbol θ_{ij} which is defined to be 1 if every $u_{ls}\eta_{rs} = u_{\lambda s}\eta_{\rho s}$ for $s \neq i, j$; i.e., θ_{ij} is zero whenever the functions of more than two particles are different; it is 1 if the two non-matching functions refer to particles i and j. Then, if we let $H = V = \sum_{i>j} V_{ij}$, (9) becomes

$$V_{AB} = \sum_{i>j} \Big\{ \int u_{li}(i)\eta_{ri}(i) \cdot u_{lj}(j)\eta_{rj}(j)\, V_{ij} \times u_{\lambda i}(i)\eta_{\rho i}(i) u_{\lambda j}(j)\eta_{\rho j}(j) d\tau - \int u_{li}(i)\eta_{ri}(i) \cdot u_{lj}(j)\eta_{rj}(j)\, V_{ij} \times u_{\lambda j}(i)\eta_{\rho j}(i) u_{\lambda i}(j)\eta_{\rho i}(j) d\tau \Big\} \theta_{ij}.$$

Here as well as in Eq. (9) the integration is understood to include a summation over spins.

Now $V_{ij} = V_{ij}' + V_{ij}'' Q_{ij}$, where V' and V'' act on the particle coordinates alone. This leads to the further decomposition

$$V_{AB} = V_{AB}' + V_{AB}''. \tag{10}$$

In V_{AB}', the summation over spins may be performed with the use of the relation

$$\sum_{\sigma\tau} \eta_a(1)\eta_b(2)\eta_c(1)\eta_d(2) = \delta(a, c)\delta(b, \delta), \tag{11}$$

so that

$$V_{AB}' = \sum_{i>j} \Big\{ \int u_{li}(1) u_{lj}(2)\, V'(12) u_{\lambda i}(1) \times u_{\lambda j}(2) d\tau \delta(r_i, \rho_i)\delta(r_j, \rho_j) - \int u_{li}(1) u_{lj}(2)\, V'(12) u_{\lambda j}(1) \times u_{\lambda i}(2) d\tau \delta(r_i, \rho_j)\delta(r_j, \rho_i) \Big\} \theta_{ij}. \tag{12}$$

This is the formula used in evaluating the Wigner and Majorana parts of the matrix elements.

In V_{AB}'', the spin summation involves a Q-operator in the manner

$$\sum_{\sigma\tau} \eta_a(1)\eta_b(2) Q_{12} \eta_c(1)\eta_d(2) \equiv Q(a, b; c, d). \tag{13}$$

This summation also reduces to δ-functions in a simple way because

$$Q\eta_1\eta_2 = \eta_2\eta_1; \quad Q\eta_1\eta_3 = \eta_1\eta_3; \quad Q\eta_1\eta_4 = \eta_2\eta_3;$$
$$Q\eta_2\eta_3 = \eta_1\eta_4; \quad Q\eta_2\eta_4 = \eta_2\eta_4; \quad Q\eta_3\eta_4 = \eta_4\eta_3;$$

and

$$Q^{-1} = Q.$$

When these relations are inserted in (13) and (11) is used, the $Q(a, b; c, d)$ are found. We then obtain

$$V_{AB}'' = \sum_{i>j} \Big\{ \int u_{li}(1) u_{lj}(2)\, V''(12) u_{\lambda i}(1) \times u_{\lambda j}(2) d\tau \cdot Q(r_i, r_j; \rho_i, \rho_j) - \int u_{li}(1) u_{lj}(2)\, V''(12) u_{\lambda j}(1) \times u_{\lambda i}(2) d\tau \cdot Q(r_i, r_j; \rho_j, \rho_i) \Big\} \theta_{ij}. \tag{14}$$

Thus far we have traced the decomposition of the general matrix element into simpler integrals

$$\int u_a(1) u_b(2) \exp(-r_{12}^2/a^2) u_c(1) u_d(2) d\tau_1 d\tau_2. \tag{15}$$

Their calculation may also be systematized. The integrations over the x, y, and z coordinates are independent, so that (15) is a product of three factors, each of the form

$$g_{lm} = \frac{1}{\pi} \int\int \xi_1^{\,l} \xi_2^{\,m} \times \exp\left[-\left(1 + \frac{1}{\sigma}\right)(\xi_1^2 + \xi_2^2) + \frac{2}{\sigma}\xi_1\xi_2 \right] d\xi_1 d\xi_2.$$

Only relatively few of the g's occur; they are listed in Table V where we have written $u \equiv 1/(\sigma+2)$. All formulae necessary in the calculation of H_{0i} have now been developed; the remainder of the work is numerical.

Results for the Ground State

The first order energy H_{00} is identical with that of Inglis (cf. his errata), since the lowest Hermite and Legendre functions agree.

$$H_{00}=(19/4)T\sigma-\{5+10w-8h+[8-2(w+h)-18(w+b)](\sigma+2)^{-1}+5(\sigma+2)^{-2}\}(\sigma/\sigma+2)^{\frac{1}{2}}B+1.43\sigma^{\frac{1}{2}}.$$

The last term is the Coulomb energy, which has been neglected in the higher approximations. The contributions of this and the doubly excited states in accordance with formula (2) are listed in Table VI for three values of σ near the energy minimum. One of these values was checked independently by using Inglis' method of oscillator functions. It is seen that the sum falls quite short of the experimental binding energy, 32 Mev. The second order contributions are smaller by about 4 Mev than those listed by Inglis; the difference is explained in his errata. Choice (*b*) gives less binding energy than Choice (*a*), as is also true for the alpha-particle.

A calculation of the contribution of all quadruply excited states is very laborious if all terms of the Hamiltonian are included. Since this contribution is smaller[8] we have computed it retaining only Majorana forces, and for the single value $\sigma=1$. The value chosen for mA is -28.7 Mev. (This gives the correct energy of the alpha-particle.) For this case $H_{00}(=-5.6$ Mev) is far smaller than the values in Table VI, because the large value of the first order kinetic energy is not affected by this choice. But the second order contribution for Majorana forces only, -7.8 Mev, is quite comparable to the value obtained including all the interactions. We may thus have confidence that the contribution of the functions of higher excitation computed with Majorana forces alone is a good approximation. It turns out to be -4.1 Mev (Inglis, reference 8, calculated -3 Mev).

Table V. *List of g's* $[u=1/(\sigma+2)]$.

$g_{00}=g=(\sigma u)^{\frac{1}{2}}$	$g_{00}=(15/8)g(1-u)^3$
$g_{11}=(1/2)gu$	$g_{01}=(15/8)gu(1-u)^2$
$g_{10}=(1/2)g(1-u)$	$g_{02}=(3/8)g(1-3u+7u^2-5u^3)$
	$g_{12}=(3/8)gu(3-6u+5u^2)$
$g_{20}=(3/4)g(1-u)^2$	$g_{30}=(105/16)g(1-u)^4$
$g_{21}=(3/4)gu(1-u)$	$g_{31}=(105/16)gu(1-u)^3$
$g_{22}=(1/4)g(1-2u+3u^2)$	$g_{32}=(15/16)g(1-4u+12u^2-16u^3+7u^4)$
	$g_{33}=(15/16)gu(3-9u+13u^2-7u^3)$
	$g_{44}=(3/16)g(3-12u+42u^2-60u^3+35u^4)$

Table VI. *Summary of numerical results. Doubly excited states.*

	Choice *a*			Choice *b*		
σ	1	1.2	1.4	1	1.2	1.4
H_{00}	-10.0	-10.8	-10.7	-7.3	-7.7	-7.1 Mev
$E_D^{(3)}$	-6.8	-7.2	-7.4	-6.0	-6.4	-6.7 Mev
Sum.	-16.8	-18.0	-18.1	-13.3	-14.1	-13.8 Mev

It is obvious that contributions due to successive stages of excitation do not decrease rapidly enough to permit an estimate of the convergence limit. There is, however, a way in which one may ascertain a lower limit of the second term in (2). We note that

$$E^{(2)}=\sum_i{}'\frac{|H_{0i}|^2}{E_0-E_i}=\frac{S_2}{E_0-E_2}+\frac{S_4}{E_0-E_4}+G,$$

where S_2 and S_4 are the sums of $|H_{0i}|^2$ taken over all doubly and quadruply excited states, respectively. They have already been calculated. G is the remainder of the sum, in which the smallest denominator is $E_0-E_6=-6T\sigma$. Hence

$$|G|<\frac{\sum_i{}'|H_{0i}|^2-S_2-S_4}{6T\sigma}.$$

But by matrix algebra, $\sum_i{}'|H_{0i}|^2=(H^2)_{00}-(H_{00})^2$. Thus

$$|G|<\frac{(H^2)_{00}-H_{00}{}^2-S_2-S_4}{6T\sigma}. \qquad (16)$$

Of all quantities needed, only $(H^2)_{00}$ remains to be calculated. A simplification arises from the fact that the matrix elements appearing in G are free from kinetic energy terms (selection rules!), which means that we may leave out all kinetic energy terms in $(H^2)_{00}$, $H_{00}{}^2$, S_2 and S_4, for they would cancel. Thus we can restrict the calculation to $(V^2)_{00}$. Again, this was done for Majorana forces only, with $(mA)\equiv B=28.7$ Mev.

$$V^2=B^2\{\sum_{i>j}J_{ij}{}^2+\sum_{i>jk}J_{ij}J_{ik}P_{ij}P_{ik}+\sum_{i>j}\sum_{k>l}J_{ij}P_{ij}J_{kl}P_{kl}\}.$$

The corresponding three terms in $(V^2)_{00}$ are given by

$$(V^2)_{00}=B^2\{0.98+1.36+1.01\}=3.35B^2.$$

Moreover, $(V_{00})^2=2.50B^2, S_2=0.29B^2, S_4=0.16B^2$, giving

$$|G|<6.6 \text{ Mev}.$$

This bound is almost certainly several Mev too great. Summarizing our results so far, we may say, even referring to the more advantageous choice of constants in Table VI, that the first and second order perturbational contributions to the binding energy of Li^6 are *in toto* smaller than (18.1+4.1+6.6) Mev=28.8 Mev. In the next section we shall show that the perturbation method, carried up to the second order, yields too large a result for the binding energy in this problem.

Variational Theory[14]

The variational procedure here adopted is that outlined in reference 2. It was carried out before the present perturbational calculations were made, unfortunately with a slightly different set of constants, namely those used in reference 2. Since we are only interested in a general correlation between variational and perturbational results a repetition of the laborious variational work with another choice of constants did not seem worthwhile.

The major difficulty lies in the large number of functions which, for obvious practical reasons, must be reduced. It is because of this necessity that a complete variational treatment of the six-body problem is very unlikely to be achieved. But it is possible, by surveying the tendency of such a calculation and correlating it with a less perfect procedure which can be carried through, to correct the result of the latter.

The functions used are the oscillator functions employed by Inglis.[8] The "types" will here be numbered in the order in which they appear in his Table IV. Only some, not even all, of the doubly excited states have been used, but the eleven types here chosen give more than 80 percent of the total perturbational contribution.

In reducing the number of functions the known H_{0i} elements served as a guide. Types with small H_{0i} were rejected. The remaining functions were combined in such a way that all ψ_i having equal H_{0i} were given the same coefficient, and hence could be taken as a single variation function. This produces as many independent functions as there are types. The word "function" in Table VII refers to such rigid linear combinations. The effect of this initial fixation of some of the functions upon the variational result could be investigated; but we feel that it is inappreciable.

The work now involves the calculation of all elements H_{ij} for the functions selected, and a subsequent reduction of the determinant. The result is equivalent to an inclusion of all higher perturbations in the Schrödinger-Rayleigh scheme, provided that they converge. The direction and extent of its deviation from the second order perturbation result indicate the correction necessary.

To explain this we indulge in a digression on a relation between the method of linear variation functions and perturbation theory. If the functions employed are orthogonal, the former leads to the equation for the energy

$$|H_{ij}-\delta_{ij}E|=0,\ i,\ j=0,\ 1\cdots n \qquad (17)$$

and E is the true solution in case the functions form a complete set. Now if in (17) all non-diagonal elements, except the H_{0i} and their conjugates, are neglected, the determinant may at once be expanded by adding rows with suitable factors, and (17) yields

$$\left(H_{00}-E+\sum_{i=1}^{n}\frac{|H_{0i}|^2}{E-H_{ii}}\right)\times(H_{11}-E)\cdots(H_{nn}-E)=0.$$

On replacing the denominator $E-H_{ii}$ by $E_0-(H_0)_{ii}$ this becomes identical with (2), after cancellation of factors producing the higher roots. The second order perturbation result is thus seen to differ from the truth in 2 respects: (1). It neglects all nondiagonal elements except those in the first row and column. (2). It neglects

TABLE VII. *Lowering of H_{00} by perturbation and variation methods (in Mev).*

Number of Functions Included	Second Order Pert. Contribution	Variational $E-H_{00}$
6	−5.53	−4.19
8	−6.85	−4.85
10	−7.05	−5.12

[14] The results of this section have already been presented at the Washington Meeting of the A. P. S., April 1938.

the difference between perturbed and unperturbed energies in the diagonal terms. Now one can easily see that inclusion of nondiagonal terms lowers the root E; as to (2) we note that replacing $E-H_{ii}$ by $E_0-(H_0)_{ii}$ lowers the root if, for the preponderant functions, $|E-H_{ii}| > |E_0-(H_0)_{ii}|$, raises it otherwise.

In the He^4 problem[3] the H_{ij}-terms neglected in the perturbation scheme were of considerable size; their effect overshadowed the inequalities of the diagonal energy differences. This is the reason why the variational method gave a greater binding energy than the other. For Li^6, we find the reverse to be the case: Nondiagonal elements are small (cancellation between a greater number of functions); the diagonal energy differences are predominantly larger than the zero order differences. The net effect is a greater perturbational than variational contribution. Table VII shows this clearly. The calculations were made for $\sigma=1$. The functions used are $(1, 2, 3, 7, 8, 16)+(6, 18)+(4, 5)$ in Inglis' table of types.

Conclusions Regarding the Ground State

The present investigation is made with the symmetric form of the Hamiltonian, the nuclear constants being specified in two definite ways. Our conclusions will be based upon choice (a) which is probably at the favorable limit of the permissible range of force parameters for producing as large as possible a binding energy of Li^6. With this choice, second order perturbation theory leads to a value certainly smaller than -28.8 Mev for the energy of Li^6. Of this -10.7 Mev are due to excited configurations.

Furthermore we have shown in the last section that perturbation theory magnifies the effect of the excited configurations. If the initial trend which is evident in Table VII persists, we may say that the true contribution of the excited states is not more than 75 percent of the perturbational one. This leads to the value $-(18.1+\frac{3}{4}\cdot 10.7)$ Mev $\doteq -26$ Mev as a lower bound for the computed energy of Li^6. The present analysis of the problem thus corroborates the conclusion of Inglis that a symmetric Hamiltonian is inadequate to produce agreement with the experimental value, -32 Mev.

Table VIII. *List of perturbing doubly excited configurations.*

Configurations	No. of Functions	Configurations	No. of Functions
$(1s)^4 2p3p$	2	$(1s)^3(2p)^2 2s$	8
$(1s)^4 2p4f$	4	$(1s)^3(2p)^2 3d$	22
$(1s)^4(3d)^2$	3	$(1s)^2(2p)^4$	12

Effect of Excited Configurations on ^3D-State

In the papers by Feenberg and Wigner[15] and by Feenberg and Phillips[16] the first order energies of the low lying levels of a large number of nuclei have been calculated. The question arises as to how much the first order arrangement of levels will be disturbed by second order effects. Li^6 offers an easy opportunity for testing this matter.

The result will be sufficiently significant if we work with Majorana forces only and make a 2nd order perturbation calculation including only the doubly excited states. For the ^3S state this procedure has already been carried through: it yields a lowering of 7.8 Mev for $B=-28.7$ Mev.

The first order function for the ^3D state is

$$\psi_0=\left(\frac{1}{6!}\right)^{\frac{1}{2}}|s\eta_1 s\eta_2 s\eta_3 s\eta_4 p_1\eta_2 p_1\eta_4|.$$

It has a first order energy

$$H_{00}=E(^3S)-3\sigma^{\frac{1}{2}}(\sigma+2)^{-7/2}B,$$

and therefore lies in this approximation (with $\sigma=1$) about 2 Mev above the ground state. It is perturbed by the doubly excited configurations given in Table VIII.

The lowering effect of these functions is 3.8 Mev for $\sigma=1$, 3.9 Mev for $\sigma=1.2$ and 1.4.

In this approximation, then, the first order $^3D-{}^3S$ energy difference is altered by 4 Mev. A correlation between computed first order levels and experimental data is therefore in general not to be expected. One should observe, however, that the order of the terms remains unchanged, which is in agreement with Feenberg and Wigner's expectation.

[15] E. Feenberg and E. Wigner, Phys. Rev. **51**, 95 (1937).
[16] E. Feenberg and M. Phillips, Phys. Rev. **51**, 597 (1937).

The Counting Losses in Geiger-Müller Counter Circuits and Recorders

HAROLD LIFSCHUTZ AND O. S. DUFFENDACK
University of Michigan, Ann Arbor, Michigan

(Received August 24, 1938)

The counting losses due to the finite recovery time of Geiger-Müller counter circuits and recorders are investigated. A description and critique of several experimental methods is given. The parallel method reported here gives the most accurate results. By this method the counting losses in a system consisting of a Geiger-Müller counter coupled by means of a Neher-Harper circuit to a scale-of-one recorder were determined. The method compares the counts registered by the scale-of-one against those registered by a vacuum tube scale-of-128 in parallel with it. The resolution times of both the scale-of-one and the G-M, Neher-Harper combination are thus found. The theoretical equations of Ruark and Brammer and Alaoglu and Smith are verified. The limitations and applicability of the Schiff-Volz formulation are also determined. Departures from the Ruark-Brammer formula for the Neher-Harper circuit are found at high counting rates. A corrected formula is derived. The speed of the Neher-Harper type of extinguishing circuit, determined in these experiments, is compared against the maximum counting speed possible with G-M counters. It is found that such circuits already approach the speed of the G-M tube itself. Existing vacuum tube scaling circuits and frequency meters are shown to be already faster than the G-M tube itself. The methods for correcting recorders and counter circuits for counting losses are given. These losses amount to about 20 percent for a Cenco recorder and one percent for most G-M counters at input rates of 1000 counts per minute. The losses increase rapidly with the input counting rate.

INTRODUCTION

THE statistical fluctuations in the number of disintegrations per minute of a radioactive substance give rise to the problem of low efficiency in the recording with simple apparatus of the individual disintegrations. In the case of a Geiger-Müller counter furnishing pulses to a scale-of-one recorder, it is well known that a large fraction of the counts are not registered by the recorder because of its finite resolution time even at rather low counting rates. Because of the statistical fluctuations in the time intervals between disintegrations, many of the counts come so close together as to fail to be resolved by the recorder. Since the short time intervals are the most probable, this effect is very large and increases rapidly with the counting rate. The recovery time of the Geiger-Müller counter and its coupling and quenching circuit (such as the Neher-Harper circuit) also causes counting losses due to this effect. Since the counting losses depend on the counting rate, the shape of observed radioactive decay curves will be distorted.

It is the purpose of the present paper to investigate the counting losses in a scale-of-one recorder and in the Geiger-Müller counter and Neher-Harper[1] coupling circuit, and to test the statistical theories of these losses which have been proposed.

METHODS

The efficiency of a recorder is defined as the ratio of the output counts to input counts. To test the efficiency of a recorder in the most direct way a known number of counts having a *random* distribution must be fed into it and the number registered observed. This procedure would have to be repeated for various input counting rates to obtain the efficiency as a function of the counting rate.

However, it is not possible directly to obtain such a known and variable random source of counts so that more indirect methods must be employed. Several methods may be used which may be designated as follows: (1) the film method;[2] (2) the multiple addition test method;[3] (3) the inverse square method; (4) the variable area method and (5) the parallel method.[4] We have in the past extensively investigated methods 1, 2, and 5 while methods 3 and 4 have sometimes

[1] H. V. Neher and W. W. Harper, Phys. Rev. **49**, 940 (1936).

[2] H. Lifschutz, O. S. Duffendack and M. M. Slawsky, Phys. Rev. **51**, 1027 (1937).

[3] O. S. Duffendack, H. Lifschutz and M. M. Slawsky, Phys. Rev. **52**, 1231 (1937).

[4] H. Lifschutz and O. S. Duffendack, Phys. Rev. **53**, 941 (1938). The present report modifies the conclusions given in this note.

been used by others in a qualitative way, mostly to test the speed of certain recording circuits.

A brief description and critique of the above methods may be given. In the film method, the electrical output of a G-M counter and Neher-Harper circuit actuated by a constant radioactive source was recorded by a commercial Western Electric sound system on standard 32 mm film. This sound system had an over-all frequency response flat to 10,000 cycles per second. This was about 150 times the speed of the single scale recorder to be calibrated. The recording of the G-M pulses was made at such a slow counting rate that the counting losses in the recording were very small and a quite accurate Poisson distribution of pulses was obtained on the film. This distribution was quantitatively tested by the method of Marsden and Barratt[5] in which the number of intervals of various lengths between pulses on the film was determined. A plot of the probability, $P(x)$, of an interval of length, x, *versus* the interval, x, showed good agreement with the theoretically predicted curve with a Poisson distribution. Of course small deviations would probably be masked by statistical fluctuations and the limited sensitivity of the method. The number of pulses on the film was counted visually. The film was then used as a known source of random counts by playing it back with the use of a standard sound head and photo-cell amplifier. The pulses from the film were fed to a single scale recording circuit operating a Cenco counter. The input to this recorder was determined from the measured running speed of the film and the total number of counts. The input rate was varied by varying the speed of the film. Thus a calibration curve for the single scale recorder could be determined.

The multiple addition test method is an approximation method. It makes use of a number of weak natural radioactive sources, the number of counts from which have been measured individually by the circuit being calibrated. The sources are so weak that the counting losses from one source are assumed to be negligible. These calibrated sources are then used in combination and the sum of the individually determined values is taken as the true input. A simple source holder with substitution dummy sources keeps the radiation scattered into the G-M counter constant. When only two sources are used this method reduces to the well-known simple addition test used for testing the linearity, with source strength, of counter circuits. However, the simple addition test cannot be used for calibrating a counter circuit. At most it can be used to determine when the departure from linearity becomes large, i.e., at what counting rates counting losses become appreciable.

The inverse square method makes use of the inverse square law of the variation of input counts of the source as a function of the distance from the counter. The variable area method employs a diaphragm which screens off the source from the counter. By varying the area of an opening in the diaphragm, it is assumed that the input counting rate to the G-M tube may be varied proportionately.

Before describing the parallel method the limitations of the previous methods may be pointed out. The film method determines the losses in the recording circuit of the G-M system only and not in the G-M tube and quenching circuit itself. The other three methods include the effect of losses in the G-M circuit. Statistical fluctuations are very small in the film method, extremely large in the multiple addition method, and fairly large in the inverse square and variable area method. In the film method the number of pulses on the film is fixed; fluctuations arise because of the possibility of changing distributions. The fluctuations are of the order $(\Delta N)^{\frac{1}{2}}$, where ΔN is the number of counts lost. In the multiple addition method the fluctuations in the individual calibrations go as $N^{\frac{1}{2}}$, where N is the total number of counts recorded. When the sources are added the total error in the strength of the combined source due to the errors in the individual sources caused by fluctuations may be very great. This makes it necessary to record an enormous number of counts. This consumes too much time at the low counting rates which must necessarily be used. The fluctuations in methods 3 and 4 are proportional to $N^{\frac{1}{2}}$ and are greater than that in the parallel method where again the fluctuations are of order $(\Delta N)^{\frac{1}{2}}$. The width of the pulses in the film method changes as the speed of the film is changed. This restricts the input counting rate to

[5] Marsden and Barratt, Proc. Phys. Soc. **23**, 367 (1911).

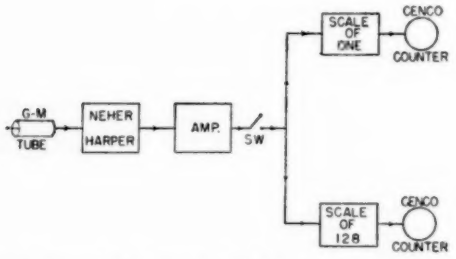

FIG. 1. Schematic diagram of set-up for parallel method.

certain limits such that the width of the pulses remains less than the resolution time of the recording circuit. Difficulties arise in methods 3 and 4 because of scattering, the lack of true point sources, and the non-uniformity of the flux of radiation over the diaphragm area. Also geometrical uncertainties in applying the inverse square law to the G-M counter cause difficulties. Many other limitations in the above methods relating to accuracy of results, flexibility, ease of application, requirements of special apparatus and sources, speed of the method and limits of counting range over which they are practicable, could easily be pointed out. In short, all the above difficulties may be best overcome by employing the parallel method. The precision and range of the results of this method are such that it only will be discussed further. The data to be presented also refer only to this method. Results were long ago obtained by the parallel method with thyratron scaling circuits. It was not until the recent development of high speed vacuum tube scaling circuits, however, that complete results were obtainable over wide enough input counting rates to allow a real test of the theory.

EXPERIMENTAL ARRANGEMENT AND PROCEDURE

The experimental arrangement for the parallel method is shown schematically in Fig. 1. The G-M counter is actuated by a constant radioactive source and is coupled by means of the Neher-Harper circuit to a scale-of-one and a scale-of-128 recorder in parallel. The circuit diagram of the Neher-Harper circuit and scale-of-one[6] is shown in Fig. 2. The scale-of-128 consisted of the high speed vacuum-tube type recently described[7] and was obtained by using a scale-of-16 and a scale-of-eight (both of the vacuum-tube type) in series. The resolution time of the vacuum tube scaling circuits was shown to be 6.5×10^{-6} second for input pulses of width 3.25×10^{-6} second.[7] The scaling ratio of 128 employed was so large that counting losses in the Cenco counter fed by the scaling circuit could be taken as negligible and actually will later be shown to have been zero. The G-M tube used was constructed of a solid nickel cylinder (about 2 cm long and 1.2 cm in diameter) and 3 mil tungsten anode wire. It was filled with hydrogen to a pressure of 136 mm of Hg. The method of preparation was as given previously[3] with the addition of thorough outgassing of the nickel cathode by means of an induction furnace to ensure a more permanent freedom from foreign gases. The counter had a long plateau of over 600 volts, which was quite flat over most of this range. The counter voltage used was 1200 volts; the counter threshold was at 1000 volts. A stabilized power supply was used to furnish this voltage to the counter. Inspection of the pulses generated by this counter, by use of a cathode-ray oscillograph showed the counts to be sharp, single pulses of uniform amplitude without the

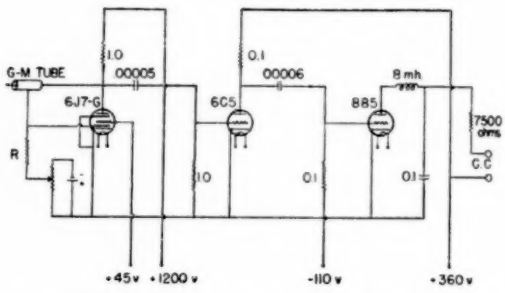

FIG. 2. The Neher-Harper circuit and scale-of-one recorder. Resistance values are in megohms and capacitance in microfarads. The amplifier indicated in Fig. 1 is not shown in this diagram.

presence of trains of spurious pulses of varying amplitude as often seen in poor counters. It was concluded that, except for losses due to its finite resolution time, this counter furnished a true Poisson distribution of pulses when actuated by a radioactive source and was thus suitable for testing the statistical counting loss theories which were fundamentally based on such a distribution.

The parallel method compares the number of counts recorded by the scale-of-one against that

[6] J. R. Dunning, Rev. Sci. Inst. **5**, 387 (1934).
[7] H. Lifschutz and J. L. Lawson, Rev. Sci. Inst. **9**, 83 (1937).

recorded by the scale-of-128. If the counting losses in the G-M circuit are negligible the scale-of-128 reading may be taken as the true number of counts, n_0, because the scaling circuit records all the counts coming from the N-H circuit. In this way the true input to the scale-of-one is determined and the output is simultaneously observed. This allows a direct calibration of the scale-of-one and also a direct test of any counting loss theory by giving the output as a function of the input. Since the input to both recorders is the same because the readings are simultaneous, it is clear that the statistical fluctuations in this method are very small. If the losses in the G-M circuit are not negligible for the counting rates used, the scale-of-128 does not record the true input, n_0, but does record all the pulses coming from the Neher-Harper circuit. Since the reading of the scale-of-one and also that of the scale-of-128 is a function of n_0, the simultaneous readings of the two recorders are described by two equations from which the unknown, n_0, may be eliminated. The way in which quantitative results are obtained may be found by examining the theory.

Theory

Ruark and Brammer,[8] and Alaoglu and Smith,[9] have given statistical theories of the counting losses in recorder circuits and have included the effect of losses in the G-M circuit. They have derived the following formulae for the observed readings of the recorders as a function of the true random input, n_0.

$$n_1=\frac{n_0}{1+n_0\sigma}\exp\left(-(\tau_1-\sigma)n_0\right) \quad \text{if} \quad \tau_1\gtrless\sigma, \tag{1a}$$

$$n_n=\frac{n_0}{n}\cdot\frac{1}{1+n_0\sigma} \quad \text{if} \quad \tau_n\leqslant n\sigma. \tag{1b}$$

Here n_1 is the observed reading of the scale-of-one, n_n that of the scaling circuit, n is the scaling ratio used, τ_1 is the resolution time of the scale-of-one and σ that of the Neher-Harper circuit. We distinguish τ_1 and τ_n as τ_n refers to the Cenco counter stage fed by the scaling circuit. These τ's are of the same order of magnitude. Here, $n=128$ and for convenience we will write hereafter τ for τ_1, and n_{128} for $n_n\cdot n$ which gives

$$n_{128}=\frac{n_0}{1+n_0\sigma}. \tag{1c}$$

The recovery time is defined as the time interval after a count which must be allowed before the circuit is ready to record another count. Clearly the statistics of a recording circuit will be different according to whether or not the recovery time of the circuit is affected by the occurrence of another count during the period of recovery. This circumstance gives rise to two formulae describing the two opposite extremes of recorder behavior. For recorders such as the Cenco counter, which can be re-excited during the period of recovery, the efficiency formula for the case of a true random input is

$$n_1=n_0\exp\left(-n_0\tau\right). \tag{2a}$$

This type of circuit is designated as Type I. A Type I recorder requires that a count, to be recorded, must be preceded by an interval τ during which no count arrives at the recorder. If the recovery time is completely unaffected by additional counts coming in during the recovery period we obtain a Type II recorder for which the efficiency formula is

$$n_1=\frac{n_0}{1+n_0\tau}. \tag{2b}$$

In order to test the theory, the circuits used must satisfy the assumptions made in deriving the formulae. In referring to Eq. (1a) it is clear that with $\tau>\sigma$ and $\sigma\to 0$ Eq. (1a) becomes

$$n_1=n_0e^{-n_0\tau}. \tag{3}$$

In other words the recorder circuit used to test Eq. (1a) must be a Type I recorder. The scale-of-one shown in Fig. 2 is such a recorder even though the Cenco counter is driven by a thyratron since the thyratron circuit is so much faster than the mechanical counter itself. This scale-of-one was also chosen because it is a widely used circuit which is very simple, reliable and faster than most other scales-of-one developed to date.[10]

[8] A. E. Ruark and F. E. Brammer, Phys. Rev. **52**, 322 (1937).

[9] L. Alaoglu and N. M. Smith, Jr., Phys. Rev. **53**, 832 (1938). See also W. B. Lewis, Proc. Camb. Phil. Soc. **33**, 549 (1937).

[10] See, e.g. W. H. Pickering, Rev. Sci. Inst. **9**, 180 (1938).

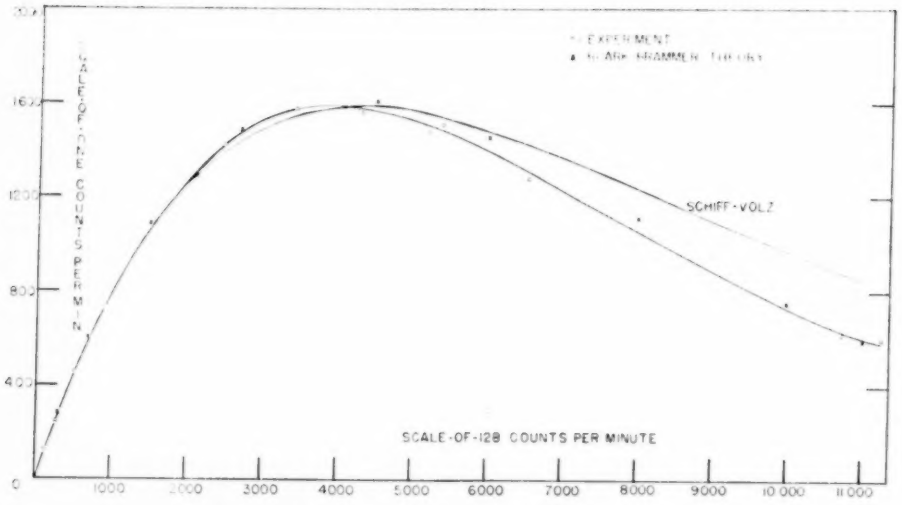

FIG. 3. The response curve for $R=20$ megohms.

Other conditions of the theory that must be met are that the recovery time of the Kth stage of scale-of-two in the scaling circuit does not exceed $2^{K-1}\sigma$, or, in other words, if we consider the first stage, its recovery time must not exceed that of the Neher-Harper circuit. From the measured resolution time of the scaling circuit given previously and preliminary measurements of σ showing it to be of the order $10^{-3}-10^{-4}$ second, it is clear that we have satisfied this condition. Likewise, it is clear that the condition $\tau_1 \gtrsim \sigma$ is met and also the condition $\tau_{128} \lesssim 128\cdot\sigma$, since the scaling ratio of 128 is so great. Moreover, rough preliminary measures of τ and σ may easily be made which also show that these latter conditions are met and later these conditions may be checked again with the final values of τ and σ.

We conclude that the circuit arrangement chosen satisfies all the conditions for providing a test of the theory.

The Eqs. (1a) and (1c) are now used to eliminate the unknown input n_0 and give

$$n_1 = n_{128} \exp\left[-n_{128}(\tau-\sigma)/(1-n_{128}\sigma)\right]. \quad (4)$$

If one takes $dn_1/dn_{128}=0$, a maximum of n_1 is found when

$$\sigma = \frac{1-[n_{128}(\tau-\sigma)]^{\frac{1}{2}}}{n_{128}}. \quad (5)$$

Defining the percent loss P as

$$P = 100\times(n_{128}-n_1)/n_{128},$$

taking dP/dn_{128} and letting $n_{128}\to 0$, we find the slope, S_0, of the percent loss curve at the origin is given by

$$dP/dn_{128} = S_0 = (\tau-\sigma)\times 100, \quad n_{128}\to 0. \quad (6)$$

Eqs. (5) and (6) allow both τ and σ to be found from experimental observations of S_0 and the value of n_{128} when n_1 is a maximum.

The experimental procedure is now clear. By using a constant radioactive source and varying its distance from the G-M counter, the experimental curves $n_1=f_1(n_{128})$ and $P=f_2(n_{128})$ may be obtained. The values of τ and σ are found from these curves as described above. The values are put back into the equations and the curves above computed theoretically. This gives a check of the theory. Moreover, τ and σ may also be found by independent methods and compared against the values of τ and σ found from the experimental curves. These values of τ and σ will be denoted by τ_{direct} and σ_{direct}. The value of τ_{direct} was found by applying *periodic* saw-tooth pulses from a sweep-circuit oscillator to the scale-of-one recorder and increasing the frequency till the maximum counting speed of the recorder was reached. This was determined from the reading of the recorder itself over a time interval measured with a stop watch. From the definition of recovery time it is clear that

$$\tau_{\text{direct}} = 1/n_{\max} \text{ (periodic)}. \quad (7)$$

Similarly, σ_{direct} was found by observing the

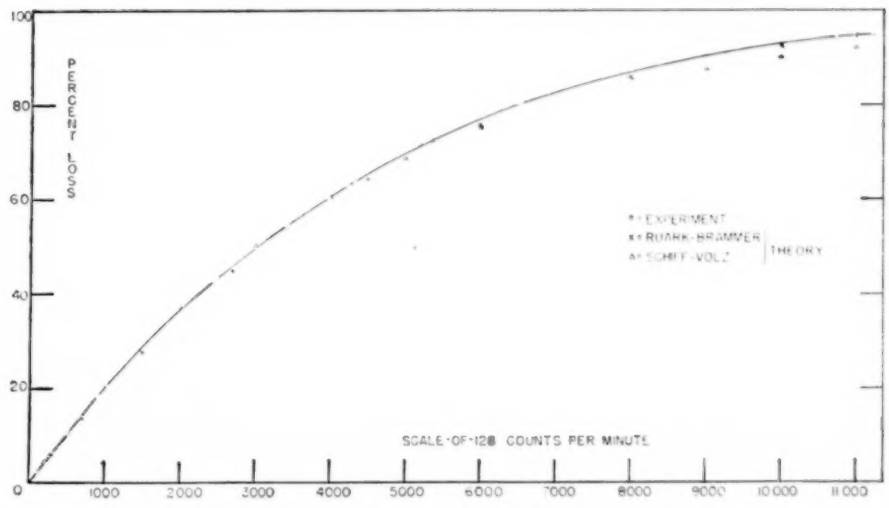

FIG. 4. The percent loss curve for $R=20$ megohms.

maximum *random* counts from the Neher-Harper circuit by means of the scale-of-128. This was accomplished simply by bringing up a strong source. Eq. (1c) shows that

$$\sigma_{\text{direct}}=1/n_{128\ \max}\ \text{(random)}. \tag{8}$$

EXPERIMENTAL RESULTS

Figures 3 and 4 show the experimental curves for n_1 and P as functions of n_{128}. The predicted maximum in n_1 is observed. It will be noted that this maximum is very broad which makes an accurate determination of n_{128} at the maximum very difficult. On the other hand, the slope at the origin in Fig. 4 may be accurately determined and so also the value of $\tau-\sigma$. The value of σ is very sensitive to the value taken for n_{128} at the maximum. Since in the case here considered σ is quite small relative to τ it was decided to use for σ the value of σ_{direct} and for $\tau-\sigma$ the value from the slope of the percent curve. These values were put into the theoretical equations to calculate the points marked "Ruark-Brammer Theory." It is seen that the agreement with the experimental curves is very good. These curves were taken by using a grid resistor, R, in the Neher-Harper circuit of 20 megohms, a correct value for the G-M tube used.

In order to allow a more complete test of the theory, σ was purposely increased by increasing the Neher-Harper grid resistor to 100 megohms and the experiments repeated. The results are shown in Figs. 5 and 6. The decrease in the slope of the percent curve is found as predicted. The value of σ relative to τ was now large enough to determine τ and σ from the observed slope and maximum in spite of the broadness of the maximum. By taking as observed values $n_{128}=3850\pm125$ counts per minute, and $\tau-\sigma=1.066\times10^{-2}$ sec. the theory gives $\sigma=0.27\times10^{-2}$ sec. and $\tau=1.34\times10^{-2}$ sec. Over the limits given for n_{128}, σ varies from 0.24×10^{-2} sec. to 0.30×10^{-2} sec. These limits include the value of $\sigma_{\text{direct}}=0.286\times10^{-2}$ sec. The values of τ and σ determined from the curves as above were put into the theoretical equations and the curves calculated again as shown in Figs. 5 and 6. The agreement between theory and experiment is again very good. Although the value of σ is very sensitive to the value of n_{128} taken, the shape of the curve is not especially sensitive to σ so that the agreement with experiment is substantially the same over the limits of σ given as for the curves shown with $\sigma=0.27\times10^{-2}$ sec.

The comparison of the values of τ and σ with τ_{direct} and σ_{direct} is shown in Table I where, as previously stated, for $R=20$ megohms, σ was taken equal to σ_{direct}. The values of σ_{direct} were also checked with a vacuum tube frequency meter.[11] It will be noted that the theoretical value of τ remains practically constant in the two determinations while only σ varies. This is, of course, exactly as it should be.

[11] H. Lifschutz, Phys. Rev. **53**, 950 (1938).

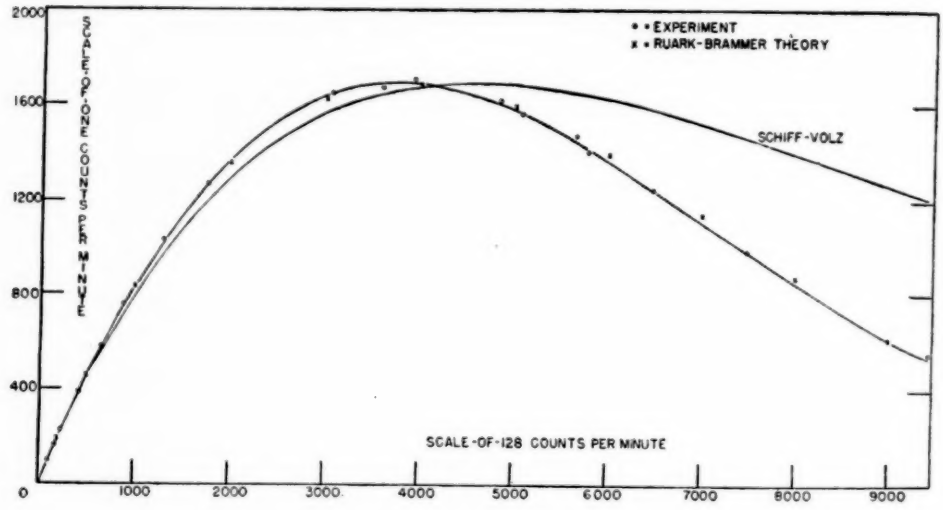

FIG. 5. The response curve for $R=100$ megohms.

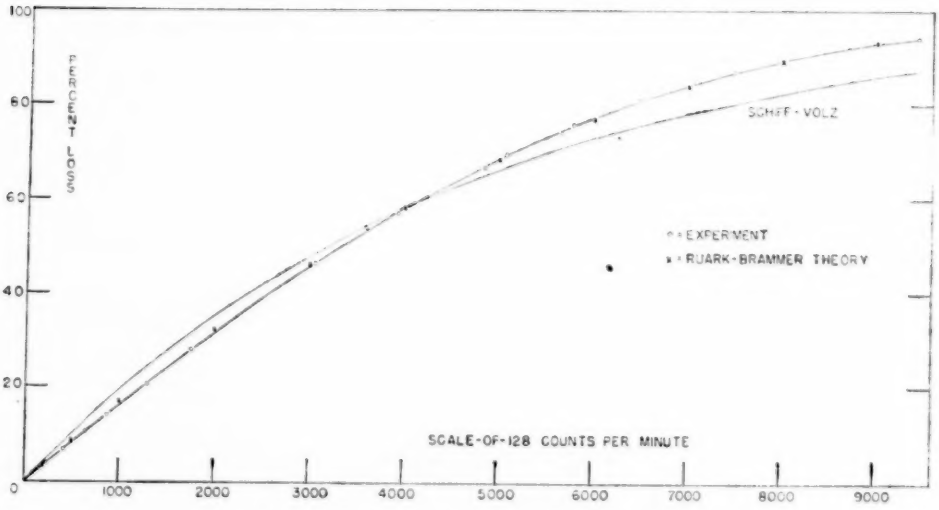

FIG. 6. The percent loss curve for $R=100$ megohms.

The original counting loss theories of Schiff[12] and Volz[13] attempted to account for counting losses in a G-M system by introducing a single recovery time, τ, to include both the effects of the counter circuit and the recording circuit. They derived the equation

$$n_1=n_0e^{-n_0\tau}. \tag{9}$$

Clearly the Ruark-Brammer and Alaoglu-Smith formulae reduce to this when $\sigma=0$. If the losses in the Neher-Harper circuit could be neglected, the theoretical Schiff-Volz curves shown in Figs. 3 to 6 should agree with the experimental curves for then $n_{128}=n_0$. Clearly they do not, showing in a striking way the effect of the resolution time σ and also showing at what counting rates the losses in the counter circuit become appreciable. As expected, the agreement of the Schiff-Volz theory is much better for the case in which $R=20$ megohms than in the case $R=100$ megohms since in the former case σ is smaller.

It is easily shown from Eq. (9) that

$$\tau=1/n_{1\,\max}, \tag{10}$$

where $n_{1\,\max}$ is the maximum random counting

[12] L. I. Schiff, Phys. Rev. **50**, 88 (1936).
[13] H. Volz, Zeits. f. Physik **93**, 539 (1935).

rate. The theoretical Schiff-Volz curves shown in Figs. 3 to 6 were calculated by determining τ from the maximum of n_1 shown in Figs. 3 and 5. The τ's determined in this way were respectively 1.39×10^{-2} sec. and 1.31×10^{-2} sec. If there were no losses in the G-M circuit, the Schiff-Volz theory would give the slope of the percent loss curve at the origin as $100\times\tau$, since then $n_{128}=n_0$. Actually values of τ are found by this method to be 1.25×10^{-2} sec. and 1.066×10^{-2} sec., which are very low as expected.

As shown above, τ, determined from the maximum of n_1, is less in the case $R=100$ megohms than in the case $R=20$ megohms. The observed maximum of n_1 increases as σ increases, since, due to σ, the short intervals are cut out by the G-M circuit. Thus the recorder is able to approach more nearly its maximum *periodic* counting rate. Accordingly, it is to be expected that τ determined experimentally from $n_{1\,\max}$ would automatically give the correct kind of average value including the effects of both the counter and the recording circuits. For this reason the use of a single resolution time to give the *over-all efficiency* of the entire counting system turns out, in practice, to give a good approximation to the truth. This is shown by Fig. 7, where n_1 is plotted against n_0 (not n_{128}) from the data for the case $R=100$ megohms. The experimental curve is computed from the Ruark-Brammer theory since this has been shown to agree with experiment. The graph is plotted up to such values of n_0 as correspond to the maximum of n_{128} in Fig. 5. One must conclude that the Schiff-Volz method is adequate to correct a G-M Type I scale-of-one system for counting losses up to its maximum counting rate with a high degree of accuracy. This is fortunate since τ is so easily determined experimentally from Eq. (10).

Experimental Precautions

The statistical fluctuations in the parallel method are quite small as shown by the smoothness of the experimental curves. The number of counts per point usually was about 10,000 to 15,000. The slope of the percent loss curve at the origin may, under these conditions, be determined with an accuracy of one or two percent. In order to obtain reproducibility all conditions of the experiments must remain quite constant. The circuit constants must not vary too much, nor the voltages. Different G-M tubes have different σ even though of similar construction and used with the same N-H circuit. This is easily shown by the very different values of the maximum random counts obtainable. The capacity of the G-M tube and its leads also influences σ quite sharply. The leads should be kept short and separated. If the counter is not electrostatically shielded, the body capacity of an observer influences the counting rate quite markedly, especially at high counting rates. In short it is essential to keep the capacity of the counter with respect to its surroundings constant. If an electrostatic shield is used to keep the charges on the glass walls of the G-M tube from changing,[14] a very large increase in σ is observed as measured by the maximum counting rate. The counter used in these experiments was used without a shield. Any effects due to charges on the walls (which were quite small for this counter) were avoided by allowing the charge to come to equilibrium after changing the source strength. Effects due to photosensitivity were also avoided by light shielding.

Table I. *Values of τ and σ in seconds.*

	$R=2\times10^7$ ohms		$R=10^8$ ohms	
	Theory	Direct	Theory	Direct
τ	1.37×10^{-2}	1.43×10^{-2}	1.34×10^{-2}	1.43×10^{-2}
σ	0.114×10^{-2}	0.114×10^{-2}	0.27×10^{-2}	0.286×10^{-2}

The Neher-Harper Circuit

The experimental method considered above, as already stated, is not especially sensitive to the effect of σ for values of σ relative to τ as given above. Since the losses in the Neher-Harper circuit are independent of the use of fast scaling circuits or frequency meters, the only way to take account of these losses is by correcting theoretically for them. Of course, faster counters and quenching circuits would also get around this difficulty up to certain counting rates. However, it seems that such faster circuits have not yet been developed.[15] The highest counting rates

[14] J. L. Lawson and A. W. Tyler, Phys. Rev. **53**, 605 (1938).
[15] See e.g. I. A. Getting, Phys. Rev. **53**, 103 (1938); A. E. Ruark, Phys. Rev. **53**, 316 (1938); H. V. Neher and W. H. Pickering, Phys. Rev. **53**, 316 (1938); E. Y. Yetter, Phys. Rev. **53**, 612 (1938).

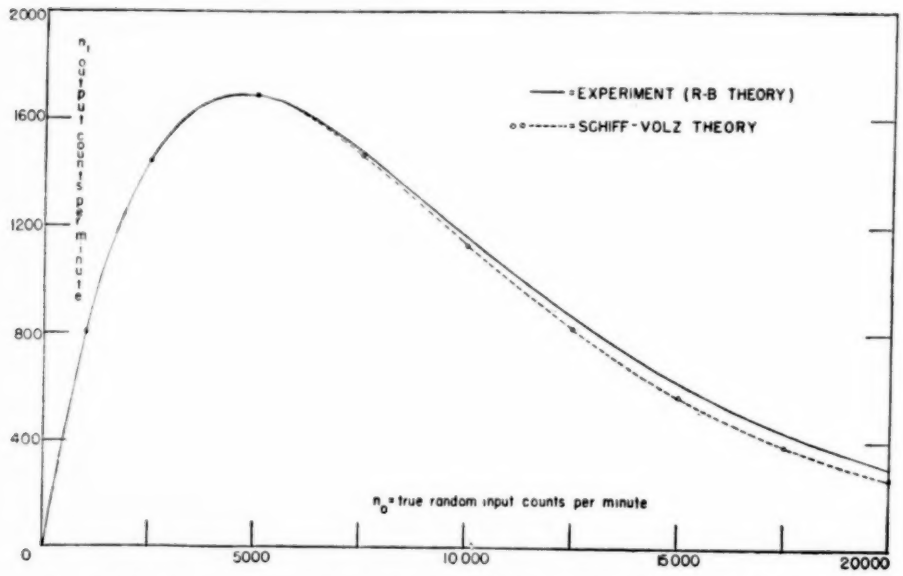

FIG. 7. Showing the approximate validity of the use of a single resolution time.

so far reported have been obtained by using the Neher-Harper circuit. Getting[15] reports values for the multivibrator type of quenching circuit of 1.2×10^5 counts per minute and probably higher values if part of the counting range of the G-M tube is sacrificed.

The counting losses due to σ are shown in Fig. 8 according to the Ruark-Brammer formula. The value of σ used corresponds to the average of most counters we have tested. In view of the magnitude of these losses it is important to know whether or not the Neher-Harper circuit does follow closely the Ruark-Brammer equation

$$n=\frac{n_0}{1+n_0\sigma} \tag{11}$$

or, perhaps, the equation

$$n=n_0\exp(-n_0\sigma). \tag{12}$$

The parallel method gives rather good support to Eq. (11), as we have seen within the limits of its sensitivity to σ. However, all counters we have tested depart from Eq. (11) at high counting rates in that they reach a maximum counting rate which is followed by a very marked decrease as the source strength is still further increased. This is in disagreement with Eq. (11), which, as noted by Ruark and Brammer, indicates a maximum *constant* value for n. Counters which showed this decrease had maximum counting rates varying from 50,000 to 175,000 random counts per minute. The effect was found both with the scale-of-128 and the frequency meter. This decrease is what would be expected if Eq. (12) were followed or might be due to a slight departure from Eq. (11). To test this point further, the following method was devised.

The grid resistor of the N-H circuit was connected by switches so that it could quickly be changed from 10^7 to 10^8 ohms. The counting rate due to a constant source was determined with the scale-of-128 for each of these grid resistor values. The grid bias was also changed with the resistor to the proper value. This procedure was repeated for all counting rates up to the maximum. Let the observed counts with the two resistors be n_7 and n_8. Then

$$n_7=\frac{n_0}{1+n_0\sigma_7}, \tag{13}$$

$$n_8=\frac{n_0}{1+n_0\sigma_8}. \tag{14}$$

Thus n_0 may be eliminated giving

$$n_8=\frac{n_7}{1+n_7(\sigma_8-\sigma_7)}, \tag{15}$$

$$P=\frac{n_7-n_8}{n_7}\times100=100\times\frac{n_7(\sigma_8-\sigma_7)}{1+n_7(\sigma_8-\sigma_7)}. \tag{16}$$

The slope of the percent curve at the origin

$$dP/dn_7 = 100(\sigma_8 - \sigma_7), \quad n_7 \to 0 \qquad (17)$$

and

$$\sigma_7 = \frac{1}{n_{7\,\max}}, \quad \sigma_8 = \frac{1}{n_{8\,\max}}. \qquad (18)$$

The experimentally observed percent loss curve could be compared with that calculated from Eqs. (16) and (18). This could also be done by the use of a formula for the N-H circuit similar to Eq. (12). Rough preliminary results show a decided disagreement with Eq. (12) and fair agreement with Eq. (11) up to $n_{7\,\max}$. A variant of this method may possibly be that of keeping the grid resistor constant and varying the N-H grid bias alone, as the observed counting rate is a function of this bias.

In view of the tendency to follow the equation

$$n = n_0/(1+n_0\sigma)$$

up to counting rates near the observed maximum and also the observed departure from this equation as shown by the failure to maintain a constant maximum counting rate, it is of interest to try to look more deeply into the mechanism of the G-M counter and N-H combination. The G-M counter has a deionization time, τ_d, which is given by the time it takes for the electric field in the counter to sweep out the positively charged ions after the discharge is extinguished. Thus, τ_d may be taken as constant. It also has a discharge time, σ, which has a lower limit equal to τ_d and which has a value which depends not only on the G-M tube but also on the extinguishing circuit. Since the counter tube cannot be re-excited by an incoming particle during the discharge period, σ, the counter itself may be classed as a Type II recorder. The extinguishing circuit introduces still another resolution time, ρ. The resolution time, ρ, of the N-H circuit would be approximately equal to σ if the succeeding circuits had no thresholds. To see this, consider a discharge in the G-M counter. In the extinguishing process, as is well known, the potential on the counter is reduced to the threshold value or very slightly below. The voltage then starts to recover at a rate depending mainly on the *RC* value of the N-H circuit. If another discharge occurs in the G-M counter when the potential has recovered to a value only slightly above the threshold value, the electrical impulse developed will be very weak since these impulses are equal to the overvoltage. The pulse thus fails to be recorded because the succeeding circuits require a certain minimum signal for response. Such circuits are the discriminator circuit, the first stage of scale-of-two in the scaling circuit or the mechanical counter stage if no scaling circuit is used. In this way the time constant of the N-H circuit does introduce an effective recovery time, $\rho > \sigma$. It is clear that a count coming within a time greater than σ and less than ρ of a preceding count will not only fail to be recorded but will re-excite the Neher-Harper circuit. In other words we may reasonably take the efficiency formula as that of a Type I recorder. If one assumes σ to be reasonably constant, the usual derivation gives for the over-all efficiency

$$n = (n_0/(1+n_0\sigma)) \exp(-n_0(\rho-\sigma)) \text{ if } \rho > \sigma \qquad (19)$$

where n is the number of counts from the N-H circuit. This, then, is the corrected Neher-Harper equation. If ρ and σ are approximately equal, this equation reduces essentially to

$$n = n_0/(1+n_0\sigma)$$

at counting rates considerably below the maximum. This explains why the parallel method showed agreement with this equation, since the counting rates were well below the maximum. The exponential "guillotine factor" in Eq. (19) is then responsible for the observed decrease after the maximum counting rate has been reached. This requires $\rho > \sigma$. Since the Neher-Harper cir-

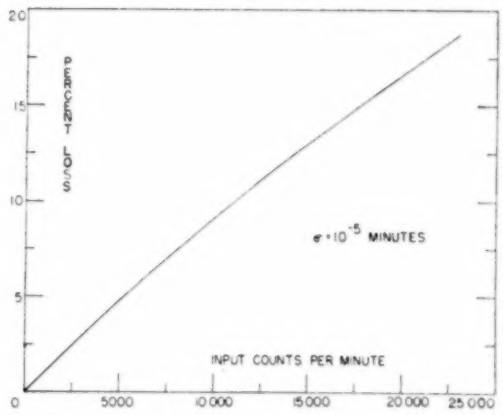

FIG. 8. The counting losses in the G-M circuit.

cuit cannot recover the voltage till the counter has stopped discharging, it is clear that $\rho > \sigma$ always. However, ρ and σ are not independent. The variation of σ by changing the N-H grid resistor shows a dependence of σ on ρ. Ruark and Brammer describe the situation by saying that the counter and circuit "work together" as a single unit so that the dependence is described by the relation $\rho \leqq \sigma$. This approximate relation, $\rho \leqq \sigma$, plus the relation $\rho > \sigma$ and Eq. (19) thus seem capable of explaining all the experimental facts. Qualitative tests of Eq. (19) with the inverse square method show a more or less exponential decay after reaching the maximum counting rate. However, it is clear that a more detailed justification of Eq. (19) would be desirable, especially in order to throw more light on the exact relationship between ρ and σ. This might lead to circuit designs which would allow σ to be decreased. It seems in the present case that enough amplification was already used to reduce ρ to a value not much greater than σ. No important increase in counting speed thus seems possible by increasing the amplification between the N-H circuit and the recorder.

The decrease in amplitude of the pulse generated by the G-M tube as described above may easily be shown in the following simple experiment. The output of the Neher-Harper circuit is applied directly to the plates of a cathode-ray oscillograph. A strong source (say one mg of radium) is moved continuously toward the G-M counter. As the input counting rate increases the amplitude of pulse in the oscillograph will be seen to drop until it almost vanishes. This effect cannot be ascribed to the regulation of the high voltage supply since the drop in applied voltage due to regulation is observed to be very small compared to the overvoltage applied to the counter.

Lyshede and Madsen[16] have measured the deionization time of G-M counters by forced quenching of the counter. The quenching was accomplished by applying periodic pulses from a thyratron oscillator to the counter in a special circuit. When the frequency was increased to such an extent that the counter discharge was not extinguished by successive pulses a direct measure of the deionization time was obtained. Values of 10^{-4} second were found for air filled counters. Hydrogen counters were three or four times faster. These values agreed with calculations of the time taken to sweep out the positive ions using the mobility of the ions, size of the counter, and electric field distribution. This agrees with similar calculations we had made (unpublished) about two years ago.

The deionization time fixes the maximum counting rate possible with G-M counters roughly as 10^6 counts per minute. Taking account of the counting losses, one could thus measure input rates up to about 10^7 per minute. The fastest counter we have measured in combination with the N-H circuit gave a maximum counting rate of the order 2×10^5 counts per minute. This is the same value as reported by Neher and Harper[1] for one of their counters. Thus about a fivefold increase in speed may be possible with faster quenching circuits. However, one must conclude that existing quenching circuits are already capable of allowing a close approach to the maximum counting speed possible. It is also clear that existing vacuum tube scaling circuits and frequency meters are already much faster than necessary for G-M work as the resolution time of these circuits is less than the deionization time of the counters themselves. For practical purposes, one is interested in attaining a close approach to the maximum speed in order that the necessity for correcting for counting losses may be avoided at ordinary counting rates, as these losses set in at relatively low counting rates. It should be stressed that whether or not counting losses are great depends not only on the counting rate at which one is working, but also on the σ of the particular counter being used, which may be quite large.

Conclusion

Alaoglu and Smith[9] have derived the statistical formulae giving the counting losses for a scaling circuit and including the effect of σ. They find

$$n_n = \frac{n_0}{n(1+n_0\sigma)}[1 - I[n_0(\tau - n\sigma), n]], \quad \text{if} \quad \tau > n\sigma \tag{19}$$

and

$$n_n = \frac{n_0}{n}\frac{1}{1+n_0\sigma} \quad \text{if} \quad \tau \leqslant n\sigma. \tag{20}$$

[16] J. M. Lyshede and J. C. Madsen, Zeits. f. Physik **108**, 777 (1938).

Here n is the scaling ratio and the function $I(n_0(\tau-n\sigma), n)$ is the ratio of the incomplete Γ-function $\Gamma(n_0(\tau-n\sigma), n)$ to the complete Γ-function, $\Gamma(n)$. The upper limit of the incomplete Γ-function is $n_0(\tau-n\sigma)$. The details may be found in the paper of Alaoglu and Smith. The interesting feature of these equations is that the counting losses in the mechanical recorder stage fed by the scaling circuit drop out when $\tau \leqslant n\sigma$ as shown by Eq. (20). This fixes the maximum scaling ratio it is necessary to use. Of course, it is assumed in the derivation that the resolving time of the scaling circuit itself is less than σ. In the parallel method reported here, the relation was satisfied so that the losses in the Cenco counter stage were zero. It is also desired to point out here, that Eqs. (19) and (20) may also be tested by using the parallel method, as was first pointed out to the authors by Smith. The simplest case would be that of comparing a scale-of-two following Eq. (19) against a circuit following Eq. (20) such as the scale-of-128 used in the present experiments. A series method similar to the parallel method, which could also be used, would involve observing the number of counts in scales-of-one connected to the output of successive stages of scales-of-two in series.

The question of the best way to correct for the counting losses due to σ in actual experimental work may be briefly discussed. The parallel method in which the scaling circuit used is compared against a scale-of-one is not sensitive enough to accurately measure small values of σ. The determination of σ from measurements of the maximum random counting rate depends on fulfilling the relation $\tau \leqslant n\sigma$. This might require a larger ratio scaling circuit than is available. To overcome this σ may purposely be increased. A frequency meter affords a convenient way of measuring σ from the maximum. In this connection the vacuum tube frequency meter already reported[11] is of interest. This frequency meter employs the same circuit as the vacuum tube scaling circuit[7] discussed above. A scaling circuit of this type may thus be built in which one of the stages of scale-of-two also serves as a frequency meter. This frequency meter could thus be used for measuring σ even though $n<\tau/\sigma$. The addition of a tank circuit would not be necessary.

For common values of τ and σ which actually occur, namely $\tau=1.5\times10^{-2}$ sec. and $\sigma=5\times10^{-4}$ sec. we obtain $n=30$. Thus a scale-of-32 would in most cases suffice for the determination of σ from the maximum as well as to prevent losses in the mechanical counter stage. We have found that a vacuum tube scale-of-eight follows a vacuum tube scale-of-16 in parallel with it up to about 30,000 counts a minute showing that the losses in the Cenco counter stage were negligible up to such counting rates. For this case σ was about 10^{-3} sec. As Alaoglu and Smith show, σ cuts out the short intervals and allows the lower ratio scaling circuit to follow the higher ratio one up to higher counting rates than would be the case if a true random input came from the Neher-Harper circuit. We may conclude then that a vacuum tube scale-of-eight is sufficient for most counting rates if means are provided for measuring and correcting for the losses due to σ, which losses would be the same no matter what the scale of the circuit.

It is a pleasure to acknowledge the very helpful discussions of the theory and its applications to the parallel method which we have had with Mr. N. M. Smith, Jr. The help of Dr. M. M. Slawsky with the earlier work, and the discussion with and encouragement of Professor S. A. Goudsmit is also deeply appreciated. Finally, support from the Horace H. Rackham Fund is gratefully acknowledged.

On the Determination of Molecular Potential Curves from Spectroscopic Data

ALBERT SPRAGUE COOLIDGE, HUBERT M. JAMES, AND E. L. VERNON
Harvard University, Cambridge, Massachusetts and Purdue University, Lafayette, Indiana

(Received August 29, 1938)

The problem of determining accurately a molecular potential curve from spectroscopic data on the system is analyzed, and the difficulties are discussed in detail. In general the principal difficulty arises from the importance in the energy expression of terms in high powers in the quantum numbers; to deal with this, recourse may be taken to a method employing graphical integration. Formulas based on the first order of the W.B.K. approximation are usually but not always adequate. One can obtain markedly better results in determining potential curves by dealing directly with the energy levels which it is desired to reproduce, rather than by the usual method of making the curve reproduce a limited number of spectroscopic constants. A method of successive approximations has proved to be particularly effective in giving accurate results. Formulas are given for the convenient manipulation of potential curves of the types suggested by Morse, Pöschl and Teller, Hylleraas, Dunham, and also a generalization of the Morse curve. This last curve has proved to be most satisfactory, combining great flexibility with relative ease of manipulation; explicit solutions for vibrational wave functions are not obtainable for it, however. The discussion is illustrated by extensive computations on the lowest $^3\Sigma_g$ state of H_2, for which a potential curve very accurate in the range of nuclear separations $1.3 \leqslant r \leqslant 2.9\, a_H$ is obtained.

§1. INTRODUCTION

IN the course of a careful theoretical study of the $1s\sigma 2s\sigma\ ^3\Sigma_g$ state of H_2 by a variational method, two of us[1] have found values for the energy of this state which differ in a surprising manner from the values given by a Morse curve constructed in the usual way to represent the experimental results. The computed and observed values of the energy agreed well at the potential minimum, for a nuclear separation $r=1.87a_H$. For $r=1.3a_H$, however, the computed energy was *lower* than the Morse curve energy by more than 0.1 electron volt, and for $r>2.7a_H$ a disagreement in the same direction, but of smaller magnitude, was found. Since our variational process could lead only to energy values above the exact theoretical value, this apparent contradiction of theory and experiment caused us to make a careful check on our theoretical work, but no errors were detected. This led us to make a critical examination of the Morse function as an approximation to the potential curve accurately derived from all available spectroscopic data, which showed that it is surprisingly in error even in the neighborhood of the minimum. Our efforts to find a better representation, accurate over the relatively small range of r in which we were interested, showed that this is a problem of unexpected difficulty, and that it is easy to overestimate the accuracy with which potential curves can be constructed by the methods used in the past.

In the present paper we wish to discuss the problem of determining analytical approximations to molecular potential curves from spectroscopic data, to describe more accurate methods than have been used heretofore, and to exhibit the accuracy of various methods, old and new, as applied to the $1s\sigma 2s\sigma\ ^3\Sigma_g$ state of H_2.

Two general methods have been employed in constructing potential curves. First we may mention that of Rydberg.[2] This is a graphical method designed to produce a curve which will give the observed vibrational and rotational energies, when these are computed by the Bohr theory with half-integral quantum numbers (or, what is the same thing, the usual approximation of the Wentzel-Brillouin-Kramers method in wave mechanics). To this approximation the energy levels depend only on the form of that part of the potential curve which lies between the limits of classical motion of the system for the energy in question. It is thus possible to construct the potential curve step by step, the energy E_v of the vth vibrational level and spacing of the rotational levels of that vibrational level providing two conditions on the construction of the potential curve for energies between E_{v-1} and E_v. Though an excellent method for determining the general form of the curve, it is of

[1] H. M. James and A. S. Coolidge, J. Chem. Phys. **6**, 730 (1938).

[2] R. Rydberg, Zeits. f. Physik **73**, 376 (1932); **80**, 514 (1933).

rather limited accuracy as concerns details, principally because of its graphical character.

The second method consists in the representation of the potential curve by an analytical expression having a generally appropriate character and containing a number of parameters; these parameters are adjusted to values appropriate to each molecular state considered. The curve most widely employed is that of Morse,[3] while other useful curves are those of Rosen and Morse,[4] Manning and Rosen,[5] Pöschl and Teller[6] and Hylleraas.[7] In each case the spectroscopic constants associated with a given curve can be determined, usually by approximate methods, as functions of the parameters in the curve; these parameters are then determined by so adjusting them as to reproduce the observed spectroscopic constants as well as possible. (The method of Hylleraas departs slightly from this procedure, as will be discussed later.)

In applying this method one encounters three difficulties, each of which may be of practical significance: the rotational levels associated with the analytical curve are always, the vibrational levels usually, known only as more or less satisfactory approximations; the "spectroscopic constants" of the state are not definite constants, but depend on the amount of observational material available and the care with which the energy levels are approximated by power series; the curves to be fitted to the data are of limited flexibility, and there may be a wide choice as to which of the observed spectroscopic properties of the system the approximate potential curve is to reproduce.

In the next three sections of this paper we shall discuss these difficulties in more detail, and shall describe a technique for dealing with them to best advantage, when the accuracy desired will justify some care in the determination of the curve. We shall then give formulas useful in fitting to observational data in various ways the curves of Morse, Pöschl and Teller, and Hylleraas, and certain series discussed by Dunham.[8] Finally we shall present and compare the results of fitting curves in a large number of ways, illustrating thereby certain principles involved in the adjustment of curves of limited flexibility, and in the deduction of the nature of the errors in a potential curve from the errors in the spectroscopic constants or energy levels associated with it.

§2. Significance of Spectroscopic Constants

We may regard as the primary spectral data for any given state the term values of the vibration-rotation levels, or the energy differences of these levels. From this it is customary to derive "spectroscopic constants," the definition of which is subject to some arbitrariness. Thus one may write

$$E_{v,K}=E_v+B_vK(K+1)-D_vK^2(K+1)^2+\cdots.$$

The energies $E_{v,K}$ are expressed in wave numbers. For any given v there will be a limited number of rotational levels known, and the coefficients E_v, B_v, $\cdots$ of this expansion will not be uniquely determined; the values depend on the number of terms used in setting up the expansion. Regarding E_v, B_v, $\cdots$ as functions of v approximately fixed for integral v, but not for other values of v, we see that in the expansions

$$E_v=C_e+\omega_e(v+\tfrac{1}{2})-\omega_ex_e(v+\tfrac{1}{2})^2+\cdots,$$
$$B_v=B_e-\alpha_e(v+\tfrac{1}{2})+\gamma_e(v+\tfrac{1}{2})-\cdots,$$

the spectroscopic constants ω_e, ω_ex_e, B_e, $\cdots$ are not definite quantities, but may depend, among other things, on the amount of spectral data available and the number of terms used in the expansions. In particular it must be realized that these expansions cannot be relied upon to give term values for vibrational levels outside of the set used in constructing them.

This point is nicely illustrated by the work of Hylleraas[9] on the $^1\Sigma_g$ state of N_2. With this state, for v up to 15, E_v can be expressed quite accurately by a series ending with the term in ω_ex_e; extrapolation of this series leads to a dissociation energy in error by 60 percent. As a second example we take the results of Sandeman[10] on the $1s\sigma 2s\sigma\ ^3\Sigma_g$ state of H_2, which form the experimental basis of the computations to be presented in this paper. He finds that the observed term

[3] P. M. Morse, Phys. Rev. **37**, 57 (1929).
[4] N. Rosen and P. M. Morse, Phys. Rev. **42**, 210 (1932).
[5] N. F. Manning and N. Rosen, Phys. Rev. **42**, 953 (1933).
[6] G. Pöschl and E. Teller, Zeits. f. Physik **83**, 143 (1933).
[7] E. A. Hylleraas, Zeits. f. Physik **96**, 643, 661 (1935).
[8] J. L. Dunham, Phys. Rev. **41**, 721 (1932).
[9] E. A. Hylleraas, Zeits. f. Physik **96**, 661 (1935).
[10] I. Sandeman, Proc. Roy. Soc., Edinburgh **55**, 49 (1935).

differences, for v up to 7, are practically all reproduced to within a few hundredths of a wave number by the series[11]

$$E_v = 4.90 + 2665.9252(v+\tfrac{1}{2}) - 72.79390(v+\tfrac{1}{2})^2 + 1.429492(v+\tfrac{1}{2})^3 - 0.1473890(v+\tfrac{1}{2})^4 + 0.01246012(v+\tfrac{1}{2})^5 - 0.000585323(v+\tfrac{1}{2})^6,$$

$$B_v = 34.22051 - 1.694884(v+\tfrac{1}{2}) + 0.03454932(v+\tfrac{1}{2})^2 - 0.002034446(v+\tfrac{1}{2})^3 + 0.00000733776(v+\tfrac{1}{2})^4.$$

The occasional deviations of greater magnitude he attributes to perturbations by other electronic levels, which have no place in a discussion of potential curves and will be ignored in this paper. He also gives a series containing a smaller, but still relatively large, number of terms:

$$E_v = 5.00 + 2665.4861(v+\tfrac{1}{2}) - 72.18137(v+\tfrac{1}{2})^2 + 1.068784(v+\tfrac{1}{2})^3 - 0.04863957(v+\tfrac{1}{2})^4$$

also fitted by least squares, and of course reproducing the observed term differences less accurately. Omission of terms in $(v+\frac{1}{2})^5$ and $(v+\frac{1}{2})^6$ has here changed the coefficient of $(v+\frac{1}{2})^4$ by a factor of three, and even the coefficient of $(v+\frac{1}{2})^2$, almost always used in curve fitting, is changed by one percent. But even in the more elaborate expression the cutting off of the series changes the coefficients by amounts which are appreciable in calculating E_v for $v>7$. One must expect an expansion adequate to represent all the vibrational levels[12] to continue well beyond the terms here given, with fairly regularly decreasing coefficients. Extrapolating Sandeman's series, we would expect as the next term $+0.00002(v+\frac{1}{2})^7$, which for $v=7$ would contribute some 27 cm^{-1} to E_v. Neglect of this and higher terms in the series has been compensated, for $v \leqslant 7$, by proper modifications of the other constants, but this compensation will not extend outside the range in question. Thus for $v=10$, when the contribution of the term in $(v+\frac{1}{2})^7$ would be some ten times greater, the error in the representation must be expected to be of this order, and to increase rapidly with v.

[11] We have added the constant term in E_v, which was obtained in the computations to be described later.

[12] There is, of course, no uniquely defined correct expansion of the functions E_v, B_v, which are specified only for a finite number of points.

§3. Energy Levels of a Potential Curve

We now turn to the problem of determining the energy levels of an analytic potential curve $U(r)$, having a minimum, which it is convenient to take as the zero for energy, at $r=r_e$ and an asymptotic value $U(\infty)=D$ which it approaches so rapidly that there is only a finite number of discrete vibrational levels E_v. (We shall throughout express U in cm^{-1}, and r in Bohr radii.) For this there is one generally useful method, that of Wentzel-Brillouin-Kramers, which provides an asymptotic expansion which converges at first very rapidly, so that only two terms, at most, need be taken. To this approximation we write, for the case of no rotation, $E_v=E_v'+E_v''$; E_v' is the first W. B. K. approximation, E_v'' the correction which arises from the second approximation. Employing the results of Dunham[13] we find

$$\oint P_v' d\rho = 2\pi B_e^{\frac{1}{2}}(v+\tfrac{1}{2}), \tag{1}$$

$$\oint P_v'' d\rho - (B_e/32)\oint (U')^2 (P_v'')^{-5} d\rho = 2\pi B_e^{\frac{1}{2}}(v+\tfrac{1}{2}), \tag{2}$$

where $\rho = r/r_e$, $B_e = Rm/\mu r_e^2$, $U' = dU/dr$,

$$(P_v')^2 = E_v' - U, \quad (P_v'')^2 = E_v' + E_v'' - U,$$

and R is the Rydberg constant, μ the reduced mass of the nuclei, m the mass of the electron. The case of rotation may be treated similarly by introducing the effective potential $U(\rho)+B_eK(K+1)/\rho^2$, assuming an energy expansion of the form $E=E_v'+E_v''+K(K+1)\times(B_v'+B_v'')+$higher terms in $K(K+1)$, and equating to zero separately the coefficient of each power of $K(K+1)$ in Dunham's relations. We thus find

$$B_v' \oint (P_v')^{-1} d\rho = B_e \oint \rho^{-2} (P_v')^{-1} d\rho, \tag{3}$$

[13] J. L. Dunham, Phys. Rev. **41**, 713 (1932).

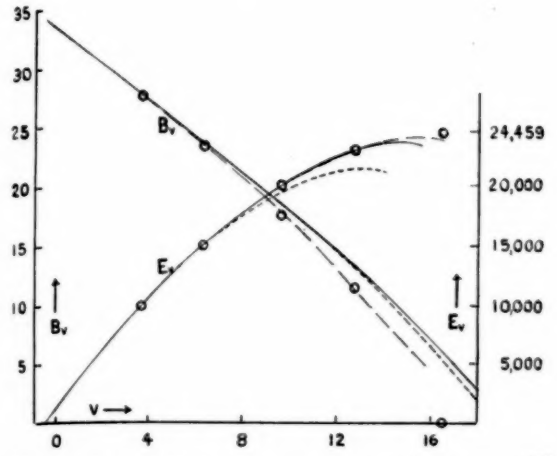

FIG. 1. E_v and B_v as determined by various methods. 0, graphical integration of Eqs. (1) and (3), curve 14. ---- calculated with Y's used in determining curve 14. — — calculated with additional Y's as described. —— calculated with Sandeman's complete constants.

$$(B_v'+B_v'')\Big\{\oint (P_v'')^{-1}d\rho + (5B_e/32)\oint (U')^2(P_v'')^{-7}d\rho\Big\} = B_e\oint \rho^{-2}(P_v'')^{-1}d\rho + (5B_e^2/32)\oint (U')^2\rho^{-2}(P_v'')^{-7}d\rho - (B_e^2/4)\oint U'\rho^{-3}(P_v'')^{-5}d\rho. \quad (4)$$

When analytical evaluation of these expressions is impracticable they can be evaluated numerically, by assuming values of E and using Eq. (1) or (2) to determine the corresponding value of v, afterward interpolating to integral values of v.

Dunham has given the results of this method in very useful form, expanding E_v, etc., in series like those employed by spectroscopists:

$$E_v = Y_{00} + Y_{10}(v+\tfrac{1}{2}) + Y_{20}(v+\tfrac{1}{2})^2 + \cdots, \quad (5)$$

$$B_v = Y_{01} + Y_{11}(v+\tfrac{1}{2}) + Y_{21}(v+\tfrac{1}{2})^2 + \cdots. \quad (6)$$

Expanding $U(r)$ about r_e in powers of

$$\xi = (r-r_e)/r_e,$$

he defines coefficients a_n by

$$U(r) = a_0\xi^2(1+a_1\xi+a_2\xi^2+\cdots). \quad (7)$$

He gives formulas for Y_{lj}' and Y_{lj}'', the parts of Y_{lj} arising from the first and second approximations of the W. B. K. method, as functions of the a_n so far as this is possible without going beyond a_6, namely, up to Y_{20}'', Y_{40}', Y_{11}'', Y_{31}', Y_{02}'', Y_{22}', Y_{13}', Y_{04}'.

In applying the results of Dunham, the principal limitation does not arise from the lack of higher terms in the W. B. K. approximation, which are of the order of the uncertainties arising from the imperfect separability of nuclear and electronic coordinates, i.e., arising from the essential vagueness in the definition of a molecular potential function. Rather, it is due to the lack of such coefficients Y_{lj} as depend on $a_7, \cdots$, and may play an essential role in determining the location of the levels for moderately large values of v. The extension of Dunham's formulas is of course possible; we believe, however, that it is more practical to estimate the necessary additional Y's by a process which is the inverse of Rydberg's, determining by numerical integration the values of E_v and B_v for large v, and so adjusting the values of the higher Y's as to reproduce these values. Thus, by graphical integration of Eq. (1) with various values of E_v', we obtain the corresponding (in general nonintegral) values of v. The resulting curve of E_v against v is tangent to the line $E=D$ for some finite value $v=v_0$ such that the next largest integer is the number of discrete vibrational levels. Similarly, the curve for B_v' (the main term in B_v), is obtained from Eq. (3); it vanishes for $v=v_0$, but it can be shown that at this point all its derivatives are infinite, so that the end-point should be disregarded when fitting the curve by a power series. These curves are, of course, subject to the errors of numerical integration as well as those due to neglect of the higher terms in the W. B. K. approximation, but they suffice to determine the higher Y's with ample precision when they are to be used only for lower v's, where they have the character of small correction terms.

An example of this procedure is illustrated in Fig. 1, which is based upon the curve numbered 14 in Table II. As will be described later, this curve was set up to reproduce the values of $Y_{10}\cdots Y_{40}$, $Y_{01}\cdots Y_{31}$ given by Sandeman for $1s\sigma 2s\sigma\ {}^3\Sigma_g$ H_2; no control of the higher Y's was

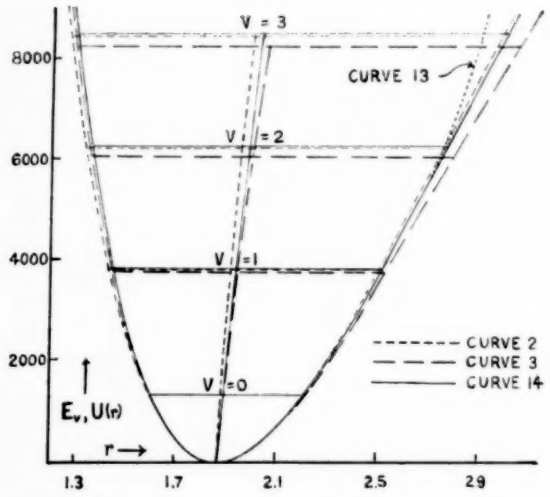

FIG. 2. Relations between E_v, r_v, and potential curves. Horizontal tie lines show values of E_v. Nearly vertical lines intersect tie lines at $r=r_v=[Rm/\mu B_v]^{\frac{1}{2}}$.

possible, and they were estimated by graphical integration. The procedure in the case of Eq. (1) is obvious; in the case of Eq. (3) the occurrence of infinities in the integrand was avoided by a change of variables:

$$\oint \rho^{-2}(E-U)^{-\frac{1}{2}}d\rho$$

$$=4\int_{r=a}^{r=g}(\rho-a)^{\frac{1}{2}}\rho^{-2}(E-U)^{-\frac{1}{2}}d(\rho-a)^{\frac{1}{2}}$$

$$+4\int_{r=b}^{r=g}(b-\rho)^{\frac{1}{2}}\rho^{-2}(E-U)^{-\frac{1}{2}}d(b-\rho)^{\frac{1}{2}}. \quad (8)$$

Here a and b are the values of ρ at the classical turning-points, and $a<g<b$. We obtain the following results:

E	10000	15000	20000	23000	24459
v	3.705	6.33	9.64	12.7	16.5
B	27.53	23.25	17.47	11.38	0.

These results lead to the following values for the higher Y's:

$$Y_{50}= 0.01061, \quad Y_{60}=-0.000705,$$
$$Y_{70}= 0.0000202, \quad Y_{80}=-0.00000022,$$
$$Y_{41}=-0.0001, \quad Y_{51}=-0.000004,$$
$$Y_{61}= 0.0000005.$$

Fig. 1 shows E_v and B_v as computed with these Y's, and for comparison the values computed with, first, only the Y's with reference to which the curve was constructed, and, second, the complete results of Sandeman, introduced for later reference. The higher Y's derived here make appreciable contributions to E_v and B_v, even for quite low values of v. Thus they contribute 14 cm^{-1} to E_v and -0.044 cm^{-1} to B_v for $v=4$, while for $v=9$ they contribute 396 cm^{-1} to E_v and -0.76 cm^{-1} to B_v.

§4. Determination of Experimental Potential Curves

We shall consider as an "experimental potential curve" any potential curve having as its energy levels the observed discrete energy levels of the molecule. Such a curve is of course not uniquely defined by the finite number of observed energy levels, but a reasonable, smooth curve which reproduces these energies should be well defined and of good accuracy everywhere. If strong perturbations affect the electronic state in question there may exist no curve whatsoever with the desired properties; a potential curve for this state is then of significance only in an intermediate stage in the theoretical treatment of these levels.

The usual process in determining an experimental potential is to refer, not to the energy levels, but to certain of the spectroscopic constants, determining a potential curve $U(r)$ such that a limited number of the Y's have the same values as the corresponding spectroscopic constants ω_e, $\omega_e x_e$, $\cdots$ in some analysis of the electronic state. The energy levels of the curve then differ from the observed energies insofar as the spectroscopic constants not used in determining the curve differ from the corresponding uncontrolled Y's of the curve. Now the spectroscopic constants appearing in the analysis are chosen to give the best possible fit on the assumption that those constants not explicitly introduced are zero. Then even if one determines the potential curve using all the available constants there remain errors in the energy levels due to the higher Y's of the curve, which will not in general be zero, and which may affect the energy levels appreciably even for low values of the quantum numbers. In any case, it is clear that the greatest difficulties will arise in properly determining the higher energy levels, and it will be correspondingly difficult properly to deter-

mine the potential curve near the classical turning points for these higher levels. The magnitude of the errors which will appear in the energy levels even under the most favorable circumstances is illustrated in Fig. 1, while Fig. 2 will illustrate the errors in the potential curve when less careful methods of curve fitting are employed.

This difficulty can be overcome, so far as the limited flexibility of the potential curve will permit, by a process of successive approximations based on the observed energy levels rather than the derived spectroscopic constants. Let it be desired to determine a potential curve of a particular form which will approximate as well as possible to the experimental curve up to a height E_w above the minimum. This is clearly to be accomplished by making the differences in the energy levels of this curve, for $E_v < E_w$, approximate as well as possible, say in a least-squares sense, to the observed energy level differences. The behavior of the energy levels and the potential curve outside of the specified region will be disregarded. As a first approximation to the desired curve we take a curve constructed in the usual way to reproduce a certain set of spectroscopic constants, which we call the controlled constants. Let the values of the uncontrolled Y's for this curve be determined; these will have roughly the same values as for the final curve. Deducting from the observed energy values the contributions to $E_{v,K}$ of these uncontrolled Y's, we obtain a set of values which we would like to reproduce by a series containing only the controlled Y's. Fitting such a series to these values by a least-squares process we obtain new values for these Y's, which serve to determine the second approximation to the desired curve. Next, the values of the uncontrolled Y's for this curve can be determined and in turn employed in a repetition of this procedure, and so on, until repetition produces no essential improvement.

We have applied this process in representing the $1s\sigma 2s\sigma\ ^3\Sigma_g$ state of H_2 by a Pöschl-Teller curve, and find that it converges rapidly, requires no excessive labor, and produces a curve which bears comparison with another curve involving twice as many disposable constants fixed in the usual way. This curve is the curve 6 of §6; where its construction and characteristics are indicated in more detail; some of its properties are tabulated in Tables II to VI.

It should be possible to form estimates of the errors in any approximate potential curve on the basis of the errors, as compared with experimental values, of the corresponding spectroscopic constants or, much better, of the energy level separations. From the point of view of the Rydberg process, one sees that an excessive computed difference of E_v and E_{v+1} indicates that the potential curve is on the average too narrow in the range between these energies, while an excessive value of B_v indicates that the mean value of the classical turning points for the vth vibration is too small. From the point of view of perturbation theory, it is clear that a depression of the potential curve in any region will depress most strongly those energy levels with turning points in the given region, and will increase or decrease the corresponding values of B_v according as the depression affects the inner or the outer branch of the potential curve. The latter effect is more clearly indicated by the behavior of the quantity $r_v = (Rm/B_v\mu)^{\frac{1}{2}}$, the effective nuclear separation for the vth level, the error in which should be a rough measure of the average lateral errors of the two branches in the neighborhood of E_v. It is also clear that an error in the curve of alternating sign will lead to errors of generally smaller magnitude in the energy levels affected.

These considerations lead also to some general principles which are useful when methods of determining a potential curve less careful than that described above are to be employed. For instance, a curve which reproduces perfectly the observed vibrational levels of a molecule may still contain very large errors if the rotational levels do not also come out right. Thus, in choosing a set of controlled constants for the construction of a curve one ought to include rotational as well as vibrational constants; a rough equality in the number of constants of each type used will probably lead to most satisfactory results. Correspondingly, to insure a reasonably wide range of application of a particular form of analytic curve it should contain at least four variable parameters, of which two can be used to give proper character to the rotational levels of the curve. Thus four-param-

TABLE I. *Constants of a Morse curve in terms of various spectroscopic constants.*

r_e	β	D	ω_e	$\omega_e x_e$	B_e	α_e
$(Rm/\mu B_e)^{\frac{1}{2}}$	$\omega_e/4(DB_e)^{\frac{1}{2}}$	**D**	$\boldsymbol{\omega_e}$	$\omega_e^2/4D$	$\mathbf{B_e}$	$3B_e^{\frac{1}{2}}/D^{\frac{1}{2}}-6B_e^2/\omega_e$
$(Rm/\mu B_e)^{\frac{1}{2}}$	$(\omega_e x_e/4B_e)^{\frac{1}{2}}$	$\omega_e^2/4\omega_e x_e$	$\boldsymbol{\omega_e}$	$\boldsymbol{\omega_e x_e}$	$\mathbf{B_e}$	$6B_e^{\frac{1}{2}}(\omega_e x_e)^{\frac{1}{2}}/\omega_e-6B_e^2/\omega_e$
$(Rm/\mu B_e)^{\frac{1}{2}}$	$(\omega_e\alpha_e/12B_e^2)^{\frac{1}{2}}$	$9\omega_e^2B_e^3/[6B_e^2+\omega_e\alpha_e]^2$	$\boldsymbol{\omega_e}$	$[6B_e^2+\omega_e\alpha_e]^2/36B_e^3$	$\mathbf{B_e}$	$\boldsymbol{\alpha_e}$

eter curves such as those of Pöschl and Teller or Rosen and Morse have a marked superiority to the three-parameter curve of Morse. Another obvious consideration is that, when one is interested only in the form of the potential curve near the minimum, as, for instance, in determining vibrational wave functions for low v, one should choose the parameters without regard to errors in the dissociation energy indicated by the curve.

These ideas will be illustrated in §6 of this paper.

§5. Formulas for the Determination of Potential Curves

We here present in a uniform notation formulas useful in determining from experimental data potential curves of Morse, Pöschl and Teller, Hylleraas, and the generalized Morse function suggested by Dunham. We write any potential curve having an asymptotic value D as

$$U(\xi)=DF(\xi), \quad \xi=(r-r_e)/r_e.$$

In addition to D and r_e, a third parameter β occurs in all these curves, while the energy formulas are conveniently expressed in terms of a constant C, where

$$C^2=4R_\infty m\beta^2/\mu r_e^2.$$

(We purposely avoid defining curves in terms of symbols such as B_e and ω_e, which we reserve for use as empirical spectroscopic constants.)

The calculation of the energy levels of any of these curves, referred to the minimum as the zero of energy, can well be based on Dunham's formulas. For the purpose of curve fitting it is convenient to have expressions for the constants defining these curves in terms of certain of the Y's. Upon identifying Y_{10}' with ω_e, $-Y_{20}'$ with $\omega_e x_e$, Y_{01}' with B_e, and $-Y_{11}'$ with α_e, one obtains formulas for computing these constants, as shown below. The error arising from the neglect of higher order terms is trivial in comparison with those due to the essential shortcomings of this method of curve fitting, as already discussed.

Morse curve

The Morse curve is defined by the three basic parameters.

$$F_M=[1-e^{-2\beta\xi}]^2.$$

One finds

$$\begin{aligned}
&Y_{00}'=0, \quad Y_{00}''=0,\\
&Y_{10}'=2CD^{\frac{1}{2}},\\
&Y_{20}'=-C^2,\\
&Y_{01}'=C^2/4\beta^2,\\
&Y_{11}'=-(3C^3/16\beta^4D^{\frac{1}{2}})(2\beta-1).
\end{aligned}$$

Y_{l0}' vanishes for all $l>2$, while Y_{l0}'' vanishes for all l; the Morse curve, for $K=0$, shares with the parabola the property of yielding the exact solution of the energy level problem in the first approximation of the W. B. K. method.

To find the constants of a curve in terms of given spectroscopic constants, one may use Table I, which gives the value of each of the quantities at the top in terms of the quantities in bold-faced type.

Pöschl-Teller curve

To define the Pöschl-Teller curve we introduce a fourth parameter τ:

$$F_P=1+\sinh^4\tau/\sinh^2(\tau+\beta\xi)-\cosh^4\tau/\cosh^2(\tau+\beta\xi).$$

This goes into the Morse curve as $\tau\to\infty$, $L=\coth 2\tau\to 1$. For the Pöschl-Teller curve also exact values can be found for the Y_{l0}, though they are not given by the first W. B. K. approximation. Defining

$$D'=D[(\cosh^4\tau+C^2/16D)^{\frac{1}{2}}-(\sinh^4\tau+C^2/16D)^{\frac{1}{2}}]^2,$$

we find

$$\begin{aligned}
&Y_{00}=D-D',\\
&Y_{10}=2CD'^{\frac{1}{2}},\\
&Y_{20}=-C^2,\\
&Y_{l0}=0, \quad l>2.
\end{aligned}$$

Closed expressions for the rotational terms do not exist, but they can be computed from Dunham's

formulas with sufficient accuracy. For Dunham's a_n we find

$$a_0=4D\beta^2,$$
$$a_1=-2L\beta,$$
$$a_2=(5L^2-8/3)\beta^2,$$
$$a_3=-(12L^3-10L)\beta^3,$$
$$a_4=\left(28L^4-\frac{98}{3}L^2+\frac{272}{45}\right)\beta^4,$$
$$a_5=-\left(64L^5-96L^3+\frac{164}{5}L\right)\beta^5.$$

Then $Y_{00}'=0$, $Y_{00}''=\frac{1}{4}C^2(L^2-1)$,
$Y_{10}'=2CD^{\frac{1}{2}}$,
$Y_{20}'=-C^2$,
$Y_{01}'=C^2/4\beta^2$,
$Y_{11}'=-(3C^3/16\beta^4D^{\frac{1}{2}})(2L\beta-1)$.

For the determination of the constants of the curve one may use either the first or the second line of the corresponding table for the Morse curves, except for the last column. To find τ one must assume in addition a value for α_e, solving either

$$2\sinh^2\tau=(1-9\omega_e^2B_e^3/D[6B_e^2+\omega_e\alpha_e]^2)^{-\frac{1}{2}}-1$$

in the first case, or, in the second

$$2\sinh^2\tau=(1-36\omega_e x_e B_e^3/[6B_e^2+\omega_e\alpha_e]^2)^{-\frac{1}{2}}-1.$$

Lotmar[14] has given comparable formulas, but they are erroneous, because of a confusion of r_e with r_0, a quantity defined in Pöschl and Teller's original paper, and in our notation given by $r_0=r_e(1-\tau/\beta)$.

Hylleraas curve

The Hylleraas curve involves three more parameters k, k_1, k_2, in terms of which are defined the intermediate quantities

$$x=e^{2(1+k)\beta\xi},\quad a=\frac{k-k_2}{1+k_2},\quad b=\frac{k-(k_1+k_2)}{1+k_1+k_2},$$
$$c=\frac{k-k_1}{1+k_1}.$$

Then $$F_H=\left[1-\frac{(1+a)(1+c)(x+b)}{(x+a)(x+c)(1+b)}\right]^2.$$

This passes into F_M upon making $k=k_1=0$, so that $a=b$, $c=0$; F_P is also the special case $k=0$, $k_1=\frac{1}{2}(\tanh\tau-1)$, $k_2=\frac{1}{2}(\coth\tau-1)$.

Exact values are not available for the energy levels. We have determined Dunham's a_n for particular curves of this type both by a straightforward expansion of the potential in powers of ξ and by a set of formulas too cumbersome to reproduce. As far as a_4, these formulas may be expressed in terms of the quantities a_1, a_2, a_3, a_4, defined in Hylleraas' paper[15] and lead to the expressions:

$$Y_{00}'=0,\qquad Y_{00}''=\tfrac{1}{4}C^2(a_1^2-a_2),$$
$$Y_{10}'=2CD^{\frac{1}{2}},$$
$$Y_{20}'=-C^2a_2,$$
$$Y_{01}'=C^2/4\beta^2,$$
$$Y_{11}'=-(3C^3/16\beta^4D^{\frac{1}{2}})(2a_1\beta-1).$$

To set up a Hylleraas curve which will reproduce certain selected spectroscopic constants, one begins by finding a set of Dunham's a_n (using a method of successive approximations if high accuracy is desired) such that when they are substituted in Dunham's formulas the desired Y_n will emerge. The task of determining a Hylleraas curve which will reproduce these a_n is most conveniently accomplished by means of the following formulas, in which we put $R=2\beta(1+k)$:

$$(D^{\frac{1}{2}}/a_0^{\frac{1}{2}})\{8R^4-12a_1R^3-(18a_1^2-24a_2)R^2-(144a_3-144a_2a_1+36a_1^3)R+144a_3a_1-144a_2^2+9a_1^4\}$$
$$=24R^3+(144a_2-108a_1^2)R-(288a_3+180a_1^3-432a_1a_2).$$
$$8640a_4\{4(a_0/D)+4(a_0/D)^{\frac{1}{2}}[-R+a_1]+[R^2-2a_1R+a_1^2]\}$$
$$=12(a_0/D)\{-512R^4+360a_1R^3+[2340a_1^2-3120a_2]R^2+[7200a_3-8640a_2a_1+2880a_1^3]R$$
$$+2160a_2^2+1080a_2a_1^2-1125a_1^4\}$$
$$+24(a_0/D)^{\frac{1}{2}}\{226R^5-406a_1R^4+[1200a_2-720a_1^2]R^3+[-3600a_3+3120a_2a_1-540a_1^3]R^2$$
$$+[3600a_3a_1-2160a_2^2-3240a_2a_1^2+1395a_1^4]R+[2160a_2^2a_1-1080a_2a_1^3+45a_1^5]\}$$
$$+\{-1136R^6+3432a_1R^5+[-4320a_2-96a_1^2]R^4+[21600a_3-15840a_2a_1+2160a_1^3]R^3$$
$$+[-43200a_3a_1+23760a_2^2+24120a_2a_1^2-7155a_1^4]R^2+[21600a_3a_1^2-38880a_2^2a_1$$
$$+6480a_2a_1^3+810a_1^5]R+[8640a_2^3-1620a_2a_1^4+270a_1^6]\},$$
$$\beta=\tfrac{1}{2}(a_0/D)^{\frac{1}{2}},$$
$$(1+k)=R(D/a_0)^{\frac{1}{2}},$$
$$k_1k_2=1+\tfrac{1}{2}(D/a_0)^{\frac{1}{2}}(a_1-R),$$
$$-(k_1+k_2)\{24+12(D/a_0)^{\frac{1}{2}}(a_1-R)\}=48+36(D/a_0)^{\frac{1}{2}}(a_1-R)+(D/a_0)\{(12a_2-3a_1^2)-12a_1R+8R^2\}.$$

[14] W. Lotmar, Zeits. f. Physik **93**, 528 (1935).

[15] It is to be noted that the $a_1\cdots a_4$ of Hylleraas' paper are simply related to, but not identical with, these quantities in our notation.

TABLE II. *Constants of potential curves.*

CODE	TYPE	r_e	D	β	τ	k	k_1	k_2
1	M	1.8678	24460	0.72836				
2	M	1.8678	24637	0.72573				
3	M	1.8678	19440	0.81700				
4	M	1.8678	20204	0.82725				
5	P-T	1.8678	24637	0.72573	0.70697			
6	P-T	1.8698	26619	0.69633	0.66959			
7	H	1.8678	24460	0.72806		−0.05382	−0.02775	1.22820
8	H	1.8678	24460	0.72806		0.12221	−0.36200	0.33728
9	H	1.8678	23248	0.74708		0.17427	−0.40643	0.32949
10	H	1.8678	24460	0.72836		−0.08041	−0.01249	1.65297
11	H	1.8672	23762	0.73930		0.27643	−0.54098	0.36442

In addition, we have considered the three curves (with $r_e = 1.8677$)

12 $V(\xi) = 51922\xi^2[1 - 1.6438\xi + 1.9588\xi^2 - 2.0945\xi^3 + 2.2775\xi^4]$,

13 $V(\xi) = 51913\xi^2[1 - 1.6409\xi + 1.9525\xi^2 - 2.0840\xi^3 + 2.2606\xi^4 - 2.965\xi^5 + 4.15\xi^6]$,

14 $V(\xi) = 24459X^2[0.72550 + 0.02948X + 0.10522X^2 + 0.05281X^3 + 0.05525X^4 + 0.02573X^5 + 0.00601X^6]$; $X = 1 - e^{-2\beta\xi}$; $\beta = 0.8552$.

TABLE III. *Dunham coefficients of potential curves.*

CODE	a_0	a_1	a_2	a_3	a_4	a_5	a_6
1	51906	−1.45672	1.23785	−0.77280	0.38776	—	—
2	51906	−1.45146	1.22893	−0.76446	0.38219	—	—
3	51906	−1.63400	1.55747	−1.09068	0.61386	—	—
4	55308	−1.65450	1.59680	−1.13224	0.64525	—	—
5	51906	−1.63400	1.93292	−2.2407	2.6672	−3.1560	—
6	51628	−1.59806	1.89923	−2.24733	2.72171	−3.2602	—
7	51861	−1.63373	1.99851	−2.94412	5.96758	—	—
8	51861	−1.63373	1.99851	−2.36007	2.67414	—	—
9	51903	−1.63396	1.96115	−2.22259	2.36103	−2.3378	2.232
10	51906	−1.63400	1.93292	−2.73312	5.96937	—	—
11	51950	−1.65287	1.99520	−2.11494	1.96573	−1.6746	1.384
12	51922	−1.64380	1.95880	−2.09450	2.27750	0	0
13	51913	−1.64090	1.95250	−2.08400	2.26000	−2.9650	4.150
14	51913	−1.64090	1.95250	−2.08400	2.26000	−2.9650	4.150

If it is desired to reproduce given values of r_e, D, a_0, a_1, a_2, a_3, the first of these equations will serve to determine R; the remaining equations then give the constants of the curve, as well as a_4. If, rather, the value of D given by the curve is of no interest, and it is desired to reproduce values of a_0, a_1, a_2, a_3, a_4, r_e then use of the first two equations will allow one to find the values of R and D needed to reproduce the given a_4, and the values for the parameters of the curves follow as before.

Hylleraas gives another method of adjusting his curve, based on a method which, if consistently carried through, would give just the principal parts of Dunham's terms, the Y_{l0}' and Y_{l1}'. However, he breaks off the vibrational series with Y_{30}', and arbitrarily substitutes a fractional expression (his Eq. (28)) which gives, upon expansion, the proper values for these quantities, and in addition a further set of Y_{l0}' which have no relation to the problem. Thus his expression for the vibrational energies does not accurately reproduce the energy levels of the curve, as he himself states. In the case of $1s\sigma 2s\sigma\ ^3\Sigma_g$ H_2 this approximate expression is a very poor approximation, and breaks down completely when one attempts to make it reproduce the observed values of ω_e, $\omega_e x_e$, $\omega_e y_e$.

Extended Morse curve

The extended Morse curve is defined by

$$F(\xi) = \sum_{n=2}^{8} c_n[1 - e^{-2\beta\xi}]^n,$$

the c's being adjustable parameters. Its manipulation differs little from that of Dunham's power series function. In either case one first finds the a_n needed to reproduce the desired Y_n. The c_n of the extended Morse curve can then be determined from the relations

$$a_0 = 4\beta^2 D c_2$$

$$a_0 a_1 = 4\beta^3 D(-2c_2 + 2c_3),$$

$$a_0 a_2 = 4\beta^4 D(7\tfrac{1}{3}c_2 - 6c_3 + 4c_4),$$

$$a_0 a_3 = 4\beta^5 D(-2c_2 + 10c_3 - 16c_4 + 8c_5),$$

$$a_0 a_4 = 4\beta^6 D(6\tfrac{2}{4}\tfrac{1}{5}c_2 - 12c_3 + 34\tfrac{2}{3}c_4 - 40c_5 + 16c_6),$$

$$a_0 a_5 = 4\beta^7 D(-\tfrac{4}{5}c_2 + 11\tfrac{2}{4}\tfrac{1}{5}c_3 - 53\tfrac{1}{3}c_4 + 106\tfrac{2}{3}c_5 - 96c_6 + 32c_7),$$

$$a_0 a_6 = 4\beta^8 D(1\tfrac{2}{3}\tfrac{7}{1}\tfrac{4}{5}c_2 - 9\tfrac{1}{5}c_3 + 64\tfrac{4}{5}c_4 - 200c_5 + 304c_6 - 224c_7 + 64c_8).$$

β may be chosen so as to satisfy the auxiliary condition, $\sum_n c_n = 1$, if it is desired to reproduce the observed dissociation energy D, or it may be used simply as an adjustable parameter to satisfy some other condition.

§6. ILLUSTRATIVE COMPUTATIONS ON $1s\sigma 2s\sigma\ ^3\Sigma_g$ H_2

In Tables II to VI we summarize the results of a variety of treatments of the $1s\sigma 2s\sigma\ ^3\Sigma_g$ state of H_2. This work was based on Sandeman's analysis of this state, as given in §2, except that some of the cruder curves were fitted to data derived from the results of Richardson and Davidson.[16] The difference for these curves is inappreciable.

[16] O. W. Richardson and P. M. Davidson, Proc. Roy. Soc. **A125**, 23 (1929).

TABLE IV. *Values of* Y_{ij}.

CURVE	Y_{00}''	Y_{10}'	Y_{10}''	Y_{20}'	Y_{20}''	Y_{30}'	Y_{40}'	Y_{01}'	Y_{01}''	Y_{11}'	Y_{11}''	Y_{21}'	Y_{31}'
1	0	2665.34	0	−72.609	0	0	0	34.216	—	−1.2037	—	−0.03288	—
2	0	2665.34	0	−72.087	0	0	0	34.216	—	−1.1899	—	−0.03276	—
3	0	2665.34	0	−91.356	0	0	0	34.216	—	−1.6709	—	−0.03647	—
4	0	2751.3	0	−93.663	0	0	0	34.216	—	−1.6709	—	+0.02419	—
5	4.82	2665.34	−0.26	−72.087	0	0	0	34.216	—	−1.6709	—	−0.00071	—
6	5.24	2655.41	−0.26	−66.223	0	0	0	34.144	−0.012	−1.5754	+0.0005	0.00292	−0.000218
7	5.66	2664.2	—	−68.66	—	0.1068	—	34.216	—	−1.6709	—	−0.0777	—
8	5.66	2664.2	—	−68.66	—	0.2080	—	34.216	—	−1.6709	—	0.0212	—
9	5.18	2665.3	−0.67	−70.630	0.033	0.2842	−0.063	34.216	−0.008	−1.6708	+0.0006	0.0212	−0.00375
10	4.82	2665.34	+4.60	−72.087	—	1.0715	—	34.216	—	−1.6709	—	−0.0826	—
11	5.16	2667.40	−0.61	−72.920	−0.016	1.2406	−0.1146	34.240	−0.002	−1.7217	−0.0008	0.0476	−0.00466
12	—	2665.92	—	−72.794	—	1.4295	—	34.221	—	−1.6949	—	0.03455	—
13, 14	4.90	2665.81	+0.11	−72.549	−0.235	1.4286	−0.1468	34.223	−0.003	−1.6895	−0.0053	0.03456	−0.00203

Table II specifies the constants which define the several curves, while Table III presents the derived values of the Dunham coefficients, as far as they have been worked out. Table IV gives for the curves the computed values of Y_{ij}' and, in certain cases, of Y_{ij}'', to illustrate the rapidity of convergence of the W. B. K. process. Table V exhibits the divergences between the curves, gives values for curve 14, the best of these curves, and the differences from this of the other curves. The location of these curves with respect to each other involves some degree of arbitrariness. In practice one would use the observed energy level separations to determine the form of the potential curve; the absolute location of the curve would be adjusted to produce as satisfactory an agreement as possible between computed and observed term values. We have considered the curves to be so located that the lowest computed energy level coincides with lowest observed energy level, a process designed to give maximum accuracy of the curve in the general neighborhood of the minimum. Finally, Table VI exhibits the errors in E_v and in $r_v=(Rm/\mu B_v)^{\frac{1}{2}}$, the effective nuclear separation for the determination of the rotational terms of the vth vibrational state. Our method of adjusting the curves gives automatically zero error in E_0; to exhibit the differences in the curves near the minimum we give also the deviation of the minima of the curves from the minimum of curve 14, which we believe to be essentially correct.

A comparison of Tables V and VI affords a test of the correlations between errors in curves and errors in energies, as discussed in §4, by taking curve 14 as the standard of comparison. (Because of the smallness of the errors of the energies of this curve, Table VI gives essentially the deviations of the energies of the other curves from those of curve 14.) The turning points are roughly 1.6 and 2.2 for $v=0$, 1.45 and 2.5 for $v=1$, 1.35 and 2.8 for $v=2$, and 1.3 and 3.0 for $v=3$; the errors for a given v in Table VI should be correlated with those in Table V for the corresponding ranges in r. Fig. 2 shows the correlation graphically for two of the cruder curves.

We now discuss the individual curves, explaining their construction and estimating their defects. For the latter purpose we shall take curve 14 as a provisional standard, later attempting an estimate of the errors in this curve, as compared to the ideal curve for the state.

TABLE V. *Deviations of potential curves from curve* 14, *(given in first line).**

CURVE	r=1.3	1.5	1.7	1.9	2.1	2.3	2.5	2.7	2.9
14	8487	2855	487	15	660	1958	3619	5461	7363
1-14	−891	−151	−4	+5	+15	+50	+91	+119	+119
2-14	−906	−154	−4	+5	+15	+52	+98	+131	+138
3-14	−433	−42	+9	+10	0	−26	−106	−258	—
4-14	+112	+109	−1	−31	−1	+56	+65	+2	−141
5-14	+32	+1	−1	+1	+1	−1	−10	−39	−87
6-14	−27	+2	+11	+1	−9	−10	−2	+8	+19
7-14	+1010	+52	+5	+5	+5	−8	−22	−65	−135
8-14	+78	+21	+5	+5	+5	0	+2	0	−5
9a-14	+3	+6	+6	+5	+5	+6	+5	−5	−30
9b-14	−2	+1	+1	0	0	+1	0	−10	−35
10-14	+5735	+39	−2	−2	−2	−4	−32	−83	−167
11-14	−13	0	−3	+1	+2	+3	+1	−2	−6
12-14	−50	0	0	0	0	+3	+50	+333	—
13-14	−7	0	0	0	0	0	+11	+122	+783

* Curves are adjusted to have the same lowest vibrational level. For curves 1 to 6, this can be calculated exactly. For curves 7, 8, and 9*a* the Hylleraas approximation has been used. 9*b* is the same curve as 9*a* relocated with the aid of the Dunham formulas, which have also been used for curves 10 to 14. Curve 14 is estimated to be correct within 1 cm^{-1} from $r=1.5$ to 2.5 inclusive, too low by about 2 cm^{-1} at 2.7, and by about 8 cm^{-1} at 2.9. At 1.3 its value is unreliable because of the steepness of the curve.

TABLE VI. *Errors in reproduction of energy levels by the potential curves.**

	Vibration						Rotation					
			Errors in E_v						Errors in $r_v \times 10^4$			
Curve	Method	Error at minimum	$v=1$	$v=2$	$v=3$	$v=4$	Method	$v=0$	$v=1$	$v=2$	$v=3$	$v=4$
1	1	5.3	−4.2	−17.6	−44.0		2	−63	−177	−269	−339	
2	1	5.2	−3.2	−14.4	−37.1		2	−65	−183	−281	−356	
3	1	10.0	−41.7	−130.1	−269.0		2	3	37	119	256	
4	1	−32.4	39.6	28.1	−38.8	−163.6	2	−1	−4	−7	−14	−30
5	1	0.5	−3.4	−14.9	−38.5	−77.0	2	0	12	41	91	155
6	1	3.6	−1.6	0.4	2.1	0.5	3	10	−8	−14	−7	10
7	5	4.9	2.9	5.9	6.3	3.2	2	6	66	206	447	
8	5	4.9	3.2	8.2	14.4	24.2	2	−1	−2	−1	−1	−6
9	5	4.8	0.8	0.1	−1.0	1.8						
	2	4.8	0.6	−1.3	−8.2	−21.2	2	−1	−2	−1	−1	−6
	3	0.0	−0.3	−5.0	−19.4	−49.1	3	1	4	20	59	127
10	2	5.0	0.3	2.2	8.0	21.5	2	6	69	216	470	
	3	−2.0	5.0	11.5	22.0	40.0						
11	3	−0.6	0.0	−1.8	−7.7	−21.2	3	−2	1	4	12	32
13	3	0.0	−0.1	−1.0	−5.4	−17.9	3	0	0	0	0	1
14	4	0.0	0.0	−0.1	−1.0	−3.4	4	0	0	2	6	18

* The approximation used in computing each set of entries is indicated in columns 2 and 8. 1 indicates use of an exact expression; 2, use of a trinomial expression in $v+\frac{1}{2}$; 3, use of all the terms given by Dunham; 4, use of Dunham's terms supplemented by results of numerical integrations; 5, use of the formula of Hylleraas.

Morse curves

Curve 1 is the Morse curve as generally constructed, reproducing experimental values of B_e, ω_e, and D, while curve 2 is designed to reproduce the experimental B_e, ω_e, $\omega_e x_e$. In the case of this particular state it happens that these two methods of construction give almost the same results, for the relation required by the Morse curve, $D=\omega_e^2/4\omega_e x_e$, is nearly satisfied by the experimental values. Usually a considerably greater difference will be found. The second method is preferable in determining the curve near the minimum. The errors in the computed E_v show that these curves tend to give excessive separations of classical turning-points, while the too-slow increase of r_v with v shows that they are too symmetrical about the minimum. Fig. 2 shows the net effect of these errors, the curves being much too low on the left and slightly too high on the right.

The Morse curve 3 was constructed in an attempt to improve the results by a better fitting of the rotational constants. It reproduces the observed α_e as well as B_e and ω_e; $\omega_e x_e$ then comes out much too large, so that the vibrational levels are very low. Fig. 2 shows that the result is an error which below $V=4000$ is approximately symmetrical; both sides of the curve are moved outward, with addition effects on E_v but compensating effects on r_v.

In constructing curve 4, which also gives the observed values of B_e and α_e, we concerned ourselves not with reproducing any vibrational constants, but with obtaining a good fit for the vibrational energy levels with $v\leqslant 4$. Both ω_e and $\omega_e x_e$ are then badly in error, but over the interesting range as a whole the energy levels and the potential curve itself are more satisfactory than for any other of the Morse curves. This is a good example of the advantages of direct fitting of energy levels over the reproduction of a limited number of spectroscopic constants; the flexibility of the Morse curve is, however, too limited to permit a really satisfactory fit.

Pöschl-Teller curves

Curve 5 is a Pöschl-Teller curve giving the observed ω_e, $\omega_e x_e$, B_e and α_e. As with the Morse function, practically the same curve is obtained if D is fixed instead of $\omega_e x_e$. (It is not possible to fix both D and $\omega_e x_e$ by sacrificing a rotational constant.) The errors in the energy levels indicate that the curve is quite good near the minimum, but that the classical turning points tend, with increasing v, to lie too far apart and too far to large r. Thus the curve must clearly lie too low on the right, as is verified by Table III, but the nature of the error on the left-hand side is not indicated by so simple an argument.

Curve 6 has been obtained by our method of energy level fitting, the energy levels used in its construction being those for $v \leqslant 4$. Since the vibrational levels of the P.-T. curve are exactly known, Y_{10} and Y_{20} could be chosen once for all to minimize the mean square errors in the computed E_v. Similar minimization of the errors in the B_v, by adjustment of Y_{01}' and Y_{11}', required the use of successive approximations, which converged rapidly. The computed E_v and B_v indicate that this curve has turning points too far apart at the bottom, (it must then be too shallow), too close together for $v=2$, 3, and too far apart above this; too far to the right for $v=0$, 4, and too far to the left in the intermediate region. In short, the errors of this curve are clearly small and of fluctuating sign, as also appears from Table IV. Since the sign of this error does fluctuate, it would of course be unjustified to assume that the magnitude of the errors in U is the same as that of the errors in E_v. In fact, the mean square error in the computed E_v is 1.2 cm^{-1}, while for $U(r)$ over the corresponding region it is about ten times as great. Comparison of this curve with curve 4 will indicate the great advantage of having one extra parameter to adjust by this method, though it is possible that the difference is unusually large for this state because of an especially appropriate character of the P.-T. curve.

Hylleraas curves

Curve 7 is a Hylleraas curve constructed as recommended by that author. According to his approximate formula for the vibrational levels these are excellently reproduced, the error remaining less than 10 cm^{-1} even up to $v=7$. The rotational terms are very bad, and indicate that beyond the range of $v=2$ the curve is as defective as the Morse curves 1 or 2, but in the opposite sense. This is caused by failure to control Y_{21} (the spectroscopic γ_e) which comes out large and with the wrong sign. (The same lack of control exists in a similar fitting of the Pöschl-Teller function, but it happens that the resulting error is there less serious.) Curve 8 represents an attempt to improve this curve by altering the value of the Hylleraas κ so as to get a satisfactory value of γ_e, while curve 9 was obtained by a general readjustment of constants to improve further the vibrational levels, as given by the Hylleraas approximation. The excellence of this result is, however, completely illusory; when E_v and r_v are computed for curve 9 from the more accurate formulas of Dunham it is found that the vibrational levels rapidly fall below the observed values as v rises, while r_v rises abruptly. Computation of the potential curve itself shows that it is little better than the Pöschl-Teller curve 5, except that it remains accurate over a somewhat larger range of r. We have not computed the exact levels of curves 7 and 8, but the magnitude of the errors in the Hylleraas approximation is evidently the same, since the errors in the computed potential curves, as compared to curve 14, are not of the character to be expected from the errors in E_v and r_v as given by that approximation.

Abandoning the Hylleraas approximate energy formula, we have determined curve 10 to give the experimental ω_e, $\omega_e x_e$, $\omega_e y_e$, D, B_e and α_e. The large size of the second order W. B. K. term Y_{10}'', and the inappropriate nature of the higher spectroscopic constants makes the result relatively poor.

Finally, abandoning preoccupation with the spectroscopic constants, we have determined curve 11 to give more satisfactory values for the energy levels, by a single application of the method of §4, with curve 9 as the starting point. The resulting curve is much the most satisfactory of the Hylleraas curves, and should be subject to further improvement by further application of this method.

We cannot recommend the Hylleraas curve as generally useful, since the curves to be described next give equal or greater flexibility and are more easily manipulated.

Series Expansion of U

Curve 12 is a Dunham curve constructed with the coefficients a_0 to a_4 given by Sandeman, and designed to make the Y_{1j}' come out equal to the observed expansion coefficients as far as $\omega_e x_e$ and γ_e.[17] We have also determined a set of

[17] Sandeman states that, for this set of a_n, Y_{10}'' has the very large value 16.5. This seems to be in error; we find the value -1.78, which is still much larger than the usual values.

a_n up to a_6 such that application of the full Dunham formulas gives Y_{lj} which, up to Y_{40}, and Y_{31}, are essentially equal to the corresponding constants in Sandeman's expansion. We have used these constants in determining curve 13, again setting equal to zero the a_n not explicitly determined. The difference of curves 12 and 13 thus illustrates the effect of failure to consider Y_{40}', Y_{31}', and the Y_{lj}''.

Finally, the extended Morse function, curve 14, has been determined, with the same set of a_n as for curve 13. These two curves agree in their first eight derivatives at their minima, but their different behavior as r becomes larger produces the differences exhibited in Table IV. Their energy levels are identical, so far as the formulas of Dunham will permit their computation; these values appear in Table VI as the levels for curve 13. A careful investigation of the higher vibrational levels, with results already stated in §3, served to determine more exactly the levels of curve 14 as shown in Table VI; the corrections for the higher levels are by no means negligible.

We may now undertake to estimate the errors in this curve in comparison with the "true" curve which gives the observed levels. Evidently this error is of the order 1 cm^{-1} for the range of $v=2$, for within this range the most important error is one of 0.0002 in r_2, corresponding to a depression of the order of 2 cm^{-1} at the outer turning point. Beyond this curve 14 becomes lower than the correct curve by a steadily increasing amount. Since this curve was taken as the standard in the preliminary estimation of the errors in the other curves, it follows that the entries in Table IV might now be corrected by subtracting the errors of curve 14. The only curve good enough to warrant this small correction is curve 6, which is evidently a better approximation for large values of r than is indicated by this table.

In order to check theoretical calculations the experimental potential curve must be located on the absolute energy scale, with zero energy that of the completely dispersed system. On this scale the energy of a normal H atom is -109678 cm^{-1}. Sandeman[18] computes a dissociation energy for H_2^+ of 21363 ± 5 cm^{-1}, a value checked experimentally, though with slightly less precision, by Beutler and Jünger.[19] Beutler and Jünger[20] also find for the ionization energy of $1s\sigma 2s\sigma\ ^3\Sigma_g$ H_2 the value 29344 ± 2 cm^{-1}. From these values one finds for the lowest energy level of this latter state the value -160385 ± 6 cm^{-1}. Using this result, and applying to curve 14 a correction of 2 cm^{-1} at $r=2.7$ and 8 cm^{-1} at $r=2.9$, we obtain the following most probable experimental values for the total and binding energies of this state:

$r=$	1.3	1.5	1.7	1.9	2.1	2.3	2.5	2.7	2.9
$-U(cm^{-1})$	153218	158850	161218	161690	161045	159747	158086	156242	154334
E(ev)	1.9885	2.6833	2.9754	3.0337	2.9540	2.7940	2.5891	2.3616	2.1262.

An appreciable uncertainty in these results, for points not too close to the minimum, arises from uncertainties in the values of the fundamental constants. U is accurately given as a function of $\xi=(r-r_e)/r_e$. The value of r_e, in cm, as deduced from B_e, depends on the values of h and μ. In atomic units its value depends on the quantity Rm/μ, which we have taken to be 119.371, corresponding to a ratio of 1838.6 for proton to electron mass. Recent discussions of the fundamental constants indicate that a slightly larger value of Rm/μ might be preferable. For comparison, we give a table of binding energies computed with $Rm/\mu=119.50$ (mass ratio 1836.6):

$r=$	1.3	1.5	1.7	1.9	2.1	2.3	2.5	2.7	2.9
E(ev) =	1.9853	2.6815	2.9747	3.0336	2.9546	2.7950	2.5904	2.3631	2.1278.

[18] I. Sandeman, Proc. Roy. Soc., Edinburgh **55**, 72 (1935).
[19] H. Beutler and H.-O. Jünger, Zeits. f. Physik **101**, 304 (1936).
[20] H. Beutler and H.-O. Jünger, Zeits. f. Physik **101**, 285 (1936).

Extension of the Theory of Complex Spectra

GEORGE H. SHORTLEY AND BERNARD FRIED
Mendenhall Laboratory of Physics, Ohio State University, Columbus, Ohio

(Received September 2, 1938)

This paper extends the tabular and formular material of the theory of complex spectra to configurations involving f and g electrons. In making these computations it was found that in practically every case significant simplification could be made over the methods previously used. In particular, for the computation of the electrostatic energies for two-electron-like almost-closed-shell configurations a simple closed formula was found which entirely replaces the previous lengthy diagonal-sum calculation. The explicit content of the paper is best exhibited by listing the section headings: I. Extension of Tables of c^k, b^k, and a^k to gp, gd, gf, gg. II. Explanation of the Regularities in the Electrostatic Energies of Two-Electron Configurations and Formulas for gp, gd, gf, gg, g^2. III. Formula Determining the Electrostatic Energies of Two-Electron-Like Configurations with Almost-Closed Shells. Values for p^5g and d^9g. IV. Matrices for Transformation of pf, df, pg, dg from LS to jj Coupling. V. Matrices of Electrostatic Interaction in jj Coupling for p^5f, (d^9p), d^9d, d^9f, d^9g.

SPECTROSCOPIC analysis is beginning more and more to involve configurations with f and g electrons.[1] For this reason we believe it useful to extend the tabular and formular material of the theory of complex spectra to the point where it will handle the simpler of the observed f- and g-electron configurations. This is the purpose of the present paper. The abstract above contains a statement of the contents by sections. In extending this material to the more complicated configurations for which the amount of computational labor is great, it became desirable to re-examine the methods of calculation with a view to simplifying them if possible. It has been found that in practically every case significant simplification could be made over the methods previously used. In one case (the determination of the electrostatic energies for almost-closed-shell configurations) it was possible to find a simple closed formula to replace the previous lengthy diagonal-sum calculation. These simplified methods of computation are discussed at the beginning of each section before the tabular results are given.

I. Extension of Tables of c^k, b^k, and a^k to gp, gf, gd, gg (Tables I and II)

The a's, b's, and c's are the Slater coefficients needed to compute the matrix of electrostatic interaction.[2] The values of the a's and b's follow at once by $8^6 14$ (TAS) from the values of the c's. The c's represent the following definite integrals:

$$c^k(lm, l'm') = \left(\frac{2}{2k+1}\right)^{\frac{1}{2}} \int_0^\pi \Theta(k, m-m')\Theta(lm)\Theta(l'm') \sin\theta \, d\theta, \tag{1}$$

$$|l-l'| \leqslant k \leqslant l+l' \qquad k+l+l' = 2g \quad (g \text{ integral}). \tag{2}$$

The direct individual evaluation of these integrals by means of Gaunt's formula $8^6 11$ is very laborious because of the sum occurring in this formula. We find, however, that it is possible to express $c^k(l, m; l', l'-\epsilon)$ as the square root of a polynomial in m and then compute from this polynomial the $2l+1$ entries with $m = l, \cdots, -l$ with but little more trouble than the direct evaluation of a single entry. We start by noting that an examination of Gaunt's derivation shows that $8^6 11$ is valid for the whole range $-l \leqslant m \leqslant l$; $-l' \leqslant m' \leqslant l'$; $-l'' \leqslant m+m' \leqslant l''$.

[1] Compare, for example, Shenstone's analysis of Cu II, which is discussed theoretically in the paper following this.
[2] See Condon and Shortley, *Theory of Atomic Spectra* [which we shall denote, following Kemble, by TAS], pp. 175–180 for definitions and previous tabulations.

TABLE I. $c^k(lm, l'm')$ and $b^k(lm, l'm')$. *We write* $c^k = \pm\sqrt{(x/D_k)}$, *where* D_k *depends only on* k, l, l'. *In the table are listed only the sign preceding the radical and the value of* x, D_k *being given at the head of each column. Since* $b^k = (c^k)^2$, $b^k = +x/D_k$. *Note that* $c^k(l'm', lm) = (-1)^{m-m'}c^k(lm, l'm')$.

$c^k(lm, l'm')$ FOR $l+l'$ EVEN

ll'	m	m'	$k=$ 0	2	4	6	8
gs	±4	0			$+\sqrt{}$ 1/9		
	±3	0			1		
	±2	0			1		
	±1	0			1		
	0	0			1		
gd	±4	±2		$+\sqrt{}$ 70/245	$-\sqrt{}$168/10672.2	$+\sqrt{}$ 1/4089.8	
	±3	±2		+ 35	− 378	+ 5	
	±2	±2		+ 15	− 540	+ 15	
	±1	±2		+ 5	− 600	+ 35	
	0	±2		+ 1	− 540	+ 70	
	∓1	±2		0	− 378	+ 126	
	∓2	±2		0	− 168	+ 210	
	∓3	±2		0	0	+ 330	
	∓4	±2		0	0	+ 495	
	±4	±1		0	+ 588	− 9	
	±3	±1		+ 35	+ 525	− 32	
	±2	±1		+ 40	+ 243	− 70	
	±1	±1		+ 30	+ 30	− 120	
	0	±1		+ 16	− 30	− 175	
	∓1	±1		+ 5	− 243	− 224	
	∓2	±1		0	− 525	− 252	
	∓3	±1		0	− 588	− 240	
	∓4	±1		0	0	− 165	
	±4	0		0	− 784	+ 45	
	±3	0		0	− 49	+ 108	
	±2	0		+ 15	+ 64	+ 168	
	±1	0		+ 30	+ 289	+ 210	
	0	0		+ 36	+ 400	+ 225	
gg	±4	±4	1	$-\sqrt{}$784/5929	$+\sqrt{}$196/123703$\frac{1}{81}$	$-\sqrt{}$ 16/20449	$+\sqrt{}$ 1/1206071$\frac{8}{49}$
	±3	±4	0	− 588	+ 490	− 84	+ 9
	±2	±4	0	− 168	+ 630	− 240	+ 45
	±1	±4	0	0	+ 490	− 480	+ 165
	0	±4	0	0	+ 196	− 720	+ 495
	∓1	±4	0	0	0	− 792	+ 1287
	∓2	±4	0	0	0	− 528	+ 3003
	∓3	±4	0	0	0	0	+ 6435
	∓4	±4	0	0	0	0	+ 12870
	±3	±3	1	− 49	− 441	+ 289	− 64
	±2	±3	0	− 525	− 70	+ 507	− 252
	±1	±3	0	− 378	+ 70	+ 540	− 720
	0	±3	0	0	+ 441	+ 300	− 1650
	∓1	±3	0	0	+ 490	+ 18	− 3168
	∓2	±3	0	0	0	− 198	− 5148
	∓3	±3	0	0	0	− 924	− 6864
	±2	±2	1	+ 64	− 121	− 484	+ 784
	±1	±2	0	− 243	− 360	− 189	+ 1764
	0	±2	0	− 540	− 121	0	+ 3150
	∓1	±2	0	0	+ 70	+ 210	+ 4620
	∓2	±2	0	0	+ 630	+ 504	+ 5544
	±1	±1	1	+ 289	+ 81	− 1	− 3136
	0	±1	0	− 30	− 81	− 210	− 4410
	∓1	±1	0	− 600	− 360	− 420	− 5040
	0	0	1	+ 400	+ 324	+ 400	+ 4900

TABLE I.—*Continued*

$c^k(lm, l'm')$ FOR $l+l'$ ODD

ll'	m	m'	$k=$	1	3	5	7
gp	±4	±1			$+\sqrt{28/147}$	$-\sqrt{1/363}$	
	±3	±1			+ 21	− 3	
	±2	±1			+ 15	− 6	
	±1	±1			+ 10	− 10	
	0	±1			+ 6	− 15	
	∓1	±1			+ 3	− 21	
	∓2	±1			+ 1	− 28	
	∓3	±1			0	− 36	
	∓4	±1			0	− 45	
	±4	0			0	+ 9	
	±3	0			+ 7	+ 16	
	±2	0			+ 12	+ 21	
	±1	0			+ 15	+ 24	
	0	0			+ 16	+ 25	
gf	±4	±3		$+\sqrt{28/63}$	$-\sqrt{42/847}$	$+\sqrt{420/143143}$	$-\sqrt{1/262914\frac{4}{7}}$
	±3	±3		+ 7	− 63	+ 1575	− 7
	±2	±3		+ 1	− 54	+ 3375	− 28
	±1	±3		0	− 30	+ 5250	− 84
	0	±3		0	− 9	+ 6300	− 210
	∓1	±3		0	0	+ 5670	− 462
	∓2	±3		0	0	+ 3150	− 924
	∓3	±3		0	0	0	− 1716
	∓4	±3		0	0	0	− 3003
	±4	±2		0	+ 70	− 1960	+ 9
	±3	±2		+ 21	+ 14	− 4235	+ 48
	±2	±2		+ 12	− 3	− 4800	+ 147
	±1	±2		+ 3	− 32	− 3125	+ 336
	0	±2		0	− 49	− 700	+ 630
	∓1	±2		0	− 30	+ 210	+ 1008
	∓2	±2		0	0	+ 3360	+ 1386
	∓3	±2		0	0	+ 7350	+ 1584
	∓4	±2		0	0	0	+ 1287
	±4	±1		0	− 42	+ 4704	− 45
	±3	±1		0	+ 14	+ 4802	− 180
	±2	±1		+ 15	+ 40	+ 1849	− 420
	±1	±1		+ 15	+ 15	+ 15	− 735
	0	±1		+ 6	− 1	− 1210	− 1050
	∓1	±1		0	− 32	− 3584	− 1260
	∓2	±1		0	− 54	− 3402	− 1260
	∓3	±1		0	0	− 294	− 990
	∓4	±1		0	0	+ 5880	− 495
	±4	0		0	0	− 7056	+ 165
	±3	0		0	− 63	− 1764	+ 480
	±2	0		0	− 3	+ 84	+ 840
	±1	0		+ 10	+ 15	+ 2166	+ 1120
	0	0		+ 16	+ 36	+ 3600	+ 1225

If in 8°11 we substitute l', $l'-\epsilon$ for lm; k, $m-l'+\epsilon$ for $l'm'$; lm for l'', $m+m'$; we can obtain the formula

$$c^k(l,m;l',l'-\epsilon)=\frac{(-1)^{g+l+\epsilon}g!}{(g-l)!(g-l')!(g-k)!(2g+1)!}\left[\frac{(2l+1)(2l'+1)}{\epsilon!(2l'-\epsilon)!}\frac{(k+l'-\epsilon-m)!}{(l-m)!}\frac{(l+m)!}{(k-l'+\epsilon+m)!}\right]^{\frac{1}{2}}$$

$$\times\sum_s(-1)^s\binom{\epsilon}{s}(2l'-s)!(2g-2l'+s)!\frac{(2g-2k)!}{(2g-2k-s)!}\frac{(k-l'+m+\epsilon)!}{(k-l'+m+s)!}. \quad (3A)$$

In the sum, $\binom{\epsilon}{s}$ is the binomial coefficient, and s runs from 0 to the lesser of ϵ and $2g-2k$.

TABLE II. $a^k(lm, l'm')$. *The value of this coefficient is independent of the signs of m and m'. As in the preceding table, we print the common denominator of several related values but once at the beginning of each group. For* $l=0$, $a^k(00, l'm') = \delta(k, 0)$ *for all* l', m'; *for* $k=0$, $a^0(lm, l'm') = 1$ *for all values of the arguments; in the table we give values only for* l, l', $k>0$. *Note that* $a^k(l'm', lm) = a^k(lm, l'm')$.

ll'	$\|m\|$	$\|m'\|$	$k=$ 2	4	6	8
gp	4	1	+ 28/385			
	3	1	+ 7			
	2	1	− 8			
	1	1	− 17			
	0	1	− 20			
	4	0	− 56			
	3	0	− 14			
	2	0	+ 16			
	1	0	+ 34			
	0	0	+ 40			
gd	4	2	+ 56/539	+ 14/2335⅔		
	3	2	+ 14	− 21		
	2	2	− 16	− 11		
	1	2	− 34	+ 9		
	0	2	− 40	+ 18		
	4	1	− 28	− 56		
	3	1	− 7	+ 84		
	2	1	+ 8	+ 44		
	1	1	+ 17	− 36		
	0	1	+ 20	− 72		
	4	0	− 56	+ 84		
	3	0	− 14	−126		
	2	0	+ 16	− 66		
	1	0	+ 34	+ 54		
	0	0	+ 40	+108		
gf	4	3	+140/1155	+ 42/3670⅓	+ 4/12269.4	
	3	3	+ 35	− 63	− 17	
	2	3	− 40	− 33	+ 22	
	1	3	− 85	+ 27	+ 1	
	0	3	−100	+ 54	− 20	
	4	2	0	− 98	− 24	
	3	2	0	+147	+102	
	2	2	0	+ 77	−132	
	1	2	0	− 63	− 6	
	0	2	0	−126	+120	
	4	1	− 84	+ 14	+ 60	
	3	1	− 21	− 21	−255	
	2	1	+ 24	− 11	+330	
	1	1	+ 51	+ 9	+ 15	
	0	1	+ 60	+ 18	−300	
	4	0	−112	+ 84	− 80	
	3	0	− 28	−126	+340	
	2	0	+ 32	− 66	−440	
	1	0	+ 68	+ 54	− 20	
	0	0	+ 80	+108	+400	
gg	4	4	+784/5929	+196/12370³¹⁄₈₁	+ 16/20449	+ 1/120607¹⁸⁄₄₉
	3	4	+196	−294	− 68	− 8
	2	4	−224	−154	+ 88	+ 28
	1	4	−476	+126	+ 4	− 56
	0	4	−560	+252	− 80	+ 70
	3	3	+ 49	+441	+289	+ 64
	2	3	− 56	+231	−374	− 224
	1	3	−119	−189	− 17	+ 448
	0	3	−140	−378	+340	− 560
	2	2	+ 64	+121	+484	+ 784
	1	2	+136	− 99	+ 22	−1568
	0	2	+160	−198	−440	+1960
	1	1	+289	+ 81	+ 1	+3136
	0	1	+340	+162	− 20	−3920
	0	0	+400	+324	+400	+4900

Alternatively if in 8^611 we substitute k, $m-l'+\epsilon$ for lm; l', $l'-\epsilon$ for $l'm'$; lm for l'', $m+m'$, we can obtain

$$c^k(l,m;l',l'-\epsilon)=\frac{(-1)^{g+l}g!}{(g-l)!(g-l')!(g-k)!(2g+1)!}\left[\frac{(2l+1)(2l'+1)}{\epsilon!(2l'-\epsilon)!}\frac{(k+l'-\epsilon-m)!}{(l-m)!}\frac{(l+m)!}{(k-l'+\epsilon+m)!}\right]^{\frac{1}{2}}$$
$$\times\sum_s(-1)^s\binom{\epsilon}{s}(2l'-s)!(2g-2l'+s)!\frac{(2g-2l)!}{(2g-2l-s)!}\frac{(l-m)!}{(l-m-\epsilon+s)!}, \quad (3B)$$

where s runs from 0 to the lesser of ϵ and $2g-2l$.

These formulas are good for the full range $-l\leqslant m\leqslant l$; hence we need consider only $\epsilon\leqslant l$ since the negative values of $l'-\epsilon$ may be covered by the formula $c^k(l,m;l',m')=c^k(l,-m;l',-m')$. For $\epsilon\leqslant l$, it may be seen that formula (3A) gives *directly* for $(c^k)^2$ a polynomial of order $2l'$ in m if $\epsilon>2g-2k$; formula (3B) gives *directly* a polynomial of order $2l'$ in m if $\epsilon>2g-2l$; while if $\epsilon<2g-2k$ and $\epsilon<2g-2l$ both formulas give polynomials of order $2l'$ *directly*. By *directly* we mean that the numerator and denominator of the rational function which these formulas give for $(c^k)^2$ come ready factorized so that the denominator may be canceled at once.[3]

The procedure for calculating the entries of Table I is then the following. In (3A) or (3B) take $l\geqslant l'$ to minimize the number of polynomials required. Then for each value of k occurring in (2), and for $\epsilon=0,1,\cdots,l'$, compute the c's as functions of m, using, in order to simplify the computation and make the sums as short as possible, (3A) if $\epsilon>2g-2k$, (3B) if $\epsilon>2g-2l$ (these inequalities are mutually exclusive), and either formula if $\epsilon<2g-2l$ and $\epsilon<2g-2k$. For example, one gets all the entries for gd from nine formulas, of which the following three are typical:

$$c^2(gm;d2)=+[(4+m)(3+m)(2+m)(1+m)/24\cdot49\cdot5]^{\frac{1}{2}}=c^2(g,-m;d,-2),$$
$$c^4(gm;d1)=+(2m-1)[5(5-m)(4+m)/6\cdot121\cdot49]^{\frac{1}{2}}\quad=c^4(g,-m;d,-1),$$
$$c^6(gm;d0)=+[5(36-m^2)(25-m^2)/4\cdot169\cdot121]^{\frac{1}{2}}\quad=c^6(g,-m;d,0).$$

These are valid for $-4\leqslant m\leqslant4$.

II. Explanation of the Regularities in the Electrostatic Energies of Two-Electron Configurations and Formulas for gp, gd, gf, gg, g^2

Inspection of the formulas for the electrostatic energies of two-electron configurations (TAS §5[7]) reveals a number of striking regularities to which attention has been called but for which, so far as we know, no proofs have been given. In order that we may justifiably take advantage of these regularities in our computations, we first indicate their general proofs.

(*a*) *In the case of ll'* (two nonequivalent electrons, cf. gp, gd, gf, gg below), *^1L and ^3L have equal coefficients of the F's and equal but opposite coefficients of the G's.*

Consider a table, such as 1^72 of TAS, in which the orbital functions are classified according to M_S and M_L. The sum of the diagonal elements of electrostatic energy for the states in the box $(1, M_L)$, with $M_S=1$, $M_L=M_L$, gives the sum of the energies of the N triplets of largest L value, if there are N states in this box. This sum is a certain linear combination of F's and G's. Consider now the diagonal sum for the corresponding box $(0, M_L)$ with $M_S=0$. This box contains $2N$ states and the diagonal sum gives the total energy of the N triplets and N singlets of highest L value. We see from the arrangement of the spins that the coefficients of the F's for this box are just twice those for $(1, M_L)$, while the coefficients of the G's vanish. The difference between the diagonal sum for $(0, M_L)$ and $(1, M_L)$ is the energy sum for the N singlets, and this sum therefore has the same F coefficients but the negative of the G coefficients of the triplet sum. By starting now with

[3] The ratio of two factorials involving m should here be treated like the ratio of two Γ functions, ignoring the fact that the factorials may be meaningless for certain values of m, for the resulting polynomials will always vanish properly for such m.

the highest M_L value, which involves only one singlet and one triplet, and working down, we prove the statement (*a*) by induction.

(*b*) *In the case of nln'l* (nonequivalent electrons of the same *l* value, cf. *gg* below) *in addition to* (*a*) *one finds that for those terms which are permitted in* nl^2 *by the exclusion principle the coefficients of the F's equal those of the corresponding G's, while for the terms excluded in* nl^2, *corresponding coefficients of F's and G's are equal and opposite.*

(*c*) *One can obtain the electrostatic energies for* nl^2 *from those for nln'l by setting* $F^k=G^k$ *and dividing by 2.*

The proof of (*c*) follows at once from the fact (TAS p. 232) that the Russell-Saunders eigenfunctions of nl^2, both the vanishing and the nonvanishing ones, may be obtained from the corresponding eigenfunctions of *nln'l* by setting $n=n'$ and dividing by $\sqrt{2}$. Then, since $G^k(nl^2) \equiv F^k(nl^2)$, a diagonal electrostatic matrix element of nl^2 in *LS* coupling is obtained from that of *nln'l* by setting $G^k=F^k$ and dividing by 2; as stated in (*c*). If this is done for one of the terms of *ll* which is excluded from l^2, the resulting energy must vanish; this requires that for such terms of *ll* the coefficients of F^k and G^k be equal and opposite. This proves one of the statements of (*b*), the other statement now follows at once from (*a*), which says that the unexcluded member of the pair of terms, ^1L, ^3L, has opposite *G* coefficients from the excluded member, and hence will have *G* coefficients equal to its *F* coefficients.

We give now the electrostatic energies of two-electron configurations involving *g* electrons. We also give the $\zeta(SL)$ which determine the absolute first-order Landé splitting (cf. TAS §4[7]). [We do not go on and calculate the complete matrices of spin-orbit interaction in *LS* coupling for these configurations because so far no one has wanted to use these matrices—even the known ones (TAS, pp. 268–269) for *pd*, d^2, *dd*—for intermediate-coupling computations because of the extreme complexity of the equations involved. Most of the complex configurations for which intermediate-coupling computations have been made involve almost-closed shells, and for these the *jj*-coupling matrices, which we do obtain, are of most interest.]

gp:

$$^1F,\ ^3F = F_0+55\,F_2\pm(\ G_3+55\,G_5) \qquad \zeta(^3F) = \tfrac{5}{8}\,\zeta_g-\tfrac{3}{8}\,\zeta_p$$
$$^1G,\ ^3G = F_0-77\,F_2\mp(\ 7\,G_3-11\,G_5) \qquad \zeta(^3G) = 1\tfrac{9}{40}\,\zeta_g+\tfrac{1}{40}\,\zeta_p$$
$$^1H,\ ^3H = F_0+28\,F_2\pm(28\,G_3+\ G_5) \qquad \zeta(^3H) = \tfrac{2}{5}\,\zeta_g+\tfrac{1}{10}\,\zeta_p$$

gd:

$$^1D,\ ^3D = F_0+110\,F_2+143\,F_4\pm(\ G_2+330\,G_4+715\,G_6) \qquad \zeta(^3D) = \tfrac{5}{6}\,\zeta_g-\tfrac{1}{3}\,\zeta_d$$
$$^1F,\ ^3F = F_0+\ 11\,F_2-286\,F_4\mp(\ 5\,G_2+957\,G_4-286\,G_6) \qquad \zeta(^3F) = 1\tfrac{3}{24}\,\zeta_g-\tfrac{1}{24}\,\zeta_d$$
$$^1G,\ ^3G = F_0-\ 65\,F_2+234\,F_4\pm(15\,G_2+883\,G_4+\ 78\,G_6) \qquad \zeta(^3G) = 1\tfrac{7}{40}\,\zeta_g+\tfrac{3}{40}\,\zeta_d$$
$$^1H,\ ^3H = F_0-\ 70\,F_2-\ 91\,F_4\mp(35\,G_2-798\,G_4-\ 13\,G_6) \qquad \zeta(^3H) = 1\tfrac{1}{30}\,\zeta_g+\tfrac{2}{15}\,\zeta_d$$
$$^1I,\ ^3I = F_0+\ 56\,F_2+\ 14\,F_4\pm(70\,G_2+168\,G_4+\ G_6) \qquad \zeta(^3I) = \tfrac{1}{3}\,\zeta_g+\tfrac{1}{6}\,\zeta_d$$

gf:

$$^1P,\ ^3P = F_0+275\,F_2+429\,F_4+\ 715\,F_6\pm(\ G_1+33\,G_3+10725\,G_5+5005\,G_7) \qquad \zeta(^3P) = \tfrac{5}{4}\,\zeta_g-\tfrac{3}{4}\,\zeta_f$$
$$^1D,\ ^3D = F_0+165\,F_2-143\,F_4-1287\,F_6\mp(\ 3\,G_1+77\,G_3+12155\,G_5-3003\,G_7) \qquad \zeta(^3D) = \tfrac{7}{12}\,\zeta_g-\tfrac{1}{12}\,\zeta_f$$
$$^1F,\ ^3F = F_0+\ 30\,F_2-299\,F_4+1170\,F_6\pm(\ 6\,G_1+97\,G_3-\ 2990\,G_5+1365\,G_7) \qquad \zeta(^3F) = \tfrac{5}{12}\,\zeta_g+\tfrac{1}{12}\,\zeta_f$$
$$^1G,\ ^3G = F_0-\ 94\,F_2+\ 39\,F_4-\ 650\,F_6\mp(10\,G_1+63\,G_3-\ 9594\,G_5-\ 455\,G_7) \qquad \zeta(^3G) = \tfrac{7}{20}\,\zeta_g+\tfrac{3}{20}\,\zeta_f$$
$$^1H,\ ^3H = F_0-159\,F_2+289\,F_4+\ 225\,F_6\pm(15\,G_1-23\,G_3+\ 8779\,G_5+\ 105\,G_7) \qquad \zeta(^3H) = 1\tfrac{9}{60}\,\zeta_g+1\tfrac{1}{60}\,\zeta_f$$
$$^1I,\ ^3I = F_0-105\,F_2-203\,F_4-\ 45\,F_6\mp(21\,G_1-91\,G_3-\ 3115\,G_5-\ 15\,G_7) \qquad \zeta(^3I) = 2\tfrac{5}{84}\,\zeta_g+1\tfrac{7}{84}\,\zeta_f$$
$$^1K,\ ^3K = F_0+140\,F_2+\ 42\,F_4+\ \ 4\,F_6\pm(28\,G_1+42\,G_3+\ 420\,G_5+\ G_7) \qquad \zeta(^3K) = \tfrac{2}{7}\,\zeta_g+\tfrac{3}{14}\,\zeta_f$$

gg:

$$^1S,\ ^3S = F_0+1540\,F_2+2002\,F_4+2860\,F_6+24310\,F_8\pm(G_0+1540\,G_2+2002\,G_4+2860\,G_6+24310\,G_8)$$
$$^1P,\ ^3P = F_0+1309\,F_2+1001\,F_4-\ 143\,F_6-19448\,F_8\mp(G_0+1309\,G_2+1001\,G_4-\ 143\,G_6-19448\,G_8)$$
$$^1D,\ ^3D = F_0+\ 883\,F_2-\ 299\,F_4-1469\,F_6+12376\,F_8\pm(G_0+\ 883\,G_2-\ 299\,G_4-1469\,G_6+12376\,G_8)$$
$$^1F,\ ^3F = F_0+\ 334\,F_2-\ 949\,F_4+\ 442\,F_6-\ 6188\,F_8\mp(G_0+\ 334\,G_2-\ 949\,G_4+\ 442\,G_6-\ 6188\,G_8)$$
$$^1G,\ ^3G = F_0-\ 230\,F_2-\ 467\,F_4+1030\,F_6+\ 2380\,F_8\pm(G_0-\ 230\,G_2-\ 467\,G_4+1030\,G_6+\ 2380\,G_8)$$
$$^1H,\ ^3H = F_0-\ 665\,F_2+\ 581\,F_4-1205\,F_6-\ \ 680\,F_8\mp(G_0-\ 665\,G_2+\ 581\,G_4-1205\,G_6-\ \ 680\,G_8)$$
$$^1I,\ ^3I = F_0-\ 791\,F_2+\ 721\,F_4+\ 601\,F_6+\ \ 136\,F_8\pm(G_0-\ 791\,G_2+\ 721\,G_4+\ 601\,G_6+\ \ 136\,G_8)$$
$$^1K,\ ^3K = F_0-\ 392\,F_2-\ 784\,F_4-\ 152\,F_6-\ \ \ 17\,F_8\mp(G_0-\ 392\,G_2-\ 784\,G_4-\ 152\,G_6-\ \ \ 17\,G_8)$$
$$^1L,\ ^3L = F_0+\ 784\,F_2+\ 196\,F_4+\ \ 16\,F_6+\ \ \ \ \ F_8\pm(G_0+\ 784\,G_2+\ 196\,G_4+\ \ 16\,G_6+\ \ \ \ G_8)$$

$$\zeta(^3P)=\zeta(^3D)=\zeta(^3F)=\zeta(^3G)=\zeta(^3H)=\zeta(^3I)=\zeta(^3K)=\zeta(^3L)=\tfrac{1}{4}\,\zeta_{ng}+\tfrac{1}{4}\,\zeta_{n'g}.$$

g^2: The formulas for the allowed terms, ^1S, ^3P, ^1D, ^3F, ^1G, ^3H, ^1I, ^3K, ^1L, are obtained from *gg* by omitting the expressions in the *G*'s. The intervals are given by $\zeta(^3P)=\zeta(^3F)=\zeta(^3H)=\zeta(^3K)=\frac{1}{25}\zeta_{ng}$.

TABLE III. *The integral* C_{uvw} [cf. (6)].*

$C_{000}=2$	$C_{112}=\frac{4}{15}$	$C_{222}=\frac{4}{35}$	$C_{334}=\frac{4}{77}$
$C_{011}=\frac{2}{3}$	$C_{123}=\frac{6}{35}$	$C_{224}=\frac{4}{35}$	$C_{336}=\frac{200}{3003}$
$C_{022}=\frac{2}{5}$	$C_{134}=\frac{8}{63}$	$C_{233}=\frac{8}{105}$	$C_{345}=\frac{40}{1001}$
$C_{033}=\frac{2}{7}$	$C_{145}=\frac{10}{99}$	$C_{235}=\frac{20}{231}$	$C_{347}=\frac{70}{1287}$
$C_{044}=\frac{2}{9}$		$C_{244}=\frac{40}{693}$	$C_{444}=\frac{36}{1001}$
		$C_{246}=\frac{10}{143}$	$C_{446}=\frac{40}{1287}$
			$C_{448}=\frac{980}{21879}$

* The table gives all nonvanishing integrals for u and $v \leq 4$. The values are independent of the order of the three subscripts.

III. Formula Determining the Electrostatic Energies of Two-Electron-Like Configurations with Almost-Closed Shells. Values for p^5g and d^9g

In §1[13] (TAS) it is shown that *the coefficients of the F's in the electrostatic energies for the configuration* $l^{m-1}l'$, which has one electron missing from the l shell, *are the negatives of those for the related two-electron configuration* ll'. It is also shown that *the coefficients of the G's vanish for the triplets*, so that if the formulas for ll' are known the computation is reduced to a determination of the coefficients of the G's for the singlets. These G singlet coefficients, in the cases where they have been previously obtained, by the lengthy diagonal-sum calculation, turn out to have the strikingly simple form shown by the formulas of p. 299, TAS. We show below the reason for this form and give for the nonvanishing G coefficients an explicit formula whose use eliminates completely the necessity for a diagonal-sum calculation for configurations of this type.

The start of the table (similar to 1[13]5, TAS) which classifies the orbital functions for $l^{m-1}l'$ according to the values of M_S and M_L is, for $M_S=0$:

$M_L=l+l'$ $\quad (-l^+, l'^+)(-l^-, l'^-)$,

$M_L=l+l'-1$ $\quad (-l+1^+, l'^+)(-l+1^-, l'^-)$
$(-l^+, l'-1^+)(-l^-, l'-1^-)$,

$M=l+l'-2$ $\quad (-l+2^+, l'^+)(-l+2^-, l'^-)$
$(-l+1^+, l'-1^+)(-l+1^-, l'-1^-)$
$(-l^+, l'-2^+)(-l^-, l'-2^-)$.

(The first entry in each parenthesis gives the quantum number m_l, m_s of the electron *missing* from the l shell, the second entry the quantum numbers of the l' electron.) The table continues in this fashion down to $M_L=|l-l'|$, and the G terms in the energies of all the singlets may be obtained by using just this part of the table.

In the diagonal sum for the box characterized by $M_S=0$, $M_L=M_L$, the coefficient of $G^k(ll')$, according to 1[13]4 (TAS), is seen to be

$$+\sum_m 2b^k(l, m; l', M_L+m). \tag{4}$$

Now we shall presently prove that

$$\sum_m b^k(l, m; l', M+m) = \frac{(2l+1)(2l'+1)}{2(2k+1)} C_{ll'k} \quad \text{if } k \geq |M| \qquad = 0 \quad \text{if } k < |M|, \tag{5}$$

so that the sum (4), when it is nonvanishing, is independent of M_L. The factor $C_{ll'k}$ is the integral of the product of three Legendre polynomials:

$$C_{ll'k}=\int_0^\pi P_l(\cos\theta)P_{l'}(\cos\theta)P_k(\cos\theta)\sin\theta\, d\theta. \tag{6}$$

Its values, which may be readily obtained from 9[6]9 (TAS) are given in Table III. From (4) and (5), and the usual diagonal-sum procedure which starts with the box with $M_S=0$, $M_L=l+l'$ and works down the table we see at once that

In the electrostatic energy for ^1L *the coefficients of all* G^k*'s vanish except that for* $k=L$, *which has the value*

$$\frac{(2l+1)(2l'+1)}{2L+1}C_{ll'L}.$$

Since $C_{ll'k}$ *vanishes unless the triangular conditions* (2) *are satisfied, only alternate singlets, those with* $L=l+l', l+l'-2, l+l'-4, \cdots, |l-l'|$ *have any nonvanishing G coefficients. The intermediate singlets, with* $L=l+l'-1, l+l'-3, \cdots$ *have the same electrostatic energies as the triplets of the same L value.*

From this rule and those enunciated at the beginning of this section we may at once write down the electrostatic energy formulas, in particular the formulas for d^9g which we shall need in our applications to Cu II in the succeeding paper. In p^5g and d^9g the only nonvanishing terms in the G's are given by

$$\begin{aligned} p^5g \text{ or } g^{17}p &\begin{cases} {}^1H: & 90G_5 \\ {}^1F: & 72G_3 \end{cases} \\ d^9g \text{ or } g^{17}d &\begin{cases} {}^1I: & 990G_6 \\ {}^1G: & 3080G_4 \\ {}^1D: & 252G_2. \end{cases} \end{aligned} \tag{7}$$

Note that these are written in terms of G_k rather than G^k ($G_k=G^k/D_k$, cf. Table I).

Proof of (5).—By the definition of $b^k=(c^k)^2$,

$$\sum_m b^k(l,\ m;\ l',\ M+m)=\sum_m b^k(l',\ M+m;\ l,\ m)$$

$$=\sum_m \frac{2}{2k+1}\int\int[\Theta_1(k,\ M)\Theta_1(l',\ M+m)\Theta_1(l,\ m)][\Theta_2(k,\ M)\Theta_2(l',\ M+m)\Theta_2(l,\ m)]\sin\theta_1\sin\theta_2\,d\theta_1\,d\theta_2$$

if $k\geqslant|M|$. b^k *and hence the sum vanish by definition for* $k<|M|$. We now introduce integrals over φ_1 and φ_2, involving a quantum number m', which vanish unless $m'=M+m$, in which case they equal $(2\pi)^{-1}$. We may then write m' for $M+m$ in the Θ factors if we introduce a sum over m'. In this way the above expression becomes

$$=\sum_m\sum_{m'}\frac{4\pi}{2k+1}\int\int\int\int[\Theta_1(kM)\Theta_2(kM)\Phi_1(M)\bar{\Phi}_2(M)][\Theta_1(l'm')\Theta_2(l'm')\bar{\Phi}_1(m')\Phi_2(m')]$$
$$\times[\Theta_1(lm)\Theta_2(lm)\Phi_1(m)\bar{\Phi}_2(m)]\sin\theta_1\sin\theta_2\,d\theta_1\,d\theta_2\,d\varphi_1\,d\varphi_2.$$

The sums over m and m' may now be evaluated by means of the spherical-harmonic addition theorem to give

$$=\frac{(2l'+1)(2l+1)}{4\pi(2k+1)}\int\int\int\int\Theta_1(kM)\Theta_2(kM)\Phi_1(M)\bar{\Phi}_2(M)P_{l'}(\cos\omega)P_l(\cos\omega)\sin\theta_1\sin\theta_2\,d\theta_1\,d\theta_2\,d\varphi_1\,d\varphi_2,$$

where ω is the angle between the directions θ_1, φ_1 and θ_2, φ_2. Now express the product $P_{l'}(\cos\omega)P_l(\cos\omega)$ as a series in

TABLE IV. Matrices for transformation from *LS* to *jj* coupling.

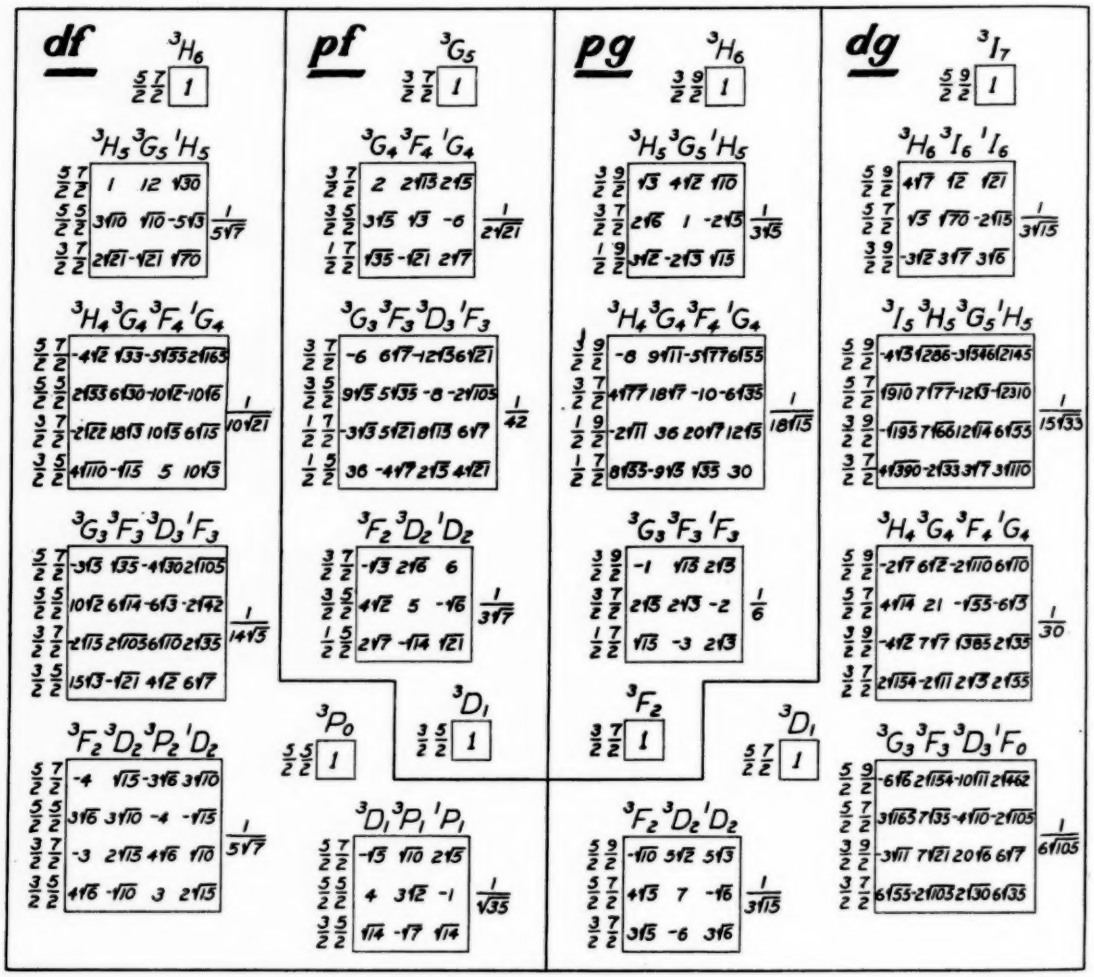

TABLE V. Matrices of electrostatic energy in *jj* coupling.

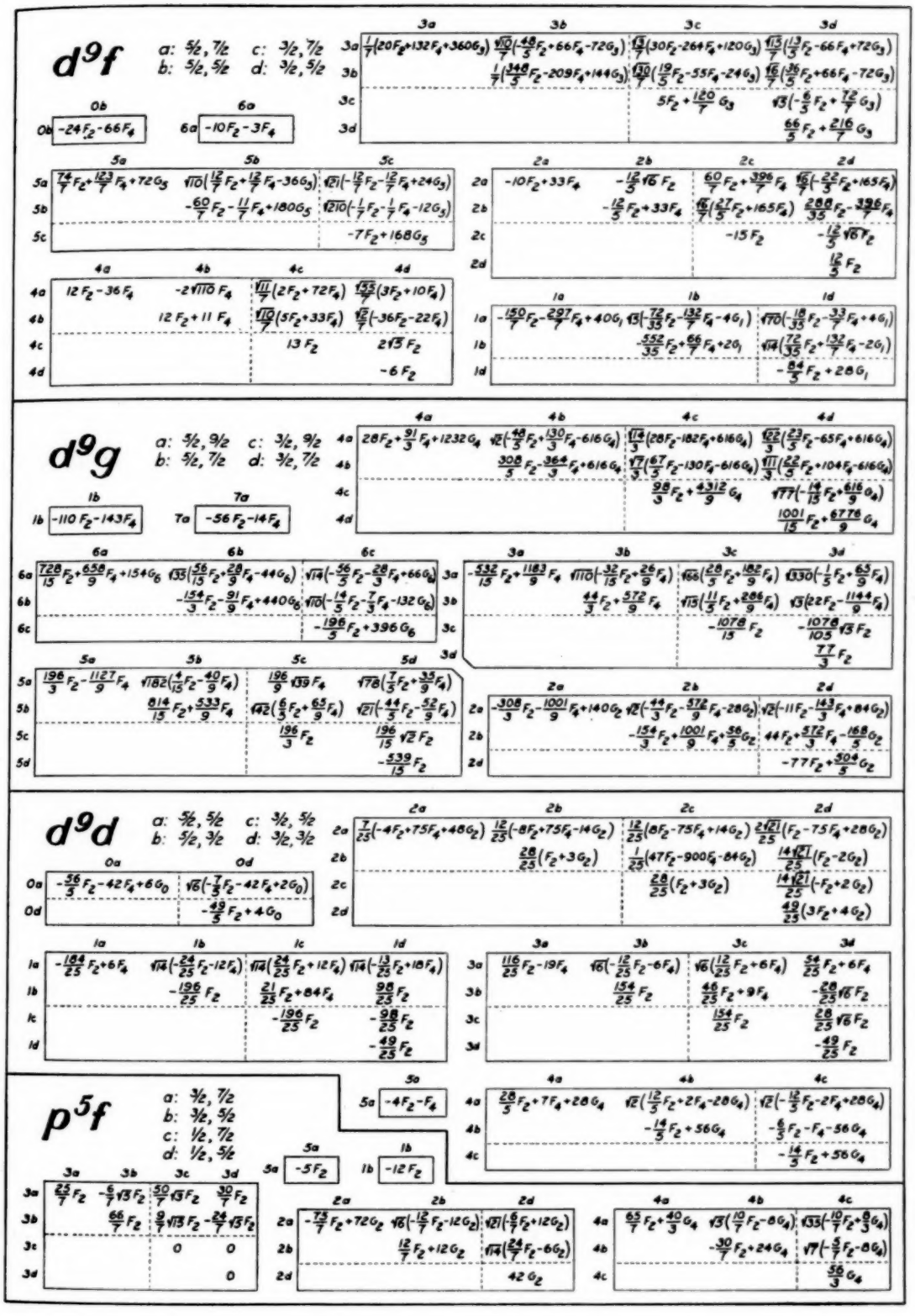

$P_\lambda(\cos\omega)$, and then expand $P_\lambda(\cos\omega)$ by the addition theorem:

$$P_{l'}(\cos\omega)P_l(\cos\omega)=\sum_\lambda \frac{2\lambda+1}{2}C_{ll'\lambda}P_\lambda(\cos\omega)=\sum_\lambda 2\pi C_{ll'\lambda}\sum_\mu \Theta_l(\lambda\mu)\Theta_{l'}(\lambda\mu)\bar{\Phi}_l(\mu)\Phi_{l'}(\mu)$$

to give

$$\sum_m b^k(l,m;l',M+m)=\frac{(2l'+1)(2l+1)}{2(2k+1)}\sum_{\lambda,\mu}C_{ll'\lambda}\int\int\Theta_l(kM)\Phi_l(M)\Theta_{l'}(\lambda\mu)\bar{\Phi}_{l'}(\mu)\sin\theta_1\,d\theta_1\,d\varphi_1$$
$$\cdot\int\int\Theta_{l'}(kM)\bar{\Phi}_{l'}(M)\Theta_l(\lambda\mu)\Phi_l(\mu)\sin\theta_2\,d\theta_2\,d\varphi_2.$$

These integrals vanish unless $\lambda\mu\equiv kM$, in which case they give the value 1, so the sum over λ, μ gives finally the result (5).

IV. Matrices for Transformation of *pf*, *df*, *pg*, *dg* from *LS* to *jj* Coupling (Table IV)

In order to find the electrostatic energy matrices needed to handle configurations like p^5f of the rare gases, d^9f and d^9g of spectra like Cu II, in *jj* coupling, we need the transformations from *LS* to *jj* coupling. The transformation matrix for the almost-closed-shell configuration $l^{m-1}l'$ is the same as that for the two-electron configuration ll' when the states are correlated as in Chapter XII, TAS. We obtain these matrices by simultaneous diagonalization of the *jj*-coupling matrices of $\boldsymbol{L}_1\cdot\boldsymbol{L}_2$ (or $\boldsymbol{L}^2$) and $\boldsymbol{S}_1\cdot\boldsymbol{S}_2$ (or $\boldsymbol{S}^2$) as sketched in §6[12], TAS. We may note one simplification in connection with this diagonalization which was not noticed when previous computations were made. In no two-electron configuration will more than four levels of the same J value occur, so the transformation factorizes into matrices of at most fourth order. For a typical J value, the four Russell-Saunders levels are ${}^1J_J$, ${}^3J{+}1_J$, ${}^3J_J$, ${}^3J{-}1_J$. The state ${}^1J_J$ may be obtained directly from the matrix $\boldsymbol{S}_1\cdot\boldsymbol{S}_2$ since it has a value of $\boldsymbol{S}_1\cdot\boldsymbol{S}_2$ different from the other three. The states ${}^3J{+}1_J$ and ${}^3J{-}1_J$ may be obtained directly from the matrix of $\boldsymbol{L}_1\cdot\boldsymbol{L}_2$ since they possess unique values of this quantity. The state ${}^3J_J$ however has the same value of $\boldsymbol{S}_1\cdot\boldsymbol{S}_2$ as the other triplets and the same $\boldsymbol{L}_1\cdot\boldsymbol{L}_2$ as the singlet. To obtain it directly involves the *simultaneous* diagonalization of the two matrices with its attendant inconvenient intermediate matrix multiplications. But this may be avoided by noting that after ${}^1J_J$, ${}^3J{+}1_J$, ${}^3J{-}1_J$ have been found, the eigenfunction for ${}^3J_J$ is the unique function orthogonal to the other three.

The phases of the *LS*-coupling states in the transformation matrices of Table IV are arbitrary but the *jj*-coupling phases are chosen in accordance with the conventions of §6[12], TAS.

V. Matrices of Electrostatic Interaction in *jj* Coupling for p^5f, (d^9p), d^9d, d^9f, d^9g (Table V)

We finally give the results of transforming the electrostatic energies of section III to *jj* coupling by means of the matrices of section IV for cases of interest in the paper following this. The electrostatic matrices for p^5p and p^5d are given on pp. 307, 313 of TAS. We note that since the electrostatic energies and the *LS*-*jj* transformations are the same, the *jj* electrostatic-energy matrix for d^9p is the same as that for p^5d, when the d^9 and the $p\,j$ values are correlated with the d and the $p^5\,j$ values respectively. Hence we do not need to give the d^9p matrix. Note however, that to conform to the *jj*-coupling phase conventions of TAS, a phase factor $(-1)^{j_1+j_2-J}$ must be applied in switching from pd to dp or from p^5d to d^9p.

Structure of the Configurations of High Azimuthal Quantum Number in Cu II and the Rare Gases

GEORGE H. SHORTLEY AND BERNARD FRIED
Mendenhall Laboratory of Physics, Ohio State University, Columbus, Ohio

(Received September 2, 1938)

The energy levels of configurations such as d^9f, d^9g of Cu II and p^5d, p^5f of the rare gases are split into two widely separated groups by the spin-orbit interaction of the almost closed shell. These groups have the two levels of the parent doublet as limits. The splitting within these groups is due to the small electrostatic interaction between the core and the outer electron and the spin-orbit interaction of the outer electron. It is found that if one neglects all of these except the leading term in the electrostatic interaction, the theory predicts that all levels should be double, two levels of different J value having the same energy. It further predicts definitely, without unknown constants, all details of the relative arrangement of these energy levels in the two groups. In the rare-gas configurations and Cu II d^9f, the levels tend to occur in these pairs and follow this arrangement approximately but the interactions which are neglected in this picture are not entirely negligible. Knowledge of the simple limiting structure should nevertheless be of value in such cases. Cu II $3d^95g$ however fits the simple picture in all details; the levels are observed to occur in pairs with precisely the energies predicted. Thus the 20 levels of this complex configuration are represented by simpler formulas and with better agreement (0.20 cm^{-1} average discrepancy) than in any other case which has been treated theoretically.

WE were led to undertake these theoretical considerations because of the peculiar structure of Cu II $3d^95g$ in which Shenstone[1] found that the 20 levels occur in 10 pairs which he was unable to resolve. We are able to explain this pairing in detail by assuming that all interactions involving the $5g$ electron are negligible except the largest term in the electrostatic interaction with the $3d^9$ core. In this approximation the theoretical formulas assume a very simple form. The intervals between double levels having the same parent j value are all predicted in terms of one parameter so that the values of 8-interval ratios are all definitely determined. The structure of this configuration is then more definitely predicted by theory than that of any other complex configuration, and the agreement with Shenstone's data is excellent. We find that a similar approximation will help to explain the observed structure of configurations like d^9f of Cu II and p^5d and p^5f of the rare gases. The simple formulas which are obtained should be of aid in the analysis of other such configurations.

I. d^9g

The observed levels of this configuration occur in two widely separated groups, the upper of which has $d^9\,{}^2D_{3/2}$ as parent, the lower, $d^9\,{}^2D_{5/2}$. If interaction between these groups is neglected, the jj-coupling electrostatic-energy matrices of the previous paper will split up as shown by the broken lines. When we add the diagonal spin-orbit interaction, we obtain the following formulas for the energy levels.[2]

Upper group

$$6c = -F_0+\tfrac{3}{2}\zeta_d-\tfrac{1961}{5}F_2+\quad 396G_6+2\zeta_g$$

$$\left.\begin{matrix}5c'\\5d'\end{matrix}\right\} = -F_0+\tfrac{3}{2}\zeta_d+\tfrac{1473}{10}F_2\quad -\tfrac{1}{4}\zeta_g\pm\tfrac{1}{2}[(\tfrac{15193}{15}F_2+\tfrac{9}{2}\zeta_g)^2+8(\tfrac{1961}{15}F_2)^2]^{\frac{1}{2}}$$

$$\left.\begin{matrix}4c'\\4d'\end{matrix}\right\} = -F_0+\tfrac{3}{2}\zeta_d+\tfrac{4971}{10}F_2+\quad 616G_4-\tfrac{1}{4}\zeta_g\pm\tfrac{1}{2}[(\tfrac{5113}{15}F_2+\tfrac{2464}{9}G_4-\tfrac{9}{2}\zeta_g)^2+308(\tfrac{143}{15}F_2-\tfrac{616}{9}G_4)^2]^{\frac{1}{2}}$$

$$\left.\begin{matrix}3c'\\3d'\end{matrix}\right\} = -F_0+\tfrac{3}{2}\zeta_d-\tfrac{2313}{10}F_2\quad -\tfrac{1}{4}\zeta_g\pm\tfrac{1}{2}[(\tfrac{14633}{15}F_2-\tfrac{9}{2}\zeta_g)^2+20(\tfrac{1543}{15}F_2)^2]^{\frac{1}{2}}$$

$$2d = -F_0+\tfrac{3}{2}\zeta_d-\quad 77F_2+\quad 504\tfrac{4}{5}G_2-\tfrac{5}{2}\zeta_g$$

[1] Shenstone, Trans. Roy. Soc. **A235**, 195 (1936). All the Cu II data are taken from this comprehensive analysis.
[2] This treatment is similar to that previously given for the rare gases: Shortley, Phys. Rev. **44**, 666 (1933); Condon and Shortley, *Theory of Atomic Spectra*, pp. 306–315.

Lower group

$$
\begin{aligned}
7a &= -F_0 - \zeta_d - 56F_2 - 14F_4 + 2\zeta_g \\
\left.\begin{matrix}6a'\\6b'\end{matrix}\right\} &= -F_0 - \zeta_d - \tfrac{7}{5}F_2 + \tfrac{63}{2}F_4 + 297G_6 - \tfrac{1}{4}\zeta_g \pm \tfrac{1}{2}[(\tfrac{1498}{15}F_2 + \tfrac{749}{9}F_4 - 286G_6 + \tfrac{9}{2}\zeta_g)^2 \\
&\qquad + 140(\tfrac{59}{15}F_2 + \tfrac{28}{9}F_4 - 44G_6)^2]^{\frac{1}{2}} \\
\left.\begin{matrix}5a'\\5b'\end{matrix}\right\} &= -F_0 - \zeta_d + \tfrac{299}{5}F_2 - \tfrac{66}{2}F_4 - \tfrac{1}{4}\zeta_g \pm \tfrac{1}{2}[(\tfrac{166}{15}F_2 - \tfrac{166}{9}F_4 + \tfrac{9}{2}\zeta_g)^2 + 728(\tfrac{4}{15}F_2 - \tfrac{40}{9}F_4)^2]^{\frac{1}{2}} \\
\left.\begin{matrix}4a'\\4b'\end{matrix}\right\} &= -F_0 - \zeta_d + \tfrac{224}{5}F_2 - \tfrac{91}{2}F_4 + 924G_4 - \tfrac{1}{4}\zeta_g \pm \tfrac{1}{2}[(\tfrac{504}{15}F_2 - \tfrac{1365}{9}F_4 - 616G_4 - \tfrac{9}{2}\zeta_g)^2 \\
&\qquad + 8(\tfrac{144}{15}F_2 - \tfrac{390}{9}F_4 + 616G_4)^2]^{\frac{1}{2}} \\
\left.\begin{matrix}3a'\\3b'\end{matrix}\right\} &= -F_0 - \zeta_d - \tfrac{52}{5}F_2 + \tfrac{195}{2}F_4 - \tfrac{1}{4}\zeta_g \pm \tfrac{1}{2}[(-\tfrac{752}{15}F_2 + \tfrac{611}{9}F_4 + \tfrac{9}{2}\zeta_g)^2 + 440(\tfrac{32}{15}F_2 - \tfrac{28}{9}F_4)^2]^{\frac{1}{2}} \\
\left.\begin{matrix}2a'\\2b'\end{matrix}\right\} &= -F_0 - \zeta_d - 77F_2 + \tfrac{378}{5}G_2 - \tfrac{1}{4}\zeta_g \pm \tfrac{1}{2}[(\tfrac{770}{15}F_2 + \tfrac{2002}{9}F_4 - \tfrac{644}{5}G_2 - \tfrac{9}{2}\zeta_g)^2 \\
&\qquad + 8(\tfrac{220}{15}F_2 + \tfrac{572}{9}F_4 + 28G_2)^2]^{\frac{1}{2}} \\
1b &= -F_0 - \zeta_d - 110F_2 - 143F_4 - \tfrac{5}{2}\zeta_g.
\end{aligned}
$$

Here F_0 is a constant which fixes the position of the configuration as a whole. ζ_d represents the spin-orbit integral for the d electrons: the configuration is split into two groups of levels with $^2D_{3/2}$ and $^2D_{5/2}$ as limits according to whether this integral occurs with coefficient $+\frac{3}{2}$ or -1; $\frac{5}{2}\zeta_d$ is the doublet splitting of the d^9 ion. Structure is given to the two groups by the smaller electrostatic integrals F_2, F_4, G_2, G_4, G_6, and the g-electron spin-orbit integral ζ_g. In the level designations, the number gives the J value, the letters a' and b' denote the higher and lower of two lower-group levels of the same J value, the letters c' and d' the higher and lower of two upper-group levels of the same J value.

In the case of Cu II $3d^95g$, the only d^9g which has been analyzed, if we follow the procedure previously used in the rare gases[2] and determine the eight integrals from the twelve linear equations expressing the energy of $7a$, the means of $6a'$ and $6b'$, of $5a'$ and $5b'$, etc., and then calculate the splitting of the levels of the same J by evaluating the radicals with these parameters, we get remarkably good agreement with observation. The parameter values obtained in this way are: $\zeta_d=828.59$, $F_2=0.3154$, $F_4=0.0027$, $G_2=0.0015$, $G_4=0.00004$, $G_6=0.0001$, $\zeta_g=0.028$ cm^{-1}. The contributions of F_4, G_2, G_4, G_6, ζ_g here are of the order of magnitude of the disagreement with experiment and of the expected error due to neglect of interaction between parents. The change in calculated values caused by setting these five integrals equal to zero is not significant. Furthermore, the levels are observed to occur in unresolved pairs, and neglect of these small parameters is just what gives this doubling.

If in the above formulas we retain only the parameters F_0, to represent the absolute position of the configuration in the energy scheme, ζ_d, to give the parent-doublet splitting, and the one integral F_2 to give structure to the groups, we find the levels to occur in pairs with energies given by the following simple formulas:

	Cu II $3d^95g$		
Upper group	Obs.	Calc.	Error
$6c,\ 5d' = -F_0 + \frac{3}{2}\zeta_d - \frac{196}{5}F_2$	2094.43	2094.34	−0.09
$5c',\ 4c' = -F_0 + \frac{3}{2}\zeta_d + \frac{343}{5}F_2$	2127.96	2128.31	0.35
$4d',\ 3c' = -F_0 + \frac{3}{2}\zeta_d + \frac{154}{5}F_2$	2116.43	2116.40	−0.03
$3d',\ 2d = -F_0 + \frac{3}{2}\zeta_d - 77F_2$	2082.65	2082.42	−0.23
Lower group			
$7a,\ 6b' = -F_0 - \zeta_d - 56F_2$	17.67	17.57	−0.10
$6a',\ 5a' = -F_0 - \zeta_d + \frac{266}{5}F_2$	52.08	51.98	−0.10
$5b',\ 4a' = -F_0 - \zeta_d + \frac{332}{5}F_2$	55.99	56.14	0.15
$4b',\ 3a' = -F_0 - \zeta_d + \frac{119}{5}F_2$	42.77	42.53	−0.24
$3b',\ 2a' = -F_0 - \zeta_d - 44F_2$	21.61	21.35	−0.26
$2b',\ 1b = -F_0 - \zeta_d - 110F_2$	0.	0.55	0.55

($F_0=-863.806$; $F_2=0.31515$, $\zeta_d=828.590$ cm^{-1})

When the observed Cu II levels are fitted to these formulas by least squares, the above parameters and computed levels are obtained. The levels are plotted in Fig. 1. These extremely simple formulas are seen to represent remarkably well the positions of the twenty levels of this configuration. The configuration is one of the most complex which has been completely analyzed, yet the formulas which represent its structure are simpler and the agreement better than in any other case which has been treated theoretically.

The two levels of a pair are, of course, not rigorously coincident, but Shenstone estimates his resolution as such that the separation of the two apparently coincident levels of different J

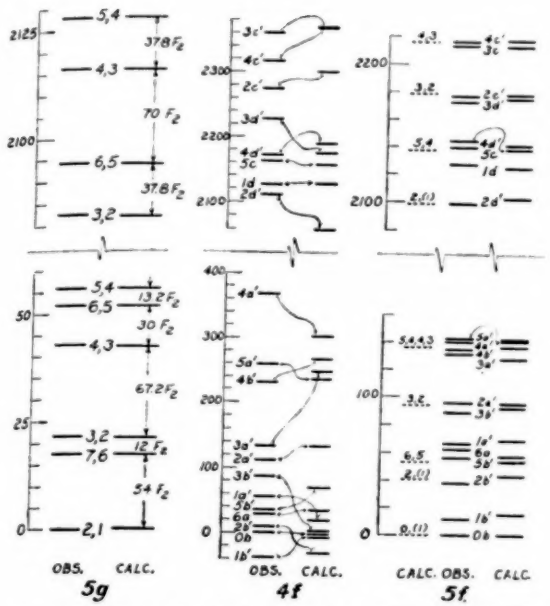

FIG. 1. Configurations $3d^9 5g$, $3d^9 4f$, and $3d^9 5f$ of Cu II. The broken lines in the $5f$ configuration show the arrangement of the levels when all parameters except F_2 are neglected; in this case the levels coincide in pairs and the relative positions are completely predicted, as in the $5g$ case above.

value must be considerably less than $\frac{1}{2}$ cm^{-1} in all cases.

To the approximation in which the above simple formulas hold, the eigenfunctions of the states are independent of the parameter values. The eigenfunctions of the actual (primed) levels are given in terms of the jj-coupling eigenfunctions by the transformation matrices of Table I. These matrices enable us to determine by means of second-order perturbation theory the amount of the electrostatic interaction between the levels of the upper and lower group, which has been neglected so far. The results here are remarkable in that this second-order interaction does not tend to split the pairs, so long as F_2 is the only significant term. $7a$, $6b'$ and $2b'$, $1b$ are not shifted at all. $6c$ interacts only with $6a'$, $5d'$ only with $5a'$, and the amount of interaction is exactly the same in these two cases. Similarly the pair $5c'$, $4c'$ interacts as a unit with $5b'$, $4a'$; the pair $4d'$, $3c'$ with $4b'$, $3a'$; and the pair $3d'$, $2d$ with $3b'$, $2a'$. In our particular case the maximum shift caused by this second-order interaction is 0.10 cm^{-1}, which is not significant.

TABLE I. *Eigenfunctions of d^9g levels.*

	$6a'$	$6b'$		$5a'$	$5b'$		$5c'$	$5d'$		$4a'$	$4b'$	
$6a$	$4\sqrt{7}$	$-\sqrt{5}$	$\frac{1}{\sqrt{117}}$	4	$\sqrt{182}$	$\frac{1}{3\sqrt{22}}$	$4\sqrt{2}$	-1	$\frac{1}{\sqrt{33}}$	1	$2\sqrt{2}$	$\frac{1}{3}$
$6b$	$\sqrt{3}$	$4\sqrt{7}$		$-\sqrt{182}$	4		1	$4\sqrt{2}$		$-2\sqrt{2}$	1	
	$4c'$	$4d'$		$3a'$	$3b'$		$3c'$	$3d'$		$2a'$	$2b'$	
$4c$	2	$\sqrt{77}$	$\frac{1}{9}$	4	$\sqrt{110}$	$\frac{1}{\sqrt{126}}$	1	$2\sqrt{3}$	$\frac{1}{\sqrt{21}}$	1	$2\sqrt{2}$	$\frac{1}{3}$
$4d$	$-\sqrt{77}$	2		$-\sqrt{110}$	4		$-2\sqrt{3}$	1		$-2\sqrt{2}$	1	

II. d^9f

The formulas for the energy levels of d^9f, interaction between parents being neglected, are

Upper levels

$$5c = -F_0 + \tfrac{3}{2}\zeta_d - 7F_2 + 168G_6 + \tfrac{3}{2}\zeta_f$$

$$\left.\begin{matrix}4c'\\4d'\end{matrix}\right\} = -F_0 + \tfrac{3}{2}\zeta_d + \tfrac{7}{2}F_2 - \tfrac{1}{4}\zeta_f \pm [(19\tfrac{9}{2}F_2 + 7\tfrac{7}{4}\zeta_f)^2 + 20F_2^2]^{\frac{1}{2}}$$

$$\left.\begin{matrix}3c'\\3d'\end{matrix}\right\} = -F_0 + \tfrac{3}{2}\zeta_d + 9\tfrac{1}{10}F_2 + 24G_2 - \tfrac{1}{4}\zeta_f \pm [(41\tfrac{1}{10}F_2 + 48\tfrac{2}{7}G_2 - 7\tfrac{7}{4}\zeta_f)^2 + 180(1\tfrac{1}{5}F_2 - 1\tfrac{2}{7}G_2)^2]^{\frac{1}{2}}$$

$$\left.\begin{matrix}2c'\\2d'\end{matrix}\right\} = -F_0 + \tfrac{3}{2}\zeta_d - 63\tfrac{1}{10}F_2 - \tfrac{1}{4}\zeta_f \pm [(87\tfrac{1}{10}F_2 - 7\tfrac{7}{4}\zeta_f)^2 + 86\tfrac{4}{25}F_2^2]^{\frac{1}{2}}$$

$$1d = -F_0 + \tfrac{3}{2}\zeta_d - 84\tfrac{1}{5}F_2 + 28G_1 - 2\zeta_f$$

Lower levels

$$6a = -F_0 - \zeta_d - 10F_2 - 3F_4 + \tfrac{3}{2}\zeta_f$$

$$\left.\begin{matrix}5a'\\5b'\end{matrix}\right\} = -F_0 - \zeta_d + F_2 + 8F_4 + 126G_5 - \tfrac{1}{4}\zeta_f \pm [(67\tfrac{7}{7}F_2 + 67\tfrac{7}{7}F_4 - 54G_5 + 7\tfrac{7}{4}\zeta_f)^2 + 1440(1\tfrac{1}{7}F_2 + \tfrac{1}{7}F_4 - 3G_5)^2]^{\frac{1}{2}}$$

$$\left.\begin{matrix}4a'\\4b'\end{matrix}\right\} = -F_0 - \zeta_d + 12F_2 - 25\tfrac{1}{2}F_4 - \tfrac{1}{4}\zeta_f \pm [(47\tfrac{1}{2}F_4 - 7\tfrac{7}{4}\zeta_f)^2 + 440F_4^2]^{\frac{1}{2}}$$

$$\left.\begin{matrix}3a'\\3b'\end{matrix}\right\} = -F_0 - \zeta_d + 32\tfrac{2}{5}F_2 - 11\tfrac{1}{2}F_4 + 36G_3 - \tfrac{1}{4}\zeta_f \pm [(124\tfrac{4}{35}F_2 - 34\tfrac{1}{14}F_4 - 108\tfrac{5}{7}G_3 - 7\tfrac{7}{4}\zeta_f)^2 + 360\tfrac{9}{49}(8\tfrac{6}{5}F_2 - 11F_4 + 12G_3)^2]^{\frac{1}{2}}$$

$$\left.\begin{matrix}2a'\\2b'\end{matrix}\right\} = -F_0 - \zeta_d - 31\tfrac{1}{5}F_2 + 33F_4 - \tfrac{1}{4}\zeta_f \pm [(119\tfrac{5}{5}F_2 - 7\tfrac{7}{4}\zeta_f)^2 + 86\tfrac{4}{25}F_2^2]^{\frac{1}{2}}$$

$$\left.\begin{matrix}1a'\\1b'\end{matrix}\right\} = -F_0 - \zeta_d - 93\tfrac{4}{5}F_2 - 33\tfrac{1}{2}F_4 + 21G_1 - \tfrac{1}{4}\zeta_f \pm [(99\tfrac{9}{35}F_2 + 363\tfrac{3}{14}F_4 - 19G_1 - 7\tfrac{7}{4}\zeta_f)^2 + 80(18\tfrac{8}{33}F_2 + 33\tfrac{3}{7}F_4 + G_1)^2]^{\frac{1}{2}}$$

$$0b = -F_0 - \zeta_d - 24F_2 - 66F_4 - 2\zeta_f.$$

TABLE II. $3d^9nf$ *parameter values.*

	$4f$	$5f$
F_0	-984.7 cm^{-1}	-921.9 cm^{-1}
F_2	10.1	3.81
F_4	-1.09	-0.013
G_1	1.27	0.949
G_3	-2.65	-0.214
G_5	0.011	0.0046
ζ_d	837.4	828.4
ζ_f	-10.4	1.508

If the eight parameters are determined from the twelve linear equations which give the means of levels of the same J value and same parent, and then used to calculate the values of the radicals, one obtains for Cu II $3d^94f$ and $3d^95f$ the parameter values of Table II and the calculated energies which are plotted in Fig. 1. It will be noted that the predicted $5f$ levels are quite good but that the $4f$ levels are badly off. The poor agreement in the case of $4f$ is due to a large interaction of $3d^94f$ and the completely overlapping configuration $3d^84s4p$ which is neglected in the present theory, but which manifests itself experimentally[1] by strong forbidden combinations of the type d^8sp-d^9g, $d^9f-d^8s^2$, d^9f-d^9s. The value of ζ_d for $3d^95f$ agrees with the value 828.6 previously found in d^9g and with the value 828 obtained from the Cu III doublet splitting. The maximum interaction which occurs between the upper and the lower group of $5f$ is found to be of the order of 0.54 cm^{-1}, which is not significant.

In this configuration also, if one neglects all integrals except F_0, ζ_d, and F_2, one obtains simple formulas which give the levels in pairs:

Upper levels

$$\begin{aligned} 5c,\ 4d' &= -F_0+\tfrac{3}{2}\tfrac{6}{7}\zeta_d- \tfrac{7}{7}F_2 \\ 4c',\ 3c' &= -F_0+\tfrac{3}{2}\tfrac{6}{7}\zeta_d+\tfrac{14}{7}F_2 \\ 3d',\ 2c' &= -F_0+\tfrac{3}{2}\tfrac{6}{7}\zeta_d+\tfrac{21}{5}F_2 \\ 2d',\ 1d &= -F_0+\tfrac{3}{2}\tfrac{6}{7}\zeta_d-\tfrac{84}{5}F_2 \end{aligned}$$

Lower levels

$$\begin{aligned} 6a,\ 5b' &= -F_0- \tfrac{1}{7}\zeta_d- \tfrac{10}{7}F_2 \\ 5a,\ 4a',\ 4b',\ 3a' &= -F_0- \tfrac{1}{7}\zeta_d+\tfrac{12}{7}F_2 \\ 3b',\ 2a' &= -F_0- \tfrac{1}{7}\zeta_d+\tfrac{4}{5}F_2 \\ 2b',\ 1a' &= -F_0- \tfrac{1}{7}\zeta_d-\tfrac{66}{35}F_2 \\ 1b',\ 0b &= -F_0- \tfrac{1}{7}\zeta_d- \tfrac{24}{7}F_2. \end{aligned}$$

This tendency toward occurring in pairs is noted in the observed $5f$ of Fig. 1. The largest splitting of the pairs occurs in the case of levels with $J=1$, which is to be expected since G_1, the largest of the neglected parameters, is not particularly small compared to F_2; but G_1 occurs only in the formulas for $J=1$. However these simple formulas give a useful qualitative picture of the location of the levels, as may be seen from the broken lines of Fig. 1, which show the arrangement of energy levels which they give with $F_2=3.79$ cm^{-1}. Levels of $J=1$ were not considered in determining this F_2 value.

III. p^5d

In the configurations p^5p, p^5d, p^5f of the rare gases one obtains a similar doubling of all energy levels if one neglects all the small interaction terms except F_2. The occurrence of this doubling is especially striking in the Ne $2p^5nd$ configurations of high n value. The reduced p^5d formulas[3] are

Upper levels

$$3c,\ 2c,\ 2d,\ 1d = -F_0+\ \tfrac{1}{5}\zeta_p$$

Lower levels

$$\begin{aligned} 4a,\ 3b' &= -F_0-\tfrac{1}{2}\tfrac{1}{5}\zeta_p-2F_2 \\ 3a',\ 2a' &= -F_0-\tfrac{1}{2}\tfrac{1}{5}\zeta_p+5F_2 \\ 2b',\ 1a' &= -F_0-\tfrac{1}{2}\tfrac{1}{5}\zeta_p \\ 1b',\ 0b &= -F_0-\tfrac{1}{2}\tfrac{1}{5}\zeta_p-7F_2. \end{aligned}$$

In the neon case the largest G coefficient, G_1, is of size comparable to F_2; this coefficient occurs only in states of $J=1$, hence the observed levels[4] are arranged very closely as in the above formulas except for those of $J=1$. The near coincidence of $3c$, $2c$, $2d$; of $4a$, $3b'$; and of $3a'$, $2a'$ is conspicuous from $4d$ to $10d$, and the arrangement of all levels of $J\neq1$ follows closely the above formulas. By determining F_2 from these levels by the above formulas and then including G_1, we may place the three $J=1$ levels satisfactorily. This method should prove of use in locating the missing levels of the argon p^5d configurations, only one of which is complete.

IV. p^5f

The formulas which are obtained for p^5f when ζ_f, G_2, G_4 are neglected are:

Upper levels

$$4c,\ 3c,\ 3d,\ 2d = -F_0+\ \tfrac{1}{5}\zeta_p$$

Lower levels

$$\begin{aligned} 5a,\ 4b' &= -F_0-\tfrac{1}{2}\tfrac{1}{5}\zeta_p- 5F_2 \\ 4a',\ 3a' &= -F_0-\tfrac{1}{2}\tfrac{1}{5}\zeta_p+10F_2 \\ 3b',\ 2a' &= -F_0-\tfrac{1}{2}\tfrac{1}{5}\zeta_p+ 3F_2 \\ 2b',\ 1b &= -F_0-\tfrac{1}{2}\tfrac{1}{5}\zeta_p-12F_2. \end{aligned}$$

The only observations of p^5f are on argon, where there are sketchy data for a number of

[3] The complete formulas are in reference 2.
[4] See the plots given in reference 2.

these configurations. At most five of the twelve levels are observed, and not even the J values of these are certain.[5] It may be that the above formulas can be of use in interpreting these observations. Perhaps the five observed levels, four lower and one upper, are at the positions of the five collapsed levels given by these formulas. On the other hand, the $J=2$ levels may be displaced from these positions because of a non-negligible G_2 value. One would not expect G_4 and ζ_f to be large enough to give significant departures for the levels of other J values. If we attempt to fit the four lower observed levels by means of the above formulas we obtain the results of Fig. 2. The level W which is observed to have the J value 4 or 3 may well be a double 4 and 3 level. The level Y is observed to be 1 or 2. No $J=1$ is expected in this vicinity so this is probably $J=2$, with a $J=3$ nearby. The level U is observed as 4 or 3. It is probably 4 with a $J=5$ nearby. The level X is definitely observed as $J=1$. A level of $J=2$ should be near. The single observed *upper* level is listed as $J=1$ or 2. It cannot be $J=1$ since there is no level in the upper group with $J=1$. This upper level is observed only for $4f$, $5f$, and $6f$. Fig. 2 indicates fairly large perturbations of these two configurations which are expected since the lower group of $5f$ is overlapped by $6p$ and the upper group of $5f$ is close to the lower of $6f$. Nevertheless, the ζ_p values obtained from the position of the upper $J=2$ level according to the above formulas—955.0 cm^{-1} for both $5f$ and $6f$—agree well with the value 954 from the A II ^2P splitting. For $2p^5 4f$ only X, Y, and the upper $J=2$ are observed. The ζ_p value calculated from the above formulas for these is 955.24 cm^{-1}, which checks in this case also the interpretation which we have given.

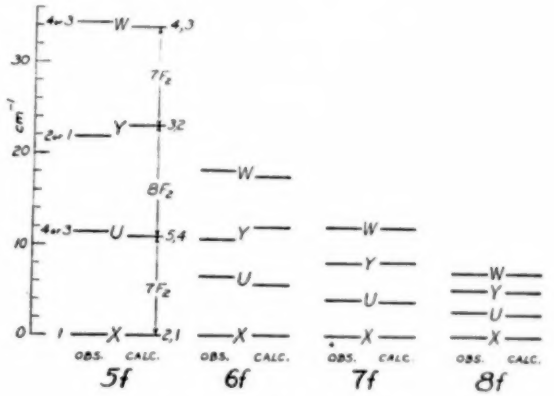

FIG. 2. Argon I $3p^5(^2P_{3/2})nf$.

[5] See Bacher and Goudsmit, *Atomic Energy States*, p. 28.

NOVEMBER 1, 1938 PHYSICAL REVIEW VOLUME 54

The Contact Difference of Potential Between Barium and Magnesium

PAUL A. ANDERSON
State College of Washington, Pullman, Washington

(Received August 15, 1938)

With the purpose of subjecting the electronic method of contact potential measurement to a thorough test for consistency with independent photoelectric work function determinations, the Volta potential Ba-Mg has been measured for some 30 pairs of surfaces and the results compared with recent careful photoelectric studies of these metals. Each surface was prepared by fractionally distilling the metal in a gettered vacuum and revaporizing a middle fraction to form a thick film on glass at room temperature. Each film was measured a few seconds after deposition and tubes of two different designs used to minimize the possibility of errors originating in tube geometry. The majority of the observed Volta potentials fell within the range of values predicted by the photoelectric data, 1.08–1.16 v, and no values below this range were found. The magnesium films were largely responsible for variations in the Volta potential and a few gave potential settings sufficiently low (work functions sufficiently high) to raise the observed Volta potentials to a maximum of 1.26 v. Since all probable contaminations should lower the work function the maximum value is regarded as the most reliable. Assuming a work function of 2.52 ev for Ba this gives 3.78 ev for the work function of Mg. Observations on the optical reflection of the magnesium surfaces suggest, however, that a work function of 3.65 ± 0.05 ev may be characteristic of mirror-like surfaces of the metal; 3.78 ev of macrocrystalline (matte) surfaces.

IN recent photoelectric determinations of the work functions of barium by Jamison and Cashman[1] and of magnesium by Cashman and

[1] Jamison and Cashman, Phys. Rev. **50**, 624 (1936).

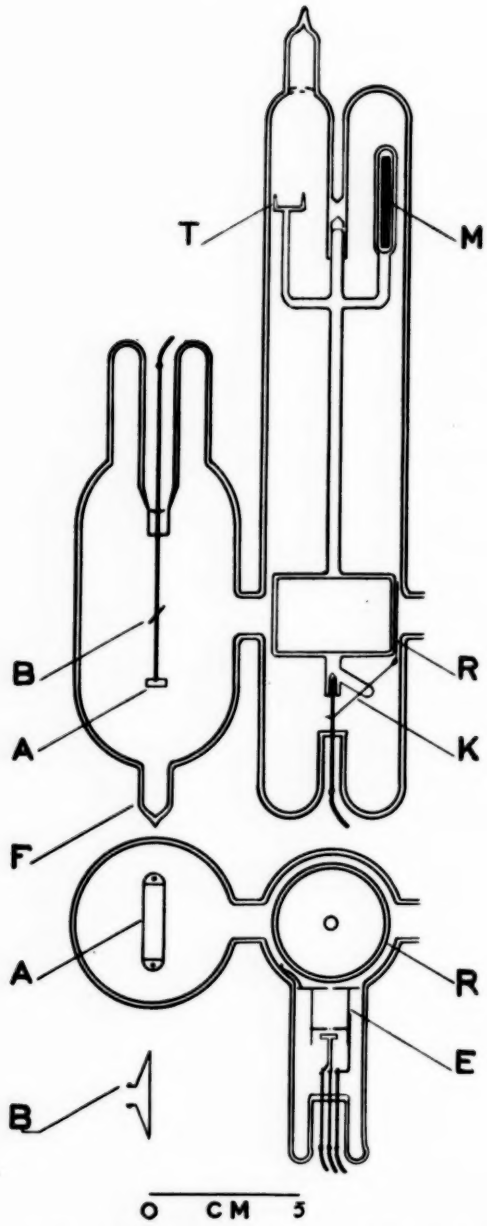

FIG. 1. Type 1 tube. First A and second B vaporizers of 0.025 mm Mo foil 8 mm wide attached to 3-lead stem with Mo rivets; one of 60 mil leads common. Films formed on Pyrex drum R were moved into reproducible positions before electron gun E by armature M and glass sights T, set on an external paper scale. Contact with films established by Pt wire embedded in R and welded to 20 mil tungsten wire brush K. Gun of 4 mil Ta foil; emitter 1 mil tungsten foil 1.5 mm wide. The second vaporizing chamber, not shown, was identical in design with the first.

Huxford,[2] and Mann and DuBridge[3] the method of preparing the metal surfaces has been similar to the fractional distillation method employed by the author in Volta potential measurements on tungsten-barium[4] and barium-silver[5] but supplemented by multiple vaporization of the middle fractions. These photoelectric studies must be regarded as among the most reliable yet made for any of the metals and the standardization of a satisfactory technique for preparing surfaces offers the possibility of testing under unusually favorable conditions the consistency of work function determinations by the photoelectric and Volta potential methods. In several instances checks of this relation, $V_{ab}=\phi_b-\phi_a$ (Sommerfeld-Eckart equation), have been reported but generally either the photoelectric or contact potential measurements, or both, have been obtained under questionable experimental conditions.

It was the purpose of the present work to make a careful study of the contact difference of potential between surfaces of barium and magnesium each prepared by fractional distillation and revaporization of the middle fraction and to compare these measurements with the photoelectric data. Since there is now abundant evidence to show that work functions are structure dependent, the barium and magnesium films were formed on glass at room temperature as in the photoelectric investigations rather than at liquid-air temperature as in our previous Volta potential studies. To minimize the possibility of undetected errors originating in tube geometry the measurements were made with tubes of two different designs.

METHOD. THE TUBES

The method of measurement, based on the determination of the shift of an electron current-retarding potential characteristic with change of work function, was that employed in previous studies.[4, 5] The scheme of preparing the metal surfaces and bringing them into the measuring position involved, in both types of tubes and for each of the metals: (1) vaporization and rejection, for other than gettering purposes, of the first half of the original sample, (2) collection on a second vaporizer of the middle fraction of metal distilled from the first vaporizing oven, (3) revaporization of this selected fraction to

[2] Cashman and Huxford, Phys. Rev. **48**, 734 (1935).
[3] Mann and DuBridge, Phys. Rev. **51**, 120 (1937).
[4] P. A. Anderson, Phys. Rev. **47**, 958 (1935).
[5] P. A. Anderson, Phys. Rev. **49**, 320 (1936).

form a thick film of the metal on a clean glass surface, and (4) provision for displacement of the freshly deposited film to a reproducible position in which it was centered before an electron gun. The tubes used in the first measurements were designed originally for work under liquid air and the movable glass receiver was a drum carried on a vertical glass spindle, Fig. 1. In the second type of tube, Fig. 2, alternate layers of barium and magnesium were deposited on a glass disk moved by magnetic control along a double glass rod track, which extended across both vaporizing chambers and the electron gun. The essential constructional details are indicated in the legends of the figures.

Materials

The magnesium was a sample of extremely high purity kindly furnished to me by Dr. Cashman and taken from the stock used by him in his photoelectric measurements. The barium, from the stock used in our previous contact potential work, was obtained from Osram and contained traces of iron as the only important impurity. As compared to samples which have been secured from other sources this barium is relatively ductile and free from absorbed gas.

Procedure

The outgassing procedure was similar to that described in previous reports except that a new high frequency bombarder has made it possible to push the heating of the metal parts to temperatures limited only by the vaporization of the tantalum. In order to eliminate the cost of liquid air, one of the tubes was pumped on an oil diffusion system and protected by two long-column charcoal traps in series. These traps were of a new design[6] which permits heating the charcoal to incandescence in an all-Pyrex system. The behavior of this tube was indistinguishable from that of the others which were pumped with mercury vapor and protected by double liquid-air traps.

After outgassing of the glass and metal parts and before seal-off the barium was melted down several times on the first vaporizing oven and a considerable fraction of it vaporized. The magnesium was treated similarly but usually could be only partially fused before a third or more of it vaporized. After seal-off the melting of the barium and vaporization of further fractions of barium and magnesium were repeated several times and the second vaporizers flashed to remove all of the first condensates. During these preliminary treatments the glass drum of the type 1 tubes was always turned into the "dumping position;" the deposits formed by direct distillation from the first vaporizers and by discarded fractions from the second vaporizers were confined to one spot on the drum while the remainder of its surface remained uncoated until the measured films were laid down. In the case of the type 2 tubes the glass disk was moved into the appropriate vaporizing chamber only when the final distillations from a second vaporizer were to be made. The first vaporization of the middle fraction of each metal was carried out at an oven temperature just sufficient to form in one to two hours on the second vaporizer a deposit adequate for the preparation of several successive fresh surfaces on the glass receiver. The initial measurement on a film was made within a few seconds of completing the final deposition and the potential settings for fixed reference current followed closely during the early history of the film. The possibility of thus detecting and following work function changes which may occur immediately after the formation of a film is one of the most useful characteristics of the method. With a negative potential on the film, i.e., under the conditions of measurement, sunlight incident

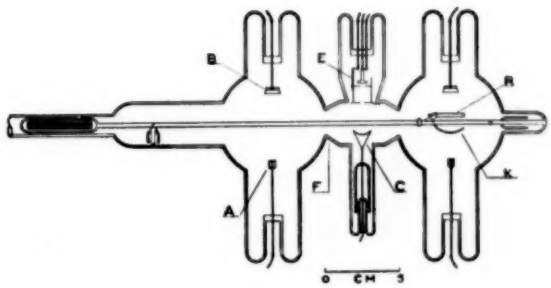

FIG. 2. Type 2 tube. First and second vaporizers, *A* and *B*, and electron gun *E* as in type 1 tube. Contact to films by Pt wire embedded in edge of 2 cm Pyrex disk *R*, 20 mil tungsten wire brush *K* and 10 mil tungsten wire spring *C* (rotated 90° in sketch). Tube flattened at *F* to prevent vapor exchange. *R* moved under gun during first vaporizations to protect it from contamination. Setting of slide determined by paper scale on armature tube.

[6] P. A. Anderson, Rev. Sci. Inst. **8**, 493 (1937).

on the tube was found to generate a large photoelectric emission from film to gun and all the measurements were carried out in a shuttered room. No detectable emission was produced by ordinary artificial light or by the light from the emitter filament. The potential applied to accelerate the electrons in the gun was 10.01 v throughout the measurements and galvanometer deflections for zero potential on the film were of the order of 950 mm. The reference deflection was 500 mm and the retarding potentials required to establish this deflection were, in a typical measurement, 10.82 v for magnesium and 12.00 v for barium. The sensitivity of measurement in terms of change in deflection per volt change in applied potential, or work function, was of the order of 1500 mm/volt. The energy of the significant fraction of the electrons collected by the film at the reference setting was a small fraction of one volt and secondary emission must have been negligible.

The Volta Potential Ba-Mg

Of the several hundred measurements made on more than 30 pairs of films the majority gave Volta potentials within the range predicted by Jamison and Cashman's photoelectric value for the work function of barium,[1] 2.52 ev, and the Mann and DuBridge[3] value for magnesium, 3.68 ev. The first series of measurements made with a type 1 tube gave reproducible Volta potentials of 1.08 v in exact agreement with the above mentioned value for barium and Cashman and Huxford's[2] value for magnesium, 3.60 ev, but in the later series most of the observations were grouped in the range 1.15–1.19 v. In several instances higher values were recorded and one pair of films gave a Volta potential of 1.26 v, the maximum value observed. Throughout the measurements the potential settings for fixed reference current were highly reproducible for the barium films and the Volta potential Ba-Ba taken on successively deposited barium surfaces was always found to be zero to ± 0.01 v whenever it was checked. Since no systematic trend in the measurements with change of tube design or between different series of observations with tubes of the same design could be detected, the variations in Volta potential apparently originated in variations between the individual magnesium surfaces. A possible clue to these variations is given by the observation that a fresh mirror-like surface of magnesium deposited on the virgin glass disk of a type 2 tube gave a Volta potential of 1.16 v against a barium film laid down upon it but as successive alternating films of the metals were deposited the magnesium surfaces took on the diffuse reflection characteristic of a finely polycrystalline metal while the Volta potential increased to 1.24 v. If residual gas was responsible for these variations it must be concluded that magnesium is sensitive to concentrations of gas which leave barium films in the same tube entirely unaffected. In tests for change of work function with aging none of the barium films studied showed a drift measurable within 72 hours. The magnesium films were somewhat less stable and in several instances exhibited drifts of 0.02–0.05 v toward lower work function within a few hours of deposition. These drifts were not, however, progressive and no changes greater than 0.05 v could be detected within 72 hours.

The Work Function of Barium

Since the value assigned to the work function of magnesium by this method depends directly upon the work function of barium, the selection of the most probable value for ϕ_{Ba} becomes of first importance. The unique advantages of barium as a reference metal lend a more general significance to such a selection. In the first of this series of contact potential studies[4] the Volta potential W-Ba was found to be 2.13 ± 0.05 v at liquid-air temperature and a value of 2.39 ± 0.05 ev was computed for ϕ_{Ba} at this temperature on the assumption that the work function of tungsten at 90°K is equal to 4.52 ev, the thermionically determined "heat function." This assumption, justified only because of our lack of information regarding the temperature coefficient of the work function of tungsten, is an approximation at best and subsequent investigations, in particular the photoelectric work of Jamison and Cashman on barium, make re-examination of our earlier value desirable. Reimann,[7] assuming zero reflection coefficient and a roughness factor of 1.3,

[7] Reimann, Phil. Mag. **20**, 594 (1935).

has computed ϕ_W to be 4.64 ev at 1500°K. More recently the same author[8] has obtained measurements yielding an average value of $d\phi_w/dT$ of 7×10^{-5} ev deg.$^{-1}$ in the range 300–1100°K while Nottingham[9] and D. B. Langmuir[10] estimate this temperature coefficient at -4×10^{-5}. Assuming $d\phi_w/dT$ to be independent of temperature, Reimann's data give 4.54 ev for ϕ_W at 90°K while the Nottingham-Langmuir data yield the value 4.70 ev at this temperature. If, now, our value for the contact difference of potential W-Ba is combined with these two divergent values for ϕ_W one obtains 2.41 and 2.57 ev, respectively, for ϕ_{Ba} at 90°K. Taking into account a temperature coefficient for barium[11] of 5×10^{-5} the calculated values of ϕ_{Ba} at room temperature become 2.42 and 2.58 ev. But if, pending settlement of its sign and magnitude, the temperature coefficient of tungsten is put equal to zero the above computation, with Reimann's work function for tungsten and our Volta potential for W-Ba, gives 2.52 ev for the work function of barium at room temperature. The extent of the discrepancy between our value for ϕ_{Ba} and that of Jamison and Cashman is evidently contingent upon uncertain data for tungsten and we have, therefore, adopted 2.52 ev as the most probable value of the barium work function at room temperature. A possible structural dependence of this work function has not been considered. Such variations are almost certainly small for barium films deposited on glass at room temperature but may be significant when such films are compared with surfaces formed at liquid-air temperature.

Mention should, finally, be made of the high value, 2.70 ev, found for ϕ_{Ba} in the photoelectric work of Suhrmann and Deponte[12] who measured a single thick film prepared by direct vaporization of a raw barium sample. It has been our experience that the first fusion of such a sample is invariably accompanied by a copious evolution of gas which, reabsorbed by the condensing surface, lowers rather than raises the work function.

[8] Reimann, Proc. Roy. Soc. **A163**, 499 (1937).
[9] Nottingham, Phys. Rev. **49**, 78 (1936).
[10] D. B. Langmuir, Phys. Rev. **49**, 428 (1936).
[11] Cashman, Phys. Rev. **52**, 512 (1937).
[12] Suhrmann and Deponte, Zeits. f. Physik **86**, 628 (1933).

The Work Function of Magnesium

In the preceding discussion of results for the Volta potential Ba-Mg emphasis has been placed upon the question of their consistency with the photoelectric data. The measurements obviously supply, also, an independent determination of the external work function of magnesium, with the barium, work function, 2.52 ev, taken as the reference metal.[5] The unweighted mean of the Volta potential values assigns 3.67 ev to ϕ_{Mg} in close agreement with the photoelectric value of Mann and DuBridge. Since, however, all of the contaminations likely to be present under the conditions of the experiment would be expected to lower the work function, it is probable that the value 3.78 ev corresponding to the maximum observed Volta potential deserves the greatest weight. Such a conclusion does not take into account a possible variation of work function with the crystal structure of the surfaces, and the observation that the maximum Volta potential was associated in at least one instance with a macroscopically crystalline rather than mirror-like surface. As compared to barium, magnesium has a relatively rigid lattice and would be expected to be less capable of spontaneously establishing its equilibrium structure. A thick film of magnesium deposited on a soft barium surface and with equilibrium crystal faces sufficiently developed to show diffuse optical reflection represents a structure very different from that of a mirror film on glass and a different work function is to be expected. This structural effect, if real, bears out the tentative conclusion[5] that the work function of a metal surface composed of equilibrium crystal faces is higher than that of a microcrystalline ("amorphous") film of the metal.

The Influence of Magnetic Fields on Persistent Currents in a Closed Superconducting Circuit†

K. C. MANN,* H. GRAYSON SMITH, AND J. O. WILHELM
McLennan Laboratory, University of Toronto, Toronto, Canada

(Received August 22, 1938)

A study has been made of the effects of external magnetic fields in preventing persistent currents from flowing in a closed superconducting circuit, in order to determine as closely as possible the field strength at which the first trace of electrical resistance appears. In agreement with earlier work by a less accurate method and with the resistance measurements of de Haas, but in contradiction to the idealized theory of the transition state, it is clearly shown that no resistance appears until the mean magnetic induction within the specimen becomes considerable. It has been found further that the amount of resistanceless current that a cylindrical specimen can carry under these conditions has a well-defined limit. The effects of very small quantities of impurities of different types have also been investigated and have been found greatly to affect the above results. When the persistent current strength was slightly above its equilibrium value, it required a measurable time to decay; the behavior was similar to the relaxation effects observed in the study of magnetic and thermal properties of superconductors.

INTRODUCTION

UP to the present time, there has been a considerable divergence in the results published on critical magnetic fields of superconducting tin. There are three main methods of measuring such fields; (1) resistance measurements of a superconducting cylindrical tin wire; (2) measurement of the field strength at which the magnetic induction in a tin specimen is complete; (3) measurements of the field strength at which persistent currents will no longer flow in a tin cylinder. Not all the work has been done with tin of the highest purity now obtainable, and it has long been suspected that small amounts of impurity such as are found in "chemically pure" materials may affect the critical field strengths.

A series of measurements taken by method (3) with the superconducting galvanometer, has already been published by two of us.[1] In that work, a single crystal of "chemically pure" tin was used, and it was felt advisable to extend the work with an improved method of measurement and even purer material. A discrepancy was found in the earlier work, which was traced to the use of an imperfect magnet, and the present paper includes corrections to the former results for the tin crystal and an extension of the method to spectroscopically pure tin.

It is important to note that method (3) gives the field strength at which the first signs of resistance appear. In longitudinal fields, this is not exactly equal to the critical field H_c as defined by other workers, since in all materials, the transition from zero to normal resistance takes place over a finite range of field strengths, and H_c is usually taken as the field strength at which the transition is complete. For very pure materials, this range is quite small, and the different methods are in fair agreement. In the present paper, the term "critical field" refers always to the field in which resistance first appears, and will be denoted by H_T in transverse fields and by H_L in longitudinal fields. The fields H_T are directly comparable with those of other workers since they mark the first appearance of resistance of the specimen when it passes into the "intermediate state" or mixed phase of normal and superconducting regions as postulated by Peierls[2] and London.[3] The *characteristic ratio*, discussed in the previous paper,[1] is H_T/H_L.

With regard to the influence of impurities on the transition, some experiments have been carried out by other workers on specimens where the amount of added impurity was considerable.[4–6] The present authors thought it advisable

† Paper presented at the Toronto meeting of the American Physical Society, June 25, 1938.

* Holder of the University of Toronto War Memorial Fellowship. At present at University of British Columbia, Vancouver, Canada.

[1] K. C. Mann and J. O. Wilhelm, Trans. Roy. Soc. Canada, III, 31, 19 (1937).

[2] R. Peierls, Proc. Roy. Soc. **A155**, 886 (1936).

[3] F. London, Physica **3**, 450 (1936).

[4] L. S. Schubnikow, W. I. Chotkewitsch, I. D. Schepelew and J. N. Rjabinin, Actes du VIIe. Congrès Int. du Froid, 457 (1936).

[5] K. Mendelssohn, Judith R. Moore and R. B. Pontius, Actes du VIIe. Congrès Int. du Froid, 431 (1936).

[6] D. Shoenberg, Proc. Roy. Soc. **A155**, 712 (1936).

that more quantitative work on this subject should be undertaken with smaller amounts of controlled impurity, and that the persistent current method might be particularly suitable for the purpose. With this end in view, we have carried out experiments, adding small but measureable amounts of impurity to spectroscopically pure tin. The effects of different types of impurities have been tried, both superconducting and nonsuperconducting. The superconducting group contained elements with transition temperatures above and also below the transition temperature of tin. In the following paper, the results of experiments are reported which give the effects of one of each of the three classes of impurities upon both transverse and longitudinal critical fields, and hence upon the characteristic ratio.

Method

In the previous work, persistent currents were induced in a superconducting circuit consisting of the superconducting galvanometer and the specimen itself. External magnetic fields were then applied and increased in steps until the persistent current could no longer flow. It was assumed that the prevention of persistent currents was due to the return of resistance, and so the field at which this occurred marked the critical field strength. It seemed advisable in the present experiment to increase the sensitivity of the current to small resistances so the circuit was slightly modified.

We may recall that in the presence of a small resistance R, a persistent current will decrease according to the law

$$I = I_0 e^{-(R/L)t}. \tag{1}$$

Hence, decreasing the self-inductance L of the circuit causes a more rapid decrease of persistent currents, and the effect of a small resistance is greatly increased. Therefore, the superconducting galvanometer, which had a high self-inductance, was replaced by a simpler circuit.

This circuit is shown diagrammatically in Fig. 1. The whole of the circuit except the test cylinder and the superconducting switch[1] consisted of lead; as lead has a high critical magnetic field, this part of the circuit always remained superconducting for the field strengths used. The cylindrical test specimen was mounted as shown

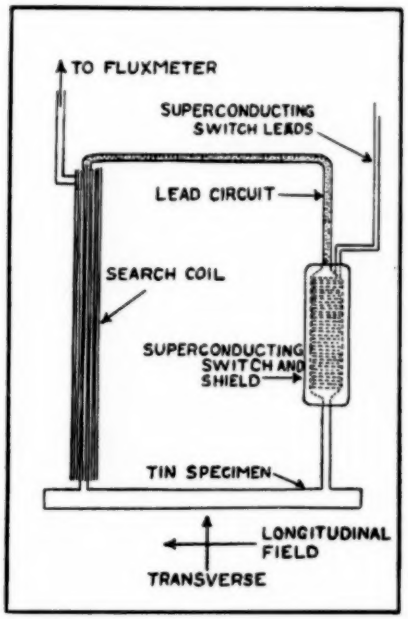

Fig. 1. Superconducting circuit for the measurement of critical magnetic fields.

to prevent the distortion of the field at the ends from affecting the readings. The superconducting switch was made of tin of larger diameter than the specimen, so that the magnitude of the current that the circuit could carry without showing resistance would be determined directly by the specimen itself. To protect the switch from outside fields, a shield of lead foil was wrapped around it. Search coils were placed before and behind the wire in a plane perpendicular to the plane of the circuit; these coils consisted of about 200 turns of fine copper wire wound around the edges of a fiber rectangle and fastened into position so that they extended down the length of one side of the circuit. They were connected to a Grassot fluxmeter as indicated. The self-inductance of the circuit when entirely superconducting was calculated to be 85 cm.

In order to use the same field coils for both transverse and longitudinal fields, a second circuit was constructed which differed from the first in that its self-inductance was slightly higher, and the specimen was in a vertical position. Both longitudinal and transverse fields were supplied by a vertical solenoid, 20 cm long, which fitted around the helium flask. The solenoid was calibrated with the fluxmeter by comparison with a standard solenoid, and it is estimated that the

field measurements are accurate to within 0.5 to 1 percent.

The inducing field (not shown in the diagram) was produced by a pair of field coils outside the helium flask, the direction of this field being perpendicular to the plane of the circuit.

All specimens were prepared by melting the constituents into a Pyrex mould and cooling rapidly. Inspection showed no large single crystal formation. Each specimen was in the form of a cylinder 40 mm long and 3.65 mm in diameter. The departure from circular cross section was small, the greatest being less than 5 percent.

The most satisfactory results were obtained by the following procedure which was repeated for each reading:

(1) The superconducting switch was applied, destroying the superconductivity of that portion of the circuit, and so preventing the circulation of persistent currents.

(2) The inducing field was switched on.

(3) The external applied field H_o (transverse or longitudinal) was switched on.

(4) The superconducting switch was removed, thus "closing" the superconducting circuit.

(5) The inducing field was switched off. This induced a persistent current through the circuit.

(6) After waiting for a certain time to allow the persistent current to decrease should there be any resistance in the specimen, the superconducting switch was applied again. Since this introduced a considerable resistance into the circuit, the persistent current dropped to zero very rapidly, and the resultant deflection of the fluxmeter was recorded. Because the fluxmeter reacted to changes of flux through the search coils due to changes of the persistent current, its readings were directly proportional to the current flowing.

TABLE I. *Data on the transverse and longitudinal critical fields for pure tin.*

TEMPERATURE	H_T	H_L	CHARACTERISTIC RATIO
3.60° °K	10.0 gauss	17.5 gauss	0.570
3.51°	17.5	30.0	0.583
3.38°	27.4	47.0	0.583
3.30°	34.7	59.5	0.584
3.17°	46.0	79.0	0.582
2.97°	61.0	105.0	0.580
2.72°	78.0	136.0	0.578

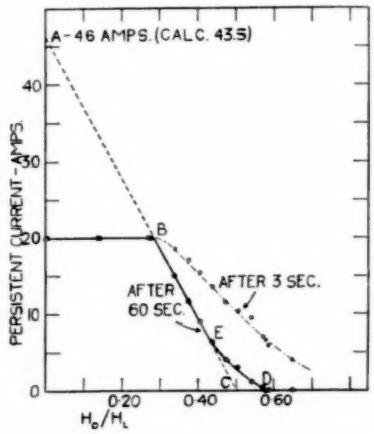

FIG. 2. Behavior of persistent currents in a pure tin cylinder in transverse magnetic fields, plotted against the ratio H_T/H_L. Temperature: 3.38° °K.

To calibrate the fluxmeter deflections directly in terms of current strength, two copper wires were soldered to the lead circuit above and below the search coils. These wires were led out of the cryostat to an outside battery circuit. At the beginning of an experiment, the temperature of the helium was kept at 4.2°K, at which temperature the lead is superconducting and the tin is not. Any current introduced through the calibration leads therefore passed entirely along the lead wire near the search coils. A deflection of 1 mm corresponded to a current of about 0.4 ampere. However, inasmuch as persistent currents of the order of 20 and 30 amperes were used in the experiments, this relatively low current sensitivity is of little importance.

EXPERIMENTAL RESULTS

(A) Spectroscopically pure tin

For comparison purposes, a complete set of experiments was carried out on a cylinder of spectroscopically pure tin (Hilger S. Lab. No. 10,000), which was investigated for both transverse and longitudinal critical fields. The results are given in Table I. Typical curves are shown plotted in Figs. 2 and 3. The broken line shows the fluxmeter readings (reduced to current strength) taken three seconds after the persistent current was induced in the circuit. The unbroken line shows the result of waiting 60 seconds after inducing the current.

Typical curves showing the decay of persistent

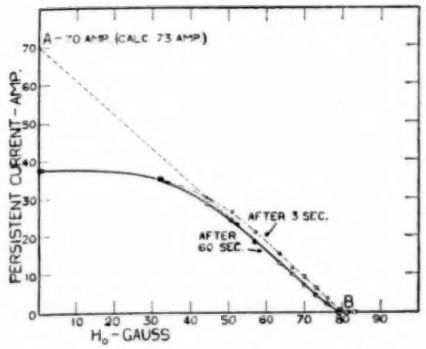

FIG. 3. Behavior of persistent currents in a pure tin cylinder in longitudinal magnetic fields. Temperature: 3.17° °K.

currents with time are given in Fig. 4. *In all cases*, it was found that a delay of 60 seconds was sufficient to bring the current strength very close to its equilibrium value.

Figure 5 is a comparison curve showing the variation of H_L with temperature. Plotted also are the results recently published on critical fields H_c by de Haas and Engelkes.[7]

(B) Single crystal of chemically pure tin

The tin single crystal was the same specimen as that used in the earlier experiments.[1] Supplementary measurements were made during the present experiment, with the improved circuit. The results are listed in Table II. Fig. 6 shows the characteristic ratio plotted against ΔT, the temperature interval measured from the transition point of tin, which is 3.72° °K.

(C) Impure tin

The three impurities that were selected as representatives of their types were *bismuth* (non-superconducting), *lead* (superconducting with a transition temperature of 7.2°K), and *thallium* (superconducting with a transition temperature of 2.37°K). The bismuth was spectroscopically pure (Hilger S. lab. No. 8016), as was the lead (Hilger S. lab. No. 8334). The thallium was commercially pure material, but since the amount of each impurity used was small, their extreme purity is not essential. The amounts of each impurity added to the tin were (1) *tin-bismuth;* 99.5 percent tin, 0.5 percent bismuth: (2) *tin-lead;* 99.5 percent tin, 0.5 percent lead: (3) *tin-thallium;* 99.3 percent tin, 0.7 percent thallium.

Experimental results for the contaminated tin are given in Table III. Typical curves for each impurity are plotted in Figs. 7, 8, and 9. It should be mentioned that, as in the case of the very pure tin, the equilibrium value of the persistent current was practically attained in an interval of 60 seconds.

DISCUSSION OF RESULTS

(A) Spectroscopically pure tin

1. Critical magnetic fields of spectroscopically pure tin.—The longitudinal critical fields for spectroscopically pure tin are slightly higher than those recently published in Leiden by de Haas and Engelkes, and at the same time are considerably higher than those for the tin single crystal. However, the low values of H_L obtained for the single crystal are not unexpected. Since it is not of extreme purity, its transition range from zero to normal resistance is probably considerable, and remembering that H_L measures the beginning of the transition, the above result is not unusual.

The transverse critical fields for spectroscopically pure tin are, within experimental error, exactly 0.58 of the longitudinal critical fields at the same temperature. The constancy of this ratio 0.58 is in direct opposition to the results for the less pure tin crystal, where the characteristic ratio was found to depend linearly

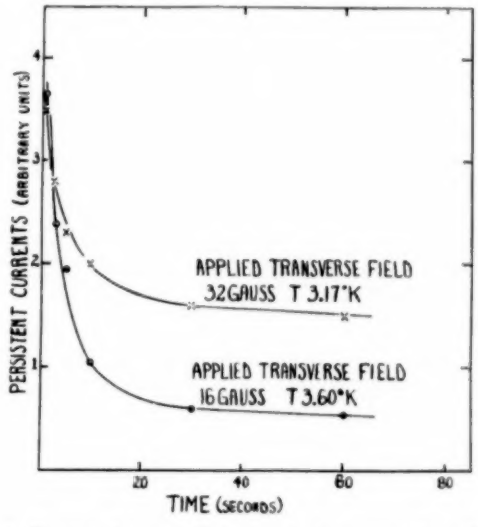

FIG. 4. Decay of persistent currents in a pure tin cylinder.

[7] W. J. de Haas and Miss A. D. Engelkes, Physica **4**, 325 (1937).

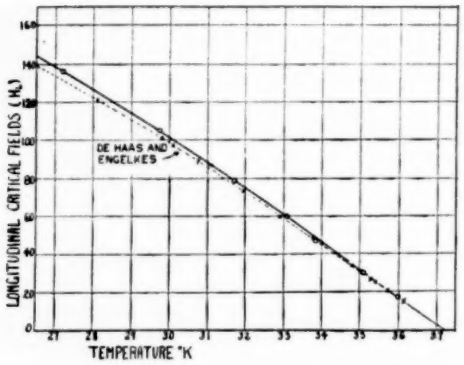

FIG. 5. Variation of longitudinal critical fields of spectroscopically pure tin with temperature.

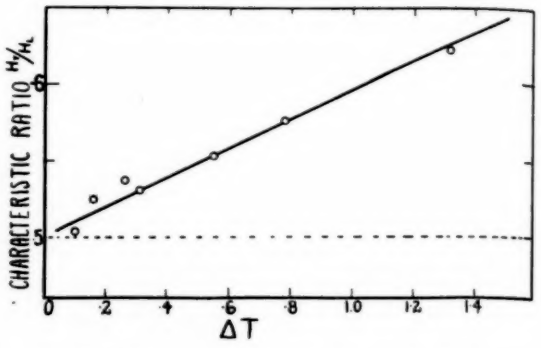

FIG. 6. Variation of the ratio H_T/H_L of a single crystal of "chemically pure" tin with temperature.

upon the temperature. Quite recently, Misener[8] at Cambridge obtained a similar temperature dependence using cylindrical wires (polycrystalline) of spectroscopically pure tin. Since workers at Leiden[9] found a constant 0.58 as the value of the ratio for a single crystal of tin, it would seem that the variation of the ratio with temperature is dependent upon some other factor than crystal structure or purity.

2. Time effects in spectroscopically pure tin.—The time effects observed in the measurements may be given a fairly simple explanation. Resistance measurements on cylinders in longitudinal and transverse fields show that in the beginning of the intermediate state, the return of resistance is not discontinuous even in the purest samples, but increases very slowly at first. In transverse fields, this resistance gradually increases to normal at H_c, while in longitudinal fields, the first small resistance in the neighborhood of H_c is followed almost at once by a very abrupt increase at H_c. If currents stronger than the critical currents are induced in a superconducting cylinder, the cylinder passes at once into some part of the intermediate state, and because of the small resistance which sets in, the current decreases. Since the resistance will depend upon the current, the decrease will not be purely exponential with the time. This decrease will continue until the current has fallen to its critical value, at which point the sample will show no resistance. In the present experiment, using the value 85 cm as the self-inductance of the circuit, we can calculate that after 60 seconds, the resistance encountered by the current is less than 10^{-11} ohm, a value which may be quoted as the upper limit of resistance at the critical field points listed above.

For longitudinal fields, the final point for zero current is almost independent of the time at which the readings were taken. This is to be expected from the above reasoning, since if there is an intermediate state in longitudinal fields, it occurs only in a small range of field strengths, and as cylinders show a relatively large resistance once the field at the surface becomes critical, persistent currents induced above the critical current value decrease to their proper value at once.

It is quite probable that a large number of the time effects observed by others can be explained in this way.

3. Critical persistent currents.—Referring to Fig. 2, we should expect the behavior of the persistent current I beyond a certain point B, to follow the line AC which represents the relation

$$2H_o+2I/r=H_L, \tag{2}$$

TABLE II. *Data on the transverse and longitudinal critical fields for a single crystal of pure tin*

TEMPERATURE	H_T	H_L	CHARACTERISTIC RATIO
3.62° °K	6.3 gauss	12.5 gauss	0.504
3.56°	10.5	20.0	0.525
3.46°	18.0	33.5	0.537
3.41°	22.0	41.5	0.530
3.17°	40.5	73.5	0.552
2.94°	58.0	100.0	0.580
2.40°	96.0	155.0	0.620

[8] A. D. Misener, Proc. Roy. Soc. **A166**, 43 (1938).
[9] W. J. de Haas, J. Voogt and J. M. Jonker, Physica **1**, 281 (1934).

where H_o is the *applied* field and r is the radius of the specimen. This line defines a boundary on the diagram at which the field on the surface of the specimen is just equal to H_L. It may be assumed that the longitudinal critical field H_L is equal to the critical field H_c for penetration as found in induction experiments, which is very nearly true for pure tin. Therefore, if a point to the right of AC represents a stable state of persistent current and field, it would give a surface field greater than H_c and so the field must penetrate into the specimen, which thereby passes into the so-called intermediate state, assumed to be a mixed phase of normal and superconducting regions. Actually, the experimental curve follows relation (2) until the point E is reached. From E to D, it departs from its linear form, and shows a greater value of I than is to be expected from a simple application of Eq. (2). At the point E then, the specimen passes into the intermediate state. Pursuing this reasoning further, we see that the current-carrying capacity of the cylinder in this state is now greater than it would have been had it remained completely superconducting, the boundary of which condition is marked by the line AC. It is quite possible that once penetration has begun, the sample breaks up in such a way that the small superconducting regions interspersed among the normal have together a greater current-carrying capacity than if the entire cylinder had remained superconducting, whether this results from a greater total superconducting surface, or from some other cause. *The current I_E represents the greatest current that the superconducting regions of the mixed phase can carry without causing a return of resistance.* As the field penetrates further, increasing the proportion of normal material, the current gradually decreases to zero at D. D marks what has been defined as H_T, the transverse critical field above which no current can flow without showing resistance. This is the only point on the diagram that is directly comparable with the results of other workers, who have uniformly used small measuring currents.

TABLE III. *Data on the transverse and longitudinal critical fields for contaminated tin.*

SPECIMEN	TEMPERATURE	H_T	H_L	CHARACTERISTIC RATIO
TIN-BISMUTH	3.60° °K		14.0 gauss	
	3.51°	16.5 gauss	27.7	0.59
	3.38°		43.5	
	3.30°		53.5	
	3.17°	40.7	71.5	0.57
	2.97°	57.5	96.5	0.59
	2.72°		130.0	
TIN-LEAD	3.60°		16.2	
	3.51°	23.5	28.3	0.83
	3.38°		46.5	
	3.30°		55.5	
	3.17°	56.0	74.5	0.76
	2.97°	74.5	100.0	0.75
	2.72°		130.0	
TIN-THALLIUM	3.60°		15.0	
	3.51°	19.5	27.0	0.72
	3.38°		43.7	
	3.30°		55.0	
	3.17°	48.0	74.0	0.65
	2.97°	67.0	101.0	0.67
	2.72°		133.0	

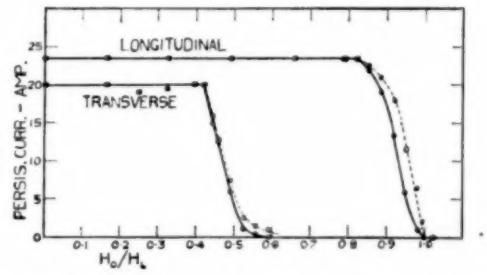

FIG. 7. Behavior of persistent currents in a tin-bismuth cylinder (99.5 percent tin, 0.5 percent bismuth) in transverse and longitudinal fields. Temperature: 2.97° °K.

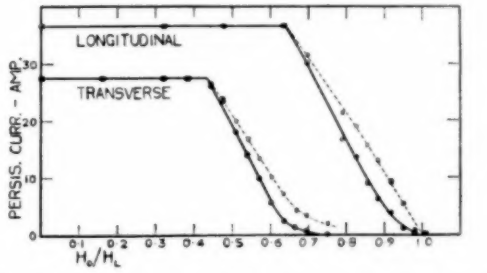

FIG. 8. Behavior of persistent currents in a tin-lead cylinder (99.5 percent tin, 0.5 percent lead) in transverse and longitudinal fields. Temperature: 2.97° °K.

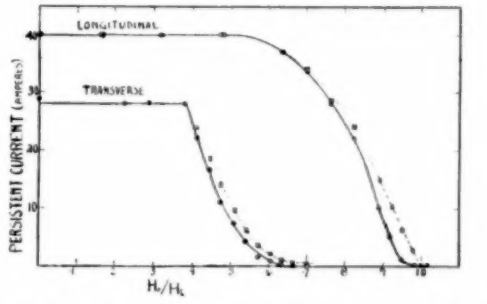

FIG. 9. Behavior of persistent currents in a tin-thallium cylinder (99.3 percent tin, 0.7 percent thallium) in transverse and longitudinal fields. Temperature: 2.97° °K.

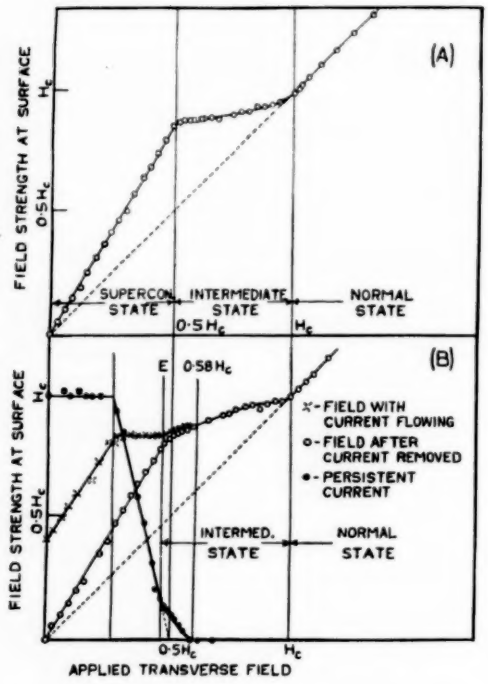

FIG. 10. The influence of persistent currents on the magnetic transition of a pure tin cylinder.

The point A should mark the critical current that the cylinder can carry in zero field without bringing on resistance, and so should be calculable by Silsbee's hypothesis, $H_L=2I_L/r$. In all cases, the agreement between calculated values and those obtained by extrapolation of EB to A was satisfactory, the disagreement generally being less than 5 percent.

4. The influence of persistent currents on induction.—A separate experiment was carried out on the spectroscopically pure cylinder in an attempt to check the accuracy of the above conclusions. This cylinder was kept in place in its superconducting circuit, and a fine bismuth wire was mounted on its surface in a diametral plane perpendicular to the direction of the applied transverse field. The bismuth wire was connected by copper leads to a potentiometer. The routine experiment was then repeated, with the exception that the resistance of the bismuth wire was measured as well as the strength of the persistent current. The results are shown in Fig. 10. 10(a) shows the strength of the magnetic field at the surface of the cylinder when no persistent current is flowing. 10(b) shows the field strength during the flow of current (after it has reached a steady value), and after it has been reduced to zero by the action of the superconducting switch. For purposes of comparison, the values of the persistent current are also plotted. The portion of the curve in the intermediate state shows an upward slope which may be explained by the fact that the ends of the bismuth wire to which the copper wires were attached, were pulled considerably away from the surface of the specimen.

Examination of the curves will show that penetration of the field into the specimen begins at the field strength represented by the line E, as was suggested above.

5. Critical persistent currents in longitudinal fields.—Referring to Fig. 3, we see that for a portion of the curve, there is a linear relationship between the strength of the persistent current I and the applied longitudinal field H_o. This is true in every case in which the pure tin was used, although the length of the linear part varies somewhat. Furthermore, an extrapolation of this line gives us AB, which in every case meets the ordinate at a point very close to the critical current for that temperature. These extrapolated values of the critical current are always slightly lower than the calculated values. It must be admitted that the calibration of the longitudinal search coils for current strength is not very certain, nor can the same reliance be placed upon this calibration that can be attributed to the transverse field search coils. However, the very consistency of its results is a point in its favor, and it is evident that some linear relation exists between persistent current and longitudinal field. Since the direction of the longitudinal field and the field due to persistent current are mutually perpendicular, we should expect the relationship to be

$$(H_o)^2+(2I/r)^2=(H_L)^2.$$

Instead, the line AB approximately represents

$$H_o+2I/r=H_L \qquad (3)$$

although the point B, which represents H_L is not exactly on the straight line. The significance of the linear relation is evident. The mutual effect of the persistent current field and the applied field is apparently independent of the direction of the latter, and depends only upon its magnitude at the surface of the cylinder.

An ideal superconductor in the form of an infinitely long cylinder would pass directly from superconducting to normal in a longitudinal field without passing through an intermediate state. In practical cases, however, cylinders do show a small intermediate state as witnessed by the finite width of the transition range. Since we conclude from our results with transverse fields that the intermediate state can carry a limited current, this should apply to longitudinal fields where there is a narrow range of mixed phase. Hence, we should expect the curve in Fig. 3 to curl slightly near the point B, in order to account for this small current-carrying capacity, and we must conclude that the actual transition from superconducting to normal begins at a field strength marked by an extrapolation from the point A to zero current, which point will be only slightly less than the point B.

(B) Impure tin

1. Effects of impurities on longitudinal critical fields.—The effect of all impurities, at least in the small amounts used here, is to lower H_L. Schubnikow and others[4] have found the reverse effect on H_c for larger amounts of impurities, and that is the conclusion reached by Mendelssohn, Moore, and Pontius.[5] Shoenberg[6] has plotted the magnetization curve of a lead sphere to which has been added 1.5 percent of bismuth, and has found that the impurity increased the critical field. It is known, however, that impurities have the effect of widening the transition range, and the critical fields reported in the papers quoted mark the points at which the magnetic transition is complete, while the critical fields in the present paper mark the points at which resistance commences. For very large impurities, i.e., for alloys, the fields at which resistance first appears have been found to be very much greater than the critical fields obtained in magnetic experiments.[10] It would be interesting to continue this work by the present method, with the use of increasing amounts of impurity.

It should be remembered that where impurities are used, there will be a considerable "locked-in" flux. With the method of measurement used in this experiment, it will be seen that each reading is a complete magnetic cycle in itself. Each reading involves increasing the total field acting on the specimen above the critical field value, because the sum of the inducing field, the applied field, and the field due to the persistent current field must be above the critical value for a short time along the sloping portion of the transition curves. Therefore, the full amount of locked-in flux should be obtained with each reading taken. The next reading releases the flux again, so that apart from a possible reduction of the persistent current below the value which would be found in a virgin cycle, the final point where no more persistent current will flow should be the same regardless of the amount of flux locked in. A study of the magnetization curve of a lead anchor ring published by Shoenberg[6] shows a considerable locked-in flux as the cycle is completed, but the indications are that if the magnetic cycle is repeated, the persistent current is reduced to zero at the same field strength as when the cycle was first begun.

The amount of reduction of H_L by impurities varies slightly with the impurity used. The superconductors reduce it only slightly, while the nonsuperconductor has a considerable effect. Lead has the least effect and thallium has slightly more than lead.

2. Effects of impurities on the transverse critical fields.—It is in the effects of impurities on H_T that abnormalities appear. These critical fields seem to be extremely sensitive to impurities. Bismuth decreases the transverse critical field in about the same ratio as it decreases the longitudinal critical field, while the superconductors increase it; lead has the greatest effect and gives characteristic ratios of 0.75 and higher. The effects of thallium lie in between the two extremes. Unfortunately, the ratios are too scattered to permit any generalization as to their dependence upon temperature.

The method also permits no definite conclusions regarding the effect of impurities on the normal transition temperatures, since this has to be obtained by an extrapolation of the H_L-T curves to zero field. We may say, however, that if such changes occur at all they are comparatively small.

[10] J. N. Rjabinin and L. W. Schubnikow, Phys. Zeits. Sowjetunion **7**, 122 (1935).

3. Effects of impurities on the resistance of the intermediate state.—An examination of the time effects in impure tin in both transverse and longitudinal fields shows definitely that the effect of impurities is to increase the resistance of the specimen in the intermediate state. Bismuth increases this resistance more than the other impurities, and consequently decreases the current the most rapidly. Thallium has the next greatest effect, and lead the least.

Equation (2) expressing the behavior of persistent currents in transverse fields does not hold for the impure samples as it does for large currents in pure tin. Nor is there any consistent linear relation between persistent current and applied longitudinal field as expressed in Eq. (3). This is hardly to be expected, for since the presence of a large locked-in flux considerably complicates any generalization, it is impossible to say just when penetration of the specimen by the field commences. Since the flux is locked in with each reading, penetration may commence as soon as the persistent current begins to be affected by the external field. If this is so, we would expect the current-carrying capacity of the intermediate state to be altered by impurities. Thus, the high transverse critical fields given by tin-lead and tin-thallium would indicate that owing to the presence of the superconducting impurities, the current-carrying capacity of the intermediate state is increased. Bismuth on the other hand must decrease it. Eqs. (2) and (3) however, are not valid over any portion of the curves.

The authors wish to express their thanks to Professor E. F. Burton, the director of the laboratory, for his constant encouragement during the course of this work.

NOVEMBER 1, 1938 PHYSICAL REVIEW VOLUME 54

Relaxation Effects Connected with the Transition Between the Superconducting and Normal States

H. GRAYSON SMITH AND K. C. MANN
McLennan Laboratory, University of Toronto, Toronto, Canada

(Received August 22, 1938)

Several authors have suggested that the relaxation effects frequently observed in experiments on the magnetic properties associated with superconductivity may be due to the slow decay, caused by a very small resistance, of eddy currents in the specimen. Similar relaxation effects have recently been observed by the authors and Wilhelm in experiments on persistent currents in a closed superconducting circuit. Viewed in the light of a marked parallelism in behavior of all time effects, these experiments definitely confirm the above suggestion. Further, a simple thermodynamic argument shows that the same cause will produce relaxation in the thermal equilibrium, and so will account also for the time effects in the calorimeter experiments of Keesom and van Laer.

INTRODUCTION

THE relaxation effects which have been observed in connection with the transition between the superconducting and normal states of a metal, when this takes place in the presence of a magnetic field, have given rise to much discussion. The effect in question can be described generally as a delay in attaining equilibrium when a change is made in either the external magnetic field or the temperature. In all cases so far reported, the relaxation effects have been found only with metals of high purity, in the transition region between the pure superconductor and the normal metal. It can reasonably be assumed, therefore, that the effects are associated with a mixture of superconducting and normal regions in a pure metal.

Different experimenters who have observed the effects have suggested various tentative explanations, but so far it has not been possible to present definite evidence of the cause, or even to show that all the effects are due to the same

cause. Several authors have suggested[1–5] that the effects observed in experiments on the magnetic properties associated with superconductivity might be due to the slow decay, caused by a very small resistance, of eddy currents induced in the specimen by the changing magnetic field. If this is the case, the phenomenon must be an irreversible one, and so must be associated with a certain amount of hysteresis in the magnetic cycle, as pointed out by Mendelssohn and Pontius.[2, 3]

Similar relaxation effects have recently been observed by the authors and Wilhelm,[6] in experiments on the prevention of persistent currents in a closed superconducting circuit by a magnetic field. In these experiments, the current in the circuit was measured directly, independently of other magnetic effects, and the decay of the current strength with time was clearly due to the presence of a very small resistance when the specimen contained suitable proportions of superconducting and normal regions. The experiments showed, in agreement with those of de Haas, Voogt and Jonker,[7] that no resistance appeared until a certain portion of the metal had passed into the normal state, and then as the transition proceeded the resistance remained finite but small over an appreciable range of magnetic field strengths. The small effective resistivity in the earlier stages of the transition region is also indicated by the experiments of Shoenberg[8, 9] on a superconducting sphere in an alternating magnetic field, where the resistance to the eddy currents was shown by an out-of-phase component in the inductance of a coil surrounding the sphere.

The experiments described in *I* show that under certain external conditions the currents induced in a superconducting metal may take an observable time to decay, and it is the purpose of the present paper to advance the proposition that all the relaxation effects which have so far been observed are due to this relatively simple cause. It is significant that the manner in which equilibrium is approached, and the conditions under which the effects are observed, are very similar in the experiments *I*, in which the resultant current strength was actually measured, and in other experiments in which the magnetic or thermal properties have been studied.

Experiments in which relaxation effects have been observed can be divided into three classes:

A. Experiments, such as *I*, in which the effect is clearly due to the decay of the current circulating around a closed circuit.

B. Experiments in which the effect is a delay in attaining equilibrium between the magnetic induction within the specimen and the external magnetic field.

C. Experiments showing a delay in attaining thermal equilibrium when the heat of transition is involved.

It is proposed to discuss these in order, and to show that there is a strong thread of continuity running through the entire series, with definite connecting links between the three types of experiment.

Delay in Establishing Magnetic Equilibrium

The largest number of observations of relaxation effects belong to class *B*, connected with experiments on the magnetic properties of simple superconducting bodies.[10] In all these cases the effect has been a delay, of very variable length, in attaining the final state of equilibrium of the magnetic induction within the body.[11]

The experiment performed by de Haas, Engelkes and Guinau[1] forms a direct link between the persistent current experiments *I* and other magnetic experiments. In this experiment the

[1] W. J. de Haas, A. D. Engelkes and O. A. Guinau, Physica **4**, 595 (1937); Leiden Comm. 247*e*.
[2] K. Mendelssohn and R. B. Pontius, Physica **3**, 327 (1936).
[3] K. Mendelssohn and R. B. Pontius, Nature **138**, 29 (1936).
[4] D. Shoenberg, Camb. Phil. Soc. Proc. **33**, 260 (1937).
[5] J. G. Daunt, Phil. Mag. **24**, 361 (1937).
[6] K. C. Mann, H. Grayson Smith and J. O. Wilhelm, Phys. Rev. **54**, 758 (1938). This paper will be referred to throughout as *I*.
[7] W. J. de Haas, J. Voogt and J. M. Jonker, Physica **1**, 281 (1934); Leiden Comm. 229*c*.
[8] D. Shoenberg, Actes du 7e Congrès Internat. du Froid **1**, 492 (1936).
[9] D. Shoenberg, Camb. Phil. Soc. Proc. **33**, 559 (1937).

[10] References 1 to 5, 12, 13 and 15; also J. N. Rjabinin and L. W. Schubnikow, Physik. Zeits. Sowjetunion **6**, 557 (1934).
[11] The experiment performed by Daunt (reference 5) is included in class *B* because it is concerned with the magnetic equilibrium. However, the effect observed, a variation with time of the shielding properties of a hollow tin cylinder, depends rather upon the proportion and distribution of the superconducting regions. It follows from the thermodynamic arguments given below that the amount of superconducting material present varies with the time in the same way as the excess eddy current.

field strength was measured inside a canal bored through a tin sphere in the direction of the external field. On account of this canal, the body has to be considered as a closed circuit, in which circulating currents can be induced. In the light of the present evidence the relaxation effects were evidently due, as the experimenters themselves suggested, to the decay with time of these currents, and the experiment should be placed along with *I* in class *A*. This is further supported by the fact that no field was observed in the canal until the external field strength was appreciably greater than the value at which penetration of flux into the sphere commenced. Since it is now known that resistance does not usually begin to appear until an appreciable part of the body has passed into the normal state, the exclusion of the field from the canal was evidently due to a resistanceless persistent current set up around the closed circuit.

Now, de Haas, Engelkes and Guinau stated further that there was no essential difference in behavior, including the relaxation effects, between the field at the surface of the sphere with the canal, and that at the surface of a similar solid sphere. We can conclude, therefore, that the effect in the solid sphere is due to the same cause as that in the bored sphere, namely to the decay of eddy currents.

Insofar as details have been reported of the relaxation effects of class *B*, the behavior has been quite similar to that in the persistent current experiments *I*. In the first place, the decay with time definitely does not follow a simple exponential law, with a rate of decay proportional to the excess.[2, 4, 5, 12] Rather, the rate of approach to equilibrium is rapid at first, and then becomes much slower as the final state is neared. This agrees with *I*, and in the latter case the shape of the decay curve could be ascribed to the fact that the small resistance depends on the amount of current flowing, in excess of the equilibrium current which the specimen can carry without resistance.

The relaxation effects have been observed in general only with pure metals.[2, 13] In *I* it was found that the resistance in the early stages of the transition was very much greater for tin contaminated with various impurities than it was for pure tin.

In experiments on spheres, and on cylinders in transverse fields where the field is considerably distorted around the body and the penetration of field proceeds gradually, the relaxation effects have been found to be more pronounced, and the times to be longer, during the earlier stages of penetration.[14] In *I* also, the small resistance which made the decay of current slow enough to be observed was associated with the earlier stages of the transition.

From the rate of decay of the persistent currents in *I* an estimate can be made of the mean resistivity of the mixture of superconducting and normal material. Towards the end of the relaxation period this was about 3×10^{-12} ohm-cm for pure tin, but the estimate is very rough since the resistance varied as the decay proceeded. With such a resistivity, the relaxation time for Foucault currents flowing around the circumference of a cylinder of radius r would be of the order of $700r^2$ seconds. The order of magnitude of the resistance observed is therefore satisfactory, although this figure is somewhat less than the times which have been observed for long cylinders in a longitudinal magnetic field.[2, 12, 15]

The Time of Relaxation

In most cases the times of relaxation which have been reported are the times required for equilibrium to be attained within the limits of measurement, and these times have varied very much in different experiments. It is well known that the secondary phenomena associated with superconductivity are very sensitive to variations in the shape and purity of the specimens, and this, as shown in *I*, includes the small resistance. However, it can be shown that in different experiments where the purity and shape are similar, the observed relaxation times can still depend very much on the way in which the experiment was carried out, principally on the magnitude of the steps in which external conditions were altered.

[12] L. W. Schubnikow, W. I. Chotkewitsch, J. D. Schepelew and J. N. Rjabinin, Physik. Zeits. Sowjetunion **10**, 165 (1936); **10** (Supp.), 36 (1936).

[13] D. Shoenberg, Proc. Roy. Soc. **A155**, 712 (1936).

[14] References 1, 4, 5, and 13. However, Mendelssohn and Pontius (reference 3) observed relaxation effects throughout the transition for a short cylinder.

[15] K. Mendelssohn, Proc. Roy. Soc. **A155**, 558 (1936).

The experiments *I*, and the general shape of the decay curves, show that the resistance increases rapidly with the amount of excess current flowing. Consequently, when the field or temperature are varied in small steps so that the currents induced are small, the effective resistivity will be extremely small, and the time required for the current to decay to half-value will be comparatively long. It can easily be seen that the whole decay curve will be extended along the time axis. Then, since experiments in which small changes have been made are usually those in which a sensitive method of measurement has been used, the time to attain "effective equilibrium" is also likely to be long.

When different experiments are compared, the association of slow relaxations with small changes of field strength seems for the most part to be confirmed. Rapid relaxations, of the order of a few seconds, have been observed by Daunt[5] when the direction of the field was suddenly changed, by Keesom and van Laer[16] with changes of the order of a third of the transition range, by the authors in *I* where every observation represented a reduction of the total field through a large part of the transition range. Slow relaxations, of several minutes, have been observed only in detailed studies of the magnetic cycle, where the field was changed in small steps.[1, 2, 3, 12, 15] On the other hand, Shoenberg[4, 13] has observed rapid relaxations in studying the magnetic cycles of spheres and short cylinders.

The Delay in Thermal Equilibrium

In experiments on the heat of transition and specific heat of tin, in the presence of a magnetic field, Keesom and van Laer[16] observed relaxation effects as the tin was heated through its transition from superconducting to normal, indicating a delay in the absorption of the heat of transition. When the metal was in its transition region, and heat was added at a uniform rate, the initial rise of temperature was greater than it ought to have been if the heat of transition had been immediately absorbed. Then, after the heating ceased, the temperature dropped again to its final equilibrium value, with a relaxation time of 20 to 40 seconds.

[16] W. H. Keesom and P. H. van Laer, Physica **3**, 173 (1936); Leiden Comm. 240*c*; Physica **4**, 499 (1937).

On the other hand, no delay was observed in the cooling due to the magneto-caloric effect, when the magnetic field was increased adiabatically. Keesom and van Laer consider that a relaxation of the order of 5 seconds ought to have been observable, and for this reason they suggest that there is some essential difference in the two cases. However, the dependence of the relaxation time on experimental conditions could cause a variation by a factor of 5 or more. Moreover, the alternating current experiments of Shoenberg[9] indicate that there is a relaxation, in this case very rapid, in the magneto-caloric effect. Hence the authors see no necessity for concluding that the cause of relaxation is different in the two cases.

Mendelssohn has reported[2, 15] that similar delays were observed in establishing magnetic equilibrium whether the field strength was altered, or the temperature changed keeping the field constant. This is to be expected if the effect is due to eddy currents, for in the transition region a change of temperature will initiate a redistribution of the field, and this will induce currents of the kind postulated. It then follows that there ought to be a relaxation in the thermal equilibrium, as observed by Keesom and van Laer.

We shall assume that when a change in external conditions is made, either of magnetic field or of temperature, the immediate change $\delta'\sigma$ in the magnetization of the superconductor is numerically less than the change $\delta\sigma$ in the equilibrium value. Then there must be a further delayed change, the relaxation, amounting to $\delta''\sigma$, where

$$\delta'\sigma+\delta''\sigma=\delta\sigma,$$

and where $\delta''\sigma$ is a function of the time, determined by the decay of the eddy currents.

In any change the external work done is $H\delta\sigma$, and if the heat absorbed is δQ we have

$$H\delta\sigma+\delta Q=\delta U+\delta U_i, \tag{1}$$

where δU_i is the kinetic, or self-inductance energy of the eddy currents. Since δU_i is always positive when an equilibrium state is disturbed by altering external conditions, the magnetic cycle as a whole may be irreversible. But the process can be said to be instantaneously

reversible in the sense that, if the time required to alter conditions is small compared with the time of relaxation, an immediate reversal will destroy the eddy currents and restore the initial conditions. Therefore, for a rapid initial change, δU_i can be treated as a part of the internal energy. Then, during the slow decay, this energy is exactly recovered as heat, and so the decay represents merely a change in the form of the internal energy, and it is permissible to apply thermodynamic relations to the problem.

Ignoring the distinction between the energy of the eddy currents and other forms of internal energy, we obtain from (1), as a fair approximation to the actual conditions,

$$\delta Q = T\delta S = C_v\delta T - T(dH/dT)_\sigma\delta\sigma. \qquad (2)$$

In this relation we can put, at least approximately,

$$(dH/dT)_\sigma = dH_c/dT,$$

where H_c is the critical field for the interruption of superconductivity, for throughout the transition region the field within the body must be nearly equal to the critical field, independent of σ.[17]

Consequently, in the first experiment of Keesom and van Laer, heating in a constant field, the rise of temperature during the heating period will be given by

$$C_v\delta' T = \delta Q + T(dH_c/dT)\delta'\sigma. \qquad (3)$$

Since dH_c/dT is a negative quantity, and $\delta'\sigma$ is positive and less than the equilibrium value $\delta\sigma$, the temperature increase $\delta' T$ must be greater than the equilibrium increase, in agreement with experiment.

After the heating is complete, we have, according to the eddy current hypothesis, a further change $\delta''\sigma$ in the magnetization, and hence a further change in temperature, given by

$$C_v\delta'' T = T(dH_c/dT)\delta''\sigma. \qquad (4)$$

This represents a delayed cooling, as observed, which follows exactly the variations in the magnetization.

Equation (4) gives also the cooling to be expected in the adiabatic magneto-caloric effect, and shows that in this case also the changes of temperature should follow the course of the magnetization, and exhibit the same kind of relaxation as has been observed in purely magnetic experiments.

The heat of transition from the superconducting to the normal state is given by[18]

$$L = -VT(H/4\pi)(dH_c/dT) = -T(dH_c/dT)\sigma, \qquad (5)$$

where $\sigma = VH_c/4\pi$ is the total change in magnetization from pure superconductor to normal metal. Eq. (2) can now be written

$$\delta Q = C_v\delta T + L\delta\sigma/\sigma.$$

But, if the mixed phase interpretation of the transition region is accepted,

$$\delta Q = C_v\delta T + L\delta r,$$

where δr is the increase in the fraction of the material which is in the normal state. From this it can be argued that the transition of the material from one state to the other in local regions also follows the changes in magnetization, and so also proceeds slowly as the excess eddy currents die out. The same presumably applies to the distribution of the normal regions, insofar as this is determined by the direction of the external field, and so the eddy current hypothesis can also account for the relaxation effects observed by Daunt.[5, 11] This suggests that the process may be similar to that suggested by Mendelssohn and Pontius,[3] that in a decreasing field the regions in which the eddy currents are located contract as the currents decay, and allow the transition to the superconducting state to proceed.

In conclusion the authors wish to express their thanks to Professor E. F. Burton for his continued encouragement and advice, and to Dr. K. Mendelssohn for his helpful correspondence.

[17] Theoretically, the internal field should be everywhere equal to H_c, if the distribution of normal and superconducting regions is regular: F. London, Physica **3**, 450 (1936).

[18] C. J. Gorter and H. Casimir, Physica **1**, 305 (1934); W. H. Keesom and P. H. van Laer, Physica **4**, 487 (1937).

LETTERS TO THE EDITOR

Prompt publication of brief reports of important discoveries in physics may be secured by addressing them to this department. Closing dates for this department are, for the first issue of the month, the eighteenth of the preceding month, for the second issue, the third of the month. Because of the late closing dates for the section no proof can be shown to authors. The Board of Editors does not hold itself responsible for the opinions expressed by the correspondents.

Communications should not in general exceed 600 words in length.

Scattering of Slow Neutrons by Paramagnetic Salts*

Bloch[1] and Schwinger[2] have investigated theoretically the polarization effects when neutrons interact with magnetized ferromagnetic material. Experiments have been performed to demonstrate these effects.[3-6] Halpern and Johnson[7, 8] have pointed out that magnetic scattering will occur in every type of magnetic material and that the magnetic and nuclear contributions to the neutron scattering may be separated by studying the scattering of certain metals in different valence states.

Preliminary results on scattering of neutrons by paramagnetic substances reported by one of us[9] indicated the necessity for making investigations of the neutron scattering at small angles.

Experiments have now been carried out in which scattering by paramagnetic substances has been studied by two methods:

(1) Measurement of the effective cross section of the paramagnetic salts as compared to the *additive* cross sections for the elements which compose them, under conditions in which neutrons scattered through angles greater than approximately 3° were not detected.

(2) Measurement of the angular distribution of the scattered neutrons.

A neutron beam approximately 100 cm long from source to boron chamber was shielded by B_4C and accurately collimated by cadmium channels. The cross sections of the compounds were then measured with the sample interposed in this beam approximately midway between the source and the detector, so that practically no scattered neutrons were detected. The cross section of an identical physical mixture was then determined as in the case of MnS, or else cross sections of the constituent elements were measured separately under the same conditions. The results are shown in Table I. The differences in column four are believed to be correct for the samples used within $\pm 0.8\times10^{-24}$ cm².

TABLE I. *Results for the observed, nuclear, and magnetic cross sections for various paramagnetic salts.*

Paramagnetic Salt	Observed Cross Section (cm²)	Nuclear Additive Cross Sections (cm²)	Magnetic Cross Section for Salt (cm²)
$MnSO_4$	33.6×10^{-24}	31.3×10^{-24}	2.3×10^{-24}
MnS	19.1	15.1*	4.0
MnO	19.9	18.1	1.8
Fe_2O_3	39.2	36.0	3.2†

* Physical mixture.
† This number should be increased by twice the magnetic scattering cross section of the metallic iron atom when unmagnetized.

The results show an increase in scattering for the paramagnetic salts over the *additive* cross sections of the elements which compose them. Carefully selected materials were used in all cases and special precautions were taken to exclude water contamination.

The angular distribution of the scattered neutrons has been studied by comparing the transmission of the paramagnetic salts when placed near the center of the beam and close to the detector. With the sample close to the detector an appreciable solid angle was subtended by the sample at the chamber. The effective change in solid angle subtended between the two points in the beam was experimentally measured with carbon as a scattering material. Iron was also used in this way and the iron and carbon data indicate a scattering cross section for iron of 8.5×10^{-24} cm² and a capture cross section for iron of 3.5×10^{-24} cm². The total cross section for iron was measured in this beam and found to be $12.0\pm0.1\times10^{-24}$ cm².

MnS gave pronounced evidence of small angle scattering. From an experimental point of view the MnS was the most favorable of the paramagnetic salts as the cross section of the negative ion was the smallest, and also a physical mixture was easily obtainable to make a comparison. A preliminary study of our data obtained with the MnS indicates that the form factor for the magnetic scattering has decreased noticeably in the region 20 to 45 degrees. These results seem to indicate conclusively the existence of magnetic scattering of slow neutrons by paramagnetic materials.

We are indebted to Professors Halpern and Johnson for many helpful discussions.

A paper giving the details of our work will follow.

MARTIN D. WHITAKER
New York University,
University Heights.

HAROLD G. BEYER
JOHN R. DUNNING
Pupin Physics Laboratories,
Columbia University,
New York, N. Y.,
October 15, 1938.

* Publication assisted by the Ernest Kempton Adams Fund for Physical Research at Columbia University.

[1] Bloch, Phys. Rev. **50**, 259 (1936).
[2] Schwinger, Phys. Rev. **51**, 544 (1937).
[3] Dunning, Powers and Beyer, Phys. Rev. **51**, 51 (1937).
[4] Hoffman, Livingston and Bethe, Phys. Rev. **51**, 214 (1937).
[5] Frisch, von Halban and Koch, Nature **139**, 756 (1937); **140**, 360 (1937).
[6] Powers (in process of publication).
[7] Halpern and Johnson, Phys. Rev. **52**, 52 (1937).
[8] Halpern and Johnson, Phys. Rev. **51**, 992 (1937).
[9] Whitaker, Phys. Rev. **52**, 384 (1937).

The Increase of X-Ray Reflection from Quartz Due to a Strong Electric Field

When a strong electric field was applied to a thin quartz plate for a long time, it was found that the intensity of x-ray reflection increased very much even after the removal of the electric field. Crystal plates free from twin and about 1 mm in thickness were cut parallel to various net planes and etched slightly with HF solution. An electrostatic field of 10~17 kv/mm was applied perpendicular to their surface. After the removal of the field, the intensity of x-ray reflection from an internal net plane was measured by the ionization spectrometer.

(1) The intensity of reflection increases at first with the length of time of application of the field, but reaches a saturation value after several hours of application.

(2) No difference is found whether the field is applied parallel or antiparallel to the electric polar axis.

(3) This effect is strongly structure sensitive,[1] but the general behavior is much the same for different crystallographic directions.

(4) The effect dies away very slowly after the removal of the field, and in some cases considerable increase in reflection is still observed after five or six days. However, at high temperatures or under the irradiation with x-rays or γ-rays, the decay is more rapid.

Further examinations are now in progress, and the definite conclusion concerning the origin of the effect must be postponed. But *there is no doubt that the increase of reflection is due to the decrease of x-ray extinction*[2] *as a result of the inhomogeneous strain.* Since the purely elastic stress shows no conceivable after-effect, and the present effect is easily destroyed by x-rays, it is natural to consider the effect to be electronic in its origin. A plausible explanation might be as follows: Electrons, after wandering through the crystal under the strong electric field, are trapped[3] by atoms at the lattice imperfection, and the stress thus produced may be the cause of inhomogeneous strain.

My sincere thanks are due to Professor S. Nishikawa for his continuous guidance and kind encouragement throughout this work.

YOSHINOBU KAKIUCHI

Physical Institute,
Tokyo Imperial University,
September 24, 1938.

[1] Smekal, *Handbuch der Physik*, 24/2.
[2] Ewald, *Handbuch der Physik*, 23/2, esp. §21 and p. 428.
[3] Gurney and Mott, Proc. Phys. Soc. **49**, 32 (1937).

Nuclear Isomerism in Element 43

We wish to report briefly an interesting case of isomerism which has appeared during an investigation of the short-lived radioactive isotopes of element 43. The irradiation of molybdenum with deuterons or slow neutrons produces a radioactive molybdenum isotope with a half-life of 65 hours which emits electrons with an upper energy limit of approximately 1 Mev. (This molybdenum activity has also been reported recently by Sagane, Kojima, Miyamoto and Ikawa.)[1] This molybdenum decays into a second activity which has a half-life of 6 hours and which emits only a line spectrum of electrons. Since the molybdenum emits electrons, the daughter activity must be ascribed to element 43; chemical identification has been carried out and has confirmed this identification of the 6-hour activity. Absorption measurements in aluminum and measurements with a magnetic spectrograph[2] indicate an energy for the electrons of about 110 kev. This line spectrum must be due to the conversion electrons of a gamma-ray of about 130 kev energy. The 6-hour activity also emits x-radiation and γ-radiation. The absorption of the x-rays in molybdenum, columbium and zirconium shows a discontinuity that is consistent with the $K\alpha$ line of element 43, which is to be expected on the basis of the interpretation given below.

The simplest and most reasonable explanation for these facts is the existence of an excited state in this isotope of element 43 which reverts to the ground state by the emission of conversion electrons and gamma-rays with a half-life of 6 hours. A line of conversion electrons corresponding to a similar transition seems to have been detected by Pontecorvo[3] during a study of the nuclear isomerism in rhodium. A more complete discussion and a description of the experiments will be published later in the *Physical Review.*

We wish to thank Professor E. O. Lawrence for the privilege of working with the cyclotron and for his interest in this problem.

We wish also to express our appreciation to Mr. D. C. Kalbfell for the photographing of the line spectrum of electrons. This research has been aided by grants from the Research Corporation.

E. SEGRÈ
G. T. SEABORG

Radiation Laboratory,
Department of Physics (E.S.),
Department of Chemistry (G.T.S.),
University of California,
Berkeley, California,
October 14, 1938.

[1] Sagane, Kojima, Mijamoto and Ikawa, Phys. Rev. **54**, 542 (1938).
[2] Kalbfell, Phys. Rev. **54**, 543 (1938).
[3] Pontecorvo, Phys. Rev. **54**, 542 (1938).

The Helium-Deuteron and Deuteron-Deuteron Nuclear Reactions—Corrections

(1) In a recent letter to the *Physical Review*, A. J. Ruhling[1] has mentioned that long range protons had been reported[2] by us from the reaction

$$_2He^3+{}_1H^2\rightarrow{}_2He^4+{}_1H^1. \qquad (1)$$

I wish to point out that these observations turned out to be erroneous, and because of the presence on the target of a trace of boron as impurity. We have obtained no evidence so far that the reaction (1) does take place.

(2) R. D. Myers[3] quotes me as reporting[2] a spherical symmetry for the neutrons from the reaction

$$_1H^2+{}_1H^2\rightarrow{}_2He^3+{}_0n^1 \qquad (2)$$

in contradiction with observations of Kempton, Browne and Maasdorp.[4] This is not so.

M. L. OLIPHANT

University of Birmingham,
Birmingham, England,
September 30, 1938.

[1] A. J. Ruhling, Phys. Rev. **54**, 308 (1938).
[2] Copenhagen Conference.
[3] R. D. Myers, Phys. Rev. **54**, 361 (1938).
[4] Kempton, Browne and Maasdorp, Proc. Roy. Soc. **A157**, 372 (1936).

Scattering of Fast Electrons

In a private communication, Professor E. J. Williams has suggested that the electron scattering data recently reported in this journal[1] could be profitably compared with his latest computations on plural and multiple scattering. For comparison with cloud chamber observations the distribution in angle projected on a plane containing the initial direction of motion must be known. According to Professor Williams the projected plural and multiple scattering for fast electrons ($\beta=v/c\approx 1$) is Gaussian with an arithmetic mean projected angle given by:[2]

$$\alpha_m = k/W = (Ze^2N^{1/2}t^{1/2})(8.10 + 0.56\log_{10}\{Z^{4/3}Nt/Z_{Pb}{}^{4/3}N_{Pb}\})/W \quad (1)$$

$$= 106/W \text{ degrees} \quad (1')$$

where t is the thickness, Z the atomic number, N the number of nuclei per cc of the scatterer and W is the kinetic plus mass energy of the electron. The numerical results, here and in what follows, are given for a lead scatterer of thickness $t=0.015$ cm as employed in the experiments and for W in Mev. In a form convenient for the treatment of the scattering of electrons of different energies we have:

$$P_M(W\alpha)d(W\alpha) = (2/\pi k)\exp(-(W\alpha/k)^2/\pi)d(W\alpha) \quad (2)$$

$$= 0.006\exp(-(W\alpha/188)^2)d(W\alpha). \quad (2')$$

The first term in brackets in k appears squared in the expression for the projected single scattering[1] as follows:

$$P_S(W\alpha)d(W\alpha) = 4\pi(Z^2e^4Nt)(W\alpha)^{-3}d(W\alpha) \quad (3)$$

$$= 2840(W\alpha)^{-3}d(W\alpha) \quad (3')$$

while the second term is a statistical factor yielded by the calculation of plural and multiple scattering from single scattering. Professor Williams also points out that the transition from multiple to single scattering ($P_M=P_S$) occurs at $\sim 4\alpha_m$, this result depending only on the statistical factor discussed above. The single scattering contributes only about 4 percent to the mean scattering angle.

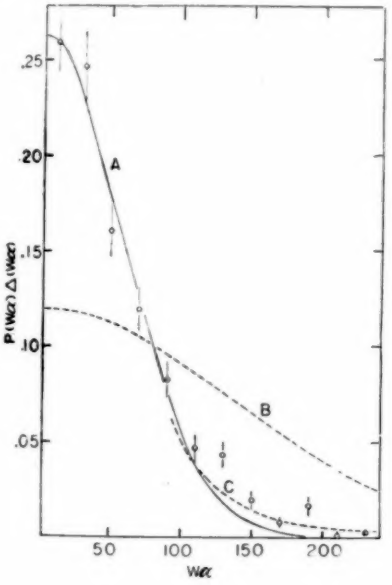

FIG. 1. Experimental and theoretical scattering of fast electrons in a lead lamina of thickness 0.015 cm. *A*, Empirical multiple scattering. *B*, Theoretical multiple scattering. *C*, Theoretical single scattering.

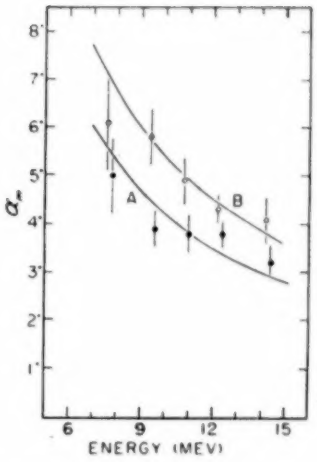

FIG. 2. Mean projected angles of scattering of fast electrons in a lead lamina of thickness 0.015 cm. *A*, For only electrons with $W\alpha\leq 120$ Mev degrees. *B*, For all electrons.

In Fig. 1 the fraction of 368 electrons (238 negatives, 130 positives) scattered by an 0.015 cm lead lamina into intervals $\Delta(W\alpha)=20$ Mev degrees is compared with equations (2′) (curve *B*) and (3′) (curve *C*). The electrons ranged in energy from 5 to 17 Mev with a mean total energy at approximately 11 Mev. A Gaussian curve (A) with $\alpha_m=45/W$ is found to fit the small angle scattering within the statistical fluctuations. The observed mean angle is thus smaller than the theoretical by a factor of 2.3 (compare (1′)). It is to be noted that any random error in measurement will tend to increase the observed mean angle. The large angle scattering is given qualitatively by the theoretical single scattering as pointed out in the first publication.[1] In Fig. 2 the observed mean angle for all electrons (open circles) and the observed mean angle for only those electrons with $W\alpha\leq 120$ Mev degrees (full circles) as functions of W are shown. The latter points fit the equation $42/W$ (curve *A*) whereas the former agree well with $55/W$ (curve *B*). The large angle scattering thus contributes approximately 25 percent of the mean angle of scattering. As this large angle scattering apparently is single, the single scattering is seen to become important at a critical angle smaller than that given by theory. These results indicate either that the statistical factor found from the plural and multiple scattering computations or the theoretical single scattering at small angles is too large. Professor Williams estimates his computational errors to be not more than three or four percent in the extreme and points out that the theoretical single scattering should hold especially for small angles as in this region the theory is independent of Dirac's treatment of spin. The preliminary experimental observations are now being supplemented by experiments with scatterers of different thickness in an attempt to discover the source of the discrepancy with theory.

W. A. FOWLER

Kellogg Radiation Laboratory,
California Institute of Technology,
Pasadena, California,
September 26, 1938.

[1] Fowler and Oppenheimer, Phys. Rev. **54**, 320 (1938).
[2] Now in publication. We are greatly indebted to Professor Williams for his kind permission to use the results of his computations before publication.